


5-2013

Variability in the Hydraulic Conductivity of a Test Pad Liner System Using Different Testing Techniques

Matthew Jonathan Nanak
University of Arkansas, Fayetteville

Follow this and additional works at: <http://scholarworks.uark.edu/etd>

 Part of the [Soil Science Commons](#), and the [Transportation Engineering Commons](#)

Recommended Citation

Nanak, Matthew Jonathan, "Variability in the Hydraulic Conductivity of a Test Pad Liner System Using Different Testing Techniques" (2013). *Theses and Dissertations*. 674.
<http://scholarworks.uark.edu/etd/674>

This Thesis is brought to you for free and open access by ScholarWorks@UARK. It has been accepted for inclusion in Theses and Dissertations by an authorized administrator of ScholarWorks@UARK. For more information, please contact scholar@uark.edu, ccmiddle@uark.edu.

VARIABILITY IN THE HYDRAULIC CONDUCTIVITY OF A TEST PAD LINER SYSTEM
USING DIFFERENT TESTING TECHNIQUES

VARIABILITY IN THE HYDRAULIC CONDUCTIVITY OF A TEST PAD LINER SYSTEM
USING DIFFERENT TESTING TECHNIQUES

A thesis submitted in partial fulfillment
of the requirements for the degree of
Master of Science in Civil Engineering

By

Matthew J. Nanak
University of Arkansas
Bachelor of Science in Civil Engineering, 2011

May 2013
University of Arkansas

ABSTRACT

Historic methods (the time lag approach, the velocity approach, and the Z-t approach), utilized to reduce two stage borehole test data, were evaluated. Two of the historic methods provided viable results and were used for this research project. Additionally, these two methods are recommended for reducing two stage borehole test data in the future.

Flexible wall permeameter and soil index laboratory testing were conducted on the soil used to construct three environmentally controlled compacted clay liners (test pads) to develop a zone of acceptance (placement window). Using the results from the laboratory testing, two acceptance criteria were evaluated, while one criterion was used for construction purposes and is recommended. Two stage borehole testing was conducted in Test Pads 1 and 2, while sealed double ring infiltrometer testing was conducted in Test Pad 3. After in-situ hydraulic conductivity testing was completed for Test Pads 1 and 2, Shelby tube and hand carved samples were obtained and laboratory testing was performed on the samples. Time domain reflectometry probes and tensiometers were used to monitor the movement of the wetting front during testing conducted in Test Pad 3.

Hydraulic conductivity results obtained from each testing method were compared. The laboratory obtained hydraulic conductivity values from testing conducted on Shelby tube samples were compared to laboratory hydraulic conductivity values obtained from testing conducted on hand carved samples. The laboratory hydraulic conductivity values obtained from testing conducted on Shelby tube and hand carved samples were compared to field hydraulic conductivity values obtained from two stage borehole hydraulic conductivity testing. The field hydraulic conductivity values obtained from two stage borehole hydraulic conductivity testing

were compared to field hydraulic conductivity values obtained from sealed double ring infiltrometer hydraulic conductivity testing.

Collection of soil specimens using Shelby tubes causes the soil to compress and thereby changes the soil parameters (unit weight and hydraulic conductivity). Results of this research project indicate that comparable hydraulic conductivities within half an order of magnitude can be obtained from two stage borehole and sealed double ring infiltrometer field testing and laboratory testing conducted on hand carved and Shelby tube flexible wall samples.

This thesis is approved for recommendation
to the Graduate Council.

Thesis Director:

Dr. Richard A. Coffman

Thesis Committee:

Dr. Norman D. Dennis

Dr. Thomas S. Soerens

THESIS DUPLICATION RELEASE

I hereby authorize the University of Arkansas Libraries to duplicate this thesis when needed for research and/or scholarship.

Agreed

Matthew J. Nanak

Refused

Matthew J. Nanak

ACKNOWLEDGMENTS

This research project would not have been possible without the help and support of various persons. I would first like to thank Dr. Richard Coffman for giving me the opportunity to conduct this project and mentoring me along the way. I would also like to thank Mark Kuss, David Peachee, and Clint Wood for helping to provide technical assistance for my research project. I would like to thank Cyrus Garner for helping me collect and analyze data for my research project. I would like to thank Camila Maldonado for helping to conduct laboratory testing. I would also like to thank everyone who helped me construct and/or remove test pads. These people include but are not limited to: Sarah Bey, Matt Blanchard, Dr. Richard Coffman, Omar Conte, Michael Deschenes, Cyrus Garner, Taylor Goldman, Elvis Ishimwe, David Peachee, Blake Peacock, Morgan Race, Kevin Tipton, Clint Wood, and Yi Zhao.

DEDICATION

This thesis document is dedicated first to my parents you have encouraged me to seek higher education and who have supported me along the way.

Dave and Margie Nanak

To my wonderful fiancée who has stood by my side along the way and who encouraged me to keep pushing through when times got rough.

Rachel Albinson

And to all of my family and friends who have helped me along the way.

TABLE OF CONTENTS

Chapter 1: Introduction	1
1.1 Background	1
1.2 Significance to the Geotechnical Engineering Community	2
1.3 Project Overview	2
1.4 Thesis Overview.....	4
Chapter 2: Literature Review	6
2.1 Introduction	6
2.2 Acceptance Criterion.....	7
2.2.1 Purpose of Acceptance Criteria	10
2.2.2 Laboratory Testing Associated with Acceptance Criteria	11
2.2.3 Field Testing Associated with Acceptance Criteria.....	12
2.3 Sealed Double Ring Infiltrometer Testing	14
2.3.1 Wetting Front Method.....	19
2.3.2 Suction Head Method	20
2.3.3 Apparent Hydraulic Conductivity Method	21
2.4 Two-Stage Borehole Testing.....	21
2.5 Calculation of Hydraulic Conductivity for TSB Testing	25
2.5.1 Soil Testing Engineers, Inc. (1983) Method.....	27
2.5.2 Daniel (1989) Method.....	29
2.5.3 Boutwell (1992) Method.....	32
2.5.4 Boutwell and Tsai (1992) Method	36
2.5.5 Trautwein and Boutwell (1994) Method.....	38

2.5.6	ASTM D6391 (2012) Method A.....	40
2.5.7	Chapuis (1999) Method	42
2.5.8	Chiasson (2005) Method.....	44
2.5.9	ASTM D6391 (2012) Method B.....	46
2.6	Time Domain Reflectometry Probes.....	47
2.7	Tensiometers	49
2.8	Flexible Wall Permeameter	50
2.9	Representative Sample Size for Hydraulic conductivity Testing.....	53
2.10	Effects of Effective Stress on Hydraulic conductivity.....	54
2.11	Laboratory Hydraulic Conductivity Compared to Field Hydraulic Conductivity	55
2.12	Conclusion.....	59
Chapter 3: Methods and Procedures.....		61
3.1	Introduction	61
3.2	Evaluating the Various Solution Methods for Two Stage Borehole Data Reduction....	62
3.3	Zone of Acceptance.....	62
3.3.1	Proctor Testing for Development of ZOA	63
3.3.2	Flexible Wall Hydraulic Conductivity Testing for Development of ZOA	65
3.4	Construction of Test Pad Box at Engineering Research Center.....	68
3.5	Placement and Removal of Soil in Test Pad Box at Engineering Research Center.....	69
3.5.1	Placement of Loose Lifts	70
3.5.2	Compaction.....	72
3.5.3	In-Situ Unit Weight Testing.....	73
3.5.4	Placement of Test Pad 1.....	73

3.5.5	Placement of Test Pad 2.....	75
3.5.6	Placement of Test Pad 3.....	77
3.5.7	Removal of Soil	78
3.6	In-Situ Hydraulic Conductivity Testing in the Test Pad Box	80
3.6.1	Two Stage Borehole Testing.....	80
3.6.2	Sealed Double Ring Infiltrometer Testing.....	85
3.6.2.1	Installation of SDRI Rings and Vertical Hydraulic Conductivity Testing.....	86
3.6.2.2	Installation of the Time Domain Reflectometry Probes and Data Collection .	92
3.6.2.3	Installation of Tensiometers and Data Collection	93
3.7	Sample Acquisition	98
3.7.1	Shelby Tube Samples.....	98
3.7.2	Hand Carved Samples.....	102
3.7.3	Disturbed Samples	104
3.8	Laboratory Testing.....	105
3.8.1	Flexible Wall Hydraulic Conductivity Testing on Samples Obtained from Test Pads	105
3.8.1.1	Shelby Tube Sample.....	106
3.8.1.2	Hand Carved Sample.....	107
3.8.2	Specific Gravity Testing.....	108
3.8.3	Hydrometer Analyses.....	110
3.8.4	Percentage Passing the No. 200 (75- μ m) Sieve.....	110
3.8.5	Atterberg Limits Testing.....	111
3.9	Conclusion.....	112

Chapter 4: Results and Discussion.....	114
4.1 Introduction	114
4.2 Evaluation of the Various Solution Methods for Two Stage Borehole Data Reduction....	115
4.3 Developing Acceptance Criterion	126
4.3.1 Proctor Testing Results	126
4.3.2 Flexible Wall Hydraulic conductivity Results on Proctor Samples.....	127
4.3.3 Zone of Acceptance	129
4.4 Test Pad Placement Results.....	132
4.5 Field Hydraulic Conductivity Testing Results	136
4.5.1 Two Stage Borehole Results for Test Pads 1 and 2	136
4.5.2 Sealed Double Ring Infiltrometer Results for Test Pad 3.....	140
4.6 Laboratory Testing Results	147
4.6.1 Hydraulic Conductivity, Dry Unit Weight, and Measured Moisture Content Results for Samples Collected from Test Pad 1	148
4.6.2 Hydraulic Conductivity, Dry Unit Weight, and Measured Moisture Content Results for Samples Collected from Test Pad 2	154
4.6.3 Soil Index Testing Results for Samples Collected from Test Pads 1 and 2.....	158
4.7 Discussion of Testing Techniques Comparisons	161
4.7.1 Discussion on Comparisons between the Hydraulic Conductivity Values Obtained from Shelby Tube and Hand Carved Samples	162
4.7.2 Discussion on the Comparisons between the Laboratory and Field (TSB) Hydraulic Conductivity Results.....	163

4.7.3	Discussion on the Comparisons between Field (TSB) and Field (SDRI) Hydraulic Conductivity Results	165
4.7.4	Discussion on the Comparisons between Laboratory and Nuclear Density Gauge Dry Unit Weight Results.....	166
4.7.5	Discussion on the Comparisons between Shelby Tube and Hand Carved Dry Unit Weight Results	168
4.7.6	Discussion on the Comparisons between Laboratory and Nuclear Density Gauge Moisture Content Results.....	169
4.7.7	Discussion on the Comparisons between Hand Carved and Shelby Tube Moisture Content Results	171
4.7.8	Discussion on the Comparisons between Shelby Tube Recovery and Push Lengths Results	173
4.7.9	Discussion on the Comparisons between TDR Probe and Nuclear Density Gauge Moisture Content Results.....	174
4.8	Conclusion.....	175
Chapter 5: Observations, Conclusions, and Recommendations		179
5.1	Introduction	179
5.2	Observations.....	179
5.3	Conclusions	180
5.4	General Recommendations	181
5.4.1	Recommendations on Development of an Acceptance Criteria	181
5.4.2	Recommendations on How to Reduce Two Stage Borehole Data	182

5.4.3	Recommendations on In-Situ Hydraulic Conductivity Testing and Sampling Soil Specimens for Laboratory Testing.....	183
5.4.4	Recommendations on SDRI Testing.....	184
5.5	Recommendations for Future Research	184
5.5.1	Recommendations for Continuing the Current Research at the Engineering Research Center	185
5.5.2	Recommendations for Nuclear Density Testing During Test Pad Removal	185
5.5.3	Recommendation for Verifying the Accuracy of the Nuclear Density Gauge	186
5.5.4	Recommendation for Evaluating the Use of Mariotte Tube for Constant Head Two Stage Borehole Testing	186
5.5.5	Recommendation for Determining Diurnal Cycles in Hydraulic Conductivity Testing	187
5.5.6	Recommendations for Evaluating the Use Shelby Tubes in a Performance Liner	187
References	189
Appendix A. Results for Zone of Acceptance Laboratory Testing	193
Appendix B. Results Obtained from Field Testing Conducted on Test Pads 1, 2, and 3 ...		209
Appendix C. Laboratory Flexible Wall Hydraulic Conductivity for Test Pads 1 and 2		222
Appendix D. Results for Soil Index Testing		254

LIST OF FIGURES

Figure 2.1. Zone of acceptance developed using the 95-percent criterion.	8
Figure 2.2. Zone of acceptance developed from APCEC criterion.	9
Figure 2.3. Zone of acceptance developed from Daniel and Benson (1990) criterion.	10
Figure 2.4. Zone of acceptance with acceptable and failed field density points.	11
Figure 2.5. Diagram of a sealed double ring infiltrometer (from Trautwein and Boutwell, 1994).	14
Figure 2.6. Constant head board device (from Neupane et al., 2005).	17
Figure 2.7. Schematic of SDRI test apparatus showing relevant dimensions for calculating hydraulic gradient (recreated from Trautwein and Boutwell, 1994).	18
Figure 2.8. Schematic of SDRI test apparatus showing relevant dimensions for wetting front method (modified from Trautwein and Boutwell, 1994).	19
Figure 2.9. Schematic of SDRI test apparatus showing relevant dimensions for suction head method (modified from Trautwein and Boutwell, 1994).	20
Figure 2.10. Schematic of SDRI test apparatus showing relevant dimensions for apparent hydraulic conductivity method (modified from Trautwein and Boutwell, 1994).	21
Figure 2.11. Schematic of two stage borehole test for both Stage 1 and Stage 2.	22
Figure 2.12. Example of steady state condition from a hydraulic conductivity test.	23
Figure 2.13. Diagram of two-stage in situ hydraulic conductivity test with Boutwell permeameter (a) Stage I (b) Stage II (from Daniel, 1989).	31
Figure 2.14. Curves of k_2/k_1 and m for $L/D = 1.0, 1.5,$ and 2.0 (from Daniel, 1989).	31
Figure 2.15. TSB data reduction nomograph (from Trautwein and Boutwell, 1994).	40

Figure 2.16. Schematic of TSB test apparatus showing relevant dimensions for calculating hydraulic conductivity for use with ASTM D6391 (2012).....	42
Figure 2.17. Photo of Campbell Scientific TDR probe (model CS645).....	48
Figure 2.18. Typical TDR probe waveform.....	48
Figure 2.19. Typical TDR verification plot.	49
Figure 2.20. Irrrometer tensiometer (modified from Irrrometer, 2012).	50
Figure 2.21. Flexible-wall permeameter diagram with rising head have falling tail (from ASTM D5084, 2012).	51
Figure 2.22. Hydraulic conductivity values measured using the TSB method and laboratory testing on one-foot block specimens as a function of hydraulic conductivity values measured from SDRI testing (data from Benson et al., 1999).	56
Figure 2.23. Field hydraulic conductivity compared to hydraulic conductivity measured in laboratory on small undisturbed specimens (data from Benson et al., 1999).	58
Figure 3.1. Equipment used for Proctor testing.	64
Figure 3.2. Calibration procedure to determine the volume of the four-inch diameter Proctor mold.	65
Figure 3.3. Two of six Trautwein flexible wall hydraulic conductivity cells used for laboratory hydraulic conductivity testing.	66
Figure 3.4. Trautwein panel boards used for laboratory hydraulic conductivity testing.	66
Figure 3.5. Components of a Trautwein hydraulic conductivity cell used for flexible wall hydraulic conductivity testing.	67
Figure 3.6. Cross section of compacted clay liner test pad constructed at the University of Arkansas Engineering Research Center.....	68

Figure 3.7. (a) Test pad box at the ERC (displaying wooden box, geosynthetic, and soil as part of first lift), and (b) raker structure for the test pad box.....	69
Figure 3.8. (a) Using the tractor to fill a bag with soil from stockpile, (b) filled soil bag being transferred from the tractor to the forklift, (c) soil bag being brought into the ERC using the forklift, (d) soil bag picked up using the forklift to place inside the test pad box, and (e) loose lift of soil in test pad box.....	71
Figure 3.9. (a) Automatic level and (b) rod used to obtain elevations measurements on a compacted lift.....	72
Figure 3.10. (a) Wacker BS700 gasoline powered rammer, (b) manual tamper.	73
Figure 3.11. Unit weight testing locations, in-situ hydraulic conductivity testing locations, and soil sampling locations within Test Pad 1.....	75
Figure 3.12. Unit weight testing locations, in-situ hydraulic conductivity testing locations, and soil sampling locations within Test Pad 2.....	76
Figure 3.13. Unit weight testing locations, in-situ hydraulic conductivity testing locations, instrumentation locations, and anticipated sample locations within Test Pad 3.....	78
Figure 3.14. (a) South wall removed from test pad box for test pad removal, and (b) electric jack being used to break up the soil.....	79
Figure 3.15. Soil being transferred from wheelbarrows to the front bucket of the tractor.	79
Figure 3.16. Augers used for Stage 1 borehole excavation for TSB testing.....	81
Figure 3.17. (a) Weight placed on recently installed casing, and (b) brushes used to roughen permeated surfaces.....	82
Figure 3.18. (a) TSB standpipe apparatus, and (b) TSB testing apparatus.....	84
Figure 3.19. Photo of extended borehole.....	85

Figure 3.20. Inner ring and outer ring used for SDRI testing (photo taken during installation). .	87
Figure 3.21. (a) Trench excavated with claw hammer (b) trench filled with bentonite slurry.	89
Figure 3.22. Inner SDRI ring under water with connected flexible bag.	91
Figure 3.23. Flexible intravenous bag filled with water and being weighted on a balance.	92
Figure 3.24. (a) Soil block cut for TDR probe, (b) TDR probe installed in the test pad.	93
Figure 3.25. (a) Figure of installed tensiometers, and (b) schematic of probe location with nominal depth.	94
Figure 3.26. Drilling a five-inch deep hole.	95
Figure 3.27. (a) Drilling an 11-inch deep hole, and (b) backfilling the annular space with bentonite.	96
Figure 3.28. (a) 3/4-inch diameter bit augered to depth of 12 inches, (b) 3/4-inch diameter bit augered to depth of 16 inches, (c) 1-inch diameter bit augered to depth of 12 inches, (d) boring after using 1-inch diameter bit to a depth of 12 inches, (e) 3/4-inch diameter drill bit attached to 12-inch long extension rod, (f) 3/4-inch diameter drill bit and 12-inch long extension rod augered into the test pad to a depth of approximately 21 inches (as determined by bottom of tape marker being 23-inches), (g) 23-inch deep probe being installed in drilled hole, and (h) vacuum pump applied to tensiometer.	97
Figure 3.29. (a) Shelby tube sampling apparatus pushing the Shelby tube into the soil, (b) retrieved, capped, and labeled of the Shelby tube, and (c) pushed Shelby tubes that have been pushed into and retrieved from the Test Pad.	99
Figure 3.30. Cross-section diagram of Shelby tubes collected from Test Pad 1.	100
Figure 3.31. Shelby tube pushed into Test Pad 2.	101
Figure 3.32. Cross-section diagram of Shelby tubes collected from Test Pad 2.	102

Figure 3.33. (a) Rough column with bucket for a guide, (b) hand carved soil column wrapped in plastic wrap, and (c) soil block wrapped in plastic.....	103
Figure 3.34. Cross-section diagram of hand carved columns collected from Test Pad 1.....	104
Figure 3.35. Cross-section diagram of hand carved columns collected from Test Pad 2.....	104
Figure 3.36. (a) Four-inch diameter soil sample prepared for hydraulic conductivity testing, (b) assembled hydraulic conductivity cell, and (c) six-inch diameter soil sample after hydraulic conductivity testing.....	106
Figure 3.37. (a) Band saw used for cutting Shelby tubes, and (b) 12-ton hydraulic bottle jack apparatus used for extruding samples.....	107
Figure 3.38. (a) Tools for trimming Shelby tube samples, (b) perforated Shelby tube sample...	107
Figure 3.39. (a) Horizontal hydraulic conductivity sample with sides (future ends) cut off, (b) photo of trimming lathe, and (c) trimmed hand carved sample.....	108
Figure 3.40. Photo of No. F-4 Quaker City Grinding Mill used for grinding soil samples.....	109
Figure 3.41. Specific gravity vacuum device.....	109
Figure 3.42. Hydrometer testing (b) spindle mixer used for dispersing hydrometer samples....	110
Figure 3.43. (a.) soil sample soaking in water (b.) photo of soil being washed.	111
Figure 3.44 (a) Soil sample prepped for Atterberg limits testing, and (b) liquid limit device with grooved soil sample.	112
Figure 3.45. Soil sample drying for plastic limit testing.....	112
Figure 4.1. (a) Velocity curve and (b) semilog curve (from Chapuis [1999]).....	122
Figure 4.2. Independently generated velocity curve (using Chapuis [1999] dataset).....	122
Figure 4.3. Comparison plot of corrected hydraulic conductivities from Stage 1 for each method.	125

Figure 4.4. Compaction curves for Standard Proctor, 75-Percent Reduced Proctor, and 50-Percent Reduced Proctor.....	127
Figure 4.5. Vertical hydraulic conductivity data for 50-percent of Standard Energy Sample 3.	128
Figure 4.6. Inflow to outflow data for 50- percent of Standard Energy Sample 3.	128
Figure 4.7. Relationship between hydraulic conductivity and molding moisture content.....	129
Figure 4.8. Relationship between dry unit weight, molding moisture content, and hydraulic conductivity.....	130
Figure 4.9. Zone of acceptance developed using the Daniel and Benson (1990) method.	131
Figure 4.10. Zone of acceptance developed using the APCEC (2007) method.	132
Figure 4.11. Dry unit weight and moisture content test measurements as obtained from nuclear density gauge for Test Pad 1.....	134
Figure 4.12. Dry unit weight and moisture content test measurements as obtained from nuclear density gauge for Test Pad 2.....	135
Figure 4.13. Dry unit weight and moisture content test measurements as obtained from nuclear density gauge for Test Pad 3.....	136
Figure 4.14. Stage 1 apparent hydraulic conductivity data for Test Pad 1.	137
Figure 4.15. Stage 2 apparent hydraulic conductivity data for Test Pad 1.	137
Figure 4.16. Stage 1 apparent hydraulic conductivity data for Test Pad 2.	139
Figure 4.17. Stage 2 apparent hydraulic conductivity data for Test Pad 2.	139
Figure 4.18. SDRI apparent hydraulic conductivity data for Test Pad 3.....	141
Figure 4.19. Soil suction data collected from Test Pad 3.	142
Figure 4.20. TDR data collected from South TRD probe located 14 inches below the soil surface.	143

Figure 4.21. Moving average for TDR data collected from South TRD probe located 14 inches below the soil surface.....	145
Figure 4.22. Moving average for each individual TDR data collected from Test Pad 3.....	146
Figure 4.23. Moving average for TDR data collected from South TRD probe at 2-inch depth.	147
Figure 4.24. Vertical hydraulic conductivity data for SE-ST-TP1 Lift 1-2 Interface.....	149
Figure 4.25. Summary plot of vertical hydraulic conductivity values obtained from the SE-ST-TP1 sample.....	150
Figure 4.26. Summary plot of vertical and horizontal hydraulic conductivity values obtained from W-HC-TP1 and E-HC-TP1 samples.....	151
Figure 4.27. Dry unit weight and moisture content results for SE-ST-TP1 before and after laboratory hydraulic conductivity testing.	152
Figure 4.28. Dry unit weight and moisture content results for HC-TP1 before and after laboratory hydraulic conductivity testing.....	153
Figure 4.29. Summary plot of vertical hydraulic conductivity values as a function of depth as obtained from the CT-ST-TP2 sample.....	155
Figure 4.30. Summary plot of vertical and horizontal hydraulic conductivity values as a function of depth as obtained from HC-TP2 samples.....	156
Figure 4.31. Dry unit weight and moisture content results for CT-ST-TP2 before and after laboratory hydraulic conductivity testing.	157
Figure 4.32. Dry unit weight and moisture content results for HC-TP2 before and after laboratory hydraulic conductivity testing.....	158
Figure 4.33 Hydrometer results from Test Pad 1 Southwest Shelby Tube Lift 1 sample (SW-ST-TP1).....	159

Figure 4.34. Summary of Atterberg limit results from samples obtained from Test Pad 1 Southwest Shelby Tube (SW-ST-TP1).....	159
Figure 4.35. Summary of Atterberg limit results and in-situ moisture content from samples obtained from Test Pad 2 Southwest Shelby Tube (SW-ST-TP2).	160
Figure 4.36. Summary of Atterberg limit results and in-situ moisture content from samples obtained from TSB Test Pad 2 cuttings (SW-TSB-TP2).....	160
Figure 4.37. Comparison between vertical hydraulic conductivity of Shelby tube samples and hand carved samples from Test Pad 1.....	162
Figure 4.38. Comparison between vertical hydraulic conductivity of Shelby tube samples and hand carved samples from Test Pad 2.....	163
Figure 4.39. Comparison between laboratory hydraulic conductivity and two stage field hydraulic conductivity for Test Pad 1.....	164
Figure 4.40. Comparison between laboratory hydraulic conductivity and two stage borehole field hydraulic conductivity for Test Pad 2.....	165
Figure 4.41. TSB vertical hydraulic conductivity from Test Pads 1 and 2 compared to SDRI hydraulic conductivity from Test Pad 3.....	166
Figure 4.42. Comparison between Shelby tube dry unit weight measurements and nuclear density gauge dry unit weight measurements from Test Pads 1 and 2.....	167
Figure 4.43. Comparison between hand carved dry unit weight measurements and nuclear density gauge dry unit weight measurements from Test Pads 1 and 2.	168
Figure 4.44. Comparison between hand carved dry unit weight measurements and Shelby tube dry unit weight measurements from Test Pads 1 and 2.	169

Figure 4.45. Comparison between Shelby tube moisture content measurements and nuclear density gauge moisture content measurements from Test Pads 1 and 2.....	170
Figure 4.46. Comparison between hand carved moisture content measurements and nuclear density gauge moisture content measurements from Test Pads 1 and 2.....	170
Figure 4.47. Comparison between hand carved moisture content measurements and Shelby tube moisture content measurements from Test Pads 1 and 2.....	172
Figure 4.48. Recovered length compared to the pushed length for Shelby tube sample acquisition.	173
Figure 4.49. Comparison between TDR probe gravimetric moisture content measurements and nuclear density gauge moisture content measurements from Test Pad 3.	174
Figure A.1. Vertical hydraulic conductivity data for Standard Energy Sample 1.	195
Figure A.2. Inflow to outflow ratio data for Standard Energy Sample 1.....	195
Figure A.3. Vertical hydraulic conductivity data for Standard Energy Sample 2.	196
Figure A.4. Inflow to outflow ratio data for Standard Energy Sample 2.....	196
Figure A.5. Vertical hydraulic conductivity data for Standard Energy Sample 3.	197
Figure A.6. Inflow to outflow ratio data for Standard Energy Sample 3.....	197
Figure A.7. Vertical hydraulic conductivity data for Standard Energy Sample 4.	198
Figure A.8. Inflow to outflow ratio data for Standard Energy Sample 4.....	198
Figure A.9. Vertical hydraulic conductivity data for Standard Energy Sample 5.	199
Figure A.10. Inflow to outflow ratio data for Standard Energy Sample 5.....	199
Figure A.11. Vertical hydraulic conductivity data for 75-percent of Standard Energy Sample 1.	200
Figure A.12. Inflow to outflow ratio data for 75-percent of Standard Energy Sample 1.	200

Figure A.13. Vertical hydraulic conductivity data for 75-percent of Standard Energy Sample 2.	201
Figure A.14. Inflow to outflow ratio data for 75-percent of Standard Energy Sample 2.	201
Figure A.15. Vertical hydraulic conductivity data for 75-percent of Standard Energy Sample 3.	202
Figure A.16. Inflow to outflow ratio data for 75-percent of Standard Energy Sample 3.	202
Figure A.17. Vertical hydraulic conductivity data for 75-percent of Standard Energy Sample 4.	203
Figure A.18. Inflow to outflow ratio data for 75-percent of Standard Energy Sample 4.	203
Figure A.19. Vertical hydraulic conductivity data for 75-percent of Standard Energy Sample 5.	204
Figure A.20. Inflow to outflow ratio data for 75-percent of Standard Energy Sample 5.	204
Figure A.21. Vertical hydraulic conductivity data for 50-percent of Standard Energy Sample 1.	205
Figure A.22. Inflow to outflow ratio data for 50-percent of Standard Energy Sample 1.	205
Figure A.23. Vertical hydraulic conductivity data for 50-percent of Standard Energy Sample 2.	206
Figure A.24. Inflow to outflow ratio data for 50-percent of Standard Energy Sample 2.	206
Figure A.25. Vertical hydraulic conductivity data for 50-percent of Standard Energy Sample 3 (previously presented as Figure 4.5).	207
Figure A.26. Inflow to outflow ratio data for 50-percent of Standard Energy Sample 3 (previously presented as Figure 4.6).	207

Figure A.27. Vertical hydraulic conductivity data for 50-percent of Standard Energy Sample 4.	208
Figure A.28. Inflow to outflow ratio data for 50-percent Reduced Energy Sample 4.....	208
Figure B.1. TDR data collected from North TRD probe at 2-inch depth.	216
Figure B.2. Moving average for TDR data collected from North TRD probe at 2-inch depth. .	216
Figure B.3. TDR data collected from South TRD probe at 2-inch depth.	217
Figure B.4. Moving average for TDR data collected from South TRD probe at 2-inch depth (previously presented as Figure 4.23).	217
Figure B.5. TDR data collected from North TRD probe at 8-inch depth.	218
Figure B.6. Moving average for TDR data collected from North TRD probe at 8-inch depth. .	218
Figure B.7. TDR data collected from South TRD probe at 8-inch depth.	219
Figure B.8. Moving average for TDR data collected from South TRD probe at 8-inch depth. .	219
Figure B.9. TDR data collected from North TRD probe at 14-inch depth.	220
Figure B.10. Moving average for TDR data collected from North TRD probe at 14-inch depth.	220
Figure B.11. TDR data collected from South TRD probe at 14-inch depth (previously presented as Figure 4.20).	221
Figure B.12. Moving average for TDR data collected from South TRD probe at 14-inch depth (previously presented as Figure 4.21).	221
Figure C.1. Vertical hydraulic conductivity data for SE-ST-TP1 Lift 1.	224
Figure C.2. Inflow to outflow data for SE-ST-TP1 Lift 1.	224
Figure C.3. Vertical hydraulic conductivity data for SE-ST-TP1 Lift 1-2 interface (previously presented as Figure 4.24).	225

Figure C.4. Inflow to outflow data for SE-ST-TP1 Lift 1-2 interface.....	225
Figure C.5. Vertical hydraulic conductivity data for SE-ST-TP1 Lift 2.	226
Figure C.6. Inflow to outflow data for SE-ST-TP1 Lift 2.	226
Figure C.7. Vertical hydraulic conductivity data for SE-ST-TP1 Lift 2-3 interface.....	227
Figure C.8. Inflow to outflow data for SE-ST-TP1 Lift 2-3 interface.....	227
Figure C.9. Vertical hydraulic conductivity data for SE-ST-TP1 Lift 3.	228
Figure C.10. Inflow to outflow data for SE-ST-TP1 Lift 3.	228
Figure C.11. Vertical hydraulic conductivity data for SE-ST-TP1 Lift 3-4 interface.	229
Figure C.12. Inflow to outflow data for SE-ST-TP1 Lift 3-4 interface.....	229
Figure C.13. Vertical hydraulic conductivity data for SE-ST-TP1 Lift 4.	230
Figure C.14. Inflow to outflow data for SE-ST-TP1 Lift 4.	230
Figure C.15. Vertical hydraulic conductivity data for W-HC-TP1 Lift 1.	231
Figure C.16. Inflow to outflow data for W-HC-TP1 Lift 1.	231
Figure C.17. Vertical hydraulic conductivity data for W-HC-TP1 Lift 2.	232
Figure C.18. Inflow to outflow data for W-HC-TP1 Lift 2.	232
Figure C.19. Vertical hydraulic conductivity data for W-HC-TP1 Lift 3.	233
Figure C.20. Inflow to outflow data for W-HC-TP1 Lift 3.	233
Figure C.21. Vertical hydraulic conductivity data for W-HC-TP1 Lift 4.	234
Figure C.22. Inflow to outflow data for W-HC-TP1 Lift 4.	234
Figure C.23. Horizontal hydraulic conductivity data for E-HC-TP1 Lift 1-2 Interface.	235
Figure C.24. Inflow to outflow data for E-HC-TP1 Lift 1-2 Interface.	235
Figure C.25. Horizontal hydraulic conductivity data for E-HC-TP1 Lift 2-3 Interface.	236
Figure C.26. Inflow to outflow data for E-HC-TP1 Lift 2-3 Interface.	236

Figure C.27. Horizontal hydraulic conductivity data for E-HC-TP1 Lift 3-4 Interface.	237
Figure C.28. Inflow to outflow data for E-HC-TP1 Lift 3-4 Interface.	237
Figure C.29. Vertical hydraulic conductivity data for CT-ST-TP1 Lift 1.	240
Figure C.30. Inflow to outflow data for CT-ST-TP2 Lift 1.	240
Figure C.31. Vertical hydraulic conductivity data for CT-ST-TP2 Lift 1-2 interface.	241
Figure C.32. Inflow to outflow data for CT-ST-TP2 Lift 1-2 interface.	241
Figure C.33. Vertical hydraulic conductivity data for CT-ST-TP2 Lift 2.	242
Figure C.34. Inflow to outflow data for CT-ST-TP2 Lift 2.	242
Figure C.35. Vertical hydraulic conductivity data for CT-ST-TP2 Lift 2-3 interface.	243
Figure C.36. Inflow to outflow data for CT-ST-TP2 Lift 2-3 interface.	243
Figure C.37. Vertical hydraulic conductivity data for CT-ST-TP2 Lift 3.	244
Figure C.38. Inflow to outflow data for CT-ST-TP2 Lift 3.	244
Figure C.39. Vertical hydraulic conductivity data for CT-ST-TP2 Lift 3-4 interface.	245
Figure C.40. Inflow to outflow data for CT-ST-TP2 Lift 3-4 interface.	245
Figure C.41. Vertical hydraulic conductivity data for CT-ST-TP2 Lift 4.	246
Figure C.42. Inflow to outflow data for CT-ST-TP2 Lift 4.	246
Figure C.43. Vertical hydraulic conductivity data for W-HC-TP2 Lift 1.	247
Figure C.44. Inflow to outflow data for W-HC-TP2 Lift 1.	247
Figure C.45. Vertical hydraulic conductivity data for W-HC-TP2 Lift 2.	248
Figure C.46. Inflow to outflow data for W-HC-TP2 Lift 2.	248
Figure C.47. Vertical hydraulic conductivity data for W-HC-TP2 Lift 3.	249
Figure C.48. Inflow to outflow data for W-HC-TP2 Lift 3.	249
Figure C.49. Vertical hydraulic conductivity data for W-HC-TP2 Lift 4.	250

Figure C.50. Inflow to outflow data for W-HC-TP2 Lift 4.	250
Figure C.51. Horizontal hydraulic conductivity data for E-HC-TP2 Lift 1-2 Interface.	251
Figure C.52. Inflow to outflow data for E-HC-TP2 Lift 1-2 Interface.	251
Figure C.53. Horizontal hydraulic conductivity data for E-HC-TP2 Lift 2-3 Interface.	252
Figure C.54. Inflow to outflow data for E-HC-TP2 Lift 2-3 Interface.	252
Figure C.55. Horizontal hydraulic conductivity data for E-HC-TP2 Lift 3-4 Interface.	253
Figure C.56. Inflow to outflow data for E-HC-TP2 Lift 3-4 Interface.	253
Figure D.1 Hydrometer results from Test Pad 1 Southwest Shelby Tube Lift 1 sample (SW ST-TP1) [previously presented as Figure 4.33].	255
Figure D.2. Hydrometer results from Test Pad 1 Southwest Shelby Tube Lift 2 sample (SW ST-TP1).....	255
Figure D.3. Hydrometer results from Test Pad 1 Southwest Shelby Tube Lift 3 sample (SW ST-TP1).....	256
Figure D.4. Hydrometer results from Test Pad 1 Southwest Shelby Tube Lift 4 sample (SW ST-TP1).....	256
Figure D.5. Hydrometer results from Test Pad 2 Southwest Shelby Tube Lift 1 sample (SW ST-TP2).....	257
Figure D.6. Hydrometer results from Test Pad 2 Southwest Shelby Tube Lift 2 sample (SW ST-TP2).....	257
Figure D.7. Hydrometer results from Test Pad 2 Southwest Shelby Tube Lift 3 sample (SW ST-TP2).....	258
Figure D.8. Hydrometer results from Test Pad 2 Southwest Shelby Tube Lift 4 sample (SW ST-TP2).....	258

Figure D.9. Hydrometer results for sample from Test Pad 2 TSB borehole (0-2in.) obtained prior to TSB testing.	259
Figure D.10. Hydrometer results for sample from Test Pad 2 TSB borehole (2-4in.) obtained prior to TSB testing.....	259
Figure D.11. Hydrometer results for sample from Test Pad 2 TSB borehole (4-6in.) obtained prior to TSB testing.....	260
Figure D.12. Hydrometer results for sample from Test Pad 2 TSB borehole (6-8in.) obtained prior to TSB testing.....	260
Figure D.13. Hydrometer results for sample from Test Pad 2 TSB borehole (8-10in.) obtained prior to TSB testing.....	261
Figure D.14. Hydrometer results for sample from Test Pad 2 TSB borehole (10-12in.) obtained after Stage 1 of TSB testing.....	261
Figure D.15. Hydrometer results for sample from Test Pad 2 TSB borehole (12-14in.) obtained after Stage 1 of TSB testing.....	262
Figure D.16. Hydrometer results for sample from Test Pad 2 TSB borehole (14-16in.) obtained after Stage 1 of TSB testing.....	262
Figure D.17. Liquid limit results from Test Pad 1 Southwest Shelby Tube Lift 1 sample (SW ST-TP1).....	263
Figure D.18. Liquid limit results from Test Pad 1 Southwest Shelby Tube Lift 2 sample (SW ST-TP1).....	263
Figure D.19. Liquid limit results from Test Pad 1 Southwest Shelby Tube Lift 3 sample (SW ST-TP2).....	264

Figure D.20. Liquid limit results from Test Pad 1 Southwest Shelby Tube Lift 4 sample (SW ST-TP1).....	264
Figure D.21. Liquid limit results from Test Pad 2 Southwest Shelby Tube Lift 1 sample (SW ST-TP2).....	265
Figure D.22. Liquid limit results from Test Pad 2 Southwest Shelby Tube Lift 2 sample (SW ST-TP2).....	265
Figure D.23. Liquid limit results from Test Pad 2 Southwest Shelby Tube Lift 3 sample (SW ST-TP2).....	266
Figure D.24. Liquid limit results from Test Pad 2 Southwest Shelby Tube Lift 4 sample (SW ST-TP2).....	266
Figure D.25. Liquid limit results for sample from Test Pad 2 TSB borehole (0-2in.) obtained prior to TSB testing.....	267
Figure D.26. Liquid limit results for sample from Test Pad 2 TSB borehole (2-4in.) obtained prior to TSB testing.....	267
Figure D.27. Liquid limit results for sample from Test Pad 2 TSB borehole (4-6in.) obtained prior to TSB testing.....	268
Figure D.28. Liquid limit results for sample from Test Pad 2 TSB borehole (6-8in.) obtained prior to TSB testing.....	268
Figure D.29. Liquid limit results for sample from Test Pad 2 TSB borehole (8-10in.) obtained prior to TSB testing.....	269
Figure D.30. Liquid limit results for sample from Test Pad 2 TSB borehole (10-12in.) obtained after Stage 1 of TSB testing.....	269

Figure D.31. Liquid limit results for sample from Test Pad 2 TSB borehole (12-14in.) obtained after Stage 1 of TSB testing.....	270
Figure D.32. Liquid limit results for sample from Test Pad 2 TSB borehole (14-16in.) obtained after Stage 1 of TSB testing.....	270

LIST OF TABLES

Table 2.1. Values of k_2/k_1 as a function of L/D and m (recreated from Soil Testing Engineers, Inc., 1983).....	28
Table 4.1. Summary of the calculated hydraulic conductivities using various solution methods with the ASTM D6391 (2010) dataset.....	118
Table A.1. Summary of Proctor data/initial data for laboratory testing (flexible wall hydraulic conductivity testing) on the Proctor samples.....	193
Table A.2. Summary final data obtained from laboratory testing (flexible wall hydraulic conductivity testing) on the Proctor samples.....	194
Table B.1. Summary of TSB data for Stage 1 conducted on Test Pad 1.....	209
Table B.2. Summary of TSB data for Stage 2 conducted on Test Pad 2.....	211
Table B.3. Summary of TSB data for Stage 1 conducted on Test Pad 2.....	212
Table B.4. Summary of TSB data for Stage 2 conducted on Test Pad 2.....	213
Table B.5. Summary of raw data obtained from SDRI test conducted on Test Pad 3.....	214
Table B.6. Summary of reduced data obtained from SDRI test conducted on Test Pad 3.....	215
Table C.1. Summary of initial data for SE-ST-TP1.....	222
Table C.2. Summary of initial data for W-HC-TP1.....	222
Table C.3. Summary of initial data for E-HC-TP1.....	222
Table C.4. Summary of final data for SE-ST-TP1.....	223
Table C.5. Summary of final data for W-HC-TP1.....	223
Table C.6. Summary of final data for E-HC-TP1.....	223
Table C.7. Summary of initial data for CT-ST-TP2.....	238
Table C.8. Summary of initial data for W-HC-TP2.....	238

Table C.9. Summary of initial data for E-HC-TP2.....	238
Table C.10. Summary of final data for CT-ST-TP2.....	239
Table C.11. Summary of final data for W-HC-TP2.....	239
Table C.12. Summary of final data for E-HC-TP2.....	239
Table D.1. Summary of soil index properties for SW-ST-TP1.....	254
Table D.2. Summary of soil index properties for SW-ST-TP2.....	254
Table D.3. Summary of soil index properties for TSB Test Pad 2 cuttings.....	254

Chapter 1: Introduction

1.1 Background

The importance of soil hydraulic conductivity to the rate of settlement has been known for over a half of century yet little evaluation on the research and application of soil hydraulic conductivity to measured clay liner hydraulic conductivity had been performed. Prior to the late 1980s, previous researchers, for example Lambe (1954), studied the theoretical hydraulic conductivity equations, of that time period, and concluded that the hydraulic conductivity equations have limited practical use and required reevaluation of the terms to determine the hydraulic conductivity of fine-grained soils.

Due to the lack of knowledge about soil hydraulic conductivity in relation to water retention, waste disposal during the same time period was conducted through a practice known as open dumping. During open dumping, waste was disposed on the natural ground surface and then buried with little to no investigation of engineering properties of the subsurface or waste. The method of waste handling changed dramatically in the early 1980's when the U.S. Environmental Protection Agency (EPA) adopted new standards for waste disposal that included an engineered bottom liner and top cap for waste containment. In response to the new landfill liner requirements, compacted clay liners (CCL) were determined to be an effective and economical solution to prevent waste from contaminating the environment. A considerable amount of research has been conducted on the performance of CCLs with respect to hydraulic conductivity and numerous papers have been published on the variance of measured in-situ hydraulic conductivity since the early 1980's. However, more research is needed to be able to effectively apply laboratory obtained measurements to characterize field performance and to assess validity of published papers.

1.2 Significance to the Geotechnical Engineering Community

As populations of cities in the United States continuously increase and older landfills reach maximum capacity, new landfills are required to handle the growing amount of waste. Due to stringent requirements and the lengthy process to obtain a permit for a new landfill, it is imperative that results obtained from laboratory tests accurately mimic the results obtained from field tests and that both tests are conducted quickly while also producing reliable data. Further research, as discussed in this thesis, on laboratory and field testing methods will help to identify ways to provide the required data within a timely manner and with an acceptable reliability.

1.3 Project Overview

Work completed by the author during undergraduate studies included the development of an acceptance criterion that was used during construction of the test pads. Eighteen Proctor tests were conducted using standard energy, 75-percent of standard energy, and 50-percent of standard energy. From these tests, Proctor curves associated with different energy levels were created for the soil being used for construction of the clay liners. After the necessary measurements were collected from the Proctor samples, samples were used for hydraulic conductivity testing to obtain measurements of the hydraulic conductivity for each sample. Data from Proctor curves were then used in conjunction with the corresponding data obtained from hydraulic conductivity testing conducted on each point to develop the acceptance criterion as presented by Daniel and Benson (1990).

Three test pads were constructed in the soils lab at the Engineering Research Center (ERC) at the University of Arkansas. Each two-foot thick compacted clay liner was constructed within a 10-foot by 10-foot wooden box. The inside of the box was lined with plastic to prevent moisture from escaping the sides of the liner. The bottom of the liner had a six-inch thick layer

of gravel to allow for drainage. The gravel was covered with woven geosynthetic to prevent soil migration. The soil was placed in eight-inch thick loose lifts and compacted into four 6-inch lifts using a gas-powered rammer and hand tamper. For quality control, the height of each loose and compacted lift was measured using an automatic level and rod and the compaction (dry unit weight and moisture content) of each lift was verified using a nuclear density gauge. The target unit weight was 96 to 104 pounds per cubic foot and the target moisture content was 20 to 24 percent.

Within Test Pads 1 and 2, two Stage Borehole (TSB) testing was conducted. A borehole was augured in the center of the test pad and the TSB was installed. A temperature effects gauge (TEG) was also installed in the test pad to obtain data to correct for temperature changes in the permeant fluid and volume changes of the testing apparatus. Stage 1 testing was conducted until steady state flow was achieved. The borehole was then advanced beyond the bottom of the casing and Stage 2 testing was conducted until steady state flow was achieved.

Within Test Pad 3, Sealed Double Ring Infiltrometer (SDRI) testing was conducted. A two-foot by two-foot sealed square ring was installed in the center of the test pad. An eight-foot by eight-foot square ring was installed around the inner ring with the inner ring centered within the outer ring. The wetting front movement was monitored using six tensiometers connected to data acquisition equipment and six time domain reflectometry (TDR) probes also connected to the same data acquisition equipment. The tensiometers were installed near the bottom of Lifts 1, 3, and 4 to measure change in soil suction, while the TDR probes were installed near the center of Lifts 2, 3, and 4 to measure change in volumetric moisture content. The TDR probes were used to determine if a change in volumetric moisture content was observed as the wetting front moved through the soil.

Disturbed and undisturbed samples were collected from Test Pads 1 and 2. Disturbed samples were collected at two-inch depth increments from the TSB borehole cuttings of Test Pad 2 during installation of the TSB and during the extension of the borehole for Stage 2. Undisturbed samples were collected from both pads after the in-situ testing was completed. Obtained undisturbed sample included 30-inch long, three-inch diameter Shelby tubes and 10-inch diameter hand-carved soil blocks. Samples were collected and stored at a constant temperature of 15 degrees Celsius in the environmental chamber at Bell Engineering Center (BEC) until commencement of laboratory testing.

Laboratory testing included soil index testing and flexible wall hydraulic conductivity testing. The soil index testing included: specific gravity, hydrometer analysis, percent passing the No. 200 sieve, and Atterberg limits. The data obtained from these tests were used to ensure uniformity of soil with depth and were also used to classify the soil. Shelby tube samples were used to test for the vertical hydraulic conductivity measurements for each lift and of each lift interface. Values of vertical hydraulic conductivity of each lift and values of horizontal hydraulic conductivity of each lift interface were obtained for the hand carved samples.

1.4 Thesis Overview

This document is divided into five chapters. Chapter 1 includes an introduction, a brief description of the research conducted, and this overview of the entire document. Chapter 2 contains a review of current literature on in-situ and laboratory hydraulic conductivity. The literature review includes a method for developing an acceptance criterion for field compaction, a discussion on in-situ and laboratory hydraulic conductivity procedures and instrumentation, and a discussion on various methods for reducing data collected from a TSB test. The methods and materials, used to conduct the research described in this document, are presented in Chapter

3. The procedures that are discussed include: developing a zone of acceptance, construction of the test box to contain the test pads, placement of each test pad constructed, conducting TSB and SDRI tests, and acquiring and testing laboratory samples. Contained in Chapter 4 are the results of the testing performed and discussion about the results. Results include: dry unit weight and moisture content measurements from the placement of test pads, in-situ hydraulic conductivity from TSB and SDRI tests, laboratory hydraulic conductivity from collected soil samples, data collected from tensiometers and time domain reflectometry probes, and soil index test results with the soil classification. Discussion is provided on the variance in measured hydraulic conductivity between the different hydraulic conductivity testing methods and includes comparison between: hand carved laboratory and Shelby tube laboratory, laboratory and field, and TSB and SDRI. Chapter 6 contains conclusions developed from review of literature and the results of the conducted research as well as recommendations for future testing.

Chapter 2: Literature Review

2.1 Introduction

Previous investigators (Benson et al., 1990) conducted research on performing in-situ and/or laboratory hydraulic conductivity tests on compacted clay liners that were constructed using an acceptance criterion based on one or more of the following: moisture content, dry unit weight, hydraulic conductivity, strength, or cracking. Historic and current acceptance criteria are discussed in Section 2.2. Two popular field testing techniques used to determine in-situ hydraulic conductivity and verify the acceptance criterion include the sealed double ring infiltrometer (SDRI) test and the two stage borehole (TSB) test. The SDRI testing methodologies and the TSB testing methodologies are presented in Sections 2.3 and 2.4, respectively. For the data collected from the TSB test, various methods have been proposed to calculate the hydraulic conductivity and are discussed in Section 2.5. To aid in determining the wetting front location as a function of time during the SDRI test, two types of instrumentation are commonly used. This instrumentation includes the use of time domain reflectometry (TDR) probes and tensiometer probes connected to a data acquisition system. The TDR probes are used to measure volumetric moisture content while the tensiometers are used to measure soil suction, as described in Sections 2.6 and 2.7, respectively.

Different states require different means of ensuring placement of soil to fulfill an acceptance criterion. Arkansas, for example, requires that moisture content and dry unit weight acceptance criteria are met and that laboratory hydraulic conductivity measurements be conducted on samples from Shelby tubes that are pushed into the production liner (Arkansas Pollution Control and Ecology Commission, 2007). However Missouri requires that a demonstration test section be constructed and that field obtained moisture content and dry unit

weight measurements meet the acceptance criteria. Furthermore, Missouri requires that field hydraulic conductivity measurements (TSB and/or SDRI) are obtained on the test pad and that laboratory flexible wall hydraulic conductivity measurements (Section 2.8) are obtained on Shelby tube samples collected from the test pad to verify the placement criteria. The size of the soil specimen used for laboratory testing (Section 2.9) and the effective stress applies to the laboratory sample (Section 2.10) are issues that must be addressed due to the problems associated with laboratory and field hydraulic conductivity testing, a comparison of historic laboratory measured hydraulic conductivity values and field measured hydraulic conductivity values is presented in Section 2.11.

2.2 *Acceptance Criterion*

Typically, laboratory testing is conducted on soil available onsite that is being considered for construction use before work begins to determine the ideal soil parameters (dry unit weight, molding moisture content, shear strength, and hydraulic conductivity). Because of the difficulty and extended testing times associated with hydraulic conductivity and strength measurements, moisture content and dry unit weight of the soil (as measured in the field using the nuclear density gauge) are commonly used as a corollary to hydraulic conductivity and strength to ensure the hydraulic conductivity and/or strength of a compacted soil deposit meet regulatory requirements. The acceptance criterion is used to accept or reject a compacted lift based on the results of nuclear density tests as discussed in Section 2.2.1.

The traditional acceptance criteria is commonly a bounded shape or zone based only on laboratory data (dry unit weight and moisture content obtained from Proctor testing) within which field dry unit weight and moisture content data must plot. The extents of this zone, known as a zone of acceptance (ZOA), vary depending on the development technique (95-percent of

standard Proctor maximum dry unit weight plus or minus two to five percent of the optimum moisture content, Arkansas Pollution Control and Ecology Commission [2007], and Daniel and Benson [1990]). The 95-percent criteria ZOA is commonly used for engineering projects where subgrade strength, and not hydraulic conductivity, is a key component in design (e.g. highway subgrade or building foundation). The ZOA is typically bounded on the top by the Proctor curve. The ZOA is bounded on the bottom by a horizontal line drawn at a value of 95 percent of the maximum dry unit weight as obtained from the Standard Proctor test and on the right and left by a range of moisture content, typically plus or minus two to five percent of the optimum moisture content (Figure 2.1).

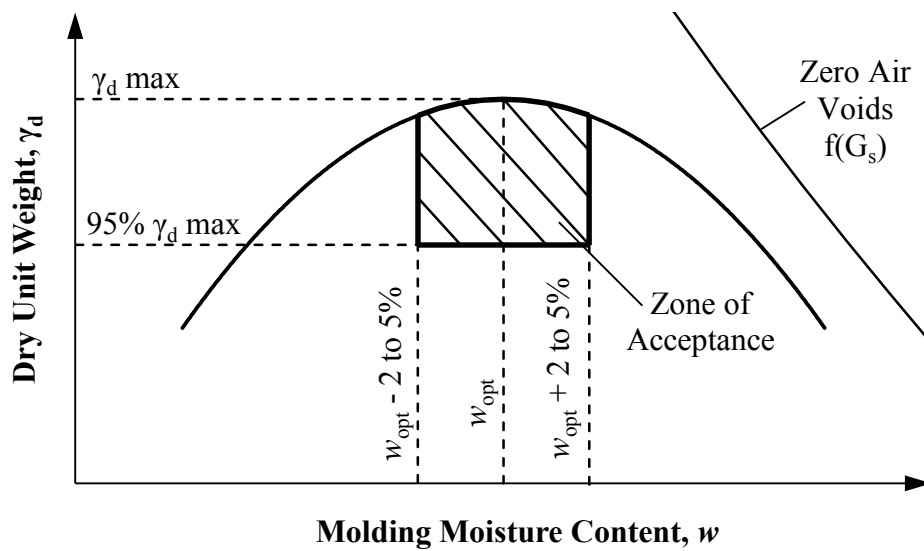


Figure 2.1. Zone of acceptance developed using the 95-percent criterion.

In the state of Arkansas, landfill construction procedures and minimum acceptable standards are outlined in Regulation 22: Solid Waste Management Rules (Arkansas Pollution Control and Ecology Commission [APCEC], 2007). The minimum standards required by the APCEC method include a minimum compaction dry unit weight for an engineered clay liner that is at, or exceeds, 90-percent of maximum dry unit weight as obtained using Standard Proctor energy and a moisture content exceeding the optimum moisture content (Figure 2.2). The

APCEC method (Figure 2.2) does not directly correlate the placement parameters of dry unit weight and moisture content with desired engineering parameters of hydraulic conductivity and/or strength. The minimum standard stated in Regulation 22 is to be used on landfill liners and caps unless an alternate ZOA is demonstrated to have acceptable shear strength and compressibility while meeting the regulated hydraulic conductivity using laboratory testing (APCEC, 2007).

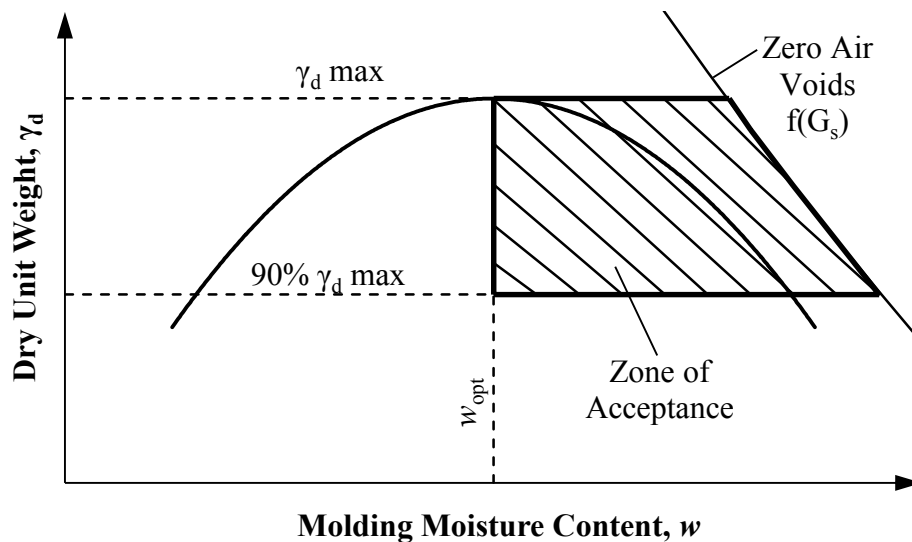


Figure 2.2. Zone of acceptance developed from APCEC criterion.

Daniel and Benson (1990) developed an alternate ZOA that directly correlates the field placement parameters of unit weight and moisture content with both hydraulic conductivity and shear strength of compacted clay liners (CCL) at various levels of compaction energy. In the Daniel and Benson (1990) method (Figure 2.3), three Proctor tests are conducted and the obtained dry unit weight and molding moisture content measurements are used to generate the Proctor curves. The Proctor samples are then used for laboratory hydraulic conductivity testing and an initial ZOA is developed based on the measured hydraulic conductivity of the soil samples being lower than a selected value and shown as open symbols in Figure 2.3. A second ZOA is developed to account for other soil properties such as shear strength or shrink/swell

characteristics. Where the two ZOAs overlap is the overall acceptance criterion or the Daniel and Benson (1990) ZOA. Note that the ZOA is typically bounded on the left by the line of optimums and on the right by the ZAV.

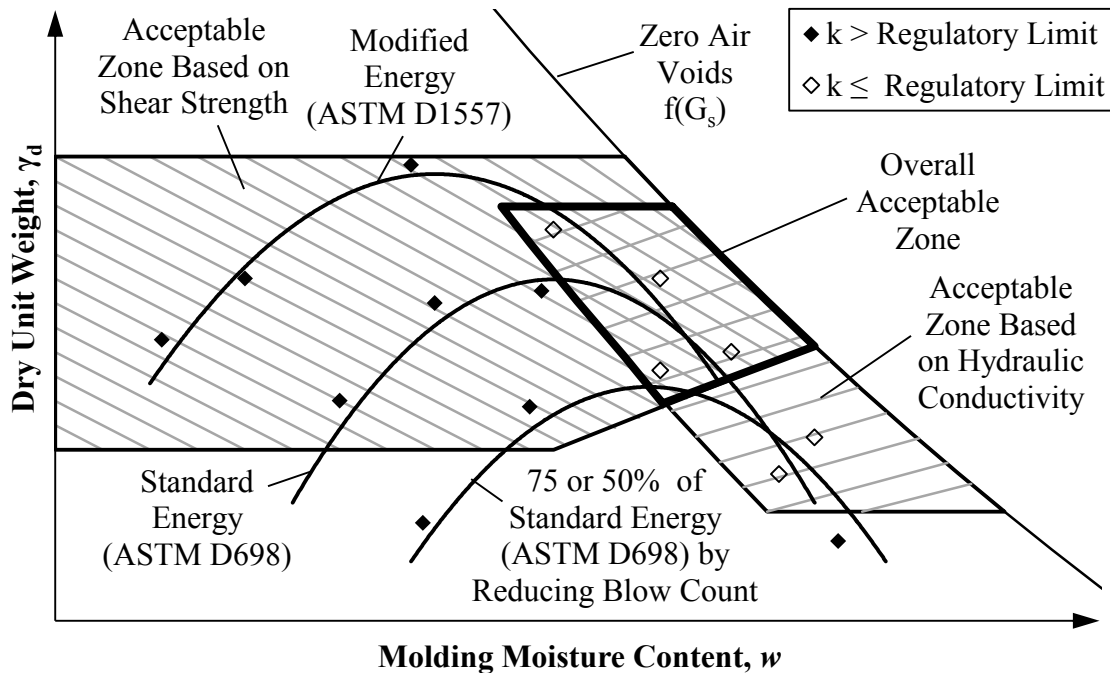


Figure 2.3. Zone of acceptance developed from Daniel and Benson (1990) criterion.

2.2.1 Purpose of Acceptance Criteria

The purpose of acceptance criteria is to ensure proper construction of compacted earthwork. Laboratory testing is used to develop an understanding of the specific material properties including: dry unit weight, moisture content, hydraulic conductivity, and shear strength. However, because of the variations between field and laboratory compaction techniques and the uncontrolled nature of the field environment, a ZOA is developed to ensure that field compaction is within an acceptable criteria based on correlations between hydraulic conductivity /shear strength and unit weight/moisture content. Following construction of the ZOA based on laboratory data, the results of the field density tests typically obtained using a nuclear density gauge are compared to the ZOA to determine if the points plot within the ZOA as shown in

Figure 2.4. Various field density tests and procedures for accepting or reworking failed lifts are presented in detail in Section 2.2.3.

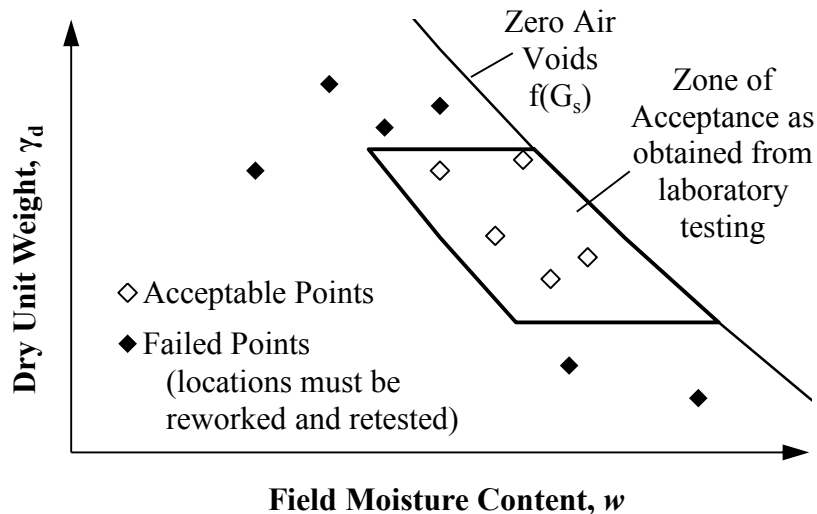


Figure 2.4. Zone of acceptance with acceptable and failed field density points.

2.2.2 Laboratory Testing Associated with Acceptance Criteria

A ZOA using the Daniel and Benson (1990) method is developed by conducting three Proctor tests using different energies. At least five standard Proctor data points and five modified Proctor data points are conducted in accordance with American Society for Testing and Materials (ASTM) D698 (2012) and ASTM D1557 (2012), respectively. Additionally, at least five Proctor data points are conducted in accordance with ASTM D698 (2012) with a deviation to the standard regarding the number of blows applied to each lift during compaction. The number of blows is reduced to 75 percent of the standard Proctor value or 50 percent of the standard Proctor value. Because the Proctor samples will be used for further testing, the moisture content will be measured from trimmings instead of soil from the center of the Proctor samples which is a deviation from ASTM D698 (2012).

Following compaction, each of the compacted samples are tested using a flexible wall permeameter, in accordance with ASTM D5084 (2012), to determine the hydraulic conductivity

of the sample. A moisture content-dry unit weight plot is generated using the data collected from each Proctor test (at least 15 total points). Compacted samples with a measured hydraulic conductivity lower than the specified acceptance criteria (passing) are differentiated from samples with a measured hydraulic conductivity that is higher than the acceptable limit (failing) via the use of symbols as shown previously in Figure 2.3. In cases where the shear strength of the constructed barrier is a design concern, further testing such as unconsolidated undrained triaxial tests or direct simple shear tests may be conducted to determine the shear strength of the soil at various moisture contents and unit weights. The measured shear strength data are then used to further refine the ZOA as shown previously in Figure 2.3.

2.2.3 Field Testing Associated with Acceptance Criteria

Proper placement and compaction of a CCL is verified in the field via the use of in-situ unit weight and moisture content measurements typically obtained using a nuclear density gauge and compared to the zone of acceptance as developed using the laboratory testing discussed in Section 2.2.2. Although the nuclear gauge test is the most common technique, two other methods, the sand cone apparatus and drive tubes, may be used to determine in-situ unit weight and moisture content.

The nuclear density test emits gamma radiation from a Cesium-137 source and the reduction in radiation caused by interaction between the compacted soil and the emitted photons is used to determine the in-situ unit weight. The nuclear density gauge is also used to measure the in-situ gravimetric moisture content of soil using the interaction of neutrons with the hydrogen atoms in water molecules within the soil. The nuclear density test is preferred over the sand cone test because it provides reliable data in a rapid manner and because it causes less disturbance to the testing site.

The sand cone method provides an accurate measurement of in-situ unit weight as the test directly measures the mass of a test sample obtained by weighing the cuttings for a given volume obtained from the sand cone. However, due to high potential for error and given the time requirement (16-24 hours) to measure gravimetric moisture content in accordance with ASTM 2216 (2012), the sand cone test is not typically conducted, but it is instead used to verify the accuracy of a nuclear density gauge for a given soil.

The drive tube test uses a drive tube of known volume that is driven into the soil using a drive tube sampler. After driving, the tube is excavated and the ends of the tube with soil protruding from the drive tube are trimmed to obtain the known volume. Drive tube sampling is preferred over the sand cone test and the nuclear density test because reliable unit weight and moisture content measurements can be obtained and because drive tube sampling has low operation cost. However, the drive tube test creates a hole with a diameter of at least three to four inches within the soil, thereby being not ideal for performance liners.

Following the placement of soil and compaction to create the CCL, field unit weight and moisture results as obtained in the field are plotted on the moisture content-unit weight plot containing the ZOA as previously shown Figure 2.4. If any of the points fall outside of the ZOA and thus are believed to not meet the specified hydraulic conductivity or strength limits, then the lift is either tilled and recompact in place or removed and replaced with different material. Typically, inability to compact soil within the ZOA in the field results from an incorrect molding moisture content or incorrect compaction energy. Once the constructed CCL is deemed acceptable, as per the specified acceptance criteria, than the next lift or next phase of construction is allowed to proceed.

2.3 Sealed Double Ring Infiltrometer Testing

The sealed double ring infiltrometer (SDRI) test (as depicted in the schematic presented in Figure 2.5) was developed by Daniel and Trautwein (1986) to accurately measure the in-situ hydraulic conductivity of hydraulic barriers and other low hydraulic conductivity soils. The SDRI is installed and the test is conducted in accordance with standard testing specifications (ASTM D5093, 2012) or following the specifications outlined by Trautwein Soil Testing Equipment Company (1987). Compared with other in-situ testing techniques (two stage borehole test), test materials are expensive and the installation is time consuming; however, data is easily collected and reliable results are obtained in one to two months (Sai and Anderson, 1990). The SDRI consists of a sealed inner ring and an unsealed outer ring, which is opened to the environment and held at ambient pressure. While either square or cylindrical rings can be used for the SDRI test, square rings are ideal because of easier fabrication and installation (ASTM D5093, 2012). The inner ring usually has a width between two and six feet (Daniel, 1989) and is inserted four to six inches into the soil (Trautwein Soil Testing Equipment Company, 1987). The outer ring is at least one foot larger than the inner ring on either side (ASTM D5093, 2012) and is inserted about 14 to 18 inches into the soil (Trautwein Soil Testing Equipment Company, 1987).

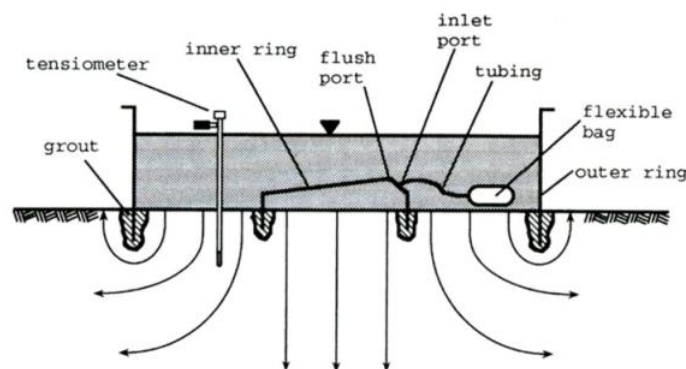


Figure 2.5. Diagram of a sealed double ring infiltrometer (from Trautwein and Boutwell, 1994).

Following the installation of the rings, the outer ring is typically filled with 12 inches of water so that the inner ring is constantly submerged (Trautwein Soil Testing Equipment Company, 1987). The purpose of the outer ring is to provide a constant head across the test area and to direct the flow of water below the inner ring (Trautwein and Boutwell, 1994). Because the outer ring extends further into the soil than the inner ring, water from beneath the inner ring is forced into a one-dimensional vertical flow path (as previously displayed in Figure 2.5). Additionally, no gradient is developed between the water in the inner and outer rings to cause water from the inner ring to flow into the outer ring because of the same head in both rings. According to Daniel (1989), the SDRI test was developed using the following assumptions: the soil is homogenous throughout the entire depth of test area, the soil is fully saturated above the wetting front, flow of the permeant below the inner ring is one-dimensional and vertical, swelling of the soil is accounted for or completed before the final hydraulic conductivity is determined, and the boundary conditions beneath the ring are negligible.

Flow from the inner ring is measured using a flexible bladder (intravenous [IV] bag) connected to the inner ring. The bladder is initially weighed on a balance and is then connected to the inner ring and placed under the water level maintained in the outer ring. The bladder is placed under the water level to ensure that an equivalent hydraulic head (equivalent to the head in the outer) is acting on the soil in both the inner and outer ring (Albrecht and Cartwright, 1989). At predetermined time intervals, the bag is disconnected from the inner ring and weighed. Because the inner ring is rigid and sealed from evaporation effects, any loss of water from the bag is assumed to be associated with water that infiltrated into the soil.

SDRI testing was designed to measure the in-situ hydraulic conductivity of soils with a hydraulic conductivity in the range of 1×10^{-5} to 1×10^{-8} cm/sec (Neupane et al., 2005). A database

containing the in-situ hydraulic conductivities of 85 test sites was presented by Benson et al. (1999). Of these sites, 74 percent were reported as having a hydraulic conductivity lower than 1×10^{-7} cm/sec with four having a hydraulic conductivity lower than 1×10^{-8} cm/sec. Even though majority of the hydraulic conductivities fall within the capable range of the SDRI test, problems in collecting readings may arise when the hydraulic conductivity values are on the order of 1×10^{-8} cm/sec. At these low hydraulic conductivities, it may take 3-6 weeks to collect a single reading and evaporation and temperature affects may contribute to inaccuracies in the reading (Neupane et al., 2005). Additionally, water loss or gain associated with handling the bladder may mask the amount of flow and result in erroneous measurements. In order to collect quick and accurate readings from low hydraulic conductivity SDRI testing, Neupane et al. (2005) developed the constant head board (CHB). The CHB is used in lieu of the flexible bladder to supply water at a assumed constant head (constant head relative to the water level inside the outer ring) to the sealed inner ring. The CHB (Figure 2.6) consists of a capillary tube attached to a board with a grid system. During testing, the board is kept horizontal and floats on the water surface maintained by the outer ring to ensure a constant head over time. The position of the water level on the grid system is easily read and tracked over time to calculate flow of water into the inner ring.

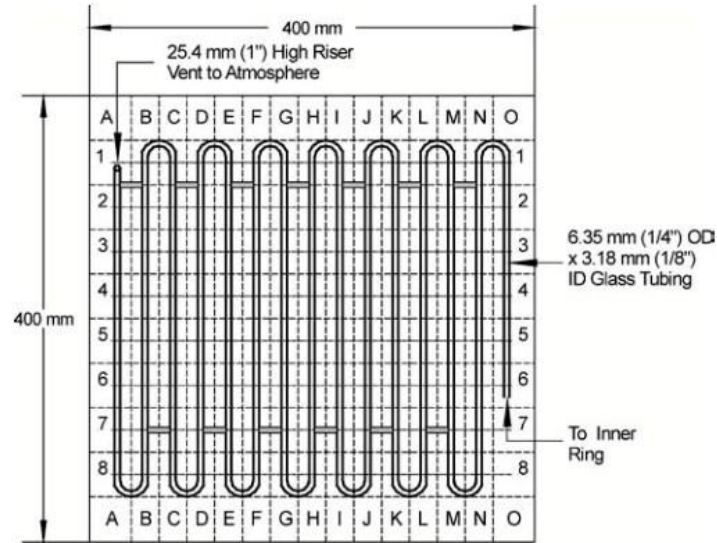


Figure 2.6. Constant head board device (from Neupane et al., 2005).

The equations used for calculating the in-situ hydraulic conductivity from the SDRI test were first proposed by Daniel and Trautwein (1986) and are presented herein as Equation 2.1 and Equation 2.2. These equations were derived from Darcy's Law (Daniel and Trautwein, 1986) and the hydraulic conductivity of the soil (k) is calculated by measuring the infiltration rate (I) and the hydraulic gradient (i). A method for calculating hydraulic gradient was not presented in Daniel and Trautwein (1986); however, a method for hydraulic gradient was presented in Trautwein and Boutwell (1994) and is presented as Equation 2.3 and shown in Figure 2.7. Calculating the hydraulic gradient is more complex due to the unsaturated nature of the soil at the beginning of the test (Trautwein and Boutwell, 1994). Three methods were proposed by Trautwein and Boutwell (1994) to estimate the hydraulic gradient and include: Wetting Front Method (Section 2.3.1), Suction Head Method (Section 2.3.2), and Apparent Hydraulic Conductivity Method (Section 2.3.3).

$$I = \frac{q}{tA} \quad \text{(Daniel and Trautwein, 1986)} \quad \text{Equation 2.1}$$

$$k = \frac{I}{i} F \quad (\text{Daniel and Trautwein, 1986}) \quad \text{Equation 2.2}$$

$$i = \frac{H + Z_w + H_s}{Z_w} \quad (\text{Trautwein and Boutwell, 1994}) \quad \text{Equation 2.3}$$

Where:

I = Infiltration rate

Q = Volume of flow

t = Test time duration

A = Area of infiltration

k = Hydraulic conductivity

i = Hydraulic gradient

F = Correction factor to account for the lateral spreading of water

H = Head of water above the soil surface

H_s = Suction head at location of the wetting front

Z_w = Depth of wetting front below the soil surface

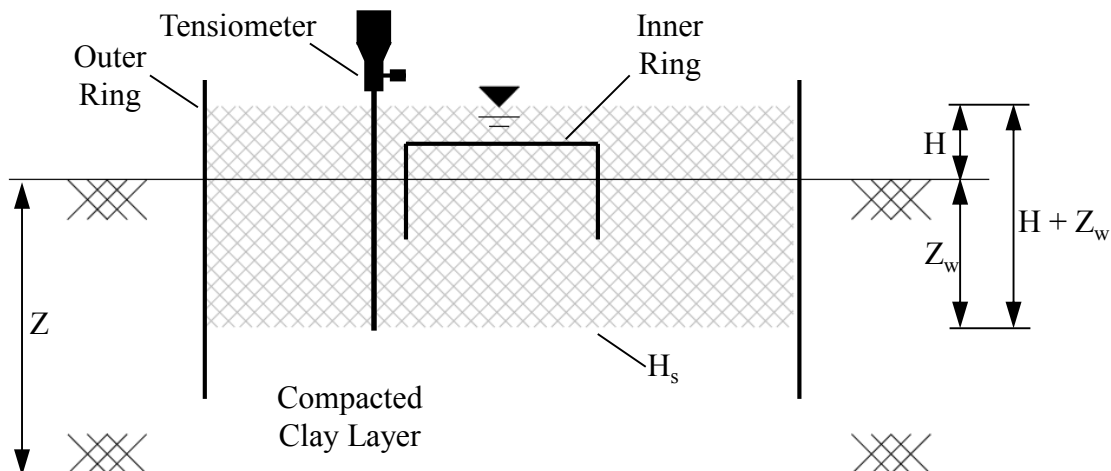


Figure 2.7. Schematic of SDRI test apparatus showing relevant dimensions for calculating hydraulic gradient (recreated from Trautwein and Boutwell, 1994).

2.3.1 Wetting Front Method

The Wetting Front Method (Equation 2.4) assumes that the suction (H_s) at the wetting front is zero because the soil becomes saturated as the water infiltrates the soil body (Trautwein and Boutwell, 1994). Soil suction, and therefore the position of the wetting front, is monitored using tensiometers at various depths. When the wetting front reaches the tensiometers, tension will be lost and the gage reading will drop to zero. As the wetting front moves through the soil, it is possible to calculate and account for the change in infiltration (Trautwein and Boutwell, 1994). While the effects of suction are not fully understood, some suction may still be acting at the wetting front; therefore, the wetting front method is considered conservative and is recommended by Trautwein and Boutwell (1994) for calculating the hydraulic gradient. A schematic of the dimensions used for the wetting front method is presented in Figure 2.8.

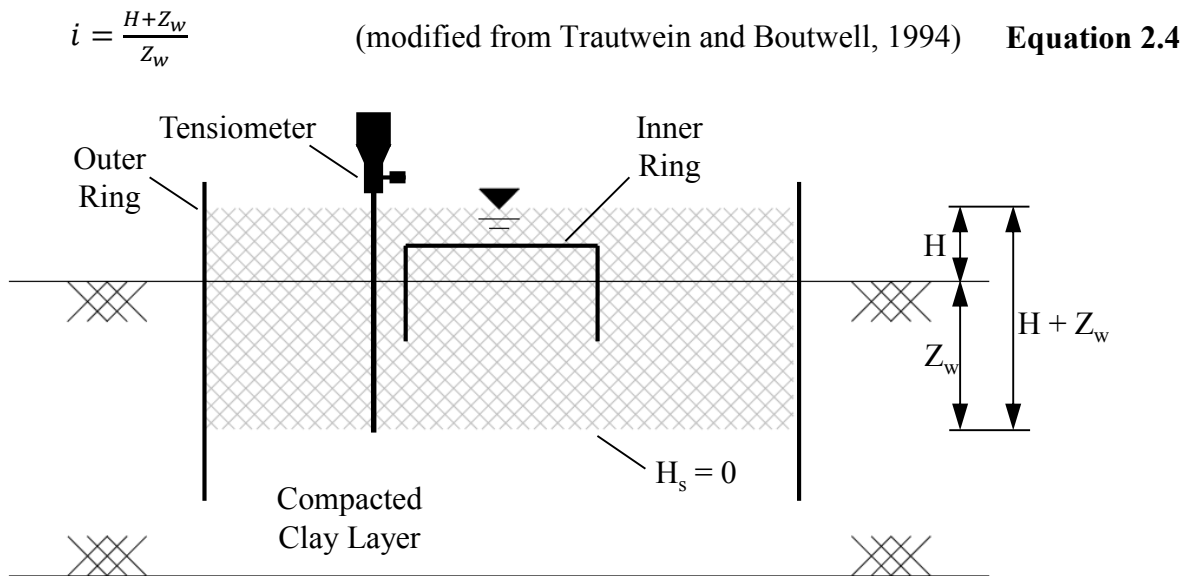


Figure 2.8. Schematic of SDRI test apparatus showing relevant dimensions for wetting front method (modified from Trautwein and Boutwell, 1994).

2.3.2 Suction Head Method

The Suction Head Method (Equation 2.5) assumes that the suction at the wetting front (H_s) is equal to the ambient suction (Trautwein and Boutwell, 1994). However, high ambient suction is typically measured resulting in calculation of high hydraulic gradients and low hydraulic conductivities. Although the suction at the wetting front is not measured, Trautwein and Boutwell (1994) suggest that the suction at the wetting front may be lower than the ambient suction. A moisture characteristic curve and the relationship between saturation and hydraulic conductivity are used to properly account for the effect of suction on infiltration rate. As stated in Trautwein and Boutwell (1994), there is a possibility that the lower hydraulic conductivity of the soil below the wetting front is restricting downward flow and thus preventing the full effects of ambient suction from acting on the sample. A schematic of the dimensions used for the suction head method is presented in Figure 2.9.

$$i = \frac{H + Z_w + H_s}{Z_w} \quad \text{(modified from Trautwein and Boutwell, 1994) \quad \text{Equation 2.5}}$$

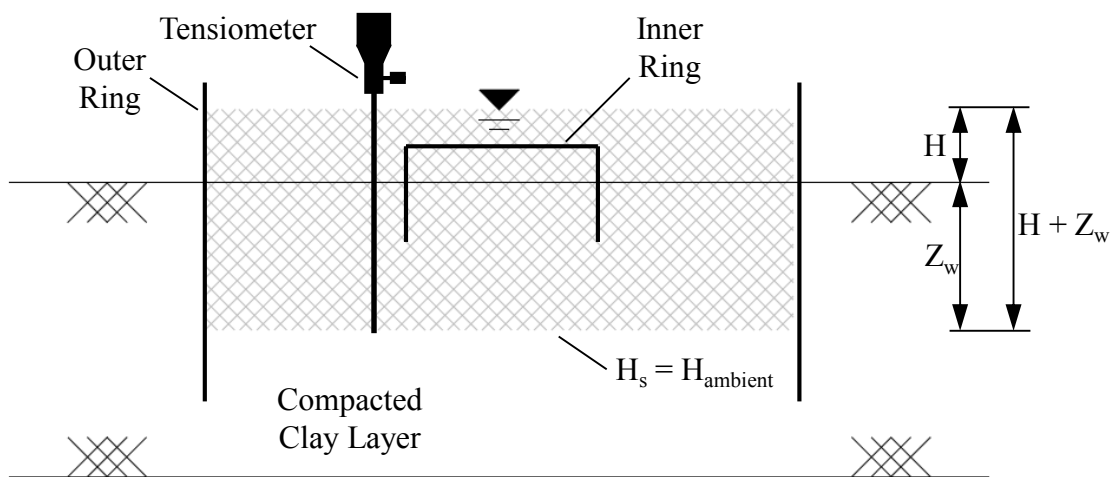


Figure 2.9. Schematic of SDRI test apparatus showing relevant dimensions for suction head method (modified from Trautwein and Boutwell, 1994).

2.3.3 Apparent Hydraulic Conductivity Method

The Apparent Hydraulic Conductivity method (Equation 2.6) is less rigorous both in terms of testing and computation because the wetting front and suction front is not monitored and is therefore unknown (Trautwein and Boutwell, 1994). Calculations are performed by assuming the depth of the wetting front (Z_w) is to equal the depth of the test pad (Z) and that the suction at the wetting front (H_s) equals zero. Because the hydraulic gradient is underestimated until the wetting front passes through the full depth of the test pad, a conservative value of vertical hydraulic conductivity is calculated (Trautwein and Boutwell, 1994). A schematic of the dimensions used for the apparent hydraulic conductivity method is presented in Figure 2.10.

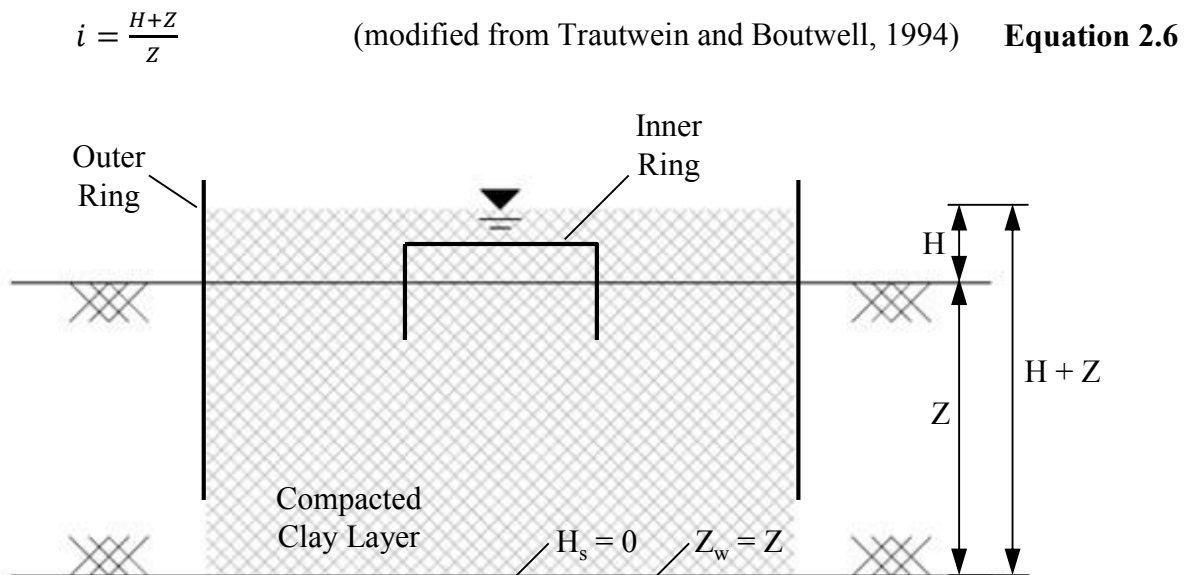


Figure 2.10. Schematic of SDRI test apparatus showing relevant dimensions for apparent hydraulic conductivity method (modified from Trautwein and Boutwell, 1994).

2.4 Two-Stage Borehole Testing

The two stage borehole (TSB) test was developed in 1983 (Soil Testing Engineers, Inc., 1983) by Dr. Gordon Boutwell and is an in-situ hydraulic conductivity test that enables measurement of both vertical hydraulic conductivity and horizontal hydraulic conductivity. As

stated in Trautwein and Boutwell (1994), the TSB test method combines two existing United States Bureau of Reclamation (USBR) test methods, E-18 and E-19 (USBR, 1974). During Stage 1 of the TSB test, a borehole is augered into the soil to the depth of interest and a casing (typically polyvinylchloride [PVC]) with an open bottom and a diameter smaller than the diameter of borehole is inserted into the borehole. To prevent flow around the outside of the casing, the casing is grouted in place using granular bentonite clay placed in lifts and wetted between each lift. During this stage, a falling head test is performed, in which permeant from inside the casing is allowed to flow into the soil and the change in head is measured using a standpipe seated on top of the casing (Figure 2.11). Instead of conducting a falling head test, a constant head test can be conducted by attaching a Mariotte tube to the standpipe as presented in ASTM D6391 (2012) Method C. With this method, a constant head is applied to the soil from the Mariotte tube while the standpipe is used to measure the flow of permeant into the soil.

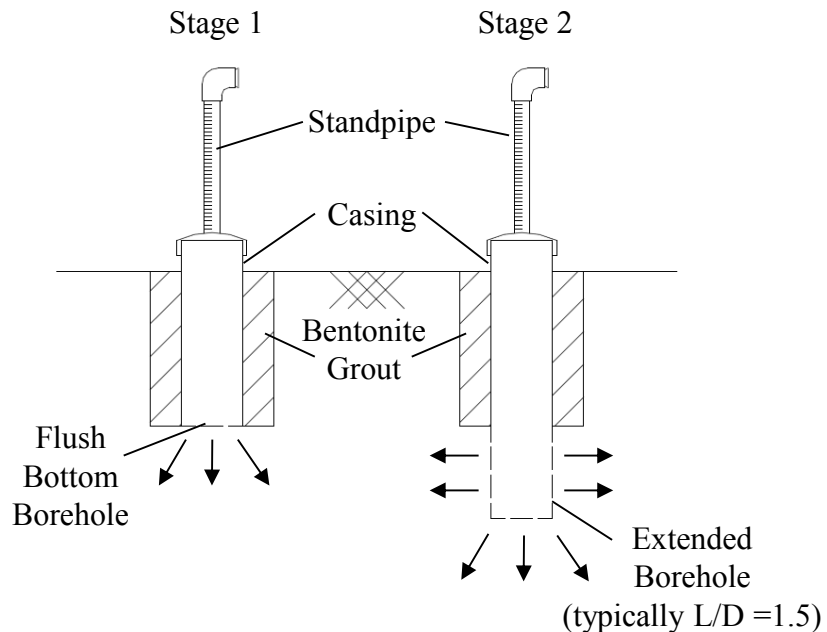


Figure 2.11. Schematic of two stage borehole test for both Stage 1 and Stage 2.

Because of the geometry associated with Stage 1 (flat bottom below the open bottom casing), only vertical flow is measured and flow is continued until the measured apparent hydraulic conductivity reaches a steady state condition (as shown in Figure 2.12). Following completion of Stage 1, an auger is placed through the center of the casing and the bottom of the borehole is advanced to a predetermined depth. Typically the depth of the open borehole below the casing is 1.5 times the inside diameter of the casing. Stage 2 is then conducted and the combined vertical and horizontal flows are measured using the same standpipe mentioned in Stage 1. In a fashion similar to Stage 1, flow in Stage 2 is continued until the apparent hydraulic conductivity readings reach a steady state condition.

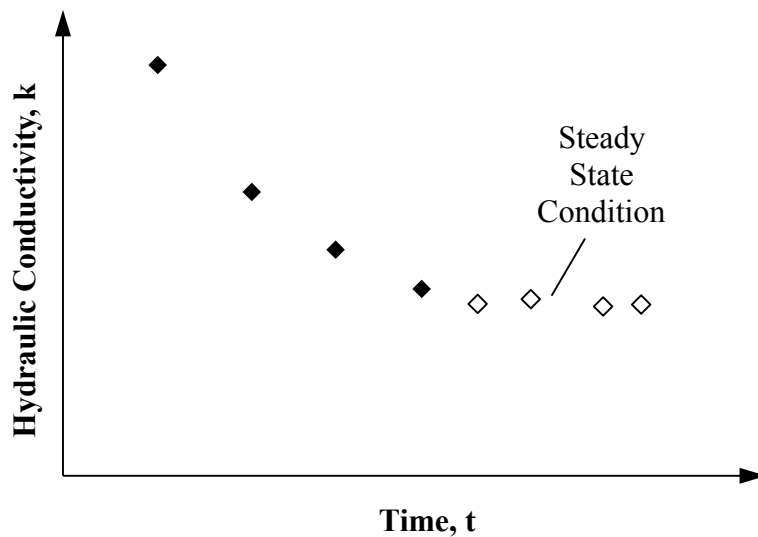


Figure 2.12. Example of steady state condition from a hydraulic conductivity test.

The measured hydraulic conductivity obtained by the TSB test is influenced by several environmental factors. An important factor is the temperature of the permeant and soil during testing (Trautwein and Boutwell, 1994). Specifically, temperature change can affect the viscosity of the permeant fluid and/or induce a volume change in the fluid resulting in a volume change within the TSB device and may also affect the soil fabric. To detect and correct for the variances caused by changes in temperature during testing, a temperature effects gauge (TEG) is installed

to monitor the temperature change of the fluid in the TEG device and to monitor the resulting volume change of the TSB device during the test.

The TEG is installed following the same procedures described for Stage 1 (at the same depth). However, the bottom of the TEG is closed to prevent water from flowing out of the bottom. Therefore any difference in water level in the standpipe is associated with volume changes in the TEG device. Additionally, a thermocouple is installed in the TEG in order to measure the temperature of the test fluid. The closed bottom and thermocouple are the only two differences between the TEG and the TSB devices. All other testing parameters are unaltered between the TEG and TSB in order to ensure compatibility and commonality between the two boreholes. While the temperature effect of the permeant fluid is accounted for, the saturation of the soil below the borehole is not. Furthermore, the wetting front depth is typically unknown during testing and may never become fully saturated.

Three advantages of the TSB testing procedure are the expedited time in which soil hydraulic conductivity values are obtained, the ability to test the hydraulic conductivity of the soil at various depths, and the ability to test the hydraulic conductivity of the soil in both the vertical and horizontal directions. TSB testing is typically completed in ten to twenty days depending on the hydraulic conductivity of the soil (Trautwein and Boutwell, 1994). The quickly obtained results help to shorten the amount of time needed to verify the acceptance criteria on test pads that were constructed using the same construction procedures (e.g. equipment, passes, lift thickness, pad thickness, and acceptance criteria) that will be used for completion of the entire project. The advantage of casing being utilized during the TSB test is that the casing can be installed at various depths to target the center of a compacted lift for vertical hydraulic conductivity and/or lift interfaces for horizontal hydraulic conductivity. Because the test is

inexpensive and tests a small surface area, multiple TSB permeameters (commonly five) are typically conducted at the same time.

The main disadvantage of the TSB testing procedure is the small testing surface area. Because soil clods can range anywhere from 0.5-10 centimeters in diameter, a test diameter of at least 20 centimeters is needed to accurately test the interfaces between soil clods and to account for the pore space in between the soil clods (Trautwein and Boutwell, 1994). The diameter of a TSB borehole is only 10 centimeters which is half of what is recommended. Even with the small test area, the TSB is still acceptable to use within homogeneous clay deposits that are compacted wet of optimum moisture content ensuring good compaction (Sai and Anderson, 1990). To account for the small testing area, it was recommended in Trautwein and Boutwell (1994) that at least five permeameters be utilized at the same time with one common TEG when TSB tests are used to validate a clay liner.

2.5 Calculation of Hydraulic Conductivity for TSB Testing

Hvorslev (1951) introduced the concept of time lag which was observed in wells during pumping. Time lag is defined as the time required to eliminate the difference between the hydrostatic groundwater pressure and the water pressure contained in well (Hvorslev, 1951). Several hidden errors in the original Hvorslev (1951) equation (the time lag response of the soil and the shape correction factor used for the measuring device) resulted in inaccuracies in the hydraulic conductivity measurements. Therefore, Hvorslev (1951) presented several cases of in-situ soil hydraulic conductivity measurements and presented equations for calculating the hydraulic conductivity for the given cases.

As mentioned previously, the TSB testing procedure is a combination of two USBR testing procedures. By completing both testing procedures into the same borehole, two equations

are formed to solve for vertical hydraulic conductivity (k_v) and horizontal hydraulic conductivity (k_h), which are the two unknowns from the Hvorslev (1951) equations. Several authors have presented different methods for calculating the hydraulic conductivity values from TSB data. Soil Testing Engineers, Inc. (1983) presented the original Hvorslev (1951) equations for calculating k_1 and k_2 and presented new equations for calculating k_v and k_h (Section 2.5.1). The Soil Testing Engineers, Inc. (1983) method was presented again in Daniel (1989) with some minor changes (Section 2.5.2). The original Hvorslev (1951) equations were modified for boundary conditions and a new method for calculating k_v and k_h was presented in Boutwell (1992) as discussed in Section 2.5.3. Other methods by Boutwell and Tsai (1992), Trautwein and Boutwell (1994), and ASTM D6391 (2012) Method A that are similar to Boutwell (1992) are discussed in Sections 2.5.4, 2.5.5, and 2.5.6, respectively.

Chapuis (1999) did not agree with the time lag approach for hydraulic conductivity. Additionally, Chapuis (1999) argued that Boutwell and Tsai (1992) implied that the top of the clay layer is an impermeable boundary and that the assumed ellipsoid flow shape is inaccurate for the geometry of the TSB permeameter. Chapuis (1999) also claimed that the anisotropy value used to obtain the hydraulic conductivity cannot be determined and therefore presented a velocity based method for calculation of hydraulic conductivity. Chiasson (2005) agrees with the use of the velocity method but notices that as the measured apparent hydraulic conductivity becomes lower, the scatter in the data becomes larger. To correct for the scatter, the Chiasson (2005) proposed the Z-t method to solve for the tested value of apparent hydraulic conductivity for soil with low hydraulic conductivity. The Chapuis (1999) and the Chiasson (2005) methods are discussed in more detail in Sections 2.5.7 and 2.5.8, respectively. Additionally, ASTM D6391 (2012) Method B, which is similar to the Chiasson (2005) method, is presented in Section

2.5.9. An evaluation of all the presented methods including the method that is proposed to be used (ASTM D6391 [2012] with Daniel [1989]) is discussed in Section 3.2.

2.5.1 *Soil Testing Engineers, Inc. (1983) Method*

The time lag equations used to calculate hydraulic conductivity based on data obtained from the TSB test originated in Hvorslev (1951) and were first presented in Soil Testing Engineers, Inc. [STEI] (1983). Case “C” (Equation 2.7) obtained from Hvorslev (1951) was used to calculate a value for the apparent hydraulic conductivity for Stage 1 (k_1) and Case “G” (Equation 2.8) obtained from Hvorslev (1951) was used to calculate a value for the apparent hydraulic conductivity for Stage 2 (k_2). A correction factor (F), which is a function of the extension length (L) to diameter (D) ratio, was added by STEI (1983) to account for the divergence between the Case “C” and Case “G” equations, and the anisotropy term (m) was removed from this equation to calculate a value for the apparent hydraulic conductivity for Stage 2 (Equation 2.9). The definition of F is presented in Equation 2.10. In order to solve for m , Soil Testing Engineers, Inc. (1983) presented an equation for calculating the k_2/k_1 ratio as a function of m and the L/D ratio (Equation 2.11). This equation was then used to generate Table 2.1 to estimate m based on the L/D ratio as a function of the k_2/k_1 ratio.

$$k_m = \frac{\pi d^2}{11D(t_2 - t_1)} \ln \frac{H_1}{H_2} \quad (\text{Hvorslev, 1951}) \quad \text{Equation 2.7}$$

$$k_h = \frac{d^2 \ln \left[\frac{mL}{D} + \sqrt{1 + \left(\frac{mL}{D} \right)^2} \right]}{8L(t_2 - t_1)} \ln \frac{H_1}{H_2} \quad (\text{Hvorslev, 1951}) \quad \text{Equation 2.8}$$

$$k_2 = \frac{1}{F} \left[\frac{\ln \frac{L}{D} + \sqrt{1 + \left(\frac{L}{D} \right)^2}}{\left(\frac{L}{D} \right)} \right] \left[\frac{d^2}{8D} * \frac{\ln \frac{H_1}{H_2}}{t_2 - t_1} \right] \quad (\text{Soil Testing Engineers, Inc., 1983}) \quad \text{Equation 2.9}$$

$$F = 1 - 0.5623e^{-1.566L/D} \quad (\text{Soil Testing Engineers, Inc., 1983}) \quad \text{Equation 2.10}$$

$$\frac{k_2}{k_1} = m \frac{\ln\left[\frac{L}{D} + \sqrt{1 + \left(\frac{L}{D}\right)^2}\right]}{\ln\left[\frac{mL}{D} + \sqrt{1 + \left(\frac{mL}{D}\right)^2}\right]} \quad (\text{Soil Testing Engineers, Inc., 1983}) \quad \text{Equation 2.11}$$

Where: k = Hydraulic conductivity

t_1 = Initial time

t_2 = Final head

H_1 = Initial head at initial time (t_1)

H_2 = Final head at final time (t_2)

d = Internal diameter of standpipe

m = Anisotropy value

D = Effective diameter (casing internal diameter or outer diameter)

L = Length of Stage 2 excavation below casing

Table 2.1. Values of k_2/k_1 as a function of L/D and m (recreated from Soil Testing Engineers, Inc., 1983)

L/D	g(m) k_2/k_1					
	m = 1	m = 2	m = 3	m = 4	m = 6	m = 10
1.00	1.00	1.22	1.45	1.69	2.13	2.95
1.25	1.00	1.27	1.55	1.81	2.32	3.25
1.50	1.00	1.31	1.62	1.92	2.48	3.51
1.75	1.00	1.35	1.69	2.01	2.61	3.73
2.00	1.00	1.38	1.74	2.08	2.72	3.91
2.50	1.00	1.42	1.82	2.20	2.90	4.21
3.00	1.00	1.46	1.89	2.29	3.04	4.44

The vertical and horizontal hydraulic conductivities (k_v and k_h , respectively) are solved for as a function of either k_1 or k_2 . Equation 2.12 and Equation 2.13 are used to solve for k_h and k_v , respectively as a function of k_1 . Equation 2.14 and Equation 2.15 are used to solve for k_h and k_v , respectively as a function of k_2 .

$$k_h = mk_1 \quad (\text{Soil Testing Engineers, Inc., 1983}) \quad \text{Equation 2.12}$$

$$k_v = \frac{1}{m} k_1 \quad (\text{Soil Testing Engineers, Inc., 1983}) \quad \text{Equation 2.13}$$

$$k_h = k_2 \frac{\ln\left[\frac{mL}{D} + \sqrt{1 + \left(\frac{mL}{D}\right)^2}\right]}{\ln\left[\frac{L}{D} + \sqrt{1 + \left(\frac{L}{D}\right)^2}\right]} \quad (\text{Soil Testing Engineers, Inc., 1983}) \quad \text{Equation 2.14}$$

$$k_v = \frac{1}{m^2} k_h \quad (\text{Soil Testing Engineers, Inc., 1983}) \quad \text{Equation 2.15}$$

The major issues with the equations presented by Soil Testing Engineers, Inc. (1983) are: the definition of the height of head, not correcting for the temperature during testing (permeant density), and not using a TEG to correct for temperature effects (volume change and viscosity). The height of the head is defined as the water level in the standpipe to the depth of the groundwater table; however, the definition does not account for a permeable base as the bottom of a clay stratum (i.e. permeable base under a test pad). The final calculated hydraulic conductivity is not corrected from test temperature to a standard temperature of 20 degrees Celsius with the R_T correction factor as found in ASTM D5084 (2012). Additionally, the temperature of the test water (and corresponding change in viscosity) and volume change effects are not monitored with a TEG. Therefore, change in environmental temperature may affect the measured hydraulic conductivity.

2.5.2 Daniel (1989) Method

The Daniel (1989) method uses the same equations presented in Soil Testing Engineers, Inc. (1983) with simplified terminologies. The hydraulic conductivity for Stage 1 (k_1) is calculated using Equation 2.16 which is the same equation as shown previous as Equation 2.7 as used by Soil Testing Engineers, Inc. (1983). The hydraulic conductivity for Stage 2 (k_2) is calculated using Equation 2.17 and the simplified A and B terms (Equation 2.18 and Equation

2.19, respectively). The A term is the top half of the quotient presented in Equation 2.8 whereas the B term is the bottom half of the quotient presented in Equation 2.8 multiplied by the correction factor (F) similar to the equation presented previously as Equation 2.10. The height and diameter terms used in the equations correspond to those defined in Figure 2.13 (previously presented). The value of m is calculated in a similar fashion to that of Soil Testing Engineers, Inc. (1983); however instead of obtaining the value of m from a table, the value is obtained from a graph (Figure 2.14). The figure was created by plotting values of the k_2/k_1 ratio and m for $L/D = 1.0, 1.5,$ and 2.0 using the previously presented Equation 2.11. As with the STEI method, the m value is then used in Equation 2.12 and Equation 2.13 (as previously presented) to calculate the horizontal hydraulic conductivity and vertical hydraulic conductivity, respectively, with respect to k_1 .

$$k_1 = \frac{\pi d^2}{11D(t_2 - t_1)} \ln \left(\frac{H_1}{H_2} \right) \quad (\text{Daniel, 1989}) \quad \text{Equation 2.16}$$

$$k_2 = \frac{A}{B} \ln \left(\frac{H_1}{H_2} \right) \quad (\text{Daniel, 1989}) \quad \text{Equation 2.17}$$

$$A = d^2 \left\{ \ln \left[\frac{L}{D} + \sqrt{1 + \left(\frac{L}{D} \right)^2} \right] \right\} \quad (\text{Daniel, 1989}) \quad \text{Equation 2.18}$$

$$B = 8D \frac{L}{D} (t_2 - t_1) \left\{ 1 - 0.562 \exp \left[-1.57 \left(\frac{L}{D} \right) \right] \right\} \quad (\text{Daniel, 1989}) \quad \text{Equation 2.19}$$

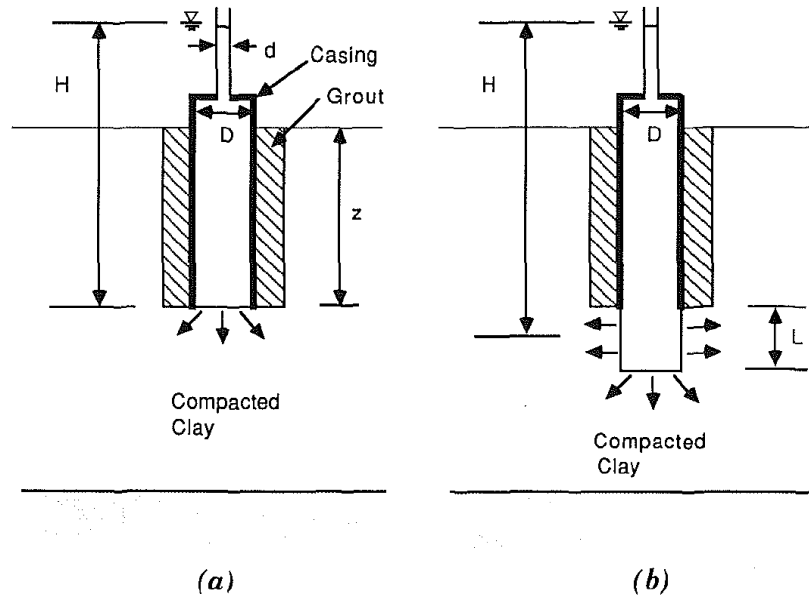


Figure 2.13. Diagram of two-stage in situ hydraulic conductivity test with Boutwell permeameter (a) Stage I (b) Stage II (from Daniel, 1989).

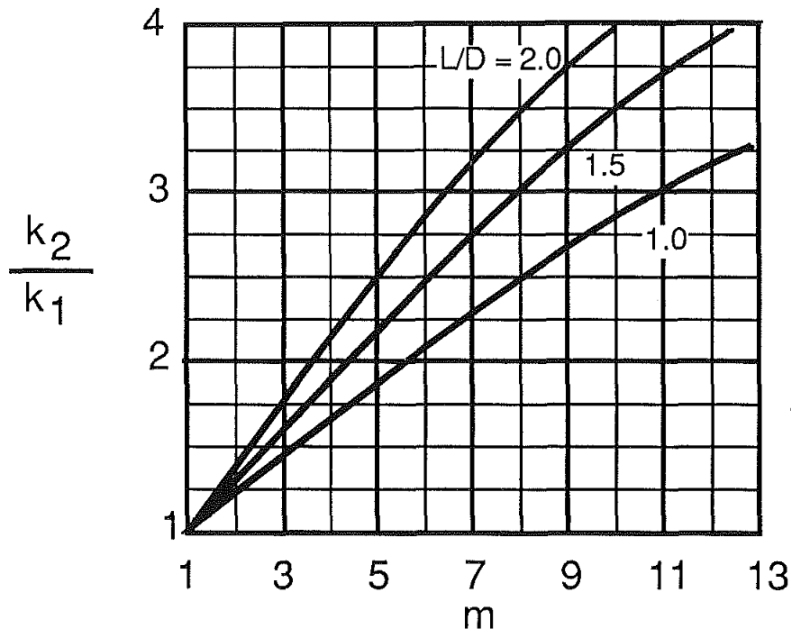


Figure 2.14. Curves of k_2/k_1 and m for $L/D = 1.0, 1.5,$ and 2.0 (from Daniel, 1989).

An issue with the Daniel (1989) method is that the head is defined as the water level in the standpipe to the depth of the bottom of the TSB casing for Stage 1 or to the depth of the TSB casing plus half of the length of the extension borehole for Stage 2. These head definitions do not

account for the location of the water table or the depth of the compacted clay stratum. Additionally, as with the Soil Testing Engineers, Inc. (1983) procedure, the temperature effects of the permeant are not taken into account in the Daniel (1989) method. Neither an R_T correction factor to address a change in viscosity in the liquid due to a temperature change or the use of a TEG to monitor the shrink and swell (volume change) of the permeameter are suggested by the Daniel (1989) method.

2.5.3 *Boutwell (1992) Method*

New time lag equations for calculating the hydraulic conductivity specific to a TSB test were presented in Boutwell (1992). The equations are still based off the original Hvorslev (1951) equations. However, the equations are further modified to include the viscosity correction factor as a function of temperature (R_T) and the geometric constant (G) that corresponds to the test geometry (including the depth to a freely draining surface). The new equation that can be utilized for both stages is presented in Equation 2.20. The viscosity correction factor as a function of temperature is calculated using Equation 2.21. The test geometry constant for Stage 1 (G_1) for the TSB test is calculated using Equation 2.22. The test geometry constant for Stage 2 (G_2) of the TSB test is calculated using Equation 2.23, which assumes no smearing of the test surface, or Equation 2.24, which accounts for smearing of the test surface. To prevent confusion with like terms, the smear zone thickness term T was changed to Z .

$$k = \frac{R_T G \ln\left(\frac{H_1}{H_2'}\right)}{(t_2 - t_1)} \quad (\text{Boutwell, 1992}) \quad \text{Equation 2.20}$$

$$R_T = \frac{2.2902 * (0.9842^T)}{T^{0.1702}} \quad (\text{ASTM D5084, 2012}) \quad \text{Equation 2.21}$$

$$G_1 = \left(\frac{\pi d^2}{11D_1}\right) \left[1 + a \left(\frac{D_1}{4b_1}\right)\right] \quad (\text{Boutwell, 1992}) \quad \text{Equation 2.22}$$

$$G2 = \left(\frac{d^2}{16Lf}\right) \{\ln[u(1, r_0, 0)] + a \ln[u(1, r_0, 2b_2)]\} \quad (\text{Boutwell, 1992}) \quad \text{Equation 2.23}$$

$$G2S = \left(\frac{d^2}{16Lf m^2}\right) \left\{ \ln[u(m, r_0 + Z, 0)] + a \ln[u(m, r_0, 2b_2)] + p \ln \left[\frac{u(m, r_0, 0)}{u(m, r_0 + Z, 0)} \right] \right\} \quad (\text{Boutwell, 1992}) \quad \text{Equation 2.24}$$

Where: k = Hydraulic conductivity

R_T = Viscosity correction factor (corrected to water as 20°C)

t_1 = Initial time

t_2 = Final time

H_1 = Initial head at initial time (t_1)

H_2 = Final head at final time (t_2)

H_2' = Corrected final head at final time (t_2), [H_2 -c]

c = Change in TEG between t_1 and t_2 with increase in height as positive

T = Average test temperature during test duration [$(T_1+T_2)/2$]

d = Internal diameter of standpipe

D_1 = Effective diameter of Stage 1 (casing internal diameter or outer diameter)

b_1 = Thickness of tested soil below casing

a = +1 for impermeable base at b_1

0 for infinite thickness of tested soil

-1 for permeable base at b_1

$f = 1 - 0.5623 \cdot \text{Exp}(-1.566 \cdot L/D_2)$

L = Length of Stage 2 extension below casing

$$u(1, r_0, 0) = \left[\frac{L}{D_2} + \sqrt{1 + \left(\frac{L}{D_2}\right)^2} \right]^2$$

$$u(1,r_0,2b_2) = \frac{\frac{4b_2+L}{D_2} + \sqrt{1 + \left(\frac{4b_2+L}{D_2}\right)^2}}{\frac{4b_2-L}{D_2} + \sqrt{1 + \left(\frac{4b_2-L}{D_2}\right)^2}}$$

$$u(m,r_0,0) = \left[\frac{mL}{D_2} + \sqrt{1 + \left(\frac{mL}{D_2}\right)^2} \right]^2$$

$$u(m,r_0,2b_2) = \frac{\frac{4mb_2+mL}{D_2} + \sqrt{1 + \left(\frac{4mb_2+mL}{D_2}\right)^2}}{\frac{4mb_2-mL}{D_2} + \sqrt{1 + \left(\frac{4mb_2-mL}{D_2}\right)^2}}$$

$$u(m,r_0+Z,0) = \left[\frac{mL}{D_2+2Z} + \sqrt{1 + \left(\frac{mL}{D_2+2Z}\right)^2} \right]^2$$

m = Anisotropy value

D_2 = Diameter of Stage 2 extension

b_2 = Distance from center of Stage 2 extension to base ($b_1 - L/2$)

p = Smear ratio (if any) [k_h/k_s]

k_s = Hydraulic conductivity of smeared zone

Z = Thickness of smeared zone

To prevent confusion of terms, the “Z” term defined as the thickness of the smeared zone is originally “T” in literature. The term was changed to “Z” in this document to prevent confusion with the “T” for average test temperature during test duration.

To solve for k_1 or k_2 , the $G1$ or $G2$ value, respectively, are used in Equation 2.20. The effective diameter of the casing (D_1) is the inner diameter of the casing unless water seeped under the casing during installation of the casing or during hydration of the bentonite, then D_1 is the outer diameter of the casing. The height of the head is defined as the water level in the standpipe to the location of the groundwater level. The depth to the groundwater level is limited

to (maximum value of) twenty times the internal diameter of the casing below the casing. The final corrected head (H_2') is found by taking the final head (H_2) and subtracting the change in head obtained from the TEG.

A new term, k' , is presented in Boutwell (1992) which is used to represent the arithmetic time weighted average for the hydraulic conductivity over the steady state condition. The term k' is calculated using Equation 2.25.

$$k'_j = \frac{\sum k_{j,i} T_i}{\sum T_i} \quad (\text{Boutwell, 1992}) \quad \text{Equation 2.25}$$

Where: k'_j = Arithmetic time-weighted average

j = 1 for Stage 1 or 2 for Stage 2

i = Time increment number

T_i = Duration of time increment i

A new method for calculating m is also presented in Boutwell (1992). The new method is based on the definition of m presented herein as Equation 2.26 as defined by Hvorslev (1951) and Boutwell (1992). The term m is applied to the geometric constants ($G1$ and $G2$) to yield $G1_m$ (Equation 2.27) and $G2_m$ (or $G2S$ as previously mentioned and defined as Equation 2.24). The vertical hydraulic conductivity value is obtained with respect to either k_1' or k_2' using Equation 2.28 or Equation 2.29; however, the use of these two equations yields an indeterminate solution because there are two equations with four unknowns. Equation 2.28 and Equation 2.29 are combined to yield one equation (Equation 2.30) with one unknown. Because the k_2/k_1 ratio, $G1$, and $G2$ are known, there is only one solution for m that will satisfy Equation 2.30. The value of m is solved for by using a trial and error approach.

$$m = \sqrt{\frac{k_h}{k_v}} \quad (\text{Hvorslev, 1951 and Boutwell, 1992}) \quad \text{Equation 2.26}$$

$$G1_m = \left(\frac{\pi d^2}{11mD_1} \right) \left[1 + a \left(\frac{D_1}{4mb_1} \right) \right] \quad (\text{Boutwell, 1992}) \quad \text{Equation 2.27}$$

$$k_v = k'_1 \left(\frac{G1_m}{G_1} \right) \quad (\text{Boutwell, 1992}) \quad \text{Equation 2.28}$$

$$k_v = k'_2 \left(\frac{G2_m}{G2} \right) \quad (\text{Boutwell, 1992}) \quad \text{Equation 2.29}$$

$$\frac{k'_2}{k'_1} = \left(\frac{G1_m}{G_1} \right) \left(\frac{G2}{G2_m} \right) \quad (\text{Boutwell, 1992}) \quad \text{Equation 2.30}$$

2.5.4 *Boutwell and Tsai (1992) Method*

The Boutwell and Tsai (1992) method uses the same equations presented in Boutwell (1992); however, several typographical mistakes were presented and the terminologies for calculating the geometric constants were simplified. All of the terminologies presented in Boutwell and Tsai (1992) are defined the same as in Boutwell (1992) except where noted below.

One of the typographical mistakes presented is contained in the equation used to calculate the value of hydraulic conductivity (Equation 2.31). The error is time difference is typically calculated by subtracting the initial time from the final time ($t_2 - t_1$). Instead, as shown in Equation 2.31, the time difference was presented as a time ratio (t_2/t_1). Not only does this discrepancy cause an error in calculation of hydraulic conductivity, it also causes an error in the dimensional analysis. Because the final time is divided by the initial time, the units of time will cancel and the calculated hydraulic conductivity will be represented in units of length which is incorrect.

$$k_v = \frac{R_T G \ln \left(\frac{H_1}{H_2} \right)}{\frac{t_2}{t_1}} \quad (\text{Boutwell and Tsai, 1992}) \quad \text{Equation 2.31}$$

Instead of presenting separate equations for calculating $G1$ and $G1_m$ and $G2$ and $G2_m$ ($G2S$), one equation was presented for both $G1(m)$ and $G2(m)$. Similar to Boutwell (1992), k_1

and k_2 are solved for using $G1(1)$ and $G2(1)$, respectively. The aforementioned Equation 2.27 is used to solve for the $G1(1)$ term assuming $m = 1$. Equation 2.32, which is similar to Equation 2.24, is used to solve for the $G2(1)$ term noting the addition of the simplified U term. The U terms in Boutwell and Tsai (1992) replaced the u terms in Boutwell (1992). However, an error was made in the simplification when the squared function was removed from U_1 and U_3 . To account for the removal of the squared function, the $\ln(U_1)$ was multiplied by two; however, the $p\ln(U_3)$ term should have also been multiplied by two (Equation 2.33) but was not. With proper procedure (ensuring no smearing of the borehole extension), this error is insignificant because then $U_3 = 1$ resulting in $p\ln(U_3) = 0$ when no smear is present.

$$G2(m) = \left(\frac{d^2}{16Lfm^2}\right) [2 \ln(U_1) + a \ln(U_2) + p \ln(U_3)] \quad \text{Equation 2.32} \quad (\text{Boutwell and Tsai, 1992})$$

$$G2(m) = \left(\frac{d^2}{16Lfm^2}\right) [2 \ln(U_1) + a \ln(U_2) + 2p \ln(U_3)] \quad \text{Equation 2.33} \quad (\text{modified from Boutwell and Tsai, 1992})$$

Where:
$$U_1 = \frac{mL}{D+2T} + \left[1 + \left(\frac{mL}{D+2T}\right)^2\right]^{1/2}$$

$$U_2 = \frac{\frac{4mb_2}{D} + \frac{mL}{D} + \left[1 + \left(\frac{4mb_2}{D} + \frac{mL}{D}\right)^2\right]^{1/2}}{\frac{4mb_2}{D} - \frac{mL}{D} + \left[1 + \left(\frac{4mb_2}{D} - \frac{mL}{D}\right)^2\right]^{1/2}}$$

$$U_3 = \frac{\frac{mL}{D} + \left[1 + \left(\frac{mL}{D}\right)^2\right]^{1/2}}{U_1}$$

Another error with the Boutwell and Tsai (1992) method is found in the definition of the a value. Boutwell and Tsai (1992) presented $a = 1$ for a clay pad with a *permeable* base at $b1$. However, an a value of positive one (+1) is for an *impermeable* base at the bottom of the clay pad. The a value should be negative one (-1) if there is a permeable base at the bottom of the clay pad (Trautwein and Boutwell, 1994). The error causes a slight error in calculation by

inverting the signage of a term found in the $G1$ and $G2$ geometric factors presented previously in Equation 2.27 and Equation 2.32, respectively.

2.5.5 *Trautwein and Boutwell (1994) Method*

The Trautwein and Boutwell (1994) method uses the same equations presented in Boutwell (1992) with similar terminology from Boutwell and Tsai (1992); however, simplified equation $G2(2)$ with an additional typographical mistake was presented. In addition, the height of the head calculation is modified to include clay stratum with a permeable base. All of the terms presented in Trautwein and Boutwell (1994) are defined in the same way as in Boutwell (1992) except where noted.

Trautwein and Boutwell (1994) presented a new equation for determining $G2(1)$ (Equation 2.34), which is used to solve for k_2 . Equation 2.34 was developed using Equation 2.32 and assuming that $m = 1$, $T = 0$, and $p = 1$. While this equation was designed to make calculating $G2(1)$ easier by not forcing the user to make assumptions, an error was presented in the $U5$ shape factor. The shape factor U_5 is presented as a matrix instead of a quotient. As presented the term is unsolvable; however, if the term is treated as a quotient instead of a matrix (Equation 2.35), then the term is solvable.

$$G2(1) = \left(\frac{d^2}{16Lf}\right) [2 \ln(U_4) + a \ln(U_5)] \quad (\text{Trautwein and Boutwell, 1994}) \quad \mathbf{Equation 2.34}$$

Where:

$$U_4 = \frac{L}{D} + \left[1 + \left(\frac{L}{D}\right)^2\right]^{1/2}$$

$$U_5 = \frac{\frac{4b_2}{D} + \frac{L}{D} + \left[1 + \left(\frac{4b_2}{D} + \frac{L}{D}\right)^2\right]^{1/2}}{\frac{4b_2}{D} - \frac{L}{D} + \left[1 + \left(\frac{4b_2}{D} - \frac{L}{D}\right)^2\right]^{1/2}}$$

$$G2(1) = \left(\frac{d^2}{16Lf}\right) [2 \ln(U_4) + a \ln(U_5)] \quad (\text{Trautwein and Boutwell, 1994}) \quad \text{Equation 2.35}$$

Where:
$$U_4 = \frac{L}{D} + \left[1 + \left(\frac{L}{D}\right)^2\right]^{1/2}$$

$$U_5 = \frac{\frac{4b_2}{D} + \frac{L}{D} + \left[1 + \left(\frac{4b_2}{D} + \frac{L}{D}\right)^2\right]^{1/2}}{\frac{4b_2}{D} - \frac{L}{D} + \left[1 + \left(\frac{4b_2}{D} - \frac{L}{D}\right)^2\right]^{1/2}}$$

In the Trautwein and Boutwell (1994) method, the height of the head used for determining H_1 and H_2 was modified to include condition for a permeable base at b_1 . For continuous soils, the height of the head is defined as distance from the water level in the standpipe to the water table and is limited (maximum value) to a distance of twenty casing diameters, $20D$, below the casing. For soils with a permeable base, the height of the head is defined as the distance between the water level in the standpipe and the first pervious layer and is also limited (maximum value) by a depth of twenty casing diameters, $20D$, below the casing. In addition to the trial and error method presented by Boutwell (1992) to solve for m , Trautwein and Boutwell (1994) utilized a figure (Figure 2.15) to solve for m where the value of m and K_v/K_1' (k_v/k_1') are approximated after K_2'/K_1' (k_2'/k_1') has been obtained.

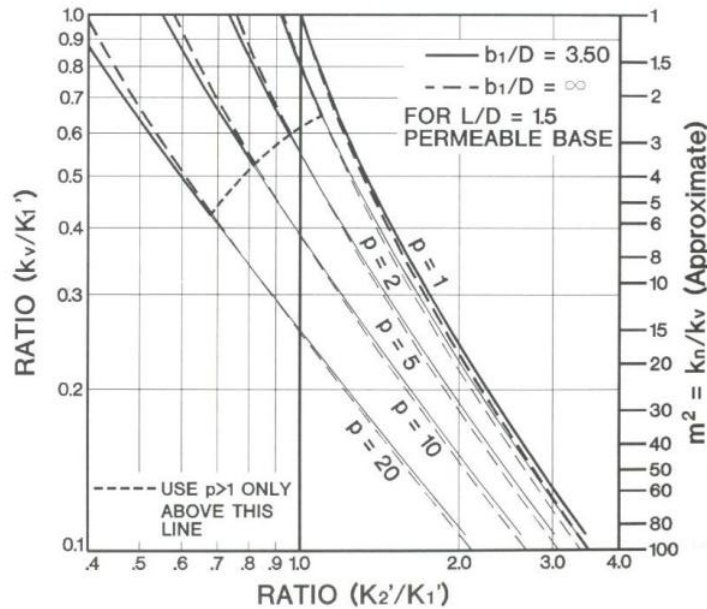


Figure 2.15. TSB data reduction nomograph (from Trautwein and Boutwell, 1994).

2.5.6 ASTM D6391 (2012) Method A

The method presented in ASTM D6391 (2012) following Method A is a simplified method from the methods presented in Boutwell (1992), Boutwell and Tsai (1992), and Trautwein and Boutwell (1994). The ASTM D6391 (2012) method contains separate equations to calculate hydraulic conductivity for Stage 1 and 2, Equation 2.36 and Equation 2.37, respectively. The difference between the two equations (Equation 2.36 and Equation 2.37) is the geometric factors. The geometric factors are calculated using Equation 2.38 for Stage 1 and Equation 2.39 through Equation 2.42 for Stage 2. The time-weighted average apparent hydraulic conductivities, k_1' and k_2' , are then calculated for Stage 1 and 2 using Equation 2.43 and Equation 2.44, respectively. The ASTM D6391 (2007) method corrects the typographical errors presented in both Boutwell and Tsai (1992) and Trautwein and Boutwell (1994); however, only the apparent hydraulic conductivities of Stages 1 and 2 and not for the vertical or horizontal hydraulic conductivities can be acquired using ASTM D6391 (2012). All of the terms presented in ASTM D6391 (2012) are defined the same as in Boutwell (1992) except where noted. The

height of head (Z) used in Equation 2.36 and Equation 2.37 is defined as the distance from the water level in the standpipe to the bottom of the casing for both Stage 1 and Stage 2 testing (as shown in Figure 2.16).

$$k_1 = \frac{R_t G_1 \ln\left(\frac{Z_1}{Z_2 t}\right)}{(t_2 - t_1)} \quad (\text{ASTM D6391, 2012}) \quad \text{Equation 2.36}$$

$$k_2 = \frac{R_t G_2 \ln\left(\frac{Z_1}{Z_2 t}\right)}{(t_2 - t_1)} \quad (\text{ASTM D6391, 2012}) \quad \text{Equation 2.37}$$

$$G_1 = \left(\frac{\pi d^2}{11D}\right) \left[1 + a \left(\frac{D}{4b_1}\right)\right] \quad (\text{ASTM D6391, 2012}) \quad \text{Equation 2.38}$$

$$G_2 = \left(\frac{d^2}{16FL}\right) G_3 \quad (\text{ASTM D6391, 2012}) \quad \text{Equation 2.39}$$

$$G_3 = 2 \ln(G_4) + a \ln(G_5) \quad (\text{ASTM D6391, 2012}) \quad \text{Equation 2.40}$$

$$G_4 = \frac{L}{D} + \left[1 + \left(\frac{L}{D}\right)^2\right]^{1/2} \quad (\text{ASTM D6391, 2012}) \quad \text{Equation 2.41}$$

$$G_5 = \frac{\left[\frac{4b_2 + L}{D}\right] + \left[1 + \left(\frac{4b_2 + L}{D}\right)^2\right]^{1/2}}{\left[\frac{4b_2 - L}{D}\right] + \left[1 + \left(\frac{4b_2 - L}{D}\right)^2\right]^{1/2}} \quad (\text{ASTM D6391, 2012}) \quad \text{Equation 2.42}$$

$$k_1' = \frac{\sum k_{1i}(t_2 - t_1)_i}{\sum (t_2 - t_1)_i} \quad (\text{ASTM D6391, 2012}) \quad \text{Equation 2.43}$$

$$k_2' = \frac{\sum k_{2i}(t_2 - t_1)_i}{\sum (t_2 - t_1)_i} \quad (\text{ASTM D6391, 2012}) \quad \text{Equation 2.44}$$

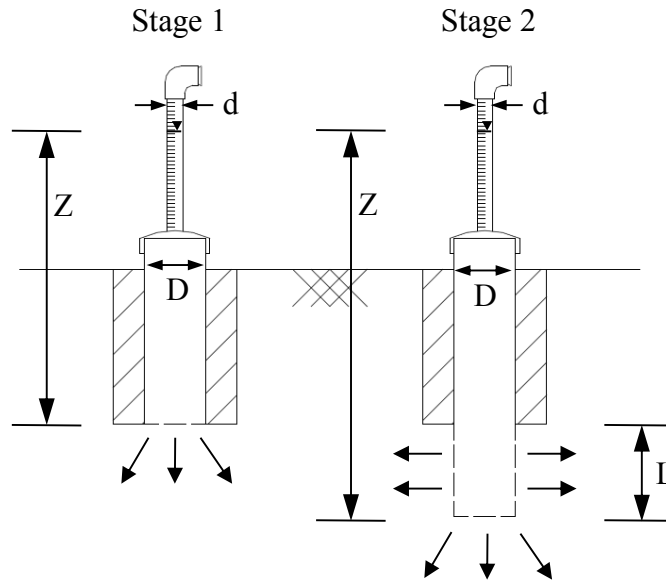


Figure 2.16. Schematic of TSB test apparatus showing relevant dimensions for calculating hydraulic conductivity for use with ASTM D6391 (2012).

An issue with ASTM D6391 (2012) is the definition of the height of head. As stated in the calculation section of the standard, the height of the head is defined as the distance from the water level in the standpipe to the bottom of the casing for both Stages 1 and 2; however, in the hand calculations presented in ASTM D6391 (2012), a W term was presented which is not addressed in the body of document. The W term accounts for the depth to the water table or the depth to a permeable layer. No depth limit, for example to a depth of twenty casing diameters below the casing, is given.

2.5.7 Chapuis (1999) Method

It was proposed in Chapuis (1999) that the velocity method be used instead of the time lag-equations. The velocity method accounts for the changing hydraulic gradient during the falling head test by plotting the calculated velocity between two readings and the average head between the same two readings. The developed velocity-head plot is only viable for one filling of the standpipe; that is, each time the standpipe is refilled, a new plot must be created.

The shape factor (C) is calculated using Equation 2.45 and one of the following equations: Equation 2.46, Equation 2.47, or Equation 2.48. The velocity between two readings is calculated by dividing the change in height by the change in time. The height of the head (H) is determined from an assumed datum (i.e. soil surface) and is corrected using the velocity-head graph. The velocity for each time increment is plotted against the average height for the same increment. A linear trend line is plotted through the points and a slope (p) is determined. The calculated shape factor (C) and the slope (p) are then used in Equation 2.49 to calculate the hydraulic conductivity for the stage. The assumed datum is adjusted for the correct piezometric level by subtracting the y-intercept from the velocity graph (or error in assumed piezometric level) to the assumed datum. Additionally, this error (H_0) is subtracted from the initial height (H) to obtain the actual head difference (H_r). To check for the value of hydraulic conductivity calculated using the velocity graph, the natural log of the actual head difference is plotted against time. A linear trend line is then plotted through the data set and a new slope (p') is determined and should be linear with no curvature. The hydraulic conductivity value is then obtained using the new slope (Equation 2.50). The hydraulic conductivity values obtained using Equation 2.49 should be similar to the hydraulic conductivity value obtained using the value obtained from the one calculated from the velocity graph. The velocity method is only recommended for determining the hydraulic conductivity associated with Stage 1 of the TSB test (Chapuis, 1999).

$$C = \frac{c}{S_{inj}} \quad (\text{Chapuis, 1999}) \quad \text{Equation 2.45}$$

$$c = 2.75D \text{ (for Stage 1)} \quad (\text{Chapuis, 1999}) \quad \text{Equation 2.46}$$

$$c = \frac{2\pi L}{\ln(2L/D)} \text{ (for Stage 2 when } L/D \geq 4) \quad (\text{Chapuis, 1999}) \quad \text{Equation 2.47}$$

$$c = 2\pi D \left(\frac{L}{D} + \frac{1}{4} \right)^{1/2} \quad (\text{for Stage 2 when } 1 \leq L/D \leq 8) \quad (\text{Chapuis, 1999}) \quad \text{Equation 2.48}$$

$$k = \frac{c}{60p} \quad (\text{Chapuis, 1999}) \quad \text{Equation 2.49}$$

$$k = \frac{cp'}{60} \quad (\text{Chapuis, 1999}) \quad \text{Equation 2.50}$$

Where:

- C = Shape factor
- c = Geometry specific shape factor
- S_{inj} = Cross-sectional area of standpipe
- D = Diameter of injection zone
- L = Length of injection zone
- k = Measured hydraulic conductivity
- p = Slope of velocity curve
- p' = Slope of corrected semilog curve

2.5.8 Chiasson (2005) Method

The method for calculating the hydraulic conductivity presented in Chiasson (2005) is similar to the velocity method proposed in Chapuis (1999); however the Chiasson (2005) method (Z-t method) is based on water elevation (Z) and time (t) and not on the average water elevation and average falling head velocity. The hydraulic conductivity is calculated using Equation 2.51 where a is an unknown constant determined from Equation 2.52 and C is the shape factor calculated using the aforementioned Equation 2.45 through Equation 2.48 [in a similar manner as Chapuis (1999)]. Three unknown variables are presented in Equation 2.52, $H(0)$, H_0 , and a . To solve for these variables, the difference between the actual measurement $Z(t)$ and the estimator of the function $Z^*(t)$ is calculated using Equation 2.53. The solution for $Z^*(t)$ is found by

minimizing the sum of the squared differences (Equation 2.54) subject to the unbiased condition presented in Equation 2.55.

$$k = \frac{a}{c} \quad (\text{Chiasson, 2005}) \quad \text{Equation 2.51}$$

$$Z^*(t) = H(0)e^{-at} + H_0 \quad (\text{modified from Chiasson, 2005}) \quad \text{Equation 2.52}$$

$$\varepsilon_j = Z(t_j) - Z^*(t_j) \quad (\text{modified from Chiasson, 2005}) \quad \text{Equation 2.53}$$

$$\text{Min} \left(\sum_{j=1}^n \varepsilon_j^2 \right) \quad (\text{Chiasson, 2005}) \quad \text{Equation 2.54}$$

$$\sum_{j=1}^n \varepsilon_j = 0 \quad (\text{Chiasson, 2005}) \quad \text{Equation 2.55}$$

Where: a = Unknown constant

$H(0)$ = True and unknown hydraulic head difference at t_0

H_0 = Unknown height of water table

A new method for determining the anisotropy value, α , was also presented in Chiasson (2005) to calculate k_v . The vertical hydraulic conductivity is calculated using Equation 2.56. A new shape factor is calculated using Equation 2.57 and α is calculated using Equation 2.58 and Equation 2.59. Note that α is different that the aforementioned a and that a is equaled to the inverse of m .

$$k_v = -\frac{1}{\alpha C'_1 m_1} \quad (\text{Chiasson, 2005}) \quad \text{Equation 2.56}$$

$$C'_1 = \frac{11D}{\sqrt{a}\pi d^2} \quad (\text{Chiasson, 2005}) \quad \text{Equation 2.57}$$

$$\alpha = \left(\frac{\lambda'_2 D}{L} \right)^2 \quad (\text{Chiasson, 2005}) \quad \text{Equation 2.58}$$

$$\lambda'_2 = \frac{m_1^2}{m_2^2} \left(\frac{11}{8\pi} \right)^2 - \frac{1}{4} \quad (\text{Chiasson, 2005}) \quad \text{Equation 2.59}$$

2.5.9 ASTM D6391 (2012) Method B

The method presented in ASTM D6391 (2012) following Method B is similar to the Z-t method presented in Chiasson (2005). For simplicity and because several terms were changed and a new hydraulic equation was presented, the equations from ASTM D6391 (2012) Method B are presented as Equation 2.60 through Equation 2.63. The calculations are conducted following the same procedures as Chiasson (2005) with the exception that the sum of the differences is divided by n before minimizing and that the shape factor is not calculated separately. Additionally, the height of head (Z) used in Equation 2.61 and Equation 2.62 is defined as the distance from the water level in the standpipe to the bottom of the casing instead of being defined as the distance from the water level in the standpipe to the water table. The Z-t method is recommended for use only on Stage 1 of the TSB test (ASTM D6391, 2012).

$$Z_t = H^* + H_0 \exp(-at) \quad (\text{ASTM D6391, 2012}) \quad \text{Equation 2.60}$$

$$\min \left(\frac{1}{n} \sum_{i=1}^n (Z_i - Z_{ti})^2 \right) \quad (\text{ASTM D6391, 2012}) \quad \text{Equation 2.61}$$

$$\sum_{i=1}^n (Z_i - Z_{ti}) = 0 \quad (\text{ASTM D6391, 2012}) \quad \text{Equation 2.62}$$

$$k = R_t a \frac{\pi d^2}{11D} \quad (\text{ASTM D6391, 2012}) \quad \text{Equation 2.63}$$

Where: Z_i = distance from the water level in the standpipe to the bottom of the casing at time t_i

Z_{ti} = Z_t from Equation 2.60 at time t_i

H^* = Constant related to the total head

H_0 = Constant related to the initial total head

a = Constant related to the hydraulic conductivity

2.6 Time Domain Reflectometry Probes

Time domain reflectometry (TDR) probes (Figure 2.17) along with data acquisition systems are commonly used to measure the real time volumetric moisture content within a soil mass by inferring the conductive ability of the soil deposit. The use of TDR probes for geotechnical engineering has been discussed in Ledieu et al. (1986), Herkelrath et al. (1991), and Siddiqui et al. (2000). TDR probes operate by sending an electrical pulse into the soil through unshielded conductors and measuring the travel time of the return signal. Soil becomes more conductive as the moisture content increases and soils with a higher moisture content will yield a shorter passage of current. Utilizing TDR probes, the measured travel time of the pulse is converted to an apparent probe length (i.e. the probe length required for the given travel time of the pulse) and is compared to the actual probe length. The comparison between the two probe lengths yields an apparent dielectric constant (K_a) for a given type of soil. The volumetric moisture content is correlated to the measured apparent dielectric constant using Equation 2.64 presented by Topp et al. (1980). Typical plots used for determining volumetric moisture content from TDR data and verification for use of the Topp et al. (1980) equation are presented in Figure 2.18 and Figure 2.19, respectively.

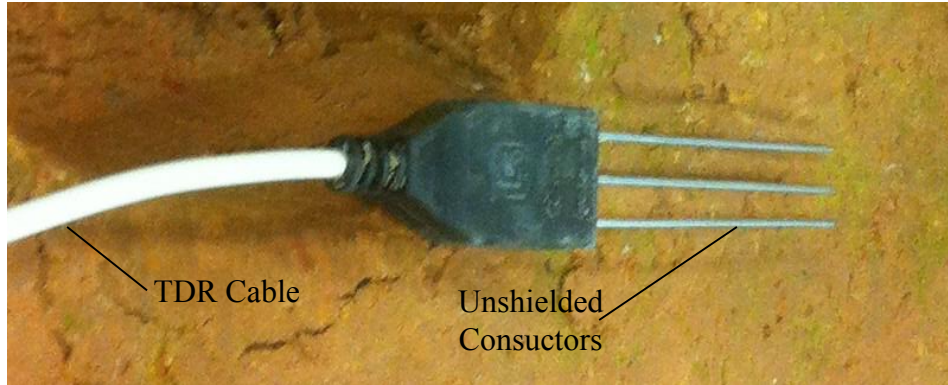


Figure 2.17. Photo of Campbell Scientific TDR probe (model CS645).

$$\theta_v = -5.3 \times 10^{-2} + 2.92 \times 10^{-2} K_a - 5.5 \times 10^{-4} K_a^2 + 4.3 \times 10^{-6} K_a^3$$

Equation 2.64
(Topp et al., 1980)

Where: θ_v = Volumetric moisture content
 K_a = Apparent dielectric constant

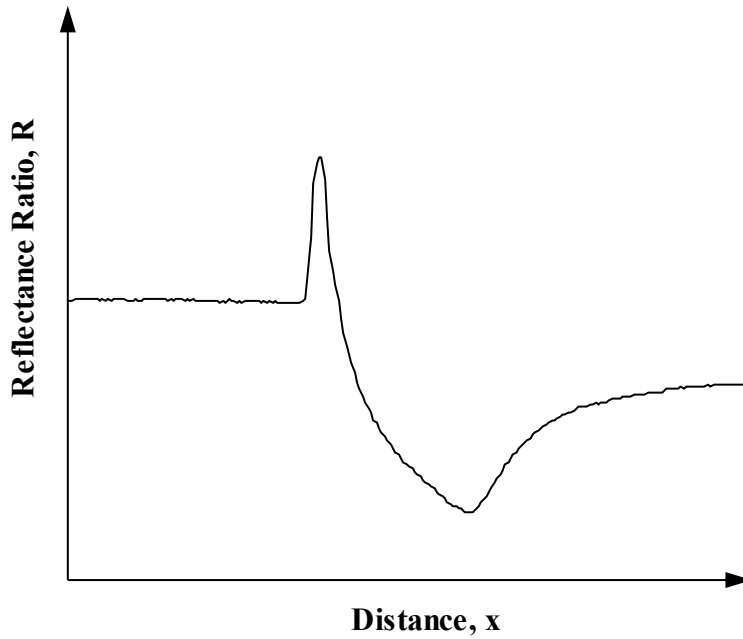


Figure 2.18. Typical TDR probe waveform.

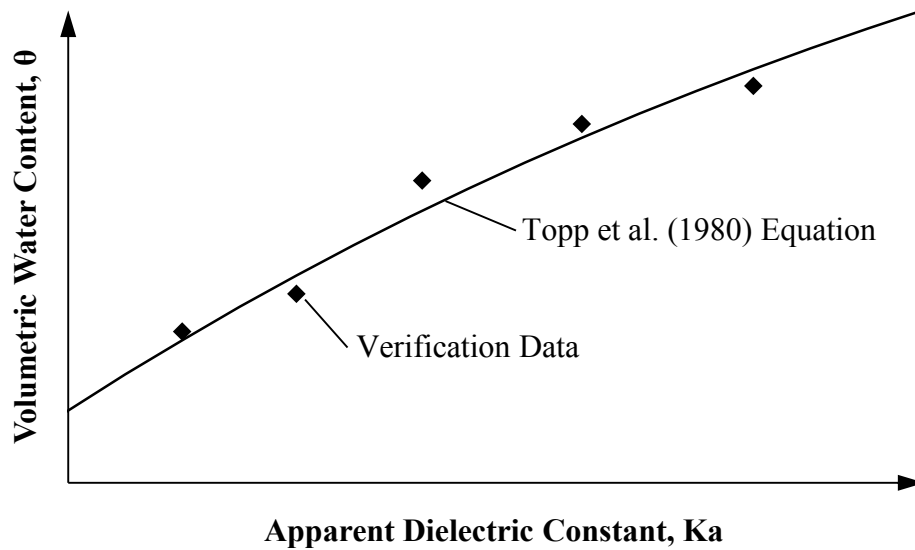


Figure 2.19. Typical TDR verification plot.

2.7 *Tensiometers*

Tensiometers are commonly used to control irrigation in agricultural fields. Specifically, tensiometers are used to measure the suction in unsaturated soils (Trautwein and Boutwell, 1994). The use of tensiometers for geotechnical engineering has been discussed in Ridley et al. (1998) and Take and Bolton (2003). The tensiometer (Figure 2.20) consists of a long plastic tube with a porous tip that is placed into the ground and a suction gauge above the ground. Before use, the porous tip is saturated to ensure no air bubbles are in the void space. Tensiometers are filled with a fluid and installed with the porous tip in close contact with the soil. The tensiometer is commonly installed by installing a pipe into the soil to create a hole and then inserting the tensiometer (Trautwein and Boutwell, 1994). The pipe being driven into the soil is a poor technique and is not recommended because the driving technique may smear the inside of the hole, compact the adjacent soils, and cause cracking in the soil. Instead, it is recommended that a hole be augured into the ground with an opening slightly smaller diameter than the porous probe (Trautwein and Boutwell, 1994). A hydraulic connection is made with the pore water in the soil and the water inside the tensiometer through the porous tip. When the soil is not fully saturated,

the pore water pressure draws suction on the tensiometer which is measured by the gauge. The gauge is a variable resistor which causes a suction dependent voltage drop relative to the input voltage. The suction in the soil is correlated from the voltage readings using Equation 2.65. As the wetting front associated with field hydraulic conductivity tests reaches the porous tip, the adjacent soils become saturated and the suction reduced to zero (Trautwein and Boutwell, 1994).

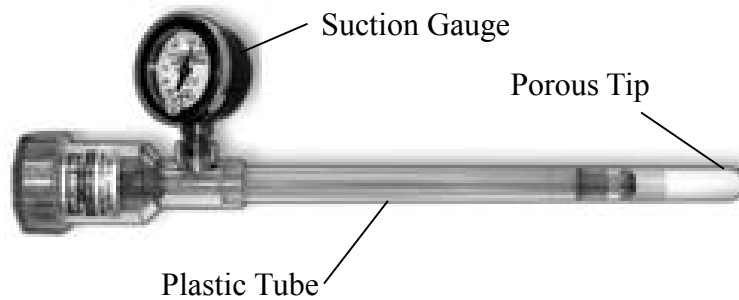


Figure 2.20. Irrrometer tensiometer (modified from Irrrometer, 2012).

$$P_s = \frac{(V_E - V_m)}{265^\circ * F_c} \quad \text{(modified from Irrrometer, 2012)} \quad \text{Equation 2.65}$$

Where:

- P_s = Measured value not corrected for soil type
- V_E = Excitation voltage
- V_m = Measured voltage
- F_c = Sensor calibration factor (0.00111 Volts/Degree/Centibar)

2.8 Flexible Wall Permeameter

The rigid-wall permeameter was commonly used for all laboratory hydraulic conductivity testing until the early 1980's when it was discovered that the permeameters were susceptible to sidewall leakage, or permeant leakage down the interior walls of the cell (Daniel, 1994). Subsequent research has involved the use of flexible wall permeameters for samples made from clay and soft soils with low hydraulic conductivity. Compared to the older rigid-wall permeameters, the flexible-wall permeameter (Figure 2.21) device allows for hydraulic

conductivity testing with the following advantages: less time required for saturation of a soil sample, controlled states of effective stress acting on the sample, and no sidewall leakage. Notable disadvantages of the flexible-wall permeameter are the higher costs associated with the equipment and more complex testing apparatus including three pressure tubes (Daniel, 1994). Additionally, the chemical properties of the flexible membrane may chemically influence and affect the properties of the soil sample on a pressure panel (Daniel, 1994). Currently, clay and soft soils are commonly tested using flexible-wall permeameters. Conversely, gravel, sand, and other hard soils are commonly tested using rigid-wall permeameters where sidewall leakage is not of importance because the hydraulic conductivity of the soil is greater than that along the sidewall. The hydraulic conductivity measured from the flexible wall hydraulic conductivity test is calculated using Equation 2.66 and then modified to a test temperature of 20 degrees Celsius using Equation 2.67.

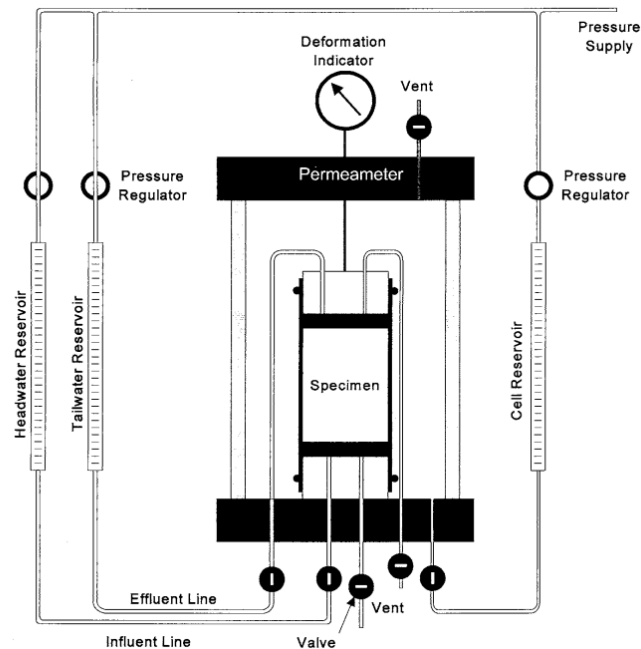


Figure 2.21. Flexible-wall permeameter diagram with rising head have falling tail (from ASTM D5084, 2012).

$$k = \frac{a_{in} * a_{out} * L}{(a_{in} + a_{out}) * A * \Delta t} \ln \left(\frac{\Delta h_1}{\Delta h_2} \right) \quad (\text{ASTM D5084 [Method C], 2012}) \quad \text{Equation 2.66}$$

$$k_{20} = R_T * k \quad (\text{ASTM D5084, 2012}) \quad \text{Equation 2.67}$$

Where: k = Measured hydraulic conductivity at test temperature

a_{in} = Cross sectional area of the reservoir containing the inflow liquid

a_{out} = Cross sectional area of the reservoir containing the outflow liquid

L = Length of specimen

A = Cross sectional area of specimen

Δt = Time interval

Δh_1 = Initial head loss across the specimen

Δh_2 = Final head loss across the specimen

k_{20} = Measured hydraulic conductivity at 20 degrees Celsius

R_T = Viscosity correction factor calculated using Equation 2.21

The effective stress acting on the sample may change the measured hydraulic conductivity of the soil while an increased back pressure should not affect the measured hydraulic conductivity given that the total stress is increased by the same amount to keep the same effective stress (Daniel, 1994). Soils contain macropores and fractures in nature which may be sealed if the effective stress on the laboratory sample is too high. To prevent changing the pore structure, the effective stress acting on the sample in the laboratory should equal the effective stress acting on the sample in the field. Because the principal stresses acting on the sample are controlled, a high back pressure is applied to increase the saturation time. This high back pressure also ensures that all of the pore air in the soil sample diffuses into solution.

However, care must be taken to avoid inducing consolidation or other changes to the properties of the soil sample (Daniel, 1994).

There are three termination criteria for flexible-wall permeameter tests: when steady state hydraulic conductivity is achieved, when two pore volumes of permeant have flown through the sample, and when the desired hydraulic conductivity is achieved. In accordance with ASTM D5084 (2012), the test is usually terminated when the hydraulic conductivity has reached steady state and at least four measurements of hydraulic conductivity are relatively equal to each other. Typically the inflow to outflow ratio is measured in order to ensure proper testing conditions (e.g. water mass balance and no leaks). When the soil is becoming saturated, the inflow will be greater than the outflow as the permeant replaces the entrained air in the sample pore spaces. However, if the soil is consolidating, the outflow may be greater than the inflow. As stated in Daniel (1994), the ideal inflow to outflow ratio is 1; however, an acceptable range for the inflow to outflow ratio is 0.9 to 1.1 (or 0.75 to 1.25 for soils with a hydraulic conductivity less than 1×10^{-8} cm/sec). Black and Lee (1973) stated that when testing unsaturated soil, full saturation may take several days to several weeks to occur. The amount of time required for saturation is dependent on the amount of time required to diffuse the pore air into the pore water (Black and Lee, 1973).

2.9 *Representative Sample Size for Hydraulic conductivity Testing*

Various hydraulic conductivity testing methods can yield different results due to the inconsistency of the soil being tested. Soil compacted in the field is not always uniform and free of clumps, cracks, and other defects (Daniel, 1984). During compaction, macrovoids forms between soil clods and lift interfaces. Evaluation of dye testing has revealed that seepage predominately occurs through the macrovoids which consequentially control the hydraulic

conductivity of the soil (Elshury et al., 1990 and Benson et al. 1994). Due to the irregularity in the soil structure, large-scale hydraulic conductivity tests may yield a higher hydraulic conductivity than a small-scale test on the same soil. Small-scale samples (i.e. Shelby tube samples) are too small to adequately characterize the macrovoid structure for soil placed in the field (Benson et al., 1997). Benson et al. (1994) suggest that a sample size with a diameter of at least one foot is required for adequate hydraulic conductivity testing. Although the recommended sample size is larger than the test area of the TSB permeameter or a laboratory Shelby tube sample, proper compaction techniques and quality control provisions taken during construction produce well compacted soil reducing the representative sample size required for hydraulic conductivity measurements (Benson et al., 1994) because of increased soil homogeneity. With good compaction, research suggests TSB and Shelby tube results are comparable to SDRI results on the same soil (Benson et al., 1999).

2.10 Effects of Effective Stress on Hydraulic conductivity

The effective stress acting on a soil sample during testing can affect the measured hydraulic conductivity. During in-situ hydraulic conductivity tests (e.g. SDRI and TSB), the effective stress acting on the soil is approximately 1.5 psi (Trast and Benson, 1995). At low effective stresses, the macropore structure of the soil will govern the hydraulic conductivity. As the effective stress increases, the macropore structure will begin to close. The micropore structure will start to govern flow when the effective stress is increased to approximately 8 psi (Boynton and Daniel, 1985). Because it is possible to conduct testing on laboratory samples at higher effective stresses, a lower value for hydraulic conductivity is obtained in the laboratory than the value obtained in the field. Research presented in Trast and Benson (1995) suggests that soils with low hydraulic conductivity (less than 1×10^{-7} cm/sec) are less susceptible to changes in

effective stress than soils with a high hydraulic conductivity. Hydraulic conductivity measurements as obtained in the laboratory on soil samples with low hydraulic conductivity are approximately 1.5 times lower than the hydraulic conductivity measurements obtained in the field (Trast and Benson, 1995).

Engineered structures (e.g. landfill liners) benefit from decreased hydraulic conductivity with increased in effective stress (Trautwein and Boutwell, 1994). The value of in-situ hydraulic conductivity of a landfill liner after waste placement (i.e. hydraulic conductivity of the bottom liner after waste is placed) should be lower than the value of in-situ hydraulic conductivity prior to fill placement due to the increase in overburden pressure acting on the liner as the waste facility places accepted waste onto the liner. While conducting an in-situ hydraulic conductivity test (e.g. SDRI or TSB), the effective stress acting on the soil is low due to the shallow test depth and the testing apparatus being opened to atmospheric pressure. As waste is placed on the bottom liner, the added weight of the waste induces a higher stress on the liner thereby increasing the effective stress. Most of the stress is applied in terms of total stress because the leachate level of the landfill is usually limited to one-foot at the bottom of the landfill. The higher effective stress acting the liner caused by the waste typically ranges from 7.2 psi to 43.5 psi (Trast and Benson, 1995).

2.11 Laboratory Hydraulic Conductivity Compared to Field Hydraulic Conductivity

Previous research has been conducted on the difference between the hydraulic conductivity measured in the laboratory compared to the hydraulic conductivity measured in the field. Additionally, various field hydraulic conductivity tests (i.e. SDRI measured hydraulic conductivity compared to TSB measured hydraulic conductivity) have been compared. With proper compaction, similar hydraulic conductivities are measured using the various test methods.

Studies between various hydraulic conductivity test results have been published by Day and Daniel (1985), Benson et al. (1994), Trast and Benson (1995), and Benson et al. (1997); however, notable research was presented in Benson et al. (1999) in which results from hydraulic conductivity tests at 85 separate sites using various testing methods were reported. The acknowledged field hydraulic conductivity was determined from the results of the SDRI tests due to the ability of the test to accurately measure the overall hydraulic conductivity of the clay liner (Sai and Anderson, 1990). A plot of TSB obtained values of hydraulic conductivity and hydraulic conductivity values obtained from 1-foot diameter block specimens as a function of field obtained hydraulic conductivity values as obtained from Benson et al. (1999) is presented in Figure 2.22. On average, the tests conducted using the SDRI, TSB, or laboratory testing on block specimen methods yield approximately the same results.

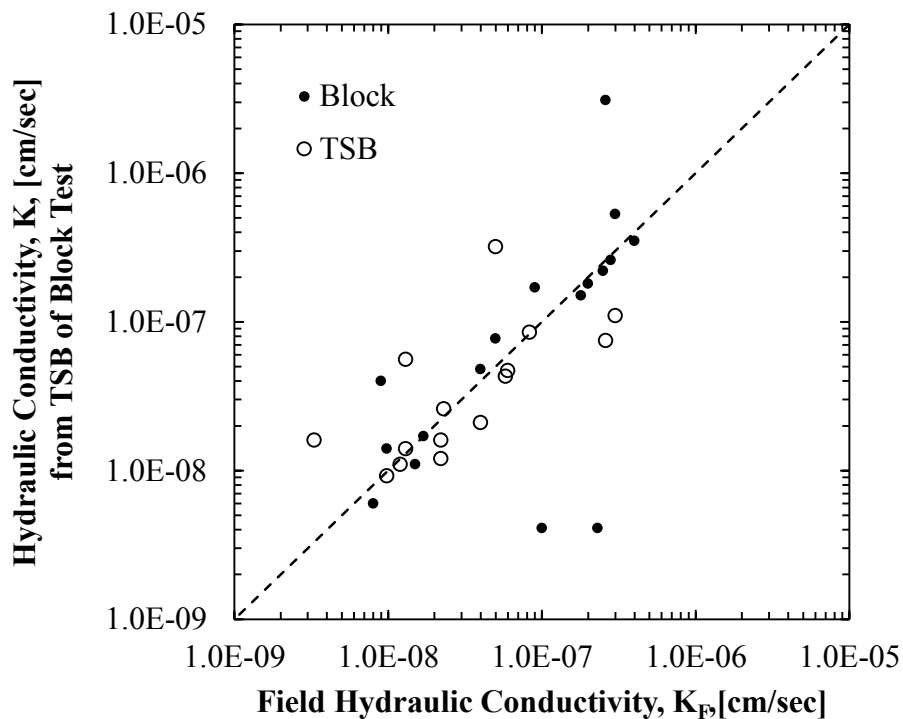


Figure 2.22. Hydraulic conductivity values measured using the TSB method and laboratory testing on one-foot block specimens as a function of hydraulic conductivity values measured from SDRI testing (data from Benson et al., 1999).

A plot of field hydraulic conductivity compared to small scale undisturbed laboratory samples (7.5-centimeter sample diameter) obtained from Benson et al. (1999) is presented in Figure 2.23. For organization purposes, Benson et al. (1999) present the P_o term which is the percentage of the field compaction data falling wet of the line of optimums. As shown in Figure 2.23, when the P_o was lower than 80-percent (i.e. poor compaction), the measured laboratory hydraulic conductivity values tended to be lower than the measured field hydraulic conductivity values. Therefore, the hydraulic conductivity values obtained from laboratory hydraulic conductivity testing underestimated the actual value of hydraulic conductivity and thereby yielded conservative results. Alternatively, when P_o was greater than 80-percent (i.e. good compaction), the measured laboratory hydraulic conductivity tended to match the measured field hydraulic conductivity plus or minus one-half an order of magnitude from a one to one ratio with the exception of three points. Based on the hydraulic conductivity data presented in Figure 2.23, pushing a Shelby tube has little effect on the hydraulic conductivity of soils compacted well and has a large effect on soils compacted poorly.

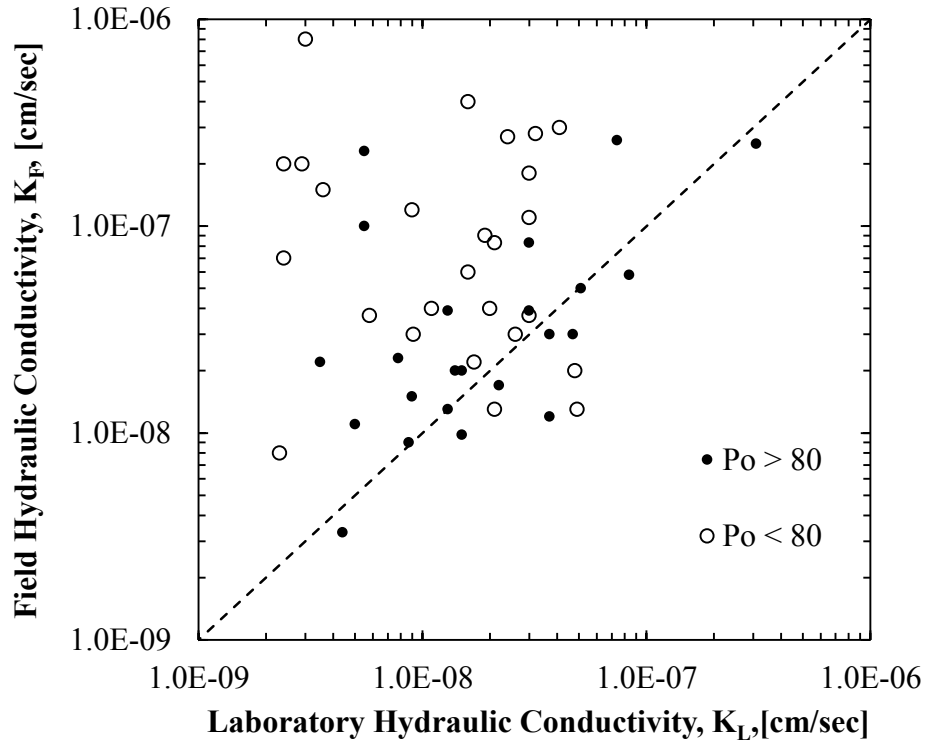


Figure 2.23. Field hydraulic conductivity compared to hydraulic conductivity measured in laboratory on small undisturbed specimens (data from Benson et al., 1999).

As previously mentioned in Section 2.9, it has been demonstrated that with proper compaction technique, the representative size of sample required for testing decreases thereby causing the SDRI and TSB tests to yield similar results (Benson et al., 1994). Additionally, as previously mentioned in Section 2.10, laboratory hydraulic conductivity tend to agree with field hydraulic conductivity tests when the laboratory tests are conducted at low effective stresses similar to the field tests (Trast and Benson, 1995). To achieve good compaction, and to ensure that the various test method will yield similar results, it is recommend by Benson et al. (1999) that at least 80 percent of the density tests on the compacted lift fall on or wet of the line of optimums. As previously mentioned in Section 2.2, the Daniel and Benson zone of acceptance is typically bounded by the line of optimums.

2.12 Conclusion

A method for developing acceptance criterion based on important soil parameters (dry unit weight, moisture content, hydraulic conductivity, and shear strength) was presented. Typically, the zone of acceptance is created by conducting laboratory tests (Proctor and flexible wall hydraulic conductivity) are conducted prior to placement of the soil in the field. Then the placed soils are accepted or rejected based on a window of dry unit weight and moisture content combinations that have been shown to produce or not to produce soils with acceptable hydraulic conductivity and shear strength properties.

Field hydraulic conductivity tests are often conducted to ensure that the hydraulic conductivity of the soil, which was placed with dry unit weight and moisture content values within the zone of acceptance, is lower than the acceptance criteria. Overviews of the sealed double ring infiltrometer (SDRI) and two stage borehole (TSB) field hydraulic conductivity testing methodologies were presented. Three methods for accounting for the wetting front during the SDRI tests were presented. Additionally, nine methods for calculating the hydraulic conductivity from a TSB test were presented with discussion about issues associated with each of the methods. Also, two methods (time domain reflectometry probes and tensiometers) for determining the location of the wetting front were presented.

Laboratory hydraulic conductivity testing conducted on field obtained samples is commonly used to validate that soils deemed to have met the dry unit weight and moisture content criteria also meet the hydraulic conductivity criteria. However, results obtained from hydraulic conductivity tests are affected by the size of the tested area and the effective stress acting on the sample during testing. It is important that the laboratory and field tests be

conducted on soils with the same macrostructure and at the same stresses as those observed in-situ.

Chapter 3: Methods and Procedures

3.1 Introduction

To evaluate the various methodologies presented in Section 2.5 for two stage borehole data reduction, the nine methodologies were analyzed for accuracy and efficiency. For construction used in this research project, a zone of acceptance was developed and used as an acceptance criterion to compact environmentally controlled clay test pads at the Engineering Research Center (ERC). The test pads were constructed inside the test pad box and verified against the zone of acceptance for thickness and compaction requirements (e.g. moisture content and dry unit weight). Following construction, the test pads were tested using either two stage borehole or sealed double ring infiltrometer hydraulic conductivity testing. After in-situ hydraulic conductivity testing was completed on either Test Pads 1 or 2, Shelby tube samples were collected. Hand carved samples were also collected from Test Pads 1 and 2 during removal of each test pad. Shelby tube, hand carved, and bag samples were transported to Bell Engineering Center (BEC) for laboratory testing (e.g. flexible wall hydraulic conductivity, specific gravity, Atterberg Limits, and grain size analysis).

The analysis of the nine methods used for two stage borehole data reductions is presented in Section 3.2. The methods used to develop the zone of acceptance are discussed in Section 3.3. The box built to contain the test pads constructed at the ERC is discussed in Section 3.4 and the placement procedure for the test pads were placed according to the procedures outlined in Section 3.5. The procedures used for two stage borehole and sealed double ring infiltrometer testing are discussed in Section 3.6 along with discussion about the instrumentation that was used to measure the wetting front movement. The procedures associated with sample collection

from the test pads (Section 3.7) and laboratory testing conducted at Bell Engineering Center (Section 3.8) are also presented.

3.2 Evaluating the Various Solution Methods for Two Stage Borehole Data Reduction

To evaluate the various methods for solving for the apparent hydraulic conductivities obtained from Stage 1 and Stage 2, the data set presented in ASTM D6391 (2010) was utilized and values of apparent hydraulic conductivity and horizontal and vertical hydraulic conductivity were calculated following the procedures outlined in each solution method. To ensure correct input and use of the data set and equations, the data set was first evaluated using the equations presented in ASTM D6391 (2010). After solving for the hydraulic conductivity of each time step utilizing the equations presented in ASTM D6391 (2010), the calculated results were compared with the results that were provided in the calculations section in ASTM D6391 (2010).

3.3 Zone of Acceptance

The soil used for this research project was Northwest Arkansas “Red Dirt”. Red dirt was selected for use because it is widely available in Northwest Arkansas and it is the soil selected for use in landfill liner construction at the Tontitown Waste Management Landfill. Two dump truck loads of sifted soil (i.e. chert nodules removed) were provided by Les Rogers of Fayetteville, Arkansas. The soil was stockpiled outside at the Engineering Research Center (ERC) until needed for research. A sample of the soil was collected from the stockpile and transported to Bell Engineering Center (BEC) for Proctor and flexible wall hydraulic conductivity testing to develop a zone of acceptance. Laboratory testing for the zone of acceptance began in September, 2010, and was completed in February, 2011. Three Proctor tests, conducted at standard energy, 75-percent of standard energy, and 50-percent of standard energy, were performed on 18 Proctor samples and the obtained data were used to develop three Proctor

curves. Following the Proctor tests, 14 of the 18 samples were extruded from the Proctor mold using a hydraulic jack and placed into a flexible wall hydraulic conductivity cell for hydraulic conductivity testing (Section 3.3.2). The Zone of Acceptance (ZOA) was developed following the Daniel and Benson (1990) method previously described in Section 2.2 using only the hydraulic conductivity requirement. The ZOA was generated to encase all of the points on the Proctor curve that possessed a hydraulic conductivity value lower than 1×10^{-7} cm/sec. The ZOA was developed to provide guidance on how to achieve field hydraulic conductivity values less than 1×10^{-7} cm/sec based on comparisons to molding moisture content and dry unit weight measurements. The procedures utilized to develop the zone of acceptance are discussed in this section.

3.3.1 Proctor Testing for Development of ZOA

Eighteen (18) Proctor samples were compacted at various energies. Seven (7) samples were compacted using standard energy in accordance with Method A of ASTM D698 (2012). The equipment used for Proctor testing is shown in Figure 3.1. For standard energy compaction, the soil was compacted in three (3) lifts inside a 1/30 of a cubic foot mold. Each lift was compacted using 25 blows from a 5.5 pound hammer dropped from a height of 12 inches. A solid Proctor mold was used to ensure no change in volume for the various samples. The volume of the Proctor mold was calibrated using the water-filled method (Figure 3.2) as described in ASTM D698 (2012). Eleven (11) samples were compacted at reduced energy by reducing the quantity of blows per layer to achieve a lower compaction effort. Six (6) of the reduced energy samples were compacted at 75 percent of standard energy using the same hammer, mold, and number of lifts as the standard Proctor but with 56 total blows (18 blows for first lift and 19 blows for second and third lifts) instead of 75 total blows (25 blows for each lift). The other five

(5) reduced energy samples were compacted at 50 percent of standard energy using the same hammer, mold, and number of lifts as the standard Proctor but with 38 total blows (12 blows for first lift and 13 blows for second and third lifts) instead of 75 total blows (25 blows for each lift). Samples were prepared using the moist preparation method. The total unit weight of the Proctor sample was calculated using Equation 3.1 and the dry unit weight was calculated using Equation 3.2. Before compaction, the mold was lubricated with silicone spray to ease in the sample extraction process.

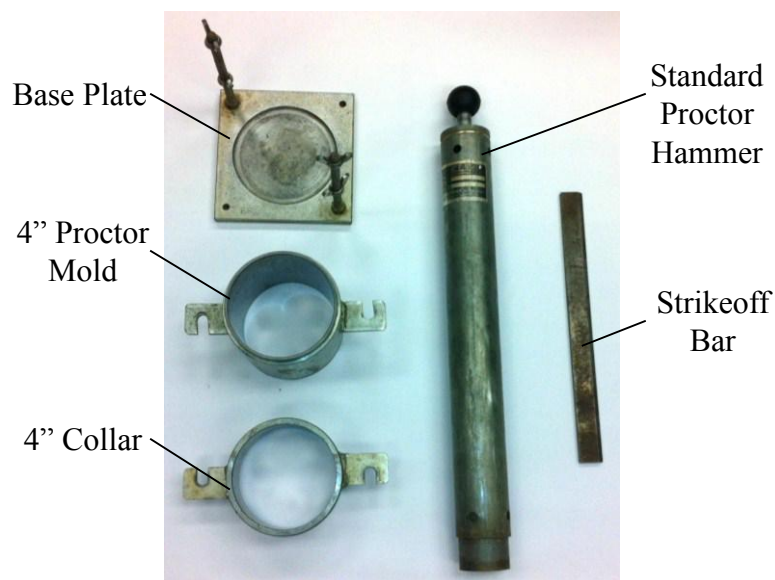


Figure 3.1. Equipment used for Proctor testing.

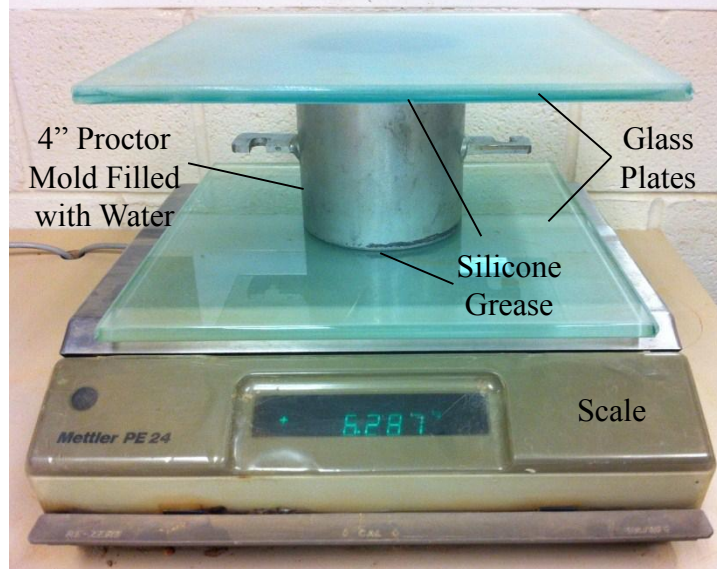


Figure 3.2. Calibration procedure to determine the volume of the four-inch diameter Proctor mold.

$$\gamma_t = \frac{(M_t - M_{md})}{V} * \gamma_w \quad (\text{modified from ASTM D698, 2012}) \quad \text{Equation 3.1}$$

$$\gamma_d = \frac{\gamma_t}{1+w} \quad (\text{modified from ASTM D698, 2012}) \quad \text{Equation 3.2}$$

Where: γ_t = Total unit weight (in pounds per cubic foot)

M_t = Total mass of completed Proctor sample and mold (in grams)

M_{md} = Mass of mold (in grams)

V = Calculated volume of mold (in cubic centimeters)

γ_w = Unit weight of water (in pounds per cubic foot)

γ_d = Dry unit weight (in pounds per cubic foot)

w = Moisture content of Proctor sample (in percent)

3.3.2 Flexible Wall Hydraulic Conductivity Testing for Development of ZOA

Flexible wall hydraulic conductivity testing was conducted on 14 of the Proctor samples following Method C of ASTM D5084 (2012). Hydraulic conductivity tests were conducted using

hydraulic conductivity cells (Figure 3.3) and pressure panel boards (Figure 3.4) obtained from Trautwein Soil Testing Equipment Company of Houston, Texas. The components of a hydraulic conductivity cell, without the soil sample, are presented in Figure 3.5.

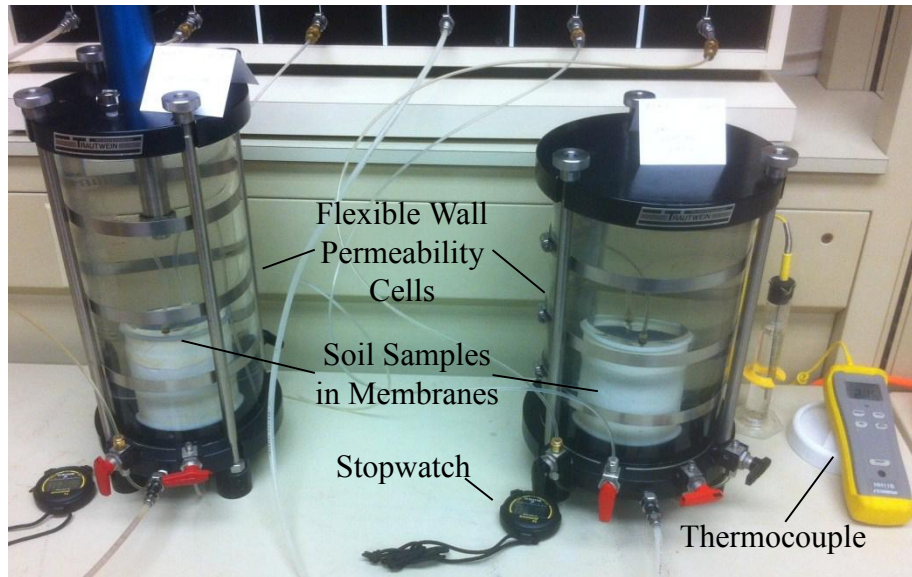


Figure 3.3. Two of six Trautwein flexible wall hydraulic conductivity cells used for laboratory hydraulic conductivity testing.



Figure 3.4. Trautwein panel boards used for laboratory hydraulic conductivity testing.

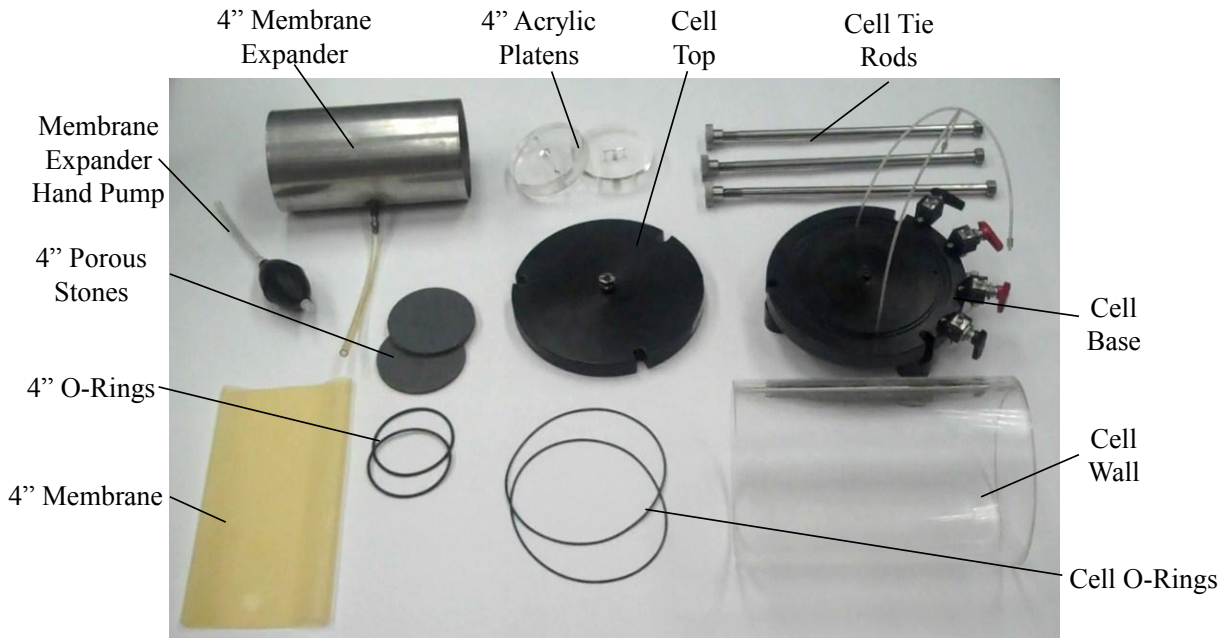


Figure 3.5. Components of a Trautwein hydraulic conductivity cell used for flexible wall hydraulic conductivity testing.

A short zero gradient saturation period of one to two days was performed to prevent fast inflow and outflow from the head water and tail water pressure tubes causing complete drainage or overfilling, respectively, between readings. Before assembling the permeameter, holes were poked into the ends of the samples using a wire brush to ensure that any smearing developed by trimming the sample was removed and did not reduced the hydraulic conductivity measurements. Twenty (20) pounds per square inch (psi) of pressure, supplied and regulated by the panel board, was used for the cell water pressure and 17 psi, also supplied and regulated by the panel board, was used for the head water and tail water pressures, resulting in an effective stress of approximately 3 psi on the soil sample. A stopwatch was used to measure the duration of each subtest and an Omega Model HH11B thermometer with a Type K thermocouple probe was used to obtain water temperature measurements. The hydraulic conductivity values of the samples were calculated using the equations presented previously in Section 2.8.

3.4 Construction of Test Pad Box at Engineering Research Center

To determine the value of the in-situ hydraulic conductivity of a small scale landfill compacted clay liner test pad that was not subjected to external environment conditions (i.e. sun, rain, ect.), a test pad box was constructed at the ERC. A schematic of the compacted clay liner test pad is presented in Figure 3.6. The test pad box (Figure 3.7) is a ten-foot by ten-foot square wooden box. Each face of the box was constructed from four 10-foot long two-inch by 12-inch timbers. Each of the facing elements was supported on the outside by multiple two-inch by four-inch wooden rakers that were secured to corresponding one-foot long, two-inch by four-inch timbers that were anchored to the floor. The bottom of the box was lined with six inches of pea gravel and covered with a sheet of geotextile obtained from the Tensar Corporation, and the sides of the box were lined with plastic sheets. The box was placed near a floor drain to collect excess water that flowed through the soil. The box was constructed during the summer of 2011 and has been used for all of the in-situ work discussed in the thesis. To accommodate construction and removal of each test pad, the front facing (South face) of the box was removed.

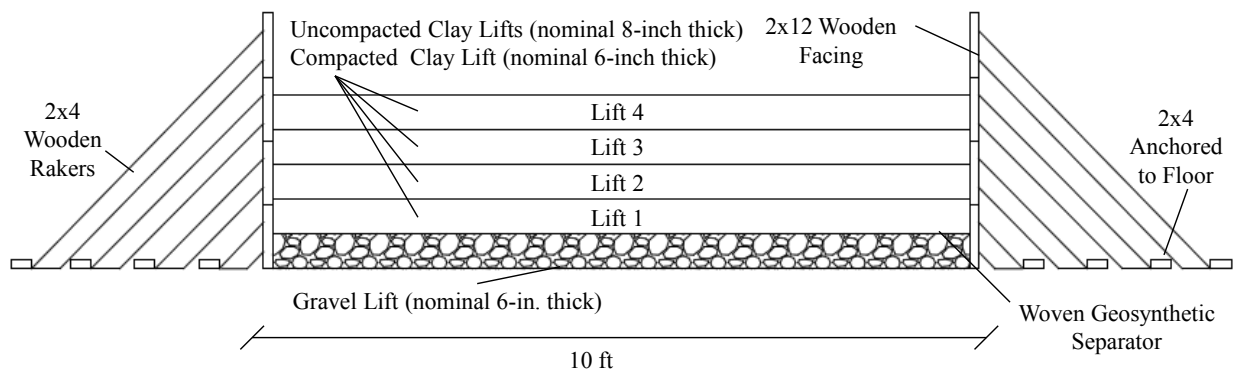


Figure 3.6. Cross section of compacted clay liner test pad constructed at the University of Arkansas Engineering Research Center.

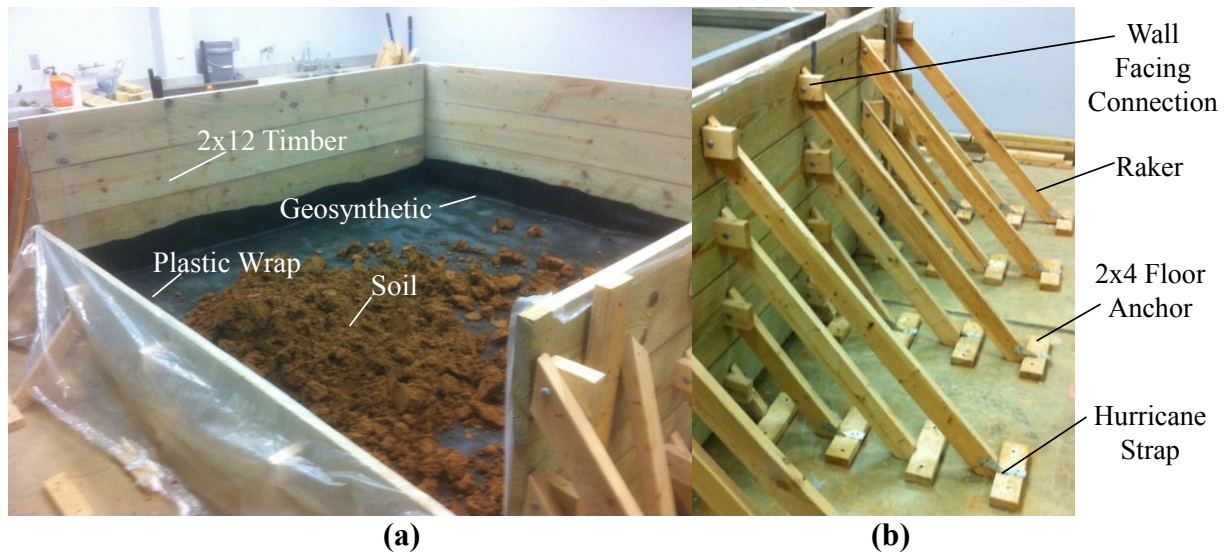


Figure 3.7. (a) Test pad box at the ERC (displaying wooden box, geosynthetic, and soil as part of first lift), and (b) raker structure for the test pad box.

3.5 Placement and Removal of Soil in Test Pad Box at Engineering Research Center

The soil used for test pad construction was stored as a stockpile outside of the ERC when not in use. The stockpile was covered with a tarp but otherwise exposed to the outside environmental conditions. Heavy equipment was used to transport the soil into the ERC and then into the test pad box where the soil was positioned by hand. After the loose lift was placed, the soil was compacted and unit weight measurements were obtained. After completion of test pad construction, in-situ hydraulic conductivity testing was conducted, then soil samples were obtained from the test pad and the test pad was removed.

Loose lifts were placed using the method discussed in Section 3.5.1, and the lifts were compacted using the method discussed in Section 3.5.2. In-situ unit weight and moisture content measurements were obtained using a nuclear density gauge (Section 3.5.3). The lift placement and testing locations for Test Pads 1, 2, and 3 are discussed in Sections 3.5.4, 3.5.5, and 3.5.6, respectively. When in-situ testing was completed, soil samples were obtained and the test pad was removed and the soil was transported to the stockpile following the procedures described in Section 3.5.7.

3.5.1 Placement of Loose Lifts

A bucket attached to the back of a tractor was used to fill bags with the soil stored in the outside stockpile (Figure 3.8a). The tractor was then used to transport the soil bag to a garage door on the West side of the ERC (Figure 3.8b). The soil bag was transferred to a forklift (Figure 3.8c) and transported inside the ERC to the soils lab where the test pad box template was located (Figure 3.8d). The forklift was used to dump the soil bag into the box and the soil was spread out by hand with rakes and shovels to obtain an eight-inch nominal loose lift thickness (Figure 3.8e). Marks were placed on the plastic around the inside sides of the box eight inches above the top woven geosynthetic (for Lift 1) or from the existing compacted lift (for Lifts 2, 3, and 4) to indicate the height of soil needed for the respective loose lift. The thickness of the loose lift was verified using a tripod mounted automatic level (Figure 3.9a) and a level rod (Figure 3.9b). The loose elevations were measured in each corner, in the center along the wall facing, and in the center of the box for each lift.



Figure 3.8. (a) Using the tractor to fill a bag with soil from stockpile, (b) filled soil bag being transferred from the tractor to the forklift, (c) soil bag being brought into the ERC using the forklift, (d) soil bag picked up using the forklift to place inside the test pad box, and (e) loose lift of soil in test pad box.



(a)



(b)

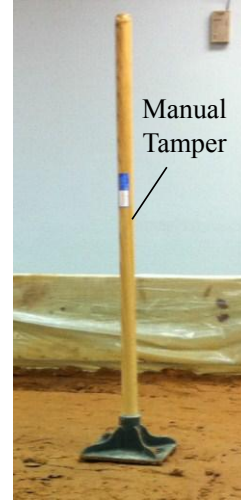
Figure 3.9. (a) Automatic level and (b) rod used to obtain elevations measurements on a compacted lift.

3.5.2 Compaction

Compaction of the clay liner was achieved using a Wacker BS700 gasoline powered rammer (Figure 3.10a). For each lift, two passes were made with the compactor. Any area that was not compacted by the compactor (e.g. the sides and corners of the box) was compacted with an eight inch square manual tamper (Figure 3.10b). For each pass, compaction started in an outer corner of the test pad and progressed in a spiral pattern towards the center of the pad. The compacted height of each lift was measured using a level and rod (previously presented in Figure 3.9) to measure the compacted lift thickness. Similar to the loose elevations, the compacted elevations were measured in each corner, in the center along the wall facing, and in the center of the box for each lift.



(a)



(b)

Figure 3.10. (a) Wacker BS700 gasoline powered rammer, (b) manual tamper.

3.5.3 *In-Situ Unit Weight Testing*

Immediately after compaction of each lift, the in-situ unit weight of the lift was measured using a nuclear density gauge. Nuclear density testing was conducted in accordance with ASTM D6938 (2012) following Procedure A. A Troxler Model 3450 nuclear gauge was used to obtain one minute long readings. Five readings were conducted for each constructed lift at a depth of four inches below the top of each lift. One reading was conducted near the center of the test pad and the other four readings were conducted along each edge of the test pad. The locations for the in-situ unit weight testing conducted in accordance with each test pad are discussed in the next three subsections.

3.5.4 *Placement of Test Pad 1*

Test Pad 1 was constructed in May of 2011 and work was completed in two days by nine personnel. The outside conditions were fair (average outside temperature of 71 degrees Fahrenheit, average relative humidity of 63 percent, and no precipitation) and the soil in the stockpile was near the desired moisture content of 20 percent. Lifts 1 and 2 were placed and compacted during Day 1 and Lifts 3 and 4 were placed and compacted during Day 2. To prevent

the soil at the surface of the test pad from drying, a sheet of plastic was placed on top of the clay when no work was being performed. Each lift was placed (3.5.1) and compacted (3.5.2) following the previously mentioned procedures except for Lift 1, which was compacted using three passes of the compactor instead of two. The nuclear density and in-situ hydraulic conductivity testing locations and locations from which soil samples were obtained following completion of the in-situ testing for Test Pad 1 are displayed in Figure 3.11. In-situ unit weight testing was conducted using the aforementioned procedure stated in Section 3.5.3. Results obtained from the nuclear density gauge for Test Pad 1 are discussed in Section 4.4. In-situ hydraulic conductivity testing was conducted using the procedure discussed later in Section 3.6.1. Results obtained from the two stage borehole testing are presented in Section 4.5.1 and Appendix B.

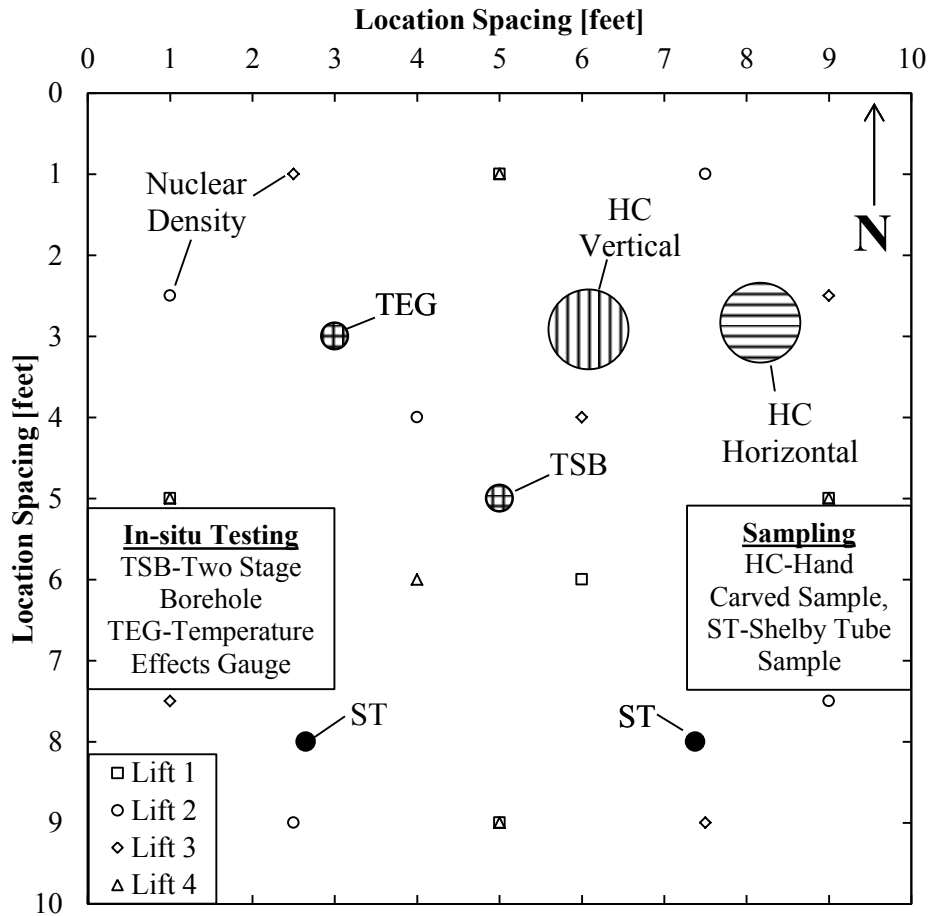


Figure 3.11. Unit weight testing locations, in-situ hydraulic conductivity testing locations, and soil sampling locations within Test Pad 1.

3.5.5 Placement of Test Pad 2

Test Pad 2 was constructed in December of 2011 and work was completed in three days by eight total personnel. The outside conditions were cold (average outside temperature of 34 degrees Fahrenheit, average relative humidity of 95 percent, and no precipitation) and the top three inches of soil in the stockpile were frozen. The soil underneath the frozen layer was workable but did contain ice that thawed when the soil was brought into the ERC causing high soil moisture contents. Lifts 1 and 2 were placed and compacted on Day 1. Lift 3 was placed on Day 1 but was compacted on Day 2, and Lift 4 was placed on Day 2 but was compacted on Day 3. As with Test Pad 1, when no work was being completed, a sheet of plastic was placed over the

test pad to prevent the soil from drying. Each lift was placed (3.5.1) and compacted (3.5.2) following the previously mentioned procedures. The nuclear density and in-situ hydraulic conductivity testing locations and locations from which soil samples were obtained following in-situ hydraulic conductivity testing for Test Pad 2 are displayed in Figure 3.12. In-situ unit weight testing was conducted using the aforementioned procedure stated in Section 3.5.3. Results obtained from the nuclear density gauge for Test Pad 1 are discussed in Section 4.4. In-situ hydraulic conductivity testing was conducted using the procedure discussed later in Section 3.6.1. Results obtained from the two stage borehole testing are presented in Section 4.5.1 and Appendix B.

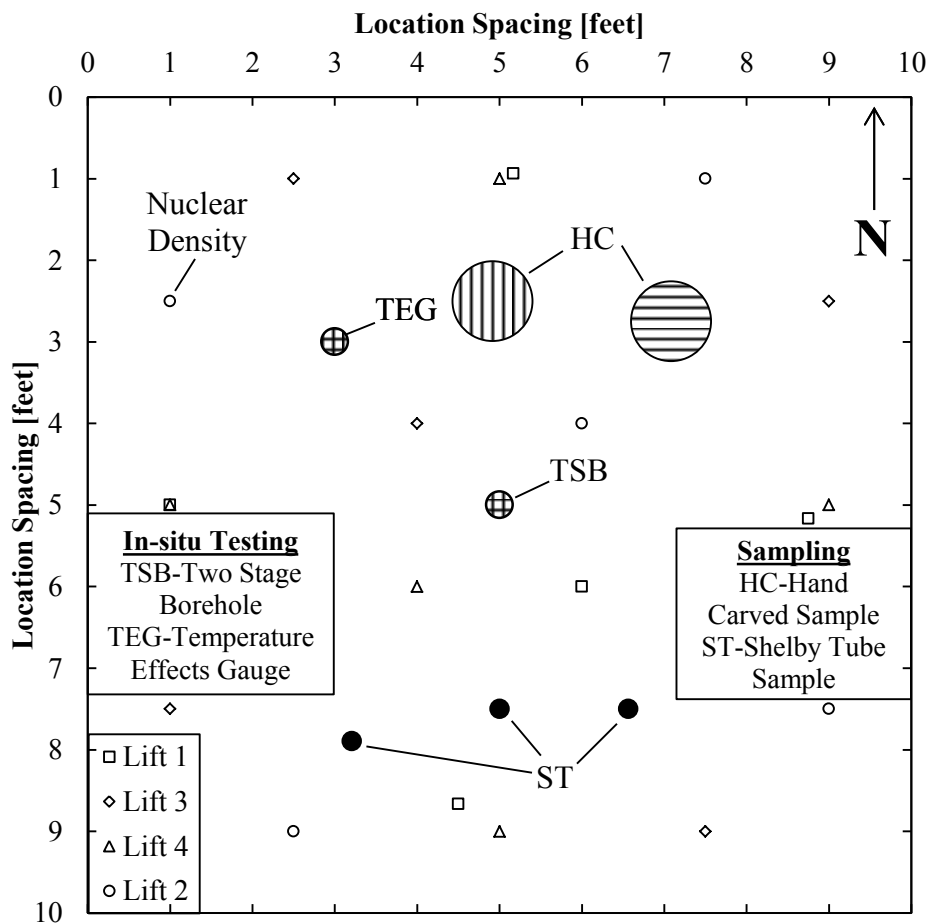


Figure 3.12. Unit weight testing locations, in-situ hydraulic conductivity testing locations, and soil sampling locations within Test Pad 2.

3.5.6 Placement of Test Pad 3

Test Pad 3 was constructed in June of 2012 and work was completed in six days with seven total personnel. The outside conditions were hot and dry (average outside temperature of 84 degrees Fahrenheit, average relative humidity of 52 percent, and no precipitation) and the soil was initially too dry for placement. A garden hose was used to add water to the soil while the soil clods in the stockpile were crushed using a bucket attached to a tractor. Lifts 1 and 2 were placed and compacted on Day 1. No work was completed on Day 2. Lift 3 was placed on Day 3; however, too much water was added and the soil was too wet (approximate moisture content of 28-30 percent based on experience with the soil) to compact. No work was conducted on Day 4 and one pass of the compactor on Lift 3 was made on Day 5. Compaction (the second pass) of Lift 3 was completed on Day 6. Lift 4 was placed and compacted on Day 6. Between Day 3 and Day 6, the top of the test pad remained exposed to allow the soil to dry; otherwise, when no work was being completed, a sheet of plastic was placed over the test pad to prevent drying. Each lift was placed (3.5.1) and compacted (3.5.2) following the previously mentioned procedures with the addition that each lift was moistened immediately before compaction (the first pass). The nuclear density and in-situ hydraulic conductivity testing locations and locations at which instrumentation was installed and from which soil samples will be obtained following the in-situ hydraulic conductivity testing for Test Pad 3 are displayed in Figure 3.13. In-situ unit weight testing was conducted using the aforementioned procedure stated in Section 3.5.3. Results obtained from the nuclear density gauge for Test Pad 1 are discussed in Section 4.4. In-situ hydraulic conductivity testing was conducted using the procedure discussed later in Section 3.6.2. Results obtained from the sealed double ring infiltrometer testing are presented in Section 4.5.2 and Appendix B.

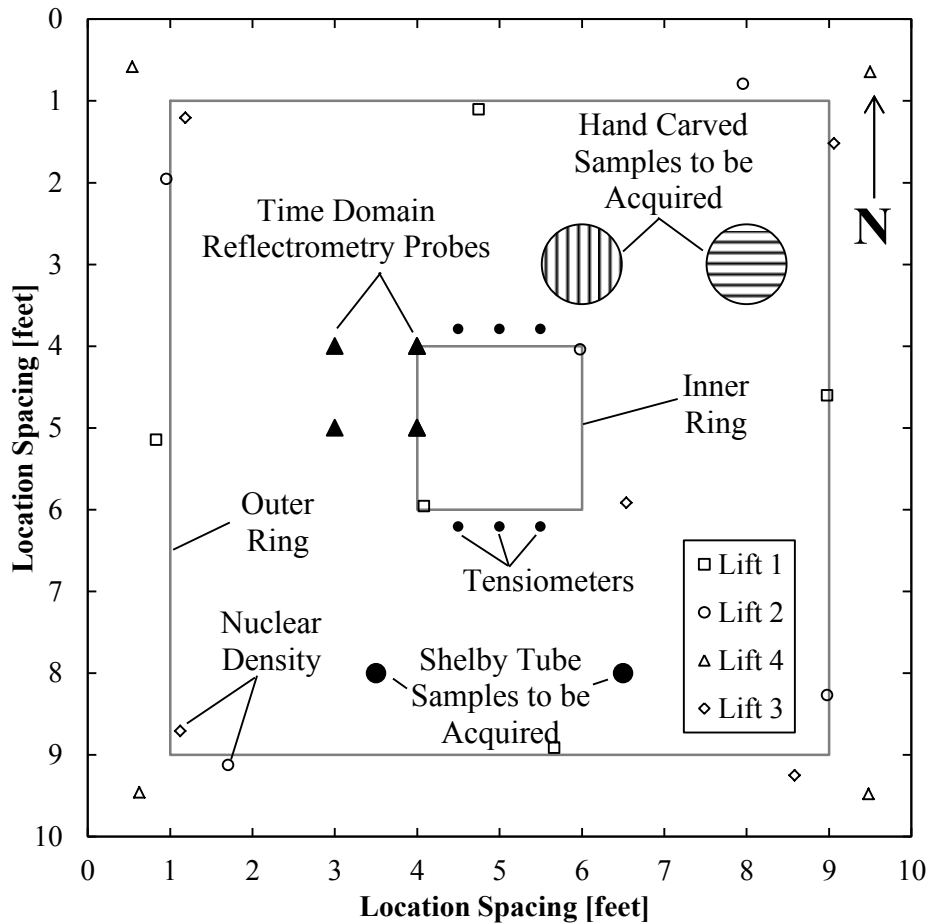


Figure 3.13. Unit weight testing locations, in-situ hydraulic conductivity testing locations, instrumentation locations, and anticipated sample locations within Test Pad 3.

3.5.7 Removal of Soil

Following the completion of the hydraulic conductivity testing (to be described in Section 3.6) and Shelby tube sample acquisition (to be described in Section 3.7.1), soil was removed from the box by removing the wall facing on the South side of the box (Figure 3.14a). An electric-powered jack hammer was used to break up the compacted test pad (Figure 3.14b) and the loose soil was loaded into wheelbarrows using shovels (large soil clods were loaded by hand). The wheelbarrows were used to transport the soil through the ERC to the garage door and the soil was then loaded in the front bucket of the tractor (Figure 3.15). The soil was then transported to the outside stockpile and dumped. After work was completed, the outside

stockpile was covered with a tarp. For Test Pads 1 and 2, most of the soil was removed in one day with a small section in the Northeast corner left in place for hand carved sampling (to be described in Section 3.7.1).

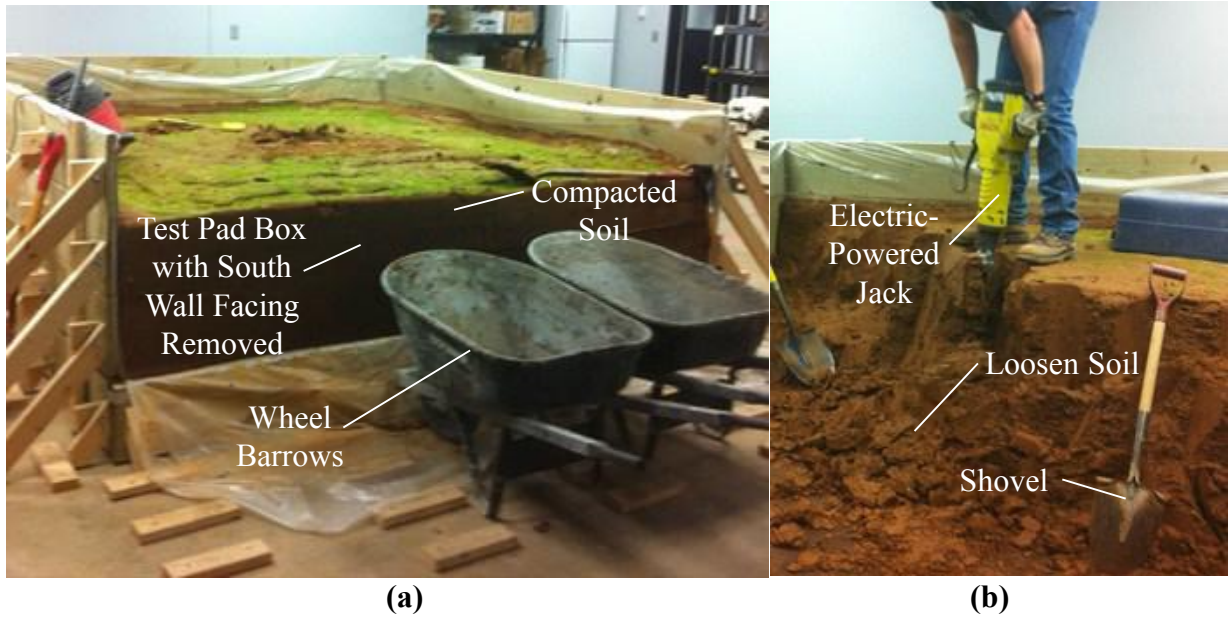


Figure 3.14. (a) South wall removed from test pad box for test pad removal, and (b) electric jack being used to break up the soil.



Figure 3.15. Soil being transferred from wheelbarrows to the front bucket of the tractor.

3.6 *In-Situ Hydraulic Conductivity Testing in the Test Pad Box*

One in-situ hydraulic conductivity test was performed within each test pad. Two stage borehole (TSB) tests were conducted within Test Pads 1 and 2 (Section 3.6.1) and a sealed double ring infiltrometer (SDRI) test was conducted within Test Pad 3 (Section 3.6.2). All of the tests were conducted until steady state flow was achieved.

3.6.1 *Two Stage Borehole Testing*

As described in Section 2.3, two stage borehole (TSB) testing was conducted in accordance with ASTM D6391 (2012) Method A. One TSB was installed in both Test Pads 1 and 2. Additionally, one temperature effects gauge (TEG) was installed in both test pads in order to monitor volumetric effects of the permeameter and permeant caused by changes in temperature.

The TSB was located in the center of the test pad and the TEG was positioned three feet from the North and West wall faces. The TSB and TEG casings were 12-inches long, made from polyvinyl chloride (PVC) DWV COEX cellular core schedule 40 pipe by Silver-Line Plastics and the bottom of the casings were installed ten inches below the soil surface. A six-inch diameter standard hand auger (Figure 3.16) was used to auger to a depth of approximately nine inches. Then a six-inch diameter flat bottom auger (Figure 3.16) was used to advance the borehole to the full depth of ten inches. The casing was centered in the borehole and the annular space outside of the casing was filled with dry pelletized bentonite (ENVIROPLUG No. 8 obtained from WYO-BEN, Inc. with at least 98-percent passing the No. 4 sieve and no more than 5-percent passing the No. 20 sieve). The dry pellets of bentonite were packed in one-inch thick lifts and then water was added to hydrate each lift as it was placed. The top inch of the annular space was packed with cuttings from the borehole to prevent the bentonite from drying out.

Installation of the TEG followed the same process as the process for installing the TSB casing. Ten-pounds of weights were added to the top of each of the casings to prevent the casing from lifting out of the test pad as the bentonite hydrated for 24 hours (Figure 3.17a). After the bentonite was hydrated, the weights were removed and the soil at the bottom of the casing was roughen with a wire brush (Figure 3.17b). A nylon sock filled with clean gravel was inserted into the casing and the standpipe apparatus was attached.

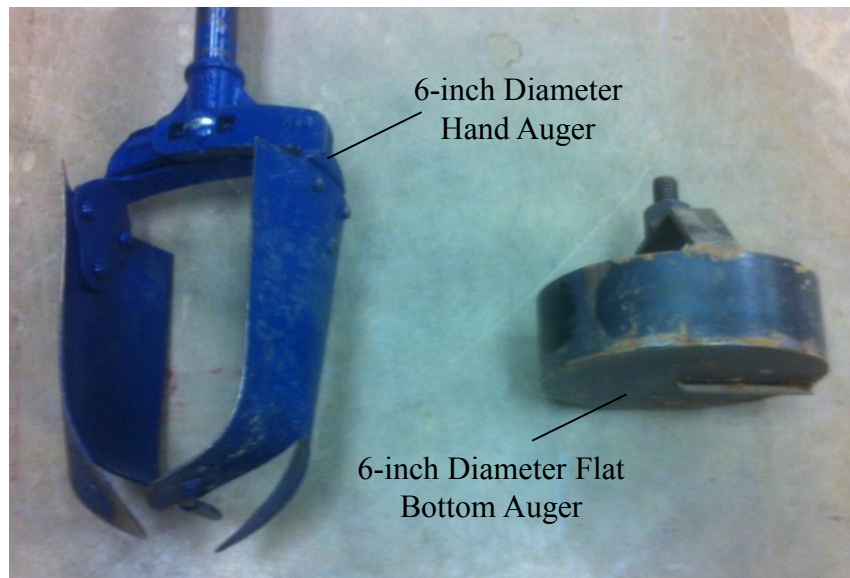


Figure 3.16. Augers used for Stage 1 borehole excavation for TSB testing.

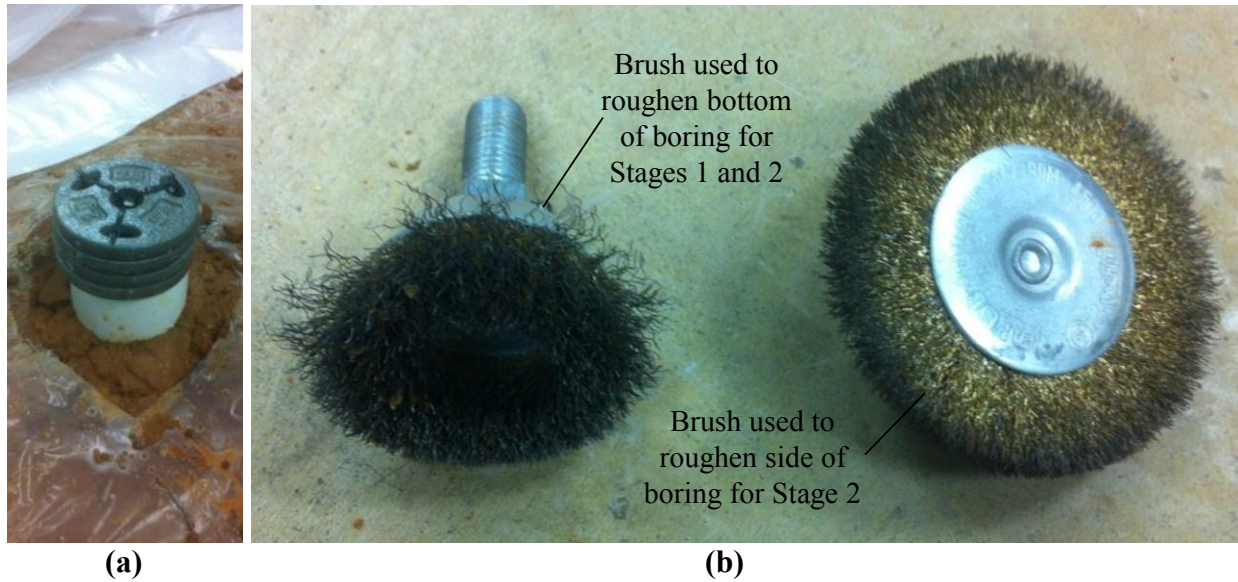


Figure 3.17. (a) Weight placed on recently installed casing, and (b) brushes used to roughen permeated surfaces.

Each standpipe apparatus (Figure 3.18a) was comprised of a clear acrylic tube with an internal diameter of 1.5 centimeters attached to a PVC cap mounted on to the top of the PVC casings by means of a rubber gasket and hose clamps. The PVC caps contained a connection for a water supply. To obtain more accurate readings and more readings for a given time period, rods with diameters of 1.315 centimeters were inserted into the tubes resulting in an effective standpipe diameter of 0.814 centimeters. Elbow pieces with rubber stoppers were attached to the top of the tube to prevent evaporation of water from the standpipes. A 1/8-inch diameter hole in the center of each rubber stopper opened the inside of the apparatus to atmospheric pressure. As described previously, the TEG was assembled in the same way as the TSB however the bottom of the TEG casing was sealed with a flat PVC cap to prevent water from escaping. Additionally, a Type K thermocouple wire was inserted through the rubber stopper and into the water in the TEG to monitor water temperature, which was measured using an Omega Model HH501DK thermocouple readout device. A second Type K thermocouple wire also connected to the Omega thermocouple readout device was used to monitor ambient temperature. The TSB and TEG were

filled with water and monitored to ensure that no air bubbles were located inside of the testing apparatus.

To conduct TSB testing, the standpipe was filled to a standpipe water level height of 15 centimeters as measured using the ruler on the standpipe. The valve used to fill the standpipe was then closed, an initial reading was obtained, and a stopwatch was started simultaneously. Consecutive readings were obtained during the TSB test including the water level in the standpipe and the elapsed time from the stopwatch. The ambient temperature, TEG water temperature, and water level of the TEG were also obtained when a reading was obtained on the TSB. When the water level reached the bottom of the standpipe (a water level of zero centimeters), the test was either restarted at an initial height of 15 centimeters or the water supply connection valve was opened to allow for continuous, unmonitored flow. When the water supply connection remained open, the elevated water supply was removed from the bucket and placed on the test pad to ensure that the water level in the standpipe did not exceed 15 centimeters; thereby preventing hydraulic fracturing of the soil. At a standpipe height of 15 centimeters, the ratio of hydraulic head to total overburden pressure is 1.45. Stage 1 was conducted until steady state flow was achieved. A photo of the TSB testing apparatus is shown in Figure 3.18b. Collection of data in Stage 2 followed the same data collection procedures as followed in Stage 1.

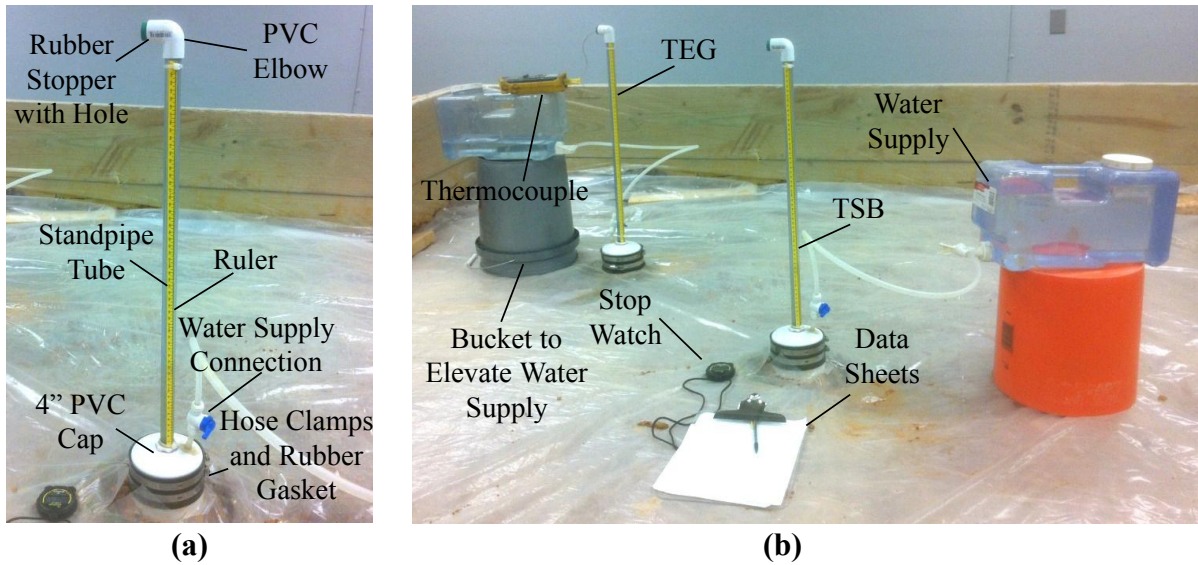


Figure 3.18. (a) TSB standpipe apparatus, and (b) TSB testing apparatus.

Following completion of Stage 1, the standpipe apparatus on the TSB was removed, the nylon sock with gravel was removed, and then the water from within the casing was removed using a vacuum. the borehole was then extended six inches below the bottom of the casing using the previously described four-inch diameter standard hand auger to a depth of 15 inches and the previously described four-inch diameter flat bottom auger to a depth of 16 inches below the soil surface. As shown in Figure 3.19, the extended borehole was roughened on the sides and bottom with the wire brushes that were previously presented in Figure 3.17. An additional nylon sock with clean gravel was inserted into the open space to account for the open volume in the borehole and then the previously used nylon sock was reinserted. The standpipe apparatus was then reconnected and Stage 2 was conducted.



Figure 3.19. Photo of extended borehole.

TSB testing on Test Pad 1 began on May 31, 2011. Stage 1 was conducted for 56 days until July 26, 2011, when the borehole was extended and Stage 2 was started. Stage 2 was conducted for four days. The results obtained from Test Pad 1 are documented in Maldonado and Coffman (2012). TSB testing in Test Pad 2 was conducted for 182 days. Stage 1 began on January 4, 2012 and was conducted until April 12, 2012. The borehole was extended on April 13, 2012 and Stage 2 was conducted until July 4, 2012. The measured TSB data was analyzed using the ASTM D6391 Method A method, as previously described in Section 2.5.6, to obtain the hydraulic conductivity values for Stage 1 and Stage 2. The Soil Testing Engineers, Inc. (1983) method for calculating the anisotropy value was utilized to calculate vertical and horizontal hydraulic conductivity values. Results obtained from the TSB testing are presented in Section 4.5.1.

3.6.2 Sealed Double Ring Infiltrometer Testing

As discussed in Section 2.3, the sealed double ring infiltrometer (SDRI) test was conducted in accordance with ASTM D5093 (2012). A two-foot by two-foot sealed inner ring

was used to measure the value of vertical hydraulic conductivity and an eight-foot by eight-foot outer ring was used to provide constant hydraulic head and to ensure one-dimensional (vertical) flow beneath the soil surface. The installation of the inner and outer rings is discussed in Section 3.6.2.1. Time domain reflectometry probes were used to measure the volumetric moisture content of the test pad at six locations as a function of time. Tensiometers were used to measure soil suction at six locations as a function of time and to monitor the movement of the wetting front through the subsurface. Installation procedures utilized for installing the TDR probes and the tensiometers are discussed in Sections 3.6.2.2 and 3.6.2.3, respectively.

3.6.2.1 Installation of SDRI Rings and Vertical Hydraulic Conductivity Testing

Sealed Double Ring Infiltrometer (SDRI) testing was conducted in accordance with ASTM D5093 (2012). The SDRI test was conducted with an eight-foot by eight-foot square outer ring and a two-foot by two-foot square inner ring (Figure 3.20). The outer ring was comprised of 1/8-inch thick aluminum sheets (folded at the top and corners), bolted together and sealed with rubber gaskets. The inner ring was obtained from Trautwein Soil Testing Equipment Company of Houston, TX.

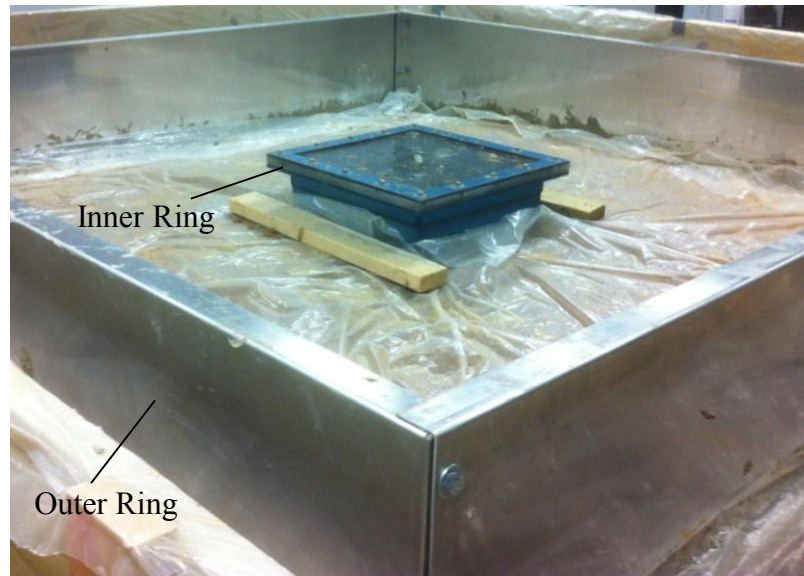


Figure 3.20. Inner ring and outer ring used for SDRI testing (photo taken during installation).

The inner ring of the SDRI test was installed by first centering the ring within the test pad. The location of the ring was marked by slightly pushing the ring into the ground. The ring would not penetrate into the soil under an applied load; therefore a thin, shallow (approximately one inch deep) trench was excavated at the location of the wall with a metal putty knife. The ring was then set in place and pushed three inches into the test pad using the weight of four grown men.

The outer ring was positioned around the inner ring and the location of the ring was marked by scoring the top of the test pad using a metal ruler around the outside of the outer ring. The ring was then removed and a chainsaw was used to cut a trench (because clay was being cut with the chainsaw, clay cuttings collected inside the housing of the chainsaw and mixed with the bar and chain oil which caused grime to collect around the rotor and prevented proper lubrication of the blade which caused over heating of the blade). The nominal depth of the trench was 5.5 inches but was limited to a depth of 4.5 inches near the buried Time domain reflectometry probe wires. Using a chainsaw for trenching yielded a clean cut, but it was difficult to manually control

the path of the chainsaw cut. The width of the chainsaw cut trench ranges from 0.25 inches to one inch. A bentonite grout, mixed at 300 percent moisture content, was manually placed in the bottom of the trench to hydraulically seal water from leaking around the outer ring. After filling the trench with bentonite, the outer ring was set in place. The ring refused to seat fully inside the trench. The initial assumption was that the trench was not excavated to the prescribe depth in all areas. Removal of the outer ring was attempted but because of the suction caused by the grout, the ring could not be removed without first removing the surrounding soil.

Because the ring could not be removed initially, the ring was left in place for two to allow the grout time to dry out and could become more workable for excavation of the ring. Two outside sides (the West and South) of the outer ring were excavated down to the bottom of the ring. After the outside sides were cleared, the ring was lifted out of the liner. The old bentonite grout was excavated and a deeper and wider trench was opened using the claw side of a claw hammer. It was confirmed after excavation with the claw hammer, the trench did not reach the prescribed depth in all areas. The trench excavated using the claw hammer had a nominal width of one inch (Figure 3.21a). Because the depth of the trench was controlled by the buried wires, the depth of the buried TDR wires served as the control depth and was measured using a ruler and a tripod mounted automatic level. The control depth was determined so that the ring would not penetrate and cut the TDR wires. The ruler and level were then used to ensure the depth of the trench around the perimeter of the ring was level with the control depth. After the trench was complete, the ring was dry fitted into the trench and checked for plum and level. The ring was then removed from the trench and the trench was halfway filled with new bentonite grout at 300 percent moisture content (Figure 3.21b). The ring was then pushed into the grout inside the trench until it was fully seated, plum, and level. Remaining voids in the trench, between the soil

walls and ring walls, were filled with the remaining grout. Four-inch by four-inch support blocks were used to brace the outer ring against the sides of the test pad box to prevent the ring from bowing. The rings were allowed to sit for four days until the tensiometers were installed (discussed later in Section 3.6.2.3) and the rings were filled with water. After the four day period, cracks were observed in the soil coming from the inner ring and, although the soil was still hydrated, desiccation cracks were noticed in the bentonite grout.

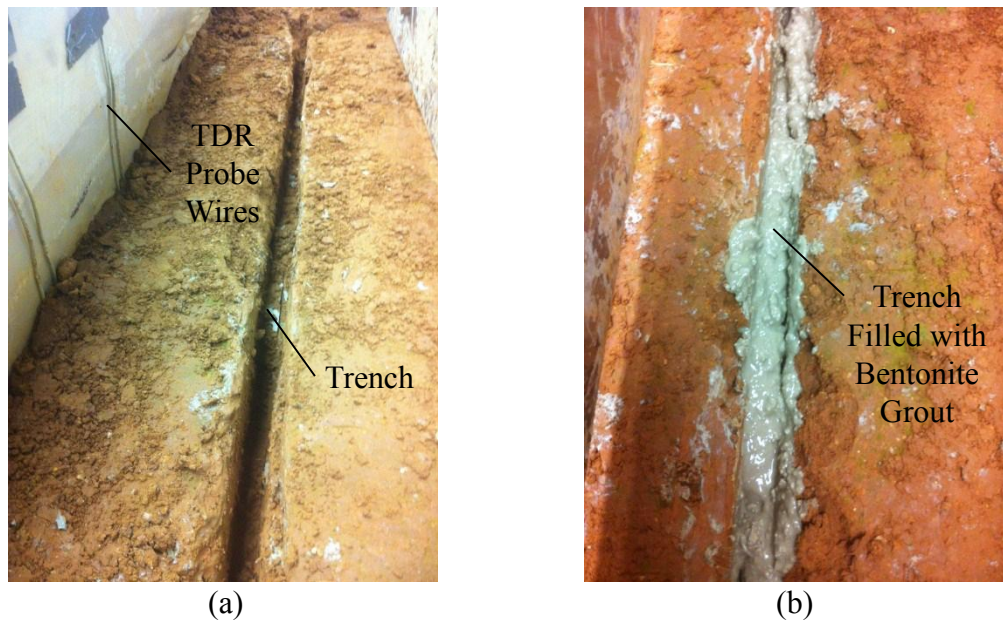


Figure 3.21. (a) Trench excavated with claw hammer (b) trench filled with bentonite slurry.

The two rings were filled simultaneously to prevent uplift of the inner ring. The outer ring was filled using a garden hose and the inner ring was filled using a water container and small tubing. Two ports were located on the top of the inner ring and were used to fill the inner ring and to remove entrapped air. During filling, leaks occurred from under the outer ring and around the rubber gaskets adjoining the panels of the outer ring. The leaks under the outer ring occurred because of the high hydraulic head forcing the bentonite grout out of the trench. These leaks were stopped by filling the holes with dry bentonite pellets and placing a soil berm on top of the bentonite trench on the outside of the outer ring to prevent the grout from being pushed

out. The leaks around the rubber gaskets occurred because the rubber was not pliable enough to form against the walls of the outer ring. These leaks were stopped by sealing the joints of the outer ring on the inside with an underwater epoxy. After the leaks were observed to have stopped, the rings were filled until the measured water level was one foot above the soil surface, as measured near the inner ring (due to undulations in the soil surface within the box). The air bubbles entrapped in the inner ring were removed using a piece of wire to push the air bubbles to the open port.

Hydraulic conductivity measurements for the SDRI test began on October 7, 2012, and are still being conducted. To begin testing, one of the ports on the inner ring was clamped off and a two-foot long piece of tubing was connected to the other port. A clamp was attached to the end of the tubing to ensure that no air bubbles entered the tubing during detaching and reattaching the flexible intravenous (IV) bag. A flexible bag was fitted with a small piece of tubing and a through connector was used to attach the bag to the tubing connected to the inner ring prior to connecting the bag to the ring. The bag was filled with tap water and the air bubbles were removed. A clamp was attached to the small piece of tubing on the bag to prevent water from escaping the bag during weighing. The bag was initially weighed using an OHAUS Explorer Pro Model EP12001 balance (Figure 3.23) and then attached to the inner ring (Figure 3.22). The bag was then connected to the inner ring with the connection made under water to prevent air bubbles from entering the bag or inner ring. Following connection of the bag to the ring both clamps were released. The time and date that the clamps were opened was recorded along with the initial weight of the bag and temperature of the water. After a given amount of time (three to five days), the clamps were closed and the bag was disconnected and reweighed. The previously mentioned required data (weight and temperature) was recorded and the bag was reconnected. This process

was repeated for each test reading. The hydraulic conductivity was calculated using the equations previously discussed in Section 2.3. During testing, the flexible bag remained submerged to ensure an equivalent hydraulic head in both the inner and outer rings. While weighing the bag, algae were noticed to be growing on the flexible bag. To minimize errors in the weight readings, the outside of the bag was always dried and wiped clean with a paper towel before being weighed.

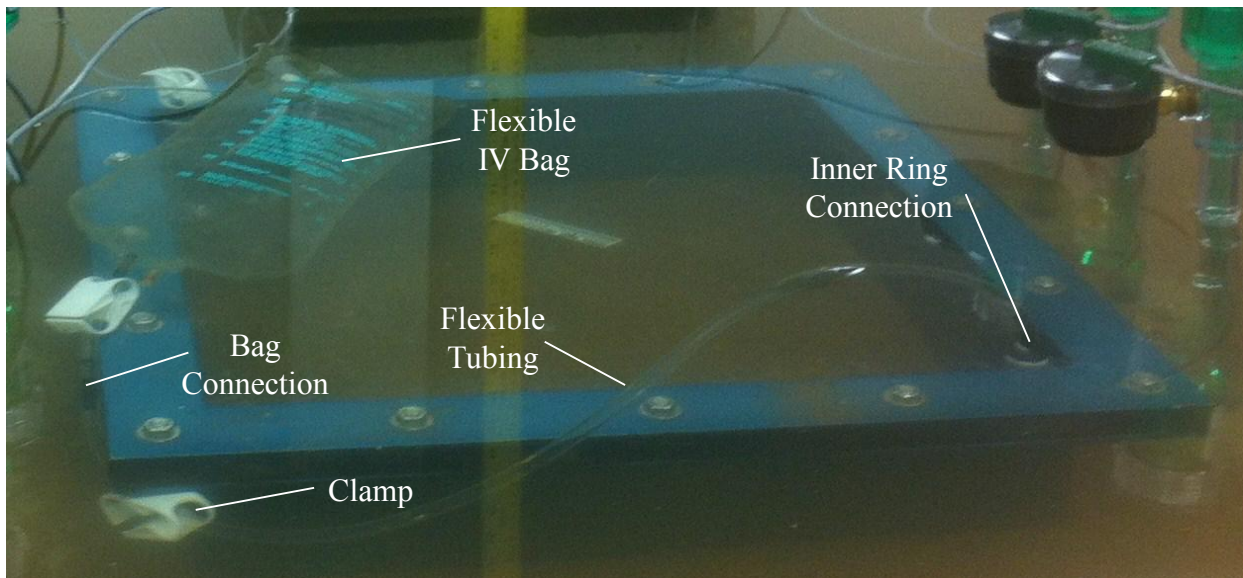


Figure 3.22. Inner SDRI ring under water with connected flexible bag.

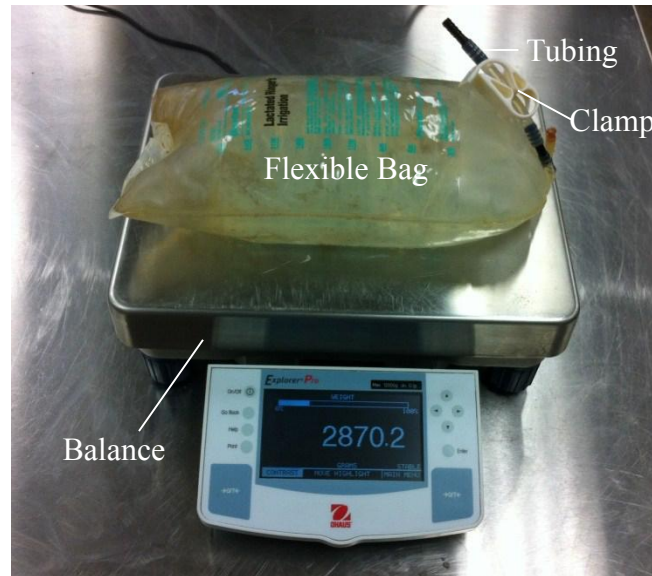


Figure 3.23. Flexible intravenous bag filled with water and being weighted on a balance.

3.6.2.2 Installation of the Time Domain Reflectometry Probes and Data Collection

Time domain reflectometry (TDR) probes were installed to monitor the location of the wetting front via changes in volumetric moisture content. The probes used for Test Pad 3 were obtained using Campbell Scientific TDR probes (model CS645) that have a rod length of 7.5 centimeters. Two TDR probes were installed in Lift 2, two TDR probes were installed in Lift 3, and two TDR probes were installed in Lift 4 (six total). At a determined location (as shown previously in Figure 3.13), a three-inch deep soil block was removed from the surface of the given lift using a sharpshooter spade shovel (Figure 3.24a). The two TDR probes in Lifts 2 and 3 were installed four feet from the West wall face with one set of probes being located four feet from the North wall facing and the other set of probes being located five feet from the North wall face. The probes in Lift 4 were installed similar to Lifts 2 and 3 in the North/South direction. However, the probes were located three feet from the West wall face. The three pronged unshielded conductors were inserted horizontally (Figure 3.24b) into the soil at a depth of two inches below the surface of the lift. A smooth excavation facing insures that the probe is in close

contact with the soil and that reliable measurement are obtained. The removed compacted soil was crumbled and recompact around the TDR probe housing. The probes were connected to a Campbell Scientific SDM-50 multiplexer that was connected to a Campbell Scientific CR-10X data collector which recorded hourly readings. Results obtained from the TDR data will be presented in Section 4.5.2.

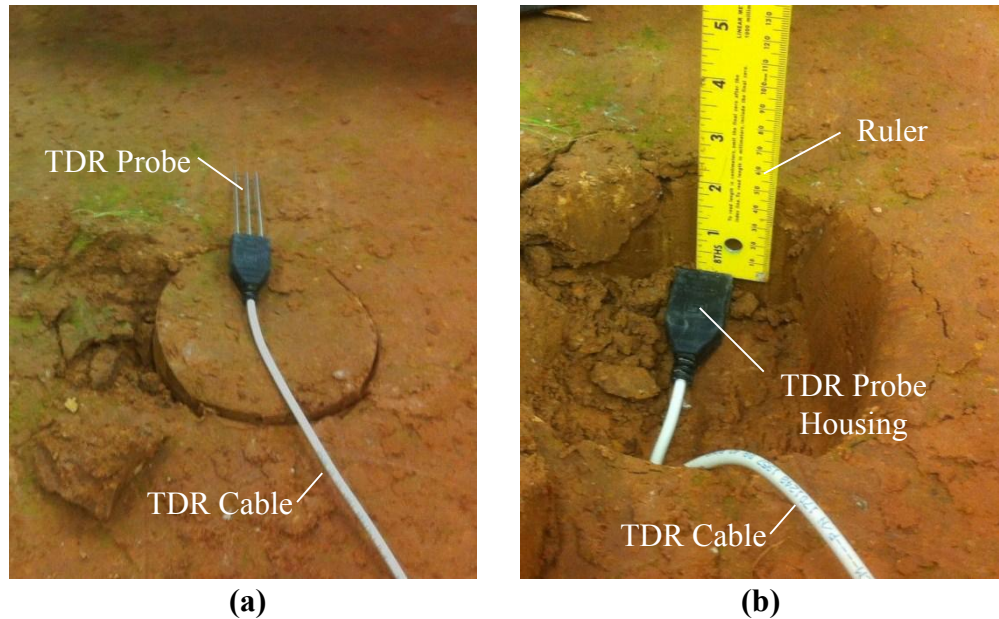


Figure 3.24. (a) Soil block cut for TDR probe, (b) TDR probe installed in the test pad.

3.6.2.3 Installation of Tensiometers and Data Collection

Six IRROMETER Model S tensiometers, with a 0.86-inch outer diameter, fitted with an “E” Gauge were installed in Test Pad 3 to monitor the wetting front during the SDRI test (Figure 3.25a). Before being installed the probes were soaked overnight in deionized deaired water to ensure saturation of the gypsum block tip. Three probes were installed 2.5 inches North of the North side of the inner ring and three probes were installed 2.5 inches South of the South side of the inner ring. The probes were installed nominally six inches apart from one another. Each tensiometer was one foot longer than the nominal installation depth to account for the one-foot height of water (one foot of head) inside of the outer ring for hydraulic conductivity testing.

Redundant probes (North and South sides) were installed at nominal depths of five inches, 11 inches, and 23 inches below the soil surface with overall probe lengths of 18 inches, 24 inches, and 36 inches, respectively (Figure 3.25b).

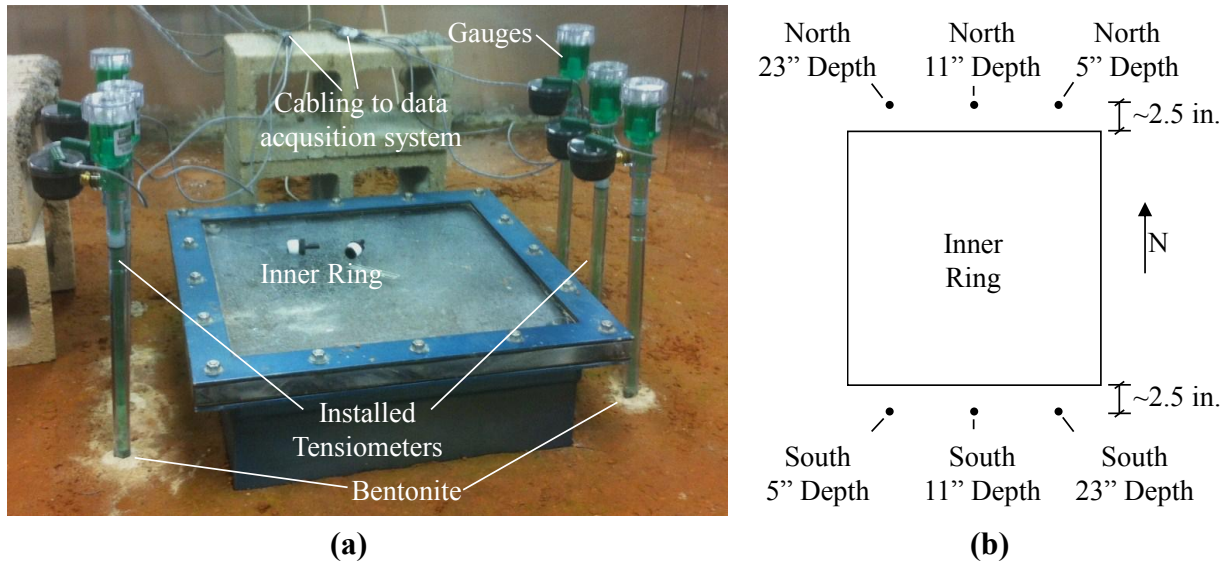


Figure 3.25. (a) Figure of installed tensiometers, and (b) schematic of probe location with nominal depth.

To install the five-inch deep probes, a five-inch deep hole was augered using an IRWIN 3/4-inch diameter by 18-inch long woodboring auger drill bit and a PORTER-CABLE 7-amp 1/2-inch variable speed hand drill (Figure 3.26). After augering, the cuttings in the bottom of the hole were cleared using small tubing connected to a shop vacuum. After vacuuming each of the five inch deep probes were then pushed into the hole until they were fully seated. Crushed bentonite (Pondseal obtained from Redmond Bentonite) passing the No. 20 (853- μ m) sieve was placed around the tensiometers at the soil surface to create a seal.

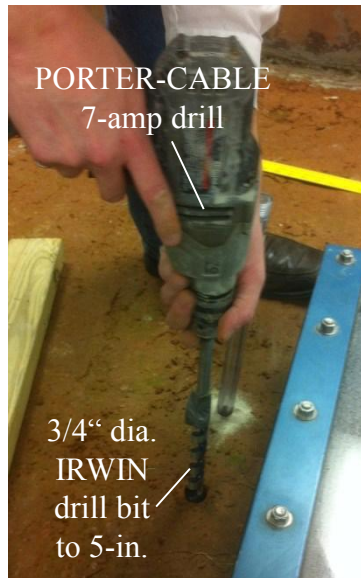


Figure 3.26. Drilling a five-inch deep hole.

The 11-inch deep probes were installed by augering an 11-inch deep hole with the aforementioned 3/4-inch diameter bit (Figure 3.27a). An IRWIN 1-inch diameter by 18-inch long woodboring auger drill bit was used to auger six inches into the previously drilled hole to reduce skin resistance in the upper six inches of the hole during probe installation. After the oversized hole was drilled, the 3/4-inch diameter bit was inserted back into the hole to full depth to ensure that the hole was cleaned and reamed. Any cuttings remaining in the hole were then removed using a vacuum and the probe was then installed to full depth (11 inches). Crushed bentonite (Pondseal obtained from Redmond Bentonite) passing the No. 20 (853- μm) sieve was placed in the annular spaces around the probes (0-6 inches deep) and around the tensiometer probes at the soil surface to create a seal (Figure 3.27b).

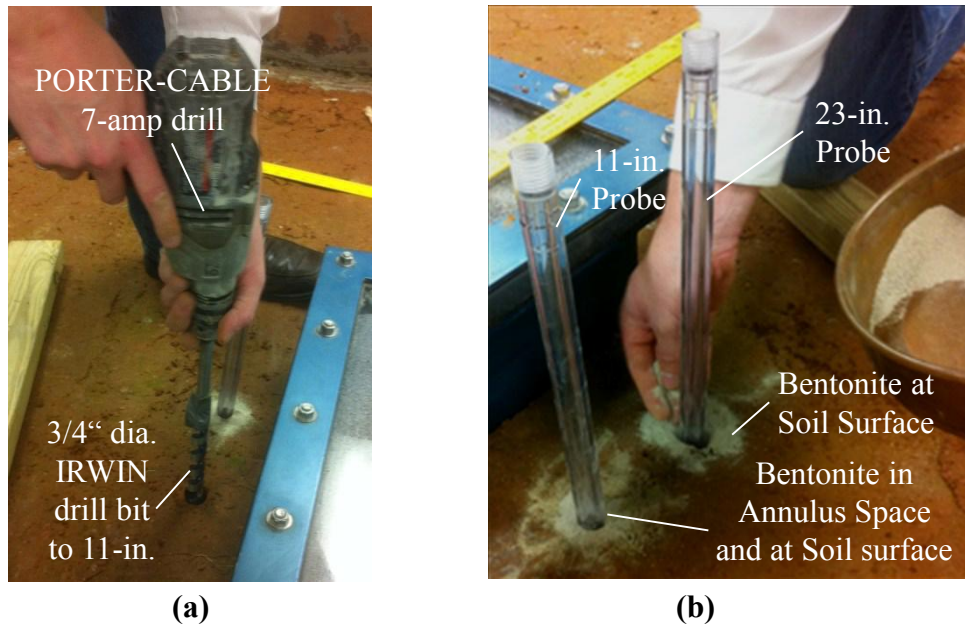


Figure 3.27. (a) Drilling an 11-inch deep hole, and (b) backfilling the annular space with bentonite.

The 23-inch deep probes were installed by using the aforementioned 3/4-inch diameter bit (Figure 3.28a) to auger the holes to a depth of 12 inches below the soil surface, which is where the augered flights on the bit ended. The hole was cleaned and then the same 3/4-inch diameter bit was used to auger to a depth of 16 inches below the soil surface (Figure 3.28b). The aforementioned one-inch diameter bit (Figure 3.28c) was then used to auger to 12 inches below the soil surface to reduce skin resistance in the upper 12 inches of the hole (Figure 3.28d) while installing the probe. An IRWIN 7/16-inch Hex Quick Connect 12-inch long Drill Bit Extension was attached to the aforementioned 3/4-inch diameter bit (Figure 3.28e) and the bit and extension were then used to extend the borings (Figure 3.28d) to a depth of 23 inches below the ground surface (Figure 3.28f). The cuttings remaining in the hole were removed using a vacuum and the probes were installed until the bottom of the hole was reached (Figure 3.28g). Crushed bentonite (Pondseal obtained from Redmond Bentonite) passing the No. 20 (853- μ m) sieve was placed in the annular spaces around the probes (0-12 inches deep) and around the tensiometer probes at the soil surface to create a seal.

Irrrometer “E” electric gauges were attached to each of the installed probes. The probes were then filled with a solution of deionized deaired water and a concentrated chemical solution supplied by the Irrrometer Company. The electric gauges were connected to a Campbell Scientific AM-416 multiplexer that was connected to the aforementioned Campbell Scientific CR-10X data collector and hourly readings were recorded via the data collector. Entrapped air in the tensiometers was removed by using a vacuum pump (Figure 3.28h). Results obtained from the tensiometer data will be presented in Section 4.5.2.

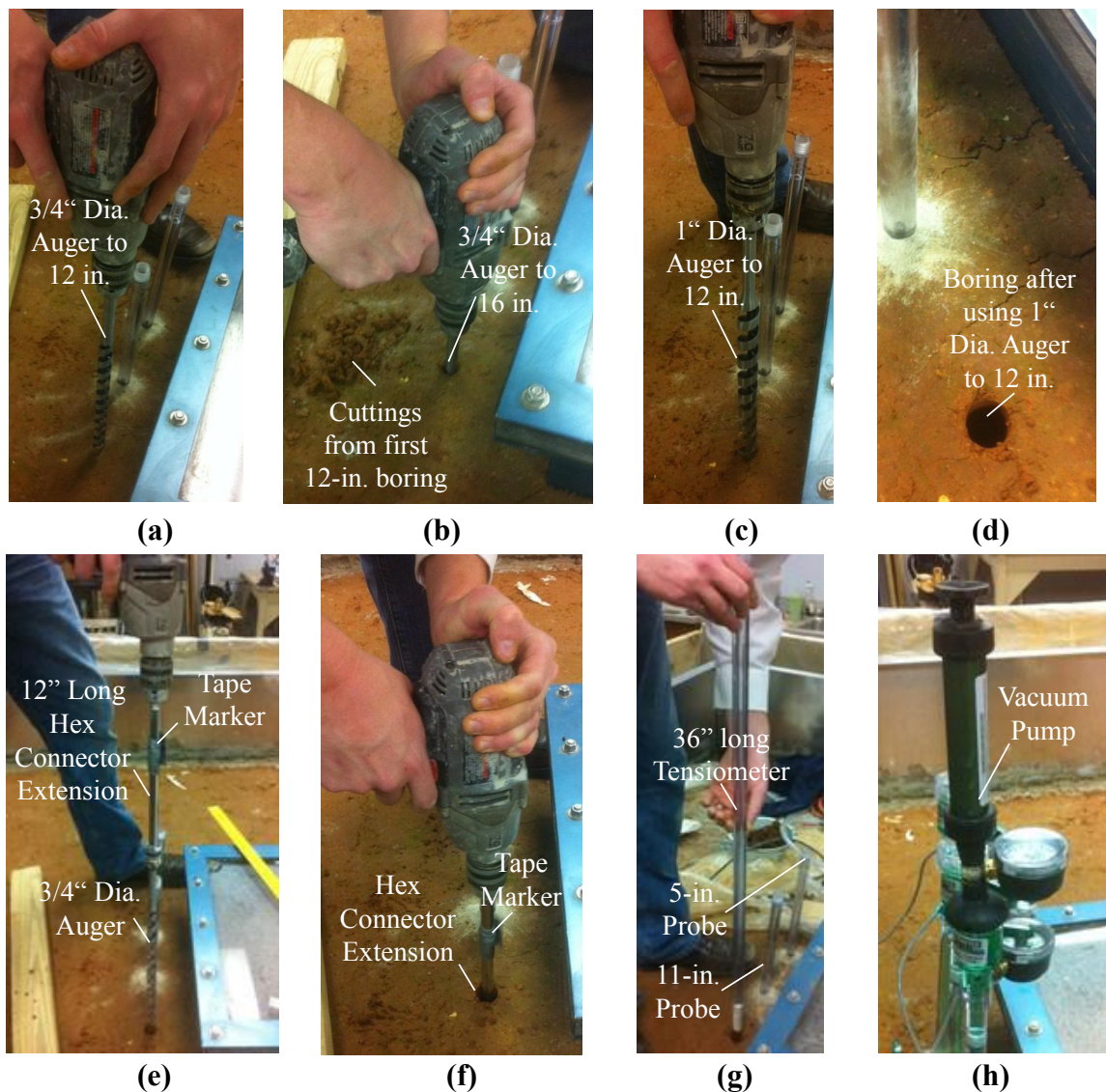


Figure 3.28. (a) 3/4-inch diameter bit augered to depth of 12 inches, (b) 3/4-inch diameter bit augered to depth of 16 inches, (c) 1-inch diameter bit augered to depth of 12 inches, (d)

borings after using 1-inch diameter bit to a depth of 12 inches, (e) 3/4-inch diameter drill bit attached to 12-inch long extension rod, (f) 3/4-inch diameter drill bit and 12-inch long extension rod augered into the test pad to a depth of approximately 21 inches (as determined by bottom of tape marker being 23-inches), (g) 23-inch deep probe being installed in drilled hole, and (h) vacuum pump applied to tensiometer.

3.7 Sample Acquisition

Soil samples were collected by: pushing Shelby tubes, collecting hand carving samples, and collecting cuttings from the TSB borings and placing them into plastic bags. Following collection of the samples, the samples were labeled and transported to BEC for laboratory testing. Samples were stored in an environmental chamber at 15-degree Celsius until either laboratory hydraulic conductivity (flexible wall hydraulic conductivity) or soil property (moisture content, specific gravity, grain size, percent passing No. 200 sieve, and Atterberg limits) testing was performed.

3.7.1 Shelby Tube Samples

Following the in-situ testing described in Section 3.6, Shelby tubes were pushed into Test Pad 1 using a forklift with a 1,500-pound concrete block mounted on the forks. A sampling apparatus was created by welding an AWJ rod with a Shelby tube sampler adapter head connected to one end to a U-channel steel beam. Thirty-six (36)-inch long thin-wall Shelby tubes were attached to the sampler adapter head and were held in place by hand on the test pad at predetermined locations. A level was used to ensure that the tubes were pushed vertically. Using the forklift, the concrete block was rested on top of the sampling apparatus and the forks of the forklift were lowered to push the Shelby tubes 24 inches into the test pad (Figure 3.29a). The specified sample depth was achieved by placing a mark on the Shelby tubes 24-inches from the sampling end of the Shelby tube and pushing the tubes until the mark reached the soil surface. The concrete block was then set aside and the forklift was used to retrieve the Shelby tubes (Figure 3.29b) by pulling up on the u-channel with the forks of the forklift. For storing the tubes,

a gasket was inserted inside each end of the Shelby tubes. The tubes were then labeled, capped, and sealed with duct tape (Figure 3.29c).

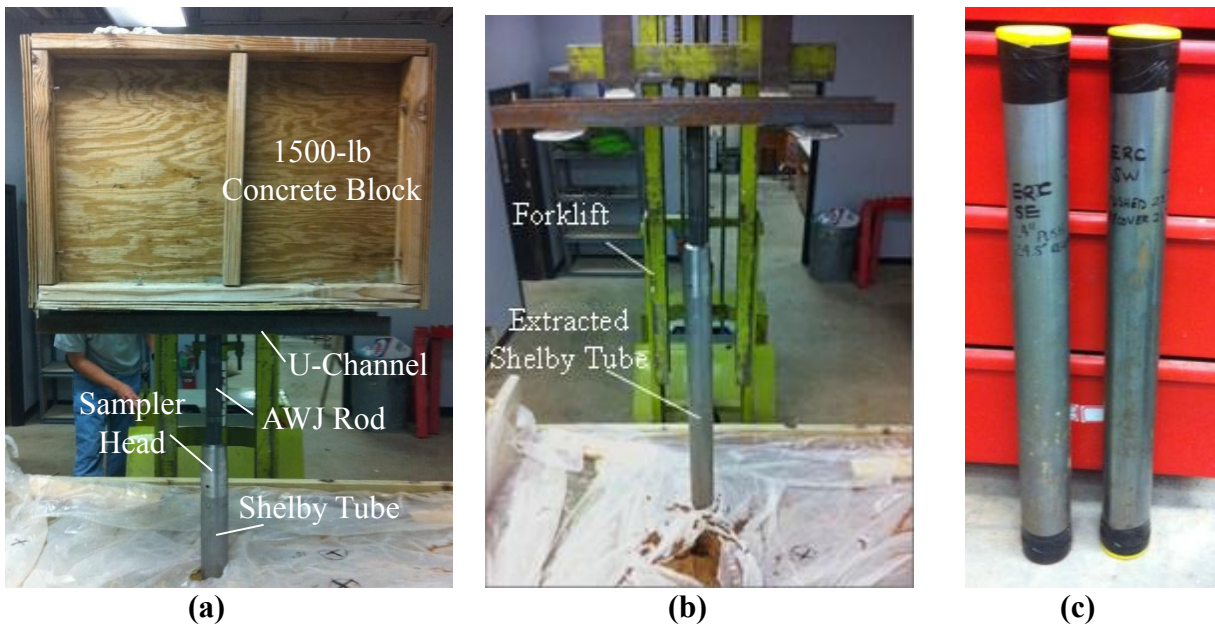


Figure 3.29. (a) Shelby tube sampling apparatus pushing the Shelby tube into the soil, (b) retrieved, capped, and labeled of the Shelby tube, and (c) pushed Shelby tubes that have been pushed into and retrieved from the Test Pad.

Two Shelby tubes were collected from Test Pad 1. The Southwest Shelby Tube (SW-ST-TP1) was used for soil properties testing. SW-ST-TP1 was pushed 23.5 inches into the soil and 21.25 inches of soil was recovered after extraction. The Southeast Shelby Tube (SE-ST-TP1) was used for flexible wall hydraulic conductivity testing. SE-ST-TP1 was pushed 24 inches into the soil and 24.5 inches of soil was recovered after extraction. A diagram of the Shelby tubes collected is presented in Figure 3.30. The tubes from Test Pad 1 were not stored in an environmental chamber prior to laboratory testing due to inexperience of storing collected field samples. Drying of the samples was noticed as will be discussed later in Section 4.6.1. To determine the thickness of each lift inside the Shelby tubes, the average measured thickness (from the rod and level measurements) of the respective lift was reduced by the ratio of the recovered length to the pushed length. For the Shelby tube used for soil index testing, the tube

was divided at each lift interface. For the Shelby tube used for laboratory hydraulic conductivity testing, the tube was divided to obtain one sample from each lift and one sample from each lift interface.

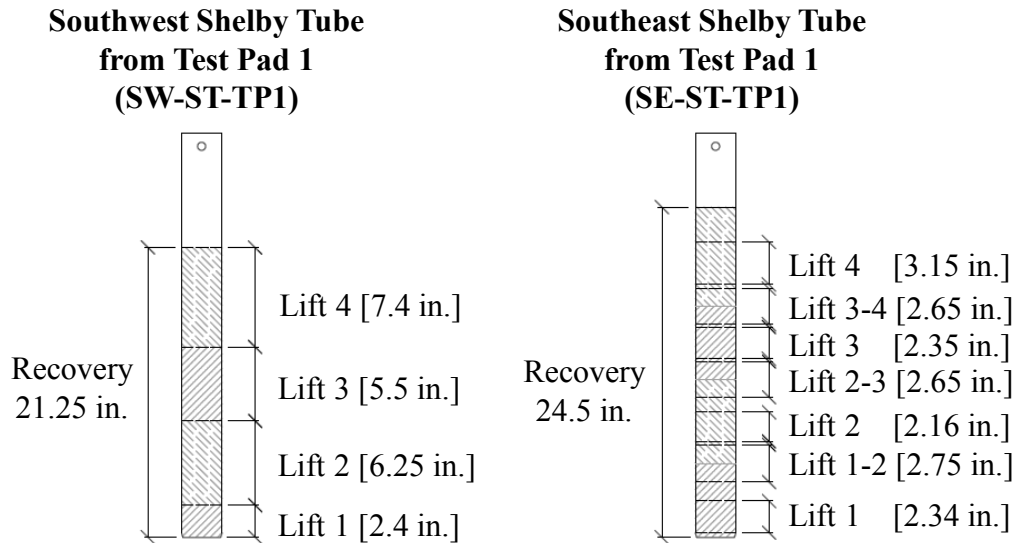


Figure 3.30. Cross-section diagram of Shelby tubes collected from Test Pad 1.

Shelby tubes pushed in Test Pad 2 were collected using the same sampling apparatus used for Test Pad 1 however the forklift that was used to push and extract the Shelby tubes into and out of Test Pad 1 was not available for sampling of Test Pad 2. Instead, the Shelby tube sampling apparatus was pushed using dead weight and human applied force. The sampling apparatus was placed in predetermined locations and a steel H-beam was placed on the U-channel. Eight Portland cement bags (each weighing 92.6 pounds) were placed on the steel beam two at a time to prevent tilting of the apparatus (Figure 3.31). The combined weight of the steel beam and concrete bags pushed the tubes 18-20 inches into the test pad. For safety concerns, human force was used to push the tubes to a depth of 24 inches instead of adding more weight to the top of the apparatus. When the tube reached the desired depth, the weight was removed and the sampler head was disconnected from the tube. A gasket was inserted inside the top of the tubes. The tubes were left in place and removed during removal of the soil from the test pad box. After

removal from the test pad, a gasket was placed in the other of the tube and the ends of the tubes were sealed with wax for storing. The tubes were then capped, labeled, sealed with duct tape, and transported to BEC and placed in the environmental chamber at 15-degree Celsius until testing.



Figure 3.31. Shelby tube pushed into Test Pad 2.

Three Shelby tubes were collected from Test Pad 2. The Southwest Shelby Tube (SW-ST-TP2) was used for soil properties testing as discussed later in Section 3.8 and results presented in Section 4.6.3. SW-ST-TP2 was pushed 24 inches into the soil and 19.75 inches of soil was recovered after extraction. The Center Shelby Tube (CT-ST-TP2) was used for flexible wall hydraulic conductivity testing as discussed later in Section 3.8.1.1 and results presented in Section 4.6.1. CT-ST-TP2 was pushed 24 inches into the soil and 21 inches of soil was recovered after extraction. The Southeast Shelby Tube (SE-ST-TP2) was not used for laboratory testing because excessive lateral deformation was noticed at the soil surface after the tube was pushed. SE-ST-TP2 was pushed 24 inches into the soil and 21.5 inches of soil was recovered after extraction. A diagram of SW-ST-TP2 and CT-ST-TP2 is presented in Figure 3.32. The Shelby tubes from Test Pad 2 were divided similar to the Shelby tubes from Test Pad 1.

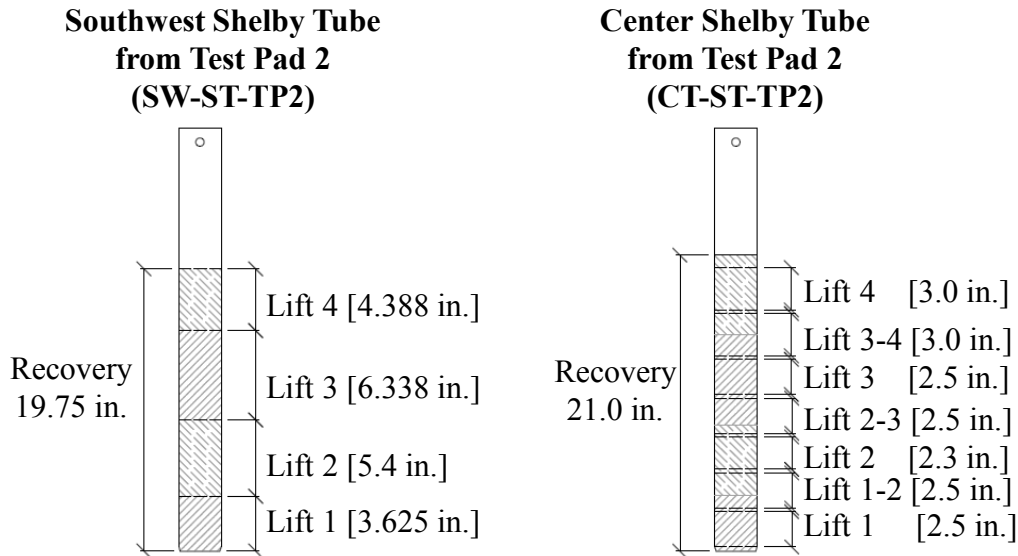


Figure 3.32. Cross-section diagram of Shelby tubes collected from Test Pad 2.

3.7.2 Hand Carved Samples

The locations of the hand carved samples (as shown previously in Figure 3.11 and Figure 3.12) were outlined by pressing a five-gallon bucket, with the bottom removed, into the test pad. The soil was then excavated to form a two inch ring around the bucket (Figure 3.33a). Starting from the top and carefully working down using the bucket as a guide, a hand saw was used to trim the soil to a nominal ten-inch diameter column. The column was then wrapped in plastic wrap (Figure 3.33b) to provide confining stress and cut into sections (using the hand saw) at the lift interfaces for vertical flow analysis or across the center of each lift for horizontal flow analysis. Each section was then completely wrapped in plastic wrap and labeled (Figure 3.33c). A total of seven samples from two hand carved samples were collected from Test Pads 1 and 2. The hand carved samples were only used for hydraulic conductivity testing as discussed later in Section 3.8.1.2 and results obtained from are discussed in Section 4.6.1.



(a) (b) (c)
Figure 3.33. (a) Rough column with bucket for a guide, (b) hand carved soil column wrapped in plastic wrap, and (c) soil block wrapped in plastic.

Two sets of hand carved columns were collected from each test pad (Test Pad 1 and Test Pad 2). The West hand carved columns (W-HC) were used for six-inch diameter vertical flow flexible wall hydraulic conductivity testing as discussed in Section 3.8.1.2 and results presented in Section 4.6.1. The East hand carved columns (E-HC) were used for four-inch diameter horizontal flow flexible wall hydraulic conductivity testing. The four-inch diameter was imposed because the lifts were six inches thick as discussed later in Section 3.8.1.2. A diagram of W-HC-TP1 and E-HC-TP1 is presented in Figure 3.34 and a diagram of W-HC-TP2 and E-HC-TP2 is presented in Figure 3.35. The average measured thickness (from the rod and level measurements) of the respective lift was used to determine the thickness of each lift in the hand carved soil column. The soil blocks from W-HC were cut apart at each interface to create four samples. The soil blocks from E-HC were cut apart at each lift midpoint to create three samples.

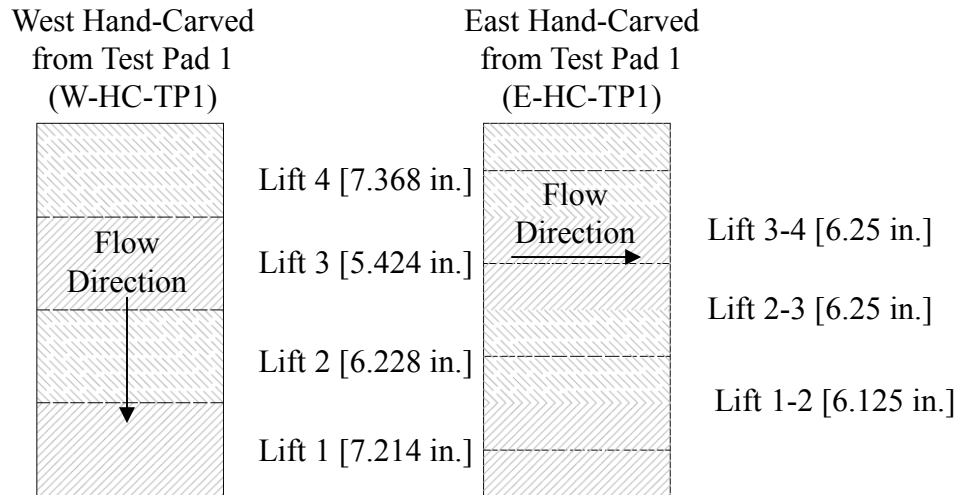


Figure 3.34. Cross-section diagram of hand carved columns collected from Test Pad 1.

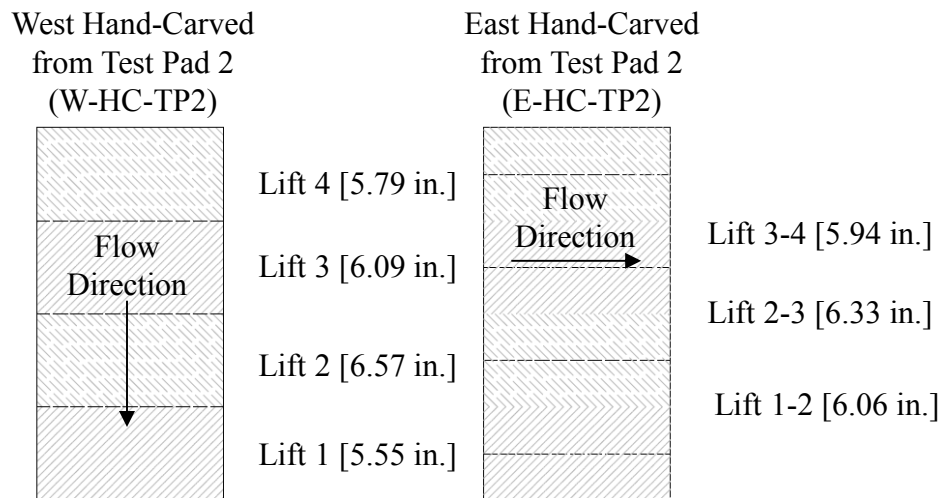


Figure 3.35. Cross-section diagram of hand carved columns collected from Test Pad 2.

3.7.3 Disturbed Samples

Disturbed samples were collected from the center of the TSB boreholes in Test Pads 1 and 2. Soil from each two-inch depth increment obtained during augering was collected and placed in a labeled plastic bag. Five samples were collected from the excavation of the borehole for the initial casing and three samples were collected from the excavation of the extension of the

borehole. The obtained samples were used for soil properties identification as described in Section 3.8 and results presented in Section 4.6.3.

3.8 *Laboratory Testing*

Laboratory testing was conducted on samples obtained from the test pad to determine soil properties with depth and to support the obtained in-situ hydraulic conductivity data. Soil samples were stored in an environmental chamber maintained at a temperature of about 15 degrees Celsius. Laboratory samples were either tested for hydraulic conductivity or for soil properties (e.g. specific gravity, particle size analysis, percent fines, and Atterberg limits).

3.8.1 *Flexible Wall Hydraulic Conductivity Testing on Samples Obtained from Test Pads*

As with the flexible wall hydraulic conductivity testing conducted on the Proctor samples as described in Section 3.3.2, flexible wall hydraulic conductivity testing was conducted on Shelby tube and hand carved samples in accordance with ASTM D5084 (2012) Method C. Hydraulic conductivity tests were conducted using cells and pressure panel boards from the Trautwein Soil Testing Equipment Company of Houston, Texas as described previously in Section 3.3.2. Images of one of the hydraulic conductivity cells used for testing are presented in Figure 3.36. The soil samples were tested using a falling head and rising tail testing technique (Method C). Thirty-five (35) psi of pressure, as supplied and regulated by the panel board, was used for the cell water pressure. Thirty-three (33) psi and 32 psi of pressure, supplied and regulated by the panel board, were used for the head water and tail water pressures, respectively. During testing of samples from Test Pad 1, the pressure to the panel board was interrupted due to a faulty laboratory air compressor. When the pressure was restored to the panel board, initial target pressures were reapplied to the samples and readings were resumed.

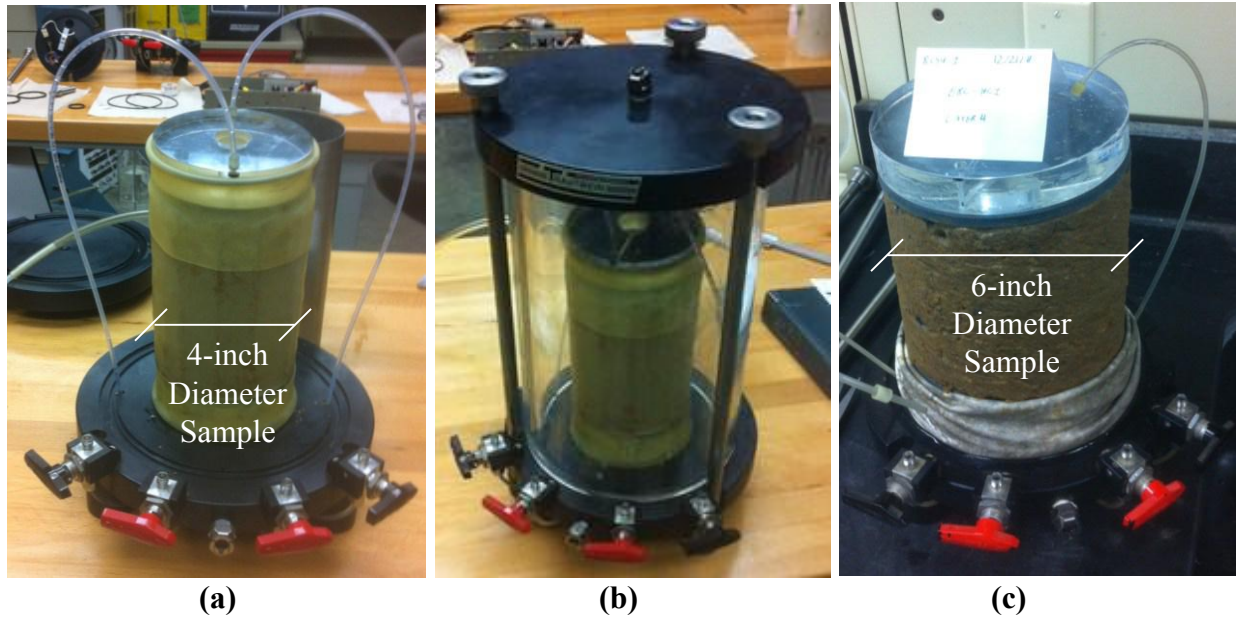


Figure 3.36. (a) Four-inch diameter soil sample prepared for hydraulic conductivity testing, (b) assembled hydraulic conductivity cell, and (c) six-inch diameter soil sample after hydraulic conductivity testing.

3.8.1.1 Shelby Tube Sample

To prevent sample disturbance caused by extruding the whole Shelby tube sample using one stroke, the lengths of each of the Shelby tubes were cut into smaller sections using a band saw (Figure 3.37a). The soil samples were extracted by using an end grinder and then a Dremel tool to spring open each of the Shelby tubes that were previously cut to the desired length using the band saw. Care was used to prevent the Dremel tool from cutting into the sample. If the sample would not slide out of the Shelby tube after it had been sprung open, it was then carefully extruded using a 12-ton hydraulic bottle jack (Figure 3.37b). The ends of each of the soil samples were then trimmed using a wire saw and a trimming mold (Figure 3.38a) to a length to diameter ratio of approximately one. Cuttings from trimming were collected in the pan shown in Figure 3.38a and were transferred to a smaller can for a moisture content test. The soil samples were trimmed to produce clean, flat edges and to remove metal shards associated with cutting the Shelby tube. The ends of the samples were also perforated with a wire brush (Figure 3.38b) to

ensure that smearing, developed during trimming of the sample, did not interfere with the hydraulic conductivity value obtained from the hydraulic conductivity testing.



Figure 3.37. (a) Band saw used for cutting Shelby tubes, and (b) 12-ton hydraulic bottle jack apparatus used for extruding samples.

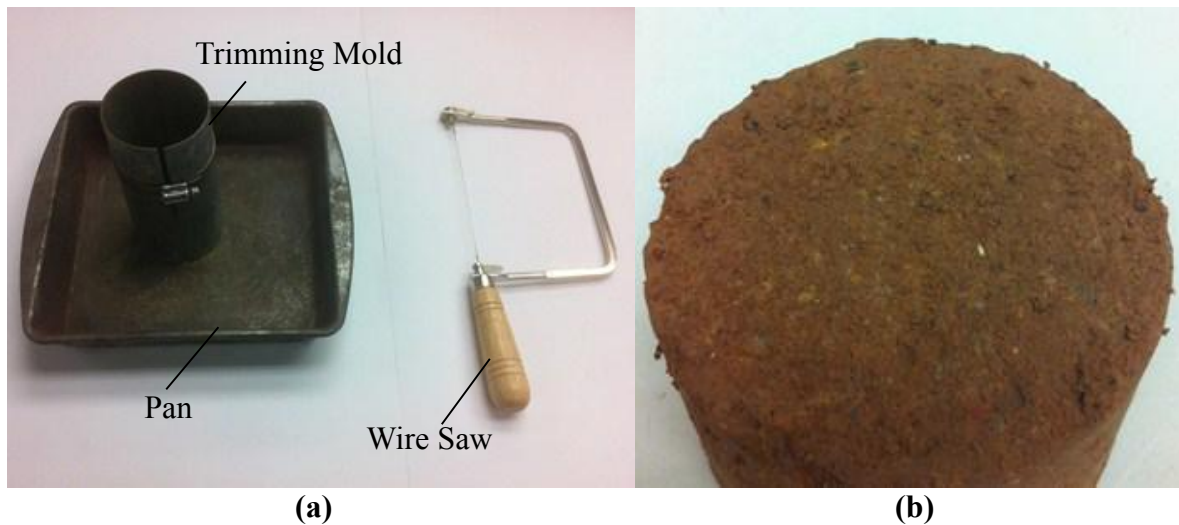


Figure 3.38. (a) Tools for trimming Shelby tube samples, (b) perforated Shelby tube sample.

3.8.1.2 Hand Carved Sample

Hand carved samples were prepared for laboratory testing by using a lathe. First, an acrylic platen was placed on top of the soil sample. A six-inch diameter platen was used to obtain samples to be tested for vertical flow and a four-inch diameter platen was used to obtain samples

to be tested for horizontal flow. For the horizontal flow samples, two sides of the block were cut off (Figure 3.39a) and then the block was rotated onto its side before the aforementioned platen was placed on the sample for trimming. The soil was trimmed using a hand saw to form a one-inch nominal ring around the platen. The soil sample was then placed in a trimming lathe (Figure 3.39b) that used an acrylic platen and two support rods (rods from permeameter cell) attached to a base plate to trim the soil sample to nominal size (six-inch diameter for vertical flow and four-inch diameter for horizontal flow). The height of the soil sample was then trimmed to ensure the soil sample could be placed into the hydraulic conductivity cell. The ends of the sample were leveled using a wire saw. A photograph of a horizontal hand carved sample that has been trimmed prior to placement in the hydraulic conductivity cell is presented in Figure 3.39c.

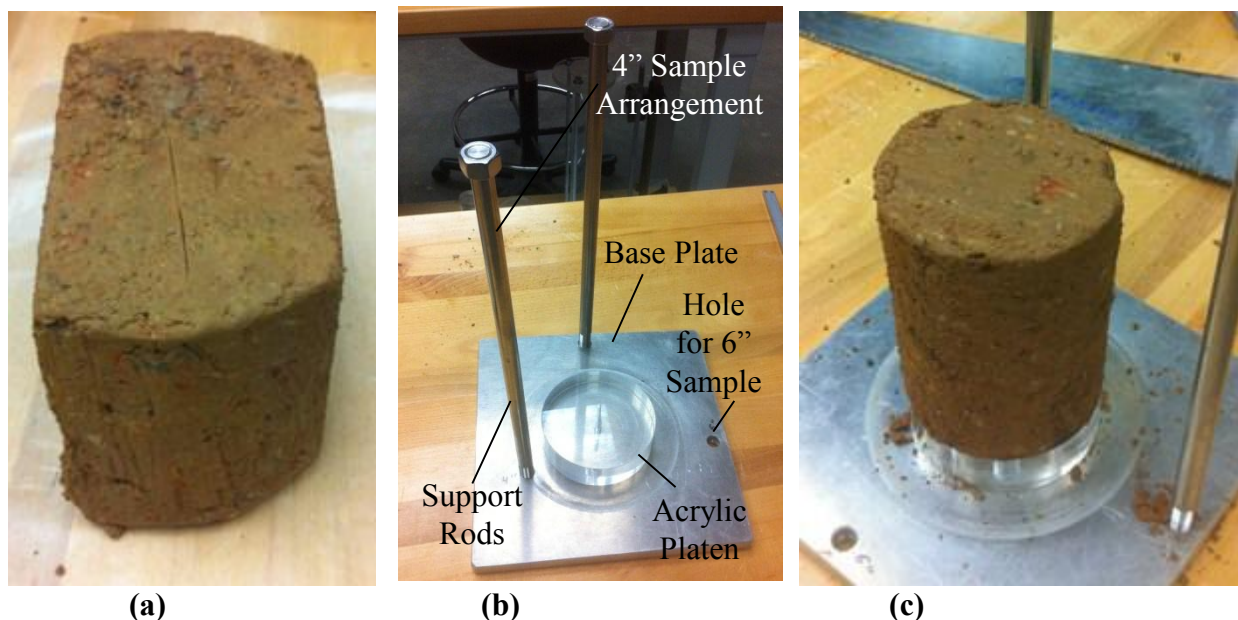


Figure 3.39. (a) Horizontal hydraulic conductivity sample with sides (future ends) cut off, (b) photo of trimming lathe, and (c) trimmed hand carved sample.

3.8.2 Specific Gravity Testing

Specific gravity testing was conducted on bagged samples collected during installation of TSB testing device and Shelby tube samples in accordance with ASTM D854 (2012) following Method B. The soil was ground up using a No. F-4 Quaker City Grinding Mill (Figure 3.40) and

then was dried in an oven. The mass of dry soil (approximately 50 grams) was weighed before testing. Instead of being vacuumed for the required two hours, the pycnometer was filled half full with water or soil and water and vacuumed for five minutes. Then the pycnometer was filled to just below the calibration mark and vacuumed for another five minutes. The vacuum apparatus is presented in Figure 3.41. Results are presented in Section 4.6.3.



Figure 3.40. Photo of No. F-4 Quaker City Grinding Mill used for grinding soil samples.

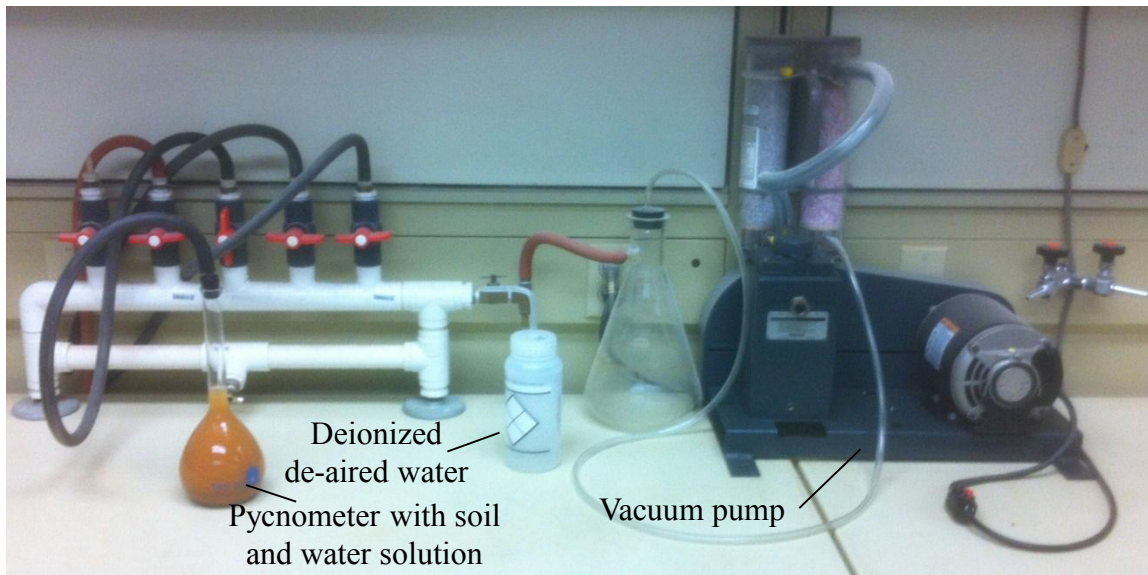


Figure 3.41. Specific gravity vacuum device.

3.8.3 Hydrometer Analyses

Hydrometer analyses (Figure 3.42a) were conducted in accordance with ASTM D422 (2012) on soil passing the No. 200 (75- μm) sieve. Instead of soaking the soil for 16 hours, the soil soaked for five minutes before being dispersed in a type A apparatus (Hamilton Beach Model HMD200) as shown in Figure 3.42b. Readings were obtained using a 152H hydrometer. Results are discussed in Section 4.6.3.

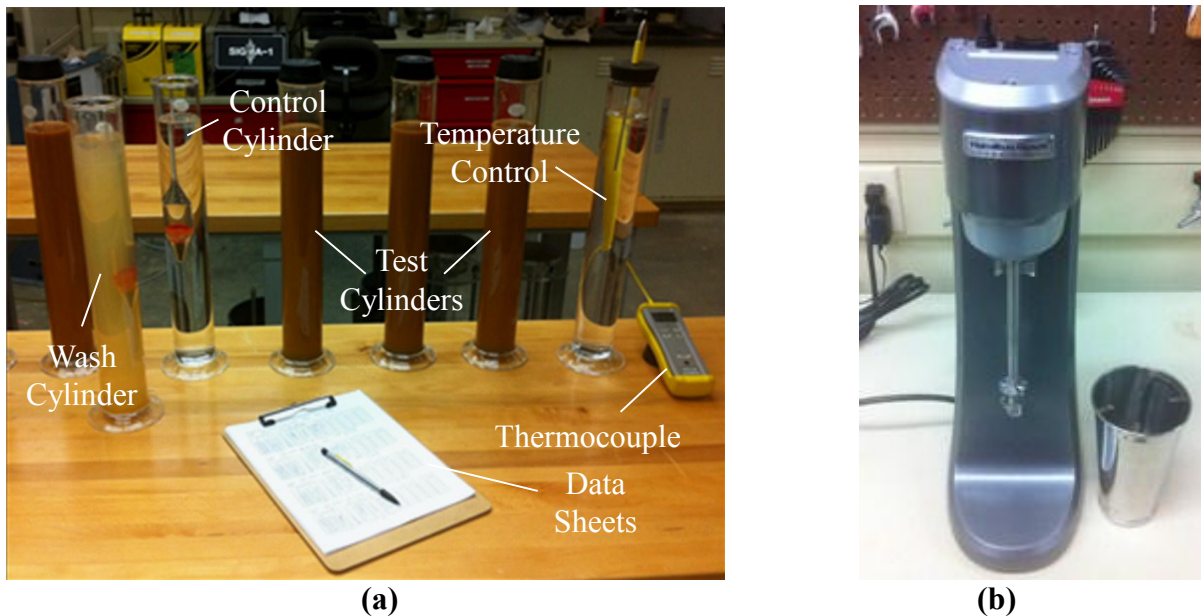


Figure 3.42. Hydrometer testing (b) spindle mixer used for dispersing hydrometer samples.

3.8.4 Percentage Passing the No. 200 (75- μm) Sieve

To determine the percentage passing the number 200 (75- μm) sieve, testing was conducted in accordance with ASTM D1140 (2012) following Method A. After obtaining an oven dry mass (approximately 100 grams), the soil was allowed to soak overnight in a beaker with deionized water (Figure 3.43a). The soil was then washed through a number four (4.75 mm) sieve nestled on top of a number 200 (75- μm) wash sieve (Figure 3.43b). The soil trapped on the sieves were collected in a tin can and dried overnight in an oven to determine the amount of dry soil retained. Results are discussed in Section 4.6.3.



(a)

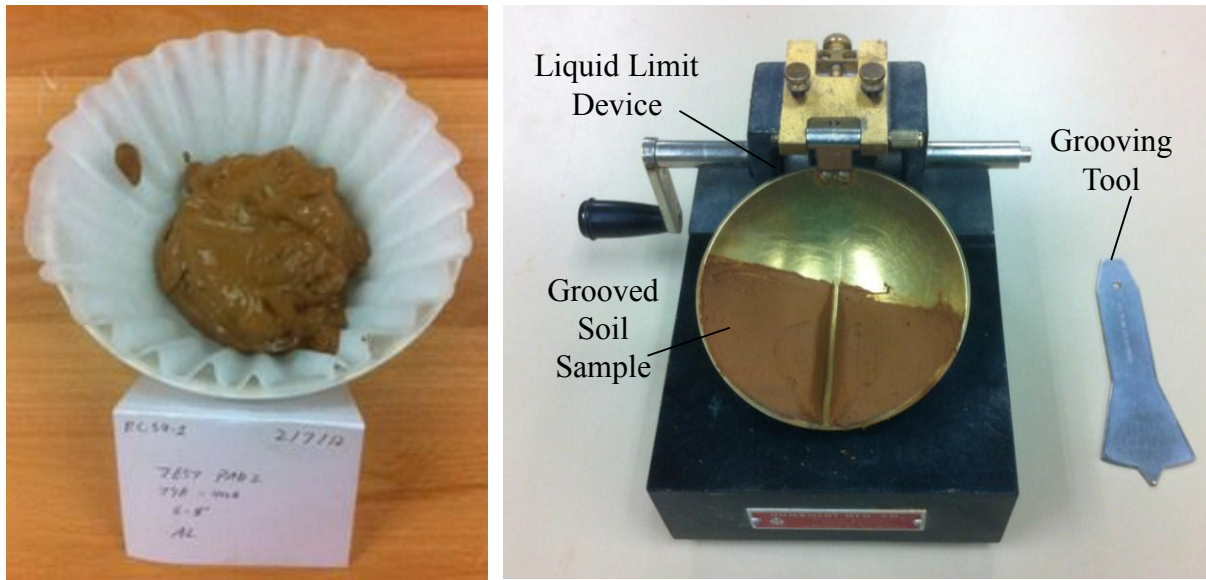


(b)

Figure 3.43. (a.) soil sample soaking in water (b.) photo of soil being washed.

3.8.5 Atterberg Limits Testing

Atterberg limits testing was conducted in accordance with ASTM D4318 (2012). The soil was not sieved prior to testing and was prepared using the wet preparation method. A slurry mixture consisting of 200 grams of moist soil and 100 grams of deionized water were mixed together using a Hamilton Beach Model HMD200 spindle mixer as shown previously in Figure 3.42b. The slurry was poured into coffee filters in ceramic bowl (Figure 3.44a) and allow to dry for 24 hours. The liquid limit test was conducted using a hand-operated liquid limit device and a metal grooving tool (Figure 3.44b). The plastic limit was hand rolled on a glass plate (Figure 3.45). Results are discussed in Section 4.6.3.



(a) (b)
Figure 3.44 (a) Soil sample prepped for Atterberg limits testing, and (b) liquid limit device with grooved soil sample.



Figure 3.45. Soil sample drying for plastic limit testing.

3.9 Conclusion

The nine methodologies presented for two stage borehole data deduction were evaluated to determine errors in the methodologies and to determine which one will be used for the analysis conducted for this research project. A zone of acceptance was developed by conducting Proctor and flexible wall hydraulic conductivity tests prior to constructing the test pads on clay

soil obtained from the soil stockpile. The zone of acceptance was then used to ensure viability of the moisture content and dry unit weight measurements obtained while constructing three environmentally controlled test pads at Engineering Research Center (ERC). The in-situ hydraulic conductivity of Test Pads 1 and 2 was tested using the two stage borehole test. The in-situ hydraulic conductivity of Test Pad 3 was tested using the sealed double ring infiltrometer, time domain reflectometry probes, and tensiometers. After completion of in-situ testing in each test pad, Shelby tubes and hand carved samples were collected and the respective test pad was then removed. Laboratory testing on the samples collected from the ERC test pads and conducted at Bell Engineering Center include flexible wall hydraulic conductivity, specific gravity, Atterberg Limits, and grain size analysis (percentage passing the number 200 [75- μm] sieve and hydrometer analysis) on the Shelby tube, hand carved, or bag samples.

Chapter 4: Results and Discussion

4.1 Introduction

The data obtained from initial Proctor testing and laboratory hydraulic conductivity testing on the Proctor samples were used to develop a zone of acceptance (ZOA) using the Daniel and Benson (1990) method and the Arkansas Pollution Control and Ecology Commission (APCEC) [2007] method. The APCEC (2007) ZOA was evaluated for accuracy against the Daniel and Benson (1990) method and the Daniel and Benson (1990) ZOA was selected as the method used to validate placement of compacted soil in the test pad box at the University of Arkansas Engineering Research Center (ERC). The data obtained from two stage borehole (TSB) testing conducted in Test Pads 1 and 2 were used to determine the in-situ and in-situ horizontal hydraulic conductivity values for the respective test pads. The sealed double ring infiltrometer (SDRI) testing conducted in Test Pad 3 was used to determine the in-situ vertical hydraulic conductivity of Test Pad 3. The vertical conductivity values measured using TSB testing conducted in Test Pads 1 and 2 were compared to vertical conductivity values measured using SDRI testing conducted in Test Pad 3 to identify differences in the values obtained from the two testing methods.

The data collected from index testing, conducted on soil samples obtained from Test Pads 1 and 2, were used to classify the soil and to validate the uniformity of the soil within Test Pads 1 and 2. The laboratory hydraulic conductivity testing conducted on Shelby tube (vertical flow) and hand carved samples (vertical flow and horizontal flow), collected from Test Pads 1 and 2, were used to validate the measured in-situ (TSB and SDRI) vertical and in-situ (TSB) horizontal hydraulic conductivity values obtained from Test Pads 1 and 2, respectively. The values obtained from laboratory hydraulic conductivity testing conducted on hand carved samples (vertical flow)

were compared to the values obtained from laboratory hydraulic conductivity testing conducted on Shelby tube samples (vertical flow) to determine if pushing the Shelby tube compresses the soil thereby affecting the hydraulic conductivity of the soil.

The results from the evaluation of the TSB data reduction methods are discussed in Section 4.2. The results used to develop the ZOA as obtained from Proctor testing and laboratory hydraulic conductivity testing are discussed in Section 4.3. Placement results for Test Pads 1, 2, and 3 are presented in Section 4.4. The results obtained from TSB testing in Test Pads 1 and 2 and the SDRI testing in Test Pad 3 are discussed in Section 4.5. The results from the flexible wall hydraulic conductivity testing, soil index testing, and soil classification testing conducted on samples obtained from the test pads are discussed in Section 4.6. The differences observed in the measured hydraulic conductivity values obtained from each of the testing techniques are discussed in Section 4.7, including: laboratory vertical flow hydraulic conductivity for hand carved samples as compared to laboratory vertical flow hydraulic conductivity for Shelby tube samples, laboratory vertical flow hydraulic conductivity for hand carved samples and Shelby tube samples as compared to TSB or SDRI vertical flow hydraulic conductivity, laboratory horizontal flow hydraulic conductivity for hand carved samples as compared to TSB horizontal flow hydraulic conductivity, and TSB vertical flow hydraulic conductivity as compared to SDRI vertical flow hydraulic conductivity.

4.2 Evaluation of the Various Solution Methods for Two Stage Borehole Data Reduction

Upon review of the data set, several discrepancies were noticed. One of the reported values in ASTM D6391 (2010) was calculated incorrectly while the other issues are associated with possible rounding errors based on the reported significant digits. On the third row of Stage 2 calculations, the corrected final height (H'_2) should be 198.9 centimeters instead of the reported

188.9 centimeters. Also, the calculated height from the bottom of the liner to the bottom of the standpipe measuring device was not calculated correctly. Based on the reported thickness of the liner below the casing (61.0 centimeters), the depth of casing (61.0 centimeters), and the length from the casing to the standpipe measuring device (22.9 centimeters), the overall length was calculated as 144.9 centimeters but was reported as 144.8 centimeters. For completeness, the internal diameter of the standpipe, the effective casing diameter for Stage 1, and the effective casing diameter for Stage 2 were reported as 1.27, 11.43, and 10.16 centimeters, respectively.

Three of the R_t correction factors, Rows 2 and 3 of Stage 1 and Row 5 of Stage 2, were reported as being 0.1 less than what was calculated for the given temperatures. Similarly, one R_t correction factor, Row 8 of Stage 2, was reported as being 0.1 greater than what was calculated for the given temperature. Additionally, several calculated hydraulic conductivity values do not coincide with the provided data. The hydraulic conductivity value in Row 3 of Stage 2 is inaccurate, mainly due to the incorrect final height reading of the standpipe. The calculated hydraulic conductivity values in Rows 2, 4, and 6 of Stage 1 and Rows 2 and 8 of Stage 2, do not coincide with the provided data because of discrepancies with the reported cumulative volumes. Because the cumulative volume is based on the previous cumulative volume, it is typically assumed that when there is a discrepancy with one of the volume measurements, the following volume measurements will also contain discrepancies. Discrepancies in the reported cumulative volumes began in Row 2 of Stage 1 and Row 4 of Stage 2. As predicted, the discrepancies continued in the successive volume calculations. After the data set and equations were verified, the various methods described in Sections 2.5.1 to 2.5.9 (including any errors and omissions in the equations reported in the literature) were used to solve for the hydraulic conductivity of the soil reported in the ASTM. Corrections to the methods and/or with modifications to the method

(as discussed in the subsequent paragraphs) were also employed in solving for the hydraulic conductivity values and the obtained value are also reported.

A summary of the calculated hydraulic conductivities as a function of the method that was used to solve for the hydraulic conductivity values is presented in Table 4.1. For calculation of m for the time lag methods and for calculation of a for the Z - t methods, the Microsoft Excel Solver function was used instead of hand solutions using the trial and error method. Since the data presented in ASTM D6391 (2010) contained a gap in the data set, the reported hydraulic conductivities are based on the final two readings for Stages 1 and 2.

Table 4.1. Summary of the calculated hydraulic conductivities using various solution methods with the ASTM D6391 (2010) dataset.

Method	Calculated Hydraulic Conductivity [cm/sec]				Notes
	k_1	k_2	k_v	k_h	
Soil Testing Engineers 1983	2.49E-08	2.02E-08	1.18E-07	5.24E-09	k_v and k_h solved with respect to k_1
Soil Testing Engineers 1983	2.49E-08	2.02E-08	1.18E-07	5.24E-09	k_v and k_h solved with respect to k_2
Soil Testing Engineers 1983	4.70E-08	4.13E-08	8.28E-08	2.67E-08	Solved correcting for H
Daniel 1989	6.95E-08	6.20E-08	1.12E-07	4.32E-08	Solved as presented
Daniel 1989	4.70E-08	4.13E-08	8.30E-08	2.66E-08	Solved correcting for H
Daniel 1989	4.70E-08	4.13E-08	7.42E-08	2.98E-08	Solved using Figure 2.14
Daniel 1989	4.70E-08	4.13E-08	8.28E-08	2.67E-08	Solved correcting for H and f
Boutwell 1992	1.46E-08	1.86E-08	7.94E-09	2.79E-08	Solved as presented
Boutwell 1992	3.20E-08	4.53E-08	1.43E-08	7.59E-08	Solved correcting for H
Boutwell and Tsai 1992	8.63E-04	6.42E-04	-1.35E-03	-4.22E-04	Solved as presented
Boutwell and Tsai 1992	7.86E-04	5.69E-04	2.23E-03	6.74E-06	Solved with correcting for a
Boutwell and Tsai 1992	1.60E-08	2.10E-08	7.79E-09	3.14E-08	Solved with correcting for t_2-t_1
Boutwell and Tsai 1992	1.46E-08	1.86E-08	7.94E-09	2.79E-08	Solved correcting for a and t_2-t_1
Boutwell and Tsai 1992	3.20E-08	4.53E-08	1.43E-08	7.59E-08	Solved correcting for a , t_2-t_1 , and H
Trautwein and Boutwell 1994	N/A				Solved as presented
Trautwein and Boutwell 1994	3.20E-08	4.53E-08	1.43E-08	7.59E-08	Solved with corrections
Trautwein and Boutwell 1994	3.20E-08	4.53E-08	1.44E-08	6.49E-08	Solved using Figure 2.15
ASTM D6391 Method A 2012	3.20E-08	4.53E-08	N/A		Solved as Method A
ASTM D6391 Method A 2012	3.20E-08	4.53E-08	1.38E-08	7.43E-08	Solved with modifications
Chapuis 1999	1.34E-04	9.22E-07	N/A		Solved as presented
Chapuis 1999	2.18E-07	9.22E-07	N/A		Solved with modifications
Chiasson 2005	2.80E-05	1.04E-05	-7.16E-04	N/A	Solved as presented
Chiasson 2005	2.64E-05	1.11E-05	N/A		Solved with R_f correction factor
ASTM D6391 Method B 2012	2.64E-05	N/A			Solved as Method B
Average	8.11E-05	5.61E-05	8.80E-06	-2.44E-05	
Standard Deviation	2.31E-04	1.74E-04	6.37E-04	9.95E-05	

The Soil Testing Engineers, Inc. (1983) and Daniel (1989) methods were both initially solved following the procedures discussed in Sections 2.5.1 and 2.5.2, respectively. The vertical and horizontal hydraulic (k_v and k_h) conductivities were obtained utilizing Equation 2.11. The k_v and k_h values obtained from the Soil Testing Engineers, Inc. [STEI] (1983) method were solved with respect to either the apparent hydraulic conductivity values obtained from Stage 1 of Stage 2. Identical k_v and k_h values, 1.18×10^{-7} cm/sec and 5.24×10^{-9} cm/sec respectively, were obtained using both techniques. The main difference between the STEI (1983) and Daniel (1989) methods

is the definition for height of head. The height of head, H , was corrected in the STEI (1983) and Daniel (1939) methods by defining H as the distance between the location of the water level in the standpipe and the location of the groundwater level (i.e. distance from the location of the water level in the standpipe to the location of the bottom of the compacted liner). When both methods (STEI [1983] and Daniel [1939]) were corrected for H , similar, but not identical, values were obtained for k . After correcting for H , k_v and k_h were calculated utilizing Figure 2.14 and respective values of 7.42×10^{-8} cm/sec and 2.98×10^{-8} cm/sec were obtained. The slight difference in the results is caused by the calculation for F in the Daniel (1989) method. Using Equation 4.1, which contains the F from Soil Testing Engineers, Inc. (1983), identical k values were obtained.

$$B = 8D \frac{L}{D} (t_2 - t_1) \left\{ 1 - 0.5623 \exp \left[-1.566 \left(\frac{L}{D} \right) \right] \right\} \quad \text{Equation 4.1}$$

(modified from Daniel, 1989)

The Boutwell (1992) method was solved following the aforementioned procedures discussed in Section 2.5.3. Values of 7.94×10^{-9} cm/sec and 2.79×10^{-8} cm/sec were obtained for k_v and k_h , respectively, by utilizing the method with no correction to the method. The H term definition was then corrected in the Boutwell (1992) method resulting in values of 1.43×10^{-8} cm/sec and 7.59×10^{-8} cm/sec for k_v and k_h , respectively.

The Boutwell and Tsai (1992) method was utilized to obtain values of hydraulic conductivity following the calculations procedures previously mentioned in Section 2.5.4 with the previously mention errors. A lower hydraulic conductivity was calculated for Stage 2 than Stage 1. The k_2/k_1 ratio value was calculated as 0.743 and the m value calculated as -0.559. The k_2/k_1 value should never be less than 1 because the hydraulic conductivity in Stage 1 should not be higher than Stage 2 due to preferential flow paths along the lift interface. However, when smearing of the borehole surface is present, a lower hydraulic conductivity in Stage 2 may be

measured (Boutwell and Tsai, 1992). Assuming that the calculated value of m was correct, negative values for the vertical and horizontal hydraulic conductivity were calculated. The Boutwell and Tsai (1992) method was reevaluated utilizing Equation 4.2 instead of Equation 2.31 (presented previously), which corrects the time difference calculation, and utilizing an a value of -1 for a permeable boundary. With both corrections, the k_2/k_1 value was calculated as 1.278 and m was calculated as 1.877. Using the corrected method, values for the vertical and horizontal hydraulic conductivity of 7.94×10^{-9} cm/sec and 2.79×10^{-8} cm/sec, respectively, were obtained. While the values are probable, the definition of the head in the permeameter must also be corrected. Correcting the Boutwell and Tsai (1992) method with the aforementioned corrections and for H , a k_2/k_1 ratio and m value of 1.413 and 2.304, respectively, were obtained. The modified procedure yielded values of vertical and horizontal hydraulic conductivity of 1.43×10^{-8} cm/sec and 7.59×10^{-8} cm/sec, respectively. Approximately a half order magnitude of difference is calculated between the corrected Boutwell and Tsai (1992) method not corrected for H and the corrected Boutwell and Tsai (1992) method corrected for H .

$$k_v = \frac{R_T G \ln\left(\frac{H_1}{H_2}\right)}{t_2 - t_1} \quad (\text{modified from Boutwell and Tsai, 1992}) \quad \text{Equation 4.2}$$

Because the U_5 term was presented by Trautwein and Boutwell (1994) as a matrix (Section 2.5.5), the Trautwein and Boutwell (1994) method cannot be solved for hydraulic conductivity as presented. Instead, the method was solved assuming that the U_5 term was a quotient (not a matrix) as previously presented in Equation 2.35 and utilizing the procedure outlined in Section 2.5.5. The corrected Trautwein and Boutwell (1994) method produced identical values for k_1 , k_2 , k_v , and k_h as compared with the corrected Boutwell (1992) and Boutwell and Tsai (1992) methods. The Trautwein and Boutwell (1994) method also presented a figure for estimating the value of m instead of using the trial-and-error method. The

approximation method utilizing the figure produced values of k_v and k_h values that were less conservative than the values of k_v and k_h obtained from the solver method.

Method A presented ASTM D6391 (2012) was used to calculate k_1 and k_2 following the aforementioned procedures discussed in Section 2.5.6. As mentioned previously, the equations used to solve for hydraulic conductivity as outlined in ASTM D6391 (2012) following Method A for solving for the hydraulic conductivities of Stage 1 and 2 are similar to those used by Boutwell (1992), Boutwell and Tsai (1992), and Trautwein and Boutwell (1994). However, a method for calculating the anisotropy value m is not presented in the ASTM D6391 (2012) method. Because the STEI (1983) and Daniel (1989) methods both presented a different way of calculating the anisotropy value m the Boutwell (1992), Boutwell and Tsai (1992), and Trautwein and Boutwell (1994) methods, for comparison, the hydraulic conductivities from Stage 1 and 2 as reported in the ASTM D6391 (2010) were used in the method of calculating the anisotropy from STEI. (1983) and Daniel (1989) to determine the horizontal and vertical hydraulic conductivity measurements. This comparison will yield to separate anisotropy values that are only depend of method used for calculation and are independent of varying term definitions. The m value obtained from the STEI (1983) and Daniel (1989) methods was 2.318 and the m value obtained from the Boutwell (1992), Boutwell and Tsai (1992), and Trautwein and Boutwell (1994) methods was 2.304. Because the two compared anisotropy values are similar, either anisotropy method can be used to solve for m .

The data set presented in Chapuis (1999) was used to validate the utilization of the Chapuis (1999) method. Figures for the velocity curve and corrected semilog curve as presented in Chapuis (1999) are presented herein, for completeness, as Figure 4.1. The hydraulic conductivity value as obtained from the data set was determined to be 1.66×10^{-7} cm/sec from

both curves; however, these results were not duplicated with initial independent calculations. Based on independent calculations of the dataset, the error in the assumed piezometric level from the velocity curve (Figure 4.2) was determined as -73.8 centimeters, instead of -80 centimeters as reported in Chapuis (1999).

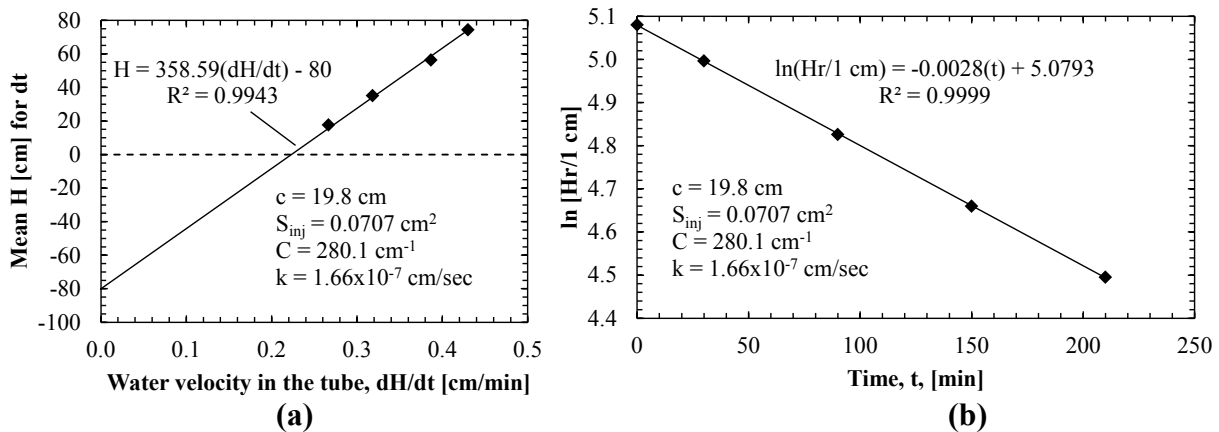


Figure 4.1. (a) Velocity curve and (b) semilog curve (from Chapuis [1999]).

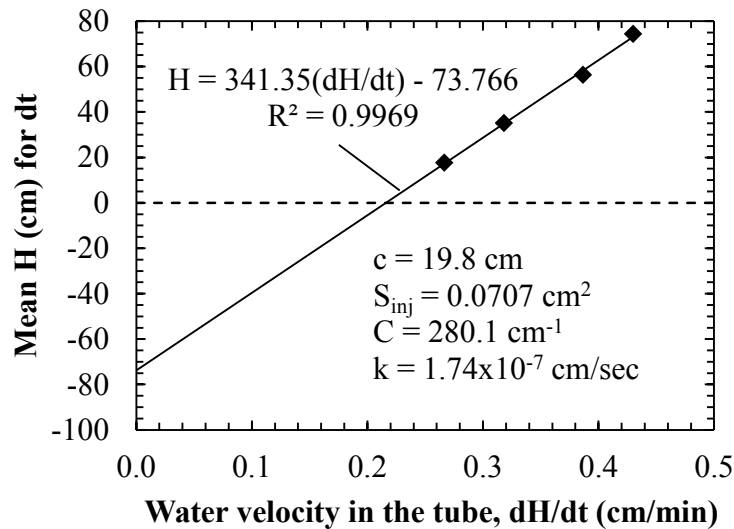


Figure 4.2. Independently generated velocity curve (using Chapuis [1999] dataset)

The initial calculated hydraulic conductivity was calculated as 0.0137 cm/sec, which is five orders of magnitude different than then the presented hydraulic conductivity. It was assumed that the presented hydraulic conductivity equation (Equation 2.49) is incorrect (as determined by dimensional analysis) and that the modified equation (Equation 4.3) should be used instead.

$$k = \frac{1}{60Cp} \quad (\text{modified from Chapuis, 1999}) \quad \text{Equation 4.3}$$

Utilizing the modified equation and the data presented in Chapuis (1999), a value of 1.74×10^{-7} cm/sec was obtained for the hydraulic conductivity, which is closer but still does not equal the value reported in Chapuis (1999). The reported value of 1.66×10^{-7} cm/sec was calculated when the modified equation was used and the y-intercept of the trend line was forced through -80 centimeters instead of intercepting at the predetermined -73.8 centimeters. For similarity, a H_0 value of -80 centimeters was utilized for the independent calculations of the semilog curve. A slope (p') of 0.00279 was obtained from the curve and used in Equation 2.50 to solve for k , which was calculated as 1.30×10^{-2} cm/sec. It was assumed that the second hydraulic equation (Equation 2.50) was also incorrect (as determined by dimensional analysis). A modified equation (Equation 4.4) was utilized which yielded a value of 1.66×10^{-7} cm/sec for the apparent hydraulic conductivity.

$$k = \frac{p'}{60C} \quad (\text{modified from Chapuis, 1999}) \quad \text{Equation 4.4}$$

Using the velocity procedure presented in Section 2.5.6 and the modified equations (Equation 4.3 and Equation 4.4), a hydraulic conductivity was calculated for both Stages 1 and 2 using the ASTM D6391 (2010) dataset. The results for the hydraulic conductivity values as obtained from the modified equations from the Chapuis (1999) method were higher than the results from the time lag methods (approximately one half to one order of magnitude higher).

The Chiasson (2005) method was initially solved following the procedures outlined in Section 2.5.8. The results for k_1 and k_2 were three orders of magnitude higher than the respective results for k_1 and k_2 as obtained from Boutwell (1992), Boutwell and Tsai (1992), and Trautwein and Boutwell (1994) methods. The Chiasson (2005) method was also used to solve for

anisotropy to solve for k_v . The Chiasson (2005) method was then reconducted utilizing the R_T correction factor. The ASTM D6391 (2012) Method B procedure was conducted as discussed in Section 2.5.9. The procedure was conducted on data obtained from Stage 1 only because shape factors were not presented for Stage 2. The results obtained utilizing the ASTM D6391 (2012) Method B procedure are identical to the results obtained utilizing the Chiasson (2005) method (as corrected by including R_T).

When used correctly, the methods for calculating Stage 1 and 2 hydraulic conductivity values as presented by Boutwell (1992), Boutwell and Tsai (1992), Trautwein and Boutwell (1994), and ASTM D6391 (2012) Method A all yield the same results. However, the methods presented by Soil Testing Engineers, Inc. (1983) and Daniel (1989) yielded higher hydraulic conductivities and therefore conservative results for the hydraulic conductivity of Stages 1 and 2. The trial and error methods for calculating the anisotropy as presented by Boutwell (1992), Boutwell and Tsai (1992), and Trautwein and Boutwell (1994) also yielded the same results; therefore, similar values of vertical and horizontal hydraulic conductivity were obtained from the different methods. The anisotropy approximation chart presented in Trautwein and Boutwell (1994) also yielded values that were close to those calculated by the solver methods. However, the approximation chart requires users to obtain values from a log-log plot and human error may be introduced in determining the correct values from the chart. A comparison plot with the final corrected hydraulic conductivity value from Stage 1 for each method is presented in Figure 4.3.

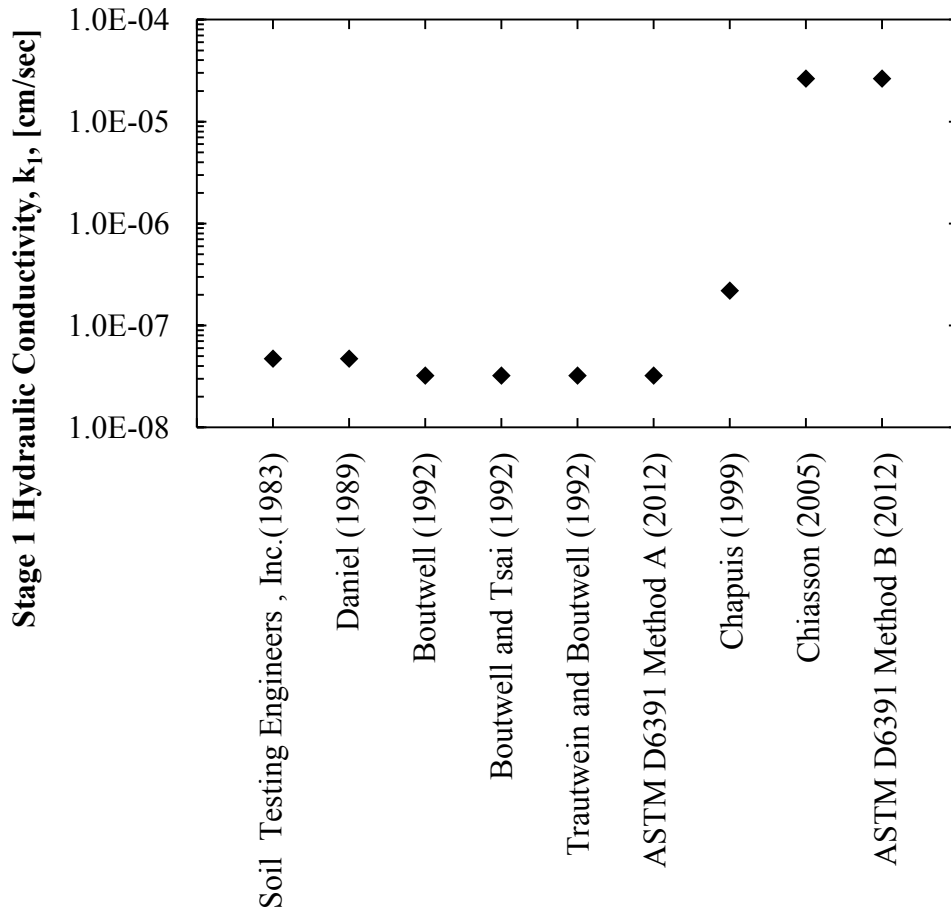


Figure 4.3. Comparison plot of corrected hydraulic conductivities from Stage 1 for each method.

To compare the anisotropy value methods presented by Soil Testing Engineers, Inc. (1983) and Daniel (1989), the Daniel (1989) method was used to calculate the vertical and horizontal hydraulic conductivity values from the apparent hydraulic conductivities presented in ASTM D6391 (2010). Similar, but slightly conservative, values for vertical and horizontal hydraulic conductivity were obtained from the modified ASTM D6391 (2010) than the values calculated from Boutwell, (1992), Boutwell and Tsai (1992), and Trautwein and Boutwell (1994) methods.

4.3 *Developing Acceptance Criterion*

Proctor testing and laboratory hydraulic conductivity testing were conducted using the procedures discussed in Section 3.2. The initial and final soil properties of each Proctor sample are presented in Table A.1 and Table A.2, respectively, in Appendix A for completeness. The Proctor curve developed using standard energy was used to determine the maximum dry unit weight and optimum moisture content for the soil. The results obtained from Proctor testing at various energies (standard energy, 75-percent of standard energy, and 50-percent of standard energy) and laboratory hydraulic conductivity testing on the Proctor samples were used to develop a Daniel and Benson (1990) ZOA and a APCEC (2007) ZOA.

4.3.1 *Proctor Testing Results*

As stated previously in Section 3.3.1, a total of 18 Proctor points were compacted. Results obtained from compaction testing and the corresponding Proctor curves are presented in Figure 4.4. The zero air voids (ZAV), 90-percent saturation, and 80-percent saturation lines based on a specific gravity of 2.67 (found from soil property testing as reported in Section 4.6.3) are also presented in Figure 4.4 for completeness. The saturated sides of the Proctor curves (the right-hand side) follow the 80-percent saturation line as the line is approximately the line of optimums (i.e. the line approximately travels through the optimum moisture content and maximum dry unit weight for each energy level). The standard Proctor has a maximum dry unit weight of 109.3 pounds per cubic feet (pcf) and an optimum moisture content of 15.5 percent (%). The 75-percent of standard Proctor has a maximum dry unit weight of 109.0 pounds per cubic feet (pcf) and an optimum moisture content of 15.6 percent (%). The 50-percent of standard Proctor has a maximum dry unit weight of 107.4 pounds per cubic feet (pcf) and an optimum moisture content of 18.1 percent (%).

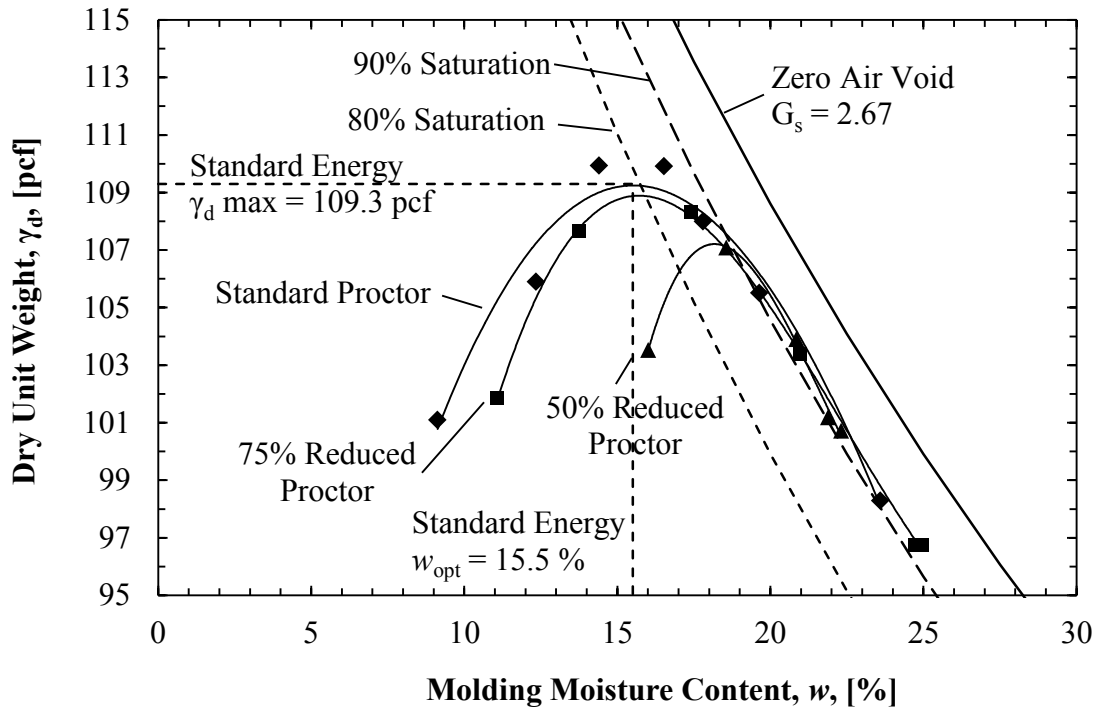


Figure 4.4. Compaction curves for Standard Proctor, 75-Percent Reduced Proctor, and 50-Percent Reduced Proctor.

4.3.2 Flexible Wall Hydraulic conductivity Results on Proctor Samples

Of the 18 Proctor tests conducted, 14 Proctor samples were selected for vertical hydraulic conductivity testing, as stated previously in Section 3.3.2. Flexible wall hydraulic conductivity testing was conducted on the samples until the measured hydraulic conductivity values reached steady state flow. A plot of a typical hydraulic conductivity test results (50-percent Reduced Proctor, Sample 4) is presented in Figure 4.5. The average of the measured steady state hydraulic conductivities (average of the points identified using open symbols, as shown in Figure 4.5) was used as the final value for hydraulic conductivity at 20-degree Celsius for each sample. The inflow to outflow ratio (Figure 4.6) was calculated for each sample to determine if the sample was still saturating (typically $Q_{in}/Q_{out} > 1$) and/or if the sample was consolidating (typically $Q_{in}/Q_{out} < 1$). As shown in Figure 4.6, the acceptable range for the inflow to outflow ratio is 0.75-1.25 as per ASTM D5084 (2012). Collected vertical hydraulic conductivity data and

corresponding inflow to outflow ratio measurements for each hydraulic conductivity test as conducted on each Proctor sample are presented in Appendix A (Figure A.1 through Figure A.28).

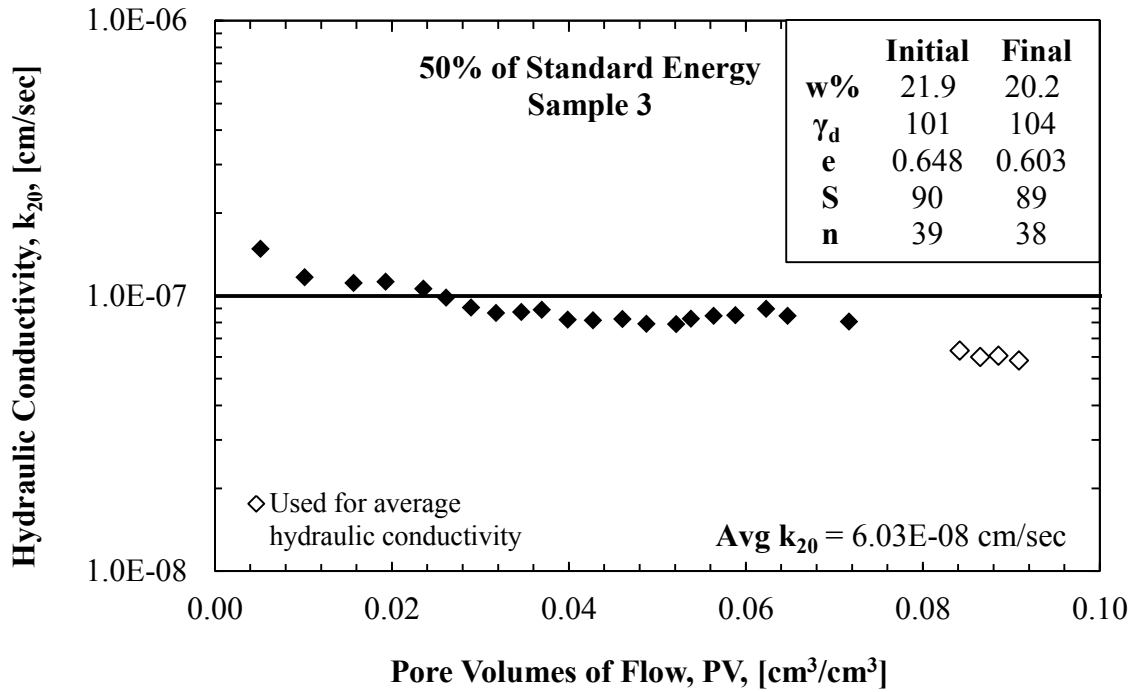


Figure 4.5. Vertical hydraulic conductivity data for 50-percent of Standard Energy Sample 3.

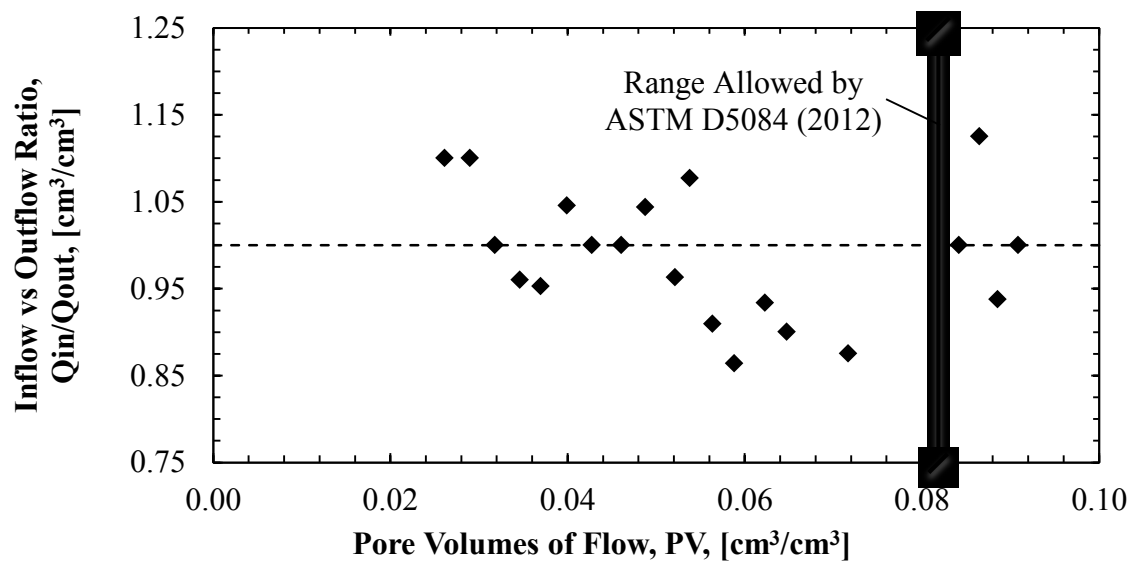


Figure 4.6. Inflow to outflow data for 50- percent of Standard Energy Sample 3.

As presented in Table A.2, full saturation of each of the 14 Proctor samples used for laboratory hydraulic conductivity testing was not achieved prior to terminating the test. The tests were terminated when steady flow was observed, often before one pore volumes of flow. Because of the low pore volume flows, the samples did not reach full saturation.

For each of the compaction energy, the average steady state flow of the measured hydraulic conductivity values were plotted against the molding moisture content of the corresponding sample to develop a relationship (Figure 4.7). As moisture content increases the hydraulic conductivity decreases, as expected. The measured hydraulic conductivity for five of the Proctor samples was lower than 1×10^{-7} centimeters per second (cm/sec), the acceptable limit.

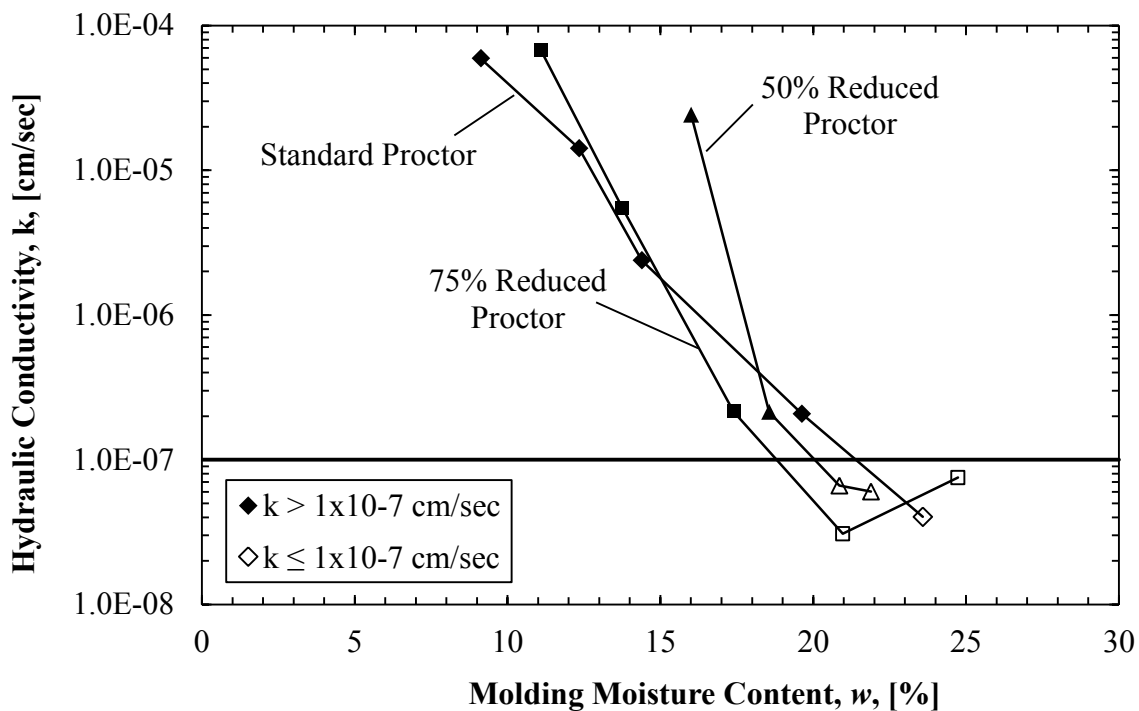


Figure 4.7. Relationship between hydraulic conductivity and molding moisture content.

4.3.3 Zone of Acceptance

A zone of acceptance (ZOA) for test pad construction was developed following the Daniel and Benson (1990) method discussed in Section 2.2. For comparison purposes, a ZOA

was also developed using the APCEC (2007) method also discussed in Section 2.2. The Proctor points corresponding to the samples used for hydraulic conductivity testing were plotted as a function of dry unit weight and molding moisture content along with the ZAV, 90-percent saturation, and 80-percent saturation lines (Figure 4.8). Closed symbols represent samples with hydraulic conductivity values greater than 1×10^{-7} cm/sec and open symbols represent samples with hydraulic conductivity values equal to or lower than 1×10^{-7} cm/sec.

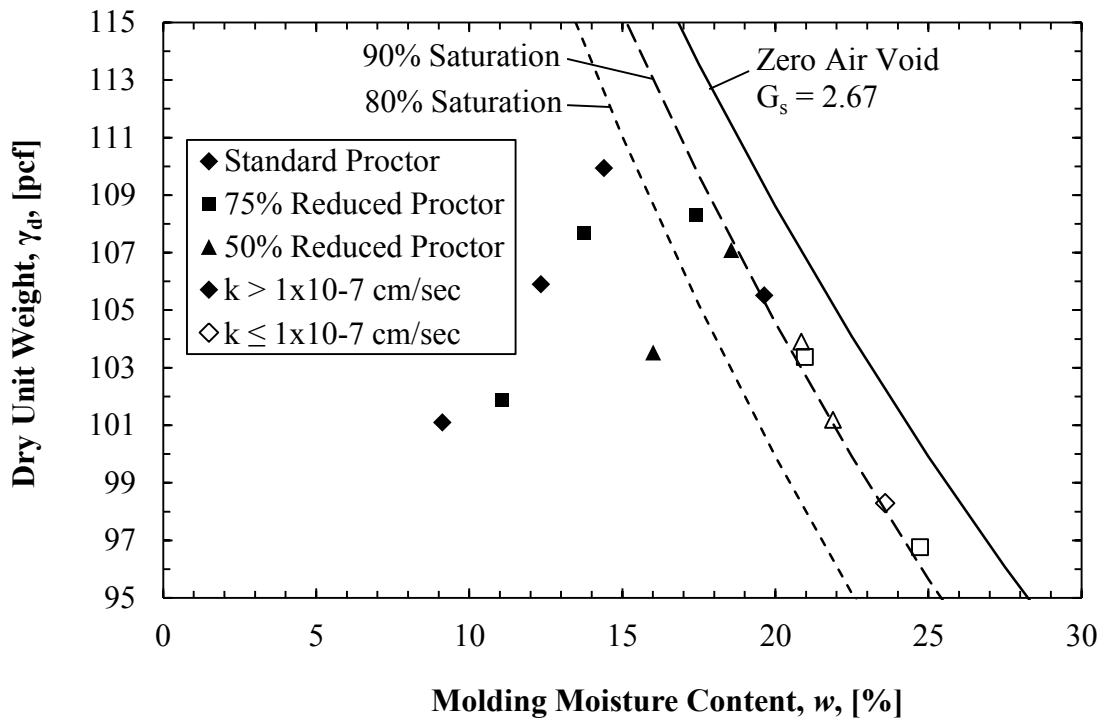


Figure 4.8. Relationship between dry unit weight, molding moisture content, and hydraulic conductivity.

The ZOA presented in Figure 4.9 was developed using the data presented previously in Figure 4.8 in accordance with Daniel and Benson (1990) and bounds the samples with an acceptable hydraulic conductivity. The ZOA is bounded at the top by a dry unit weight of 104 pcf and at the bottom by a dry unit weight of 96 pcf. The ZOA is bounded on the left side by the 80-percent saturation line (corresponding to the line of optimums) and on the right side by the ZAV line. For this research project, the ZOA created using the Daniel and Benson (1990)

method is based only on acceptable hydraulic conductivity (less than 1×10^{-7} cm/sec which is the regulatory limit for municipal solid waste landfills) and does not account for the shear strength or shrink/swell conditions of the soil.

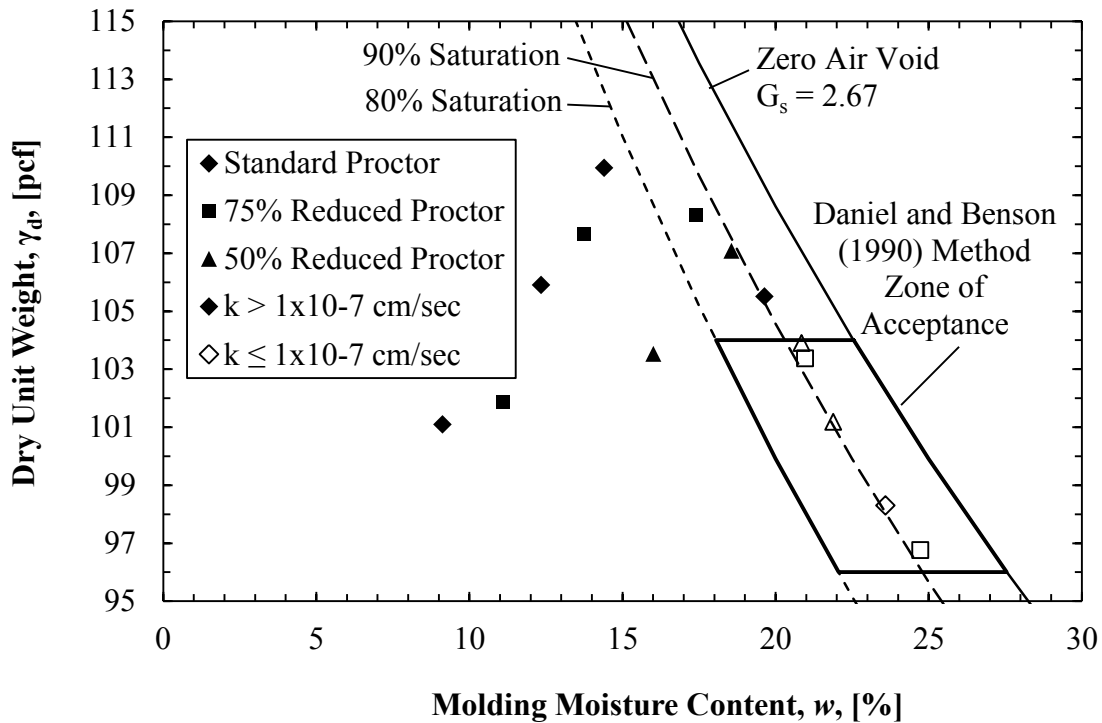


Figure 4.9. Zone of acceptance developed using the Daniel and Benson (1990) method.

The ZOA developed from the APCEC (2007) method also used the data presented previously in Figure 4.8 (only the standard Proctor data but also includes the reduced data for comparison purposes) and is presented in Figure 4.10. The top of the ZOA is bounded by the value of the maximum dry unit weight from the standard Proctor (109.3 pcf) and the bottom is bounded by the value of the 90 percent of the maximum dry unit weight from the standard Proctor (98.4 pcf = $0.9[109.3 \text{ pcf}]$). The left side of the ZOA is bounded by the value of the optimum moisture content (15.5%) and the right side is bounded by the ZAV line. The APCEC (2007) method includes points that were tested in the laboratory as not having an acceptable hydraulic conductivity (closed points with a hydraulic conductivity greater than 1×10^{-7} cm/sec,

the regulatory limit for municipal solid waste landfills) and does not include points that were tested in the laboratory as having an acceptable hydraulic conductivity (open points with a hydraulic conductivity less than 1×10^{-7} cm/sec, the regulatory limit for municipal solid waste landfills).

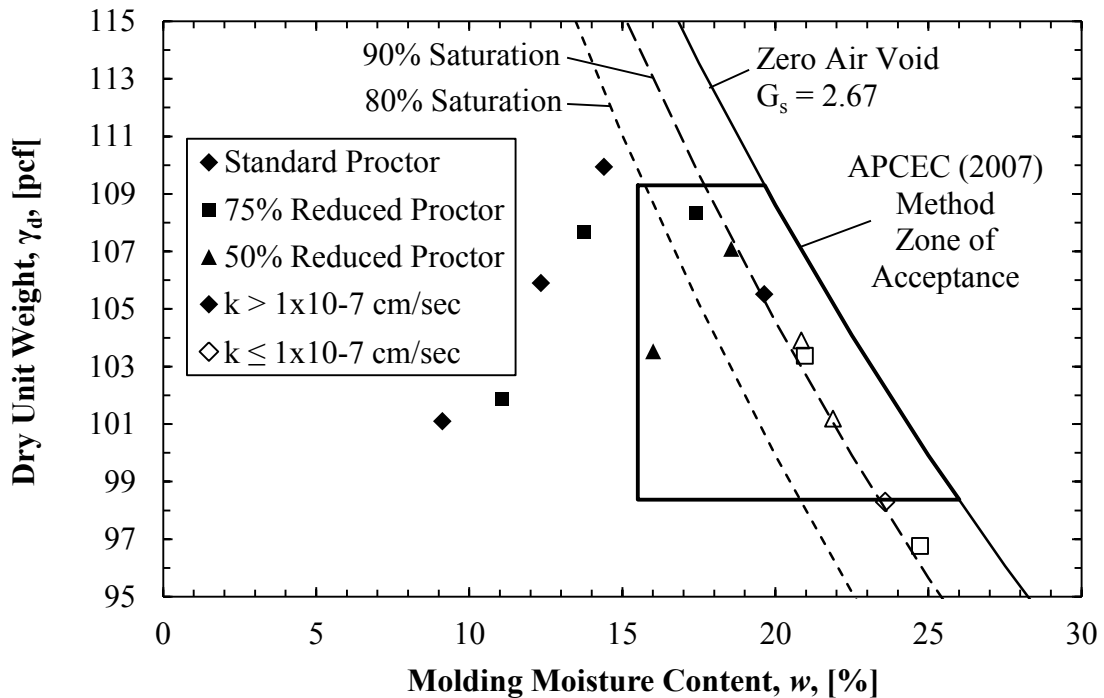


Figure 4.10. Zone of acceptance developed using the APCEC (2007) method.

4.4 Test Pad Placement Results

Test Pad 1 was placed as stated in Section 3.5.4. The results of density measurements obtained from the nuclear density gauge are presented in Figure 4.11. All five density tests from Lift 1 of Test Pad 1 plotted outside of the ZOA; therefore, Lift 1 was over compacted resulting in a higher dry unit weight than desired. In normal liner construction, when compaction requirements for a lift are not met, the lift is reworked (tilled up or replaced with other material) and recompact. However, Lift 1 was not reworked due to the inability to easily rework the soil in place and due to Lift 1 being on the bottom of the liner. Also, because Lift 1 was below the

area of interest for hydraulic conductivity testing, the lift was allowed to remain in place, as it was initially constructed, without rework.

In addition to the Lift 1 data plotting outside of the ZOA, the collected data from Lift 1 plotted above the ZAV. It is not physically possible for soils to be compacted with a dry unit weight and moisture content to the right/above the ZAV. The nuclear density tests are believed to have plotted above the ZOA due to the measured specific gravity (2.67) used for developing the ZAV being inaccurate. However, this value of specific gravity was utilized in calculating the ZOA line because it was the average value measured from the laboratory samples (as discussed on Section 4.6.3). The error is not believed to exist with the nuclear density gauge because all five points plotted outside the ZAV. Additionally, the nuclear density gauge passed a standard count calibration before use and the same nuclear gauge was used to conduct the remaining tests on the subsequent lifts which the obtained values plotted inside of the ZOA and were deemed acceptable (based on the values obtained for dry unit weight and moisture content, which are a corollary to measurements of hydraulic conductivity values).

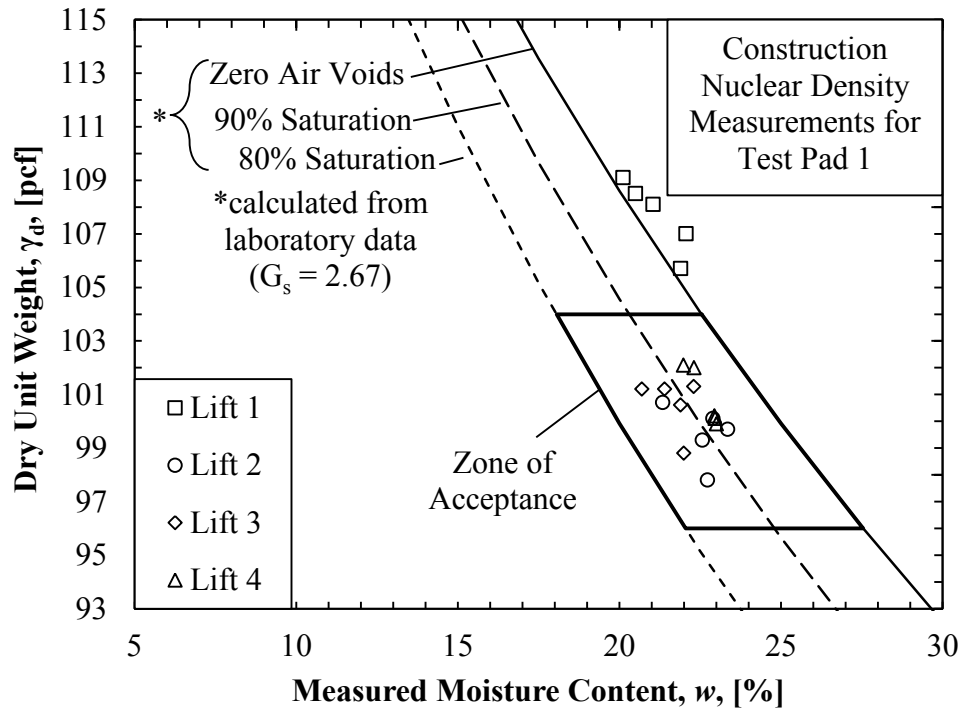


Figure 4.11. Dry unit weight and moisture content test measurements as obtained from nuclear density gauge for Test Pad 1.

Test Pad 2 was placed as stated in Section 3.5.5. The results of unit weight measurements obtained from the nuclear density gauge are presented in Figure 4.12. As previously mentioned, the ice in the stockpiled soil was believed to have caused some areas of the test pad to contain excess moisture. However, even with the excess moisture, all but one test (from Lift 3) plotted within the ZOA. Since the test that failed was on the outside edge of the test pad and the results from the other four tests from Lift 3 plotted within the ZOA, the lift was deemed acceptable and Lift 4 was then placed on top of Lift 3.

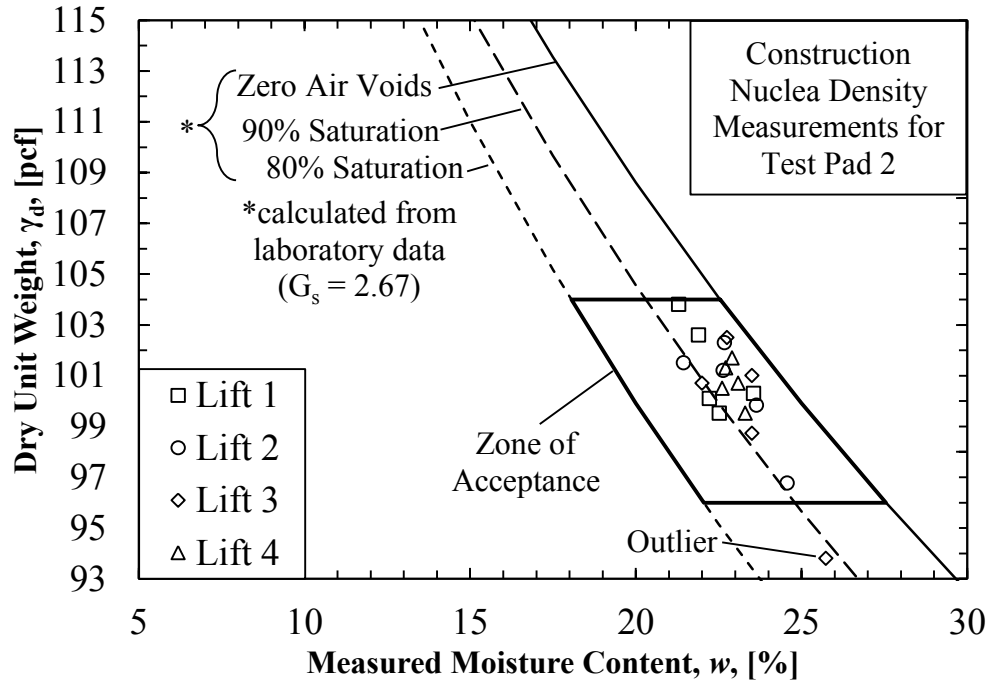


Figure 4.12. Dry unit weight and moisture content test measurements as obtained from nuclear density gauge for Test Pad 2.

Test Pad 3 was placed as stated in Section 3.5.5. The results of unit weight measurements obtained from the nuclear density gauge are presented in Figure 4.13. Water was added to the excessively dry soil to increase the moisture content and workability of the soil. Four unit weight tests from Lift 1 plotted outside of the ZOA. This was caused by the molding moisture content being too low during compaction resulting in a higher unit weight than desired. Lift 1 was not reworked due to the inability of easily reworking the soil and because the lift was below the area of interest for hydraulic conductivity testing. All but two of the unit weight tests from Lift 2 fell within the ZOA. Even though two of the tests from Lift 2 failed (the tests were located in the Northwest corner and in the center), it was deemed acceptable and Lift 3 was then placed on top of Lift 2. Only four unit weight tests were conducted on Lift 4 in the area outside of the outer ring. As previously mentioned, a unit weight test was not conducted inside the outer ring to ensure that the test hole for the nuclear density did not accelerate the vertical flow of water in a concentrated area.

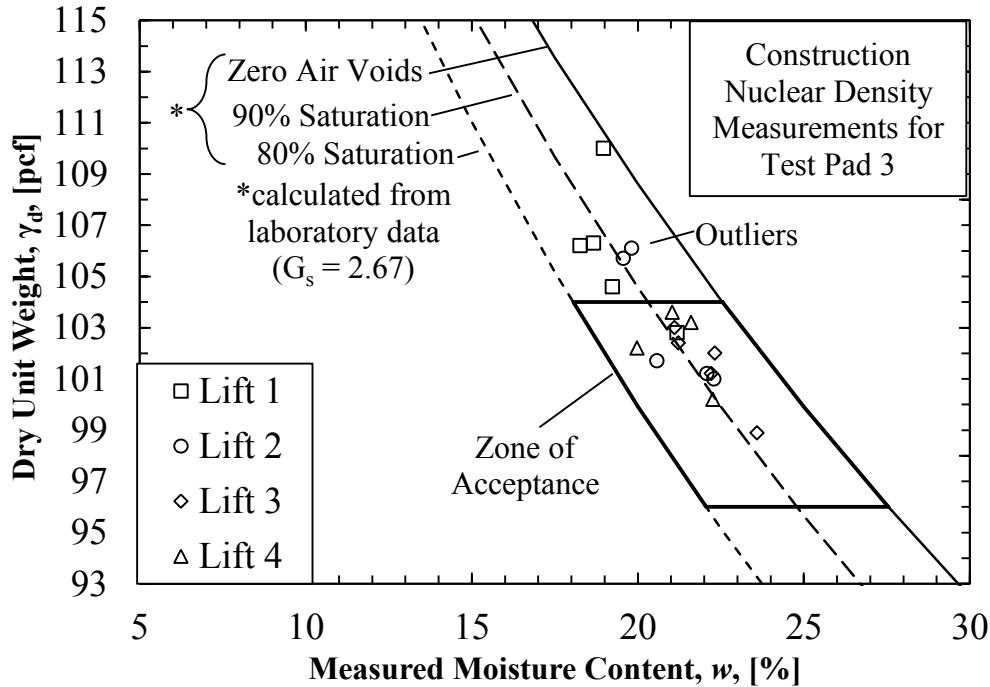


Figure 4.13. Dry unit weight and moisture content test measurements as obtained from nuclear density gauge for Test Pad 3.

4.5 Field Hydraulic Conductivity Testing Results

Two types of testing techniques, two stage borehole (TSB) and sealed double ring infiltrometer (SDRI), were used to measure the field hydraulic conductivity. The hydraulic conductivity results obtained from the TSB testing conducted on Test Pads 1 and 2 using the procedures stated in Section 3.6.1 are provided in Section 4.5.1. The results obtained from the SDRI testing conducted on Test Pad 3 using the procedures stated in Section 3.6.2 are provided in Section 4.5.2.

4.5.1 Two Stage Borehole Results for Test Pads 1 and 2

Stage 1 was conducted on Test Pad 1 for 499 hours. The measured hydraulic conductivity data obtained during Stage 1 are presented in Figure 4.14. The time weighted average apparent hydraulic conductivity value obtained from Stage 1 (k_1) is 1.09×10^{-8} cm/sec. Stage 2 was conducted on Test Pad 1 for 23 hours. The measured hydraulic conductivity data obtained during

Stage 2 are presented in Figure 4.15. The time weighted average apparent hydraulic conductivity value obtained from Stage 2 (k_2) is 1.50×10^{-8} cm/sec.

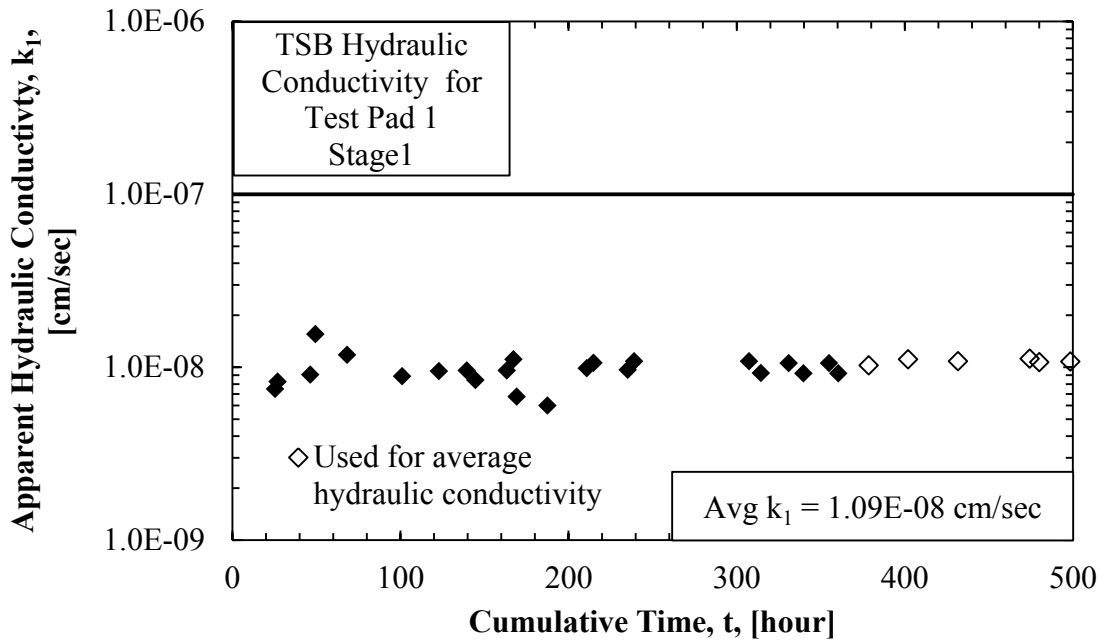


Figure 4.14. Stage 1 apparent hydraulic conductivity data for Test Pad 1.

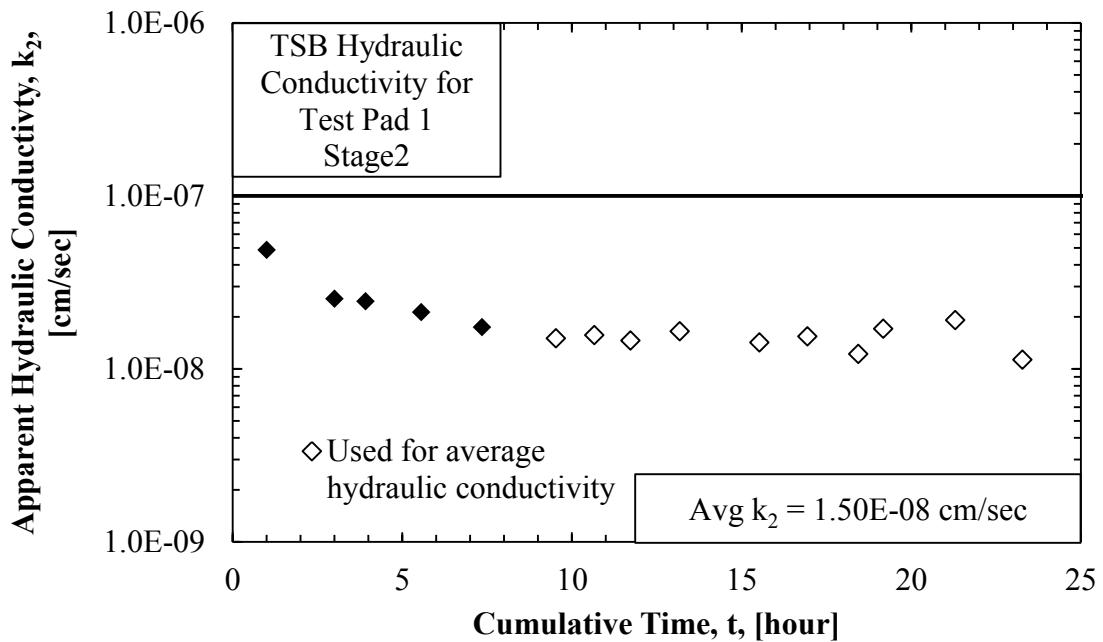


Figure 4.15. Stage 2 apparent hydraulic conductivity data for Test Pad 1.

The k_2/k_1 ratio value is 1.37 resulting in an anisotropy value (m) of 2.19 (as calculated using the Microsoft Excel® Solver function) using the Soil Testing Engineers, Inc. (1983) method and an anisotropy value (m) of 2.22 (as calculated using the Microsoft Excel® Solver function) using the Boutwell (1992) method. Using the Soil Testing Engineers, Inc. (1983) method a vertical hydraulic conductivity value ($k_{v,20^\circ\text{C}}$) of 4.98×10^{-9} cm/sec and a horizontal hydraulic conductivity value ($k_{h,20^\circ\text{C}}$) of 2.39×10^{-8} cm/sec was obtained. Using the Boutwell (1992) method a vertical hydraulic conductivity value ($k_{v,20^\circ\text{C}}$) of 5.13×10^{-9} cm/sec and a horizontal hydraulic conductivity value ($k_{h,20^\circ\text{C}}$) of 2.52×10^{-8} cm/sec was obtained. The TSB data obtained during Stages 1 and 2 for Test Pads 1 and 2 are presented in Appendix B (Table B.1 through Table B.4)

Stage 1 was conducted on Test Pad 2 for 262 hours. The measured hydraulic conductivity data obtained during Stage 1 for Test Pad 2 are presented in Figure 4.16. The time weighted average apparent hydraulic conductivity value obtained from Stage 1 (k_1) is 2.18×10^{-8} cm/sec. Stage 2 was conducted on Test Pad 2 for 44 hours. The measured hydraulic conductivity data obtained during Stage 2 for Test Pad 2 are presented in Figure 4.17. The time weighted average apparent hydraulic conductivity value obtained from Stage 2 (k_2) is 3.13×10^{-8} cm/sec.

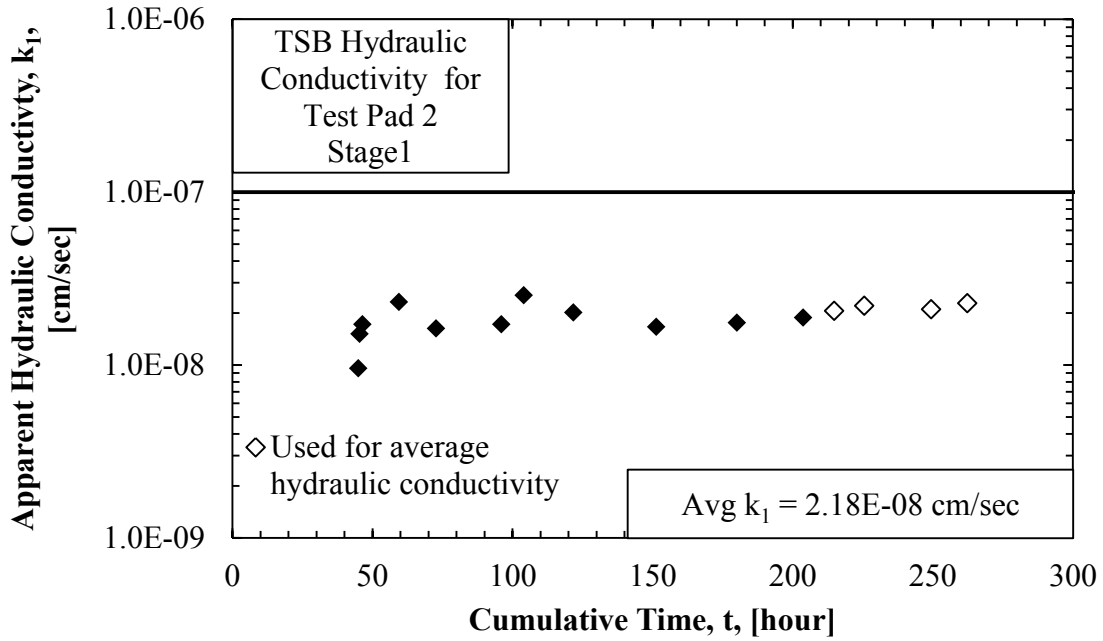


Figure 4.16. Stage 1 apparent hydraulic conductivity data for Test Pad 2.

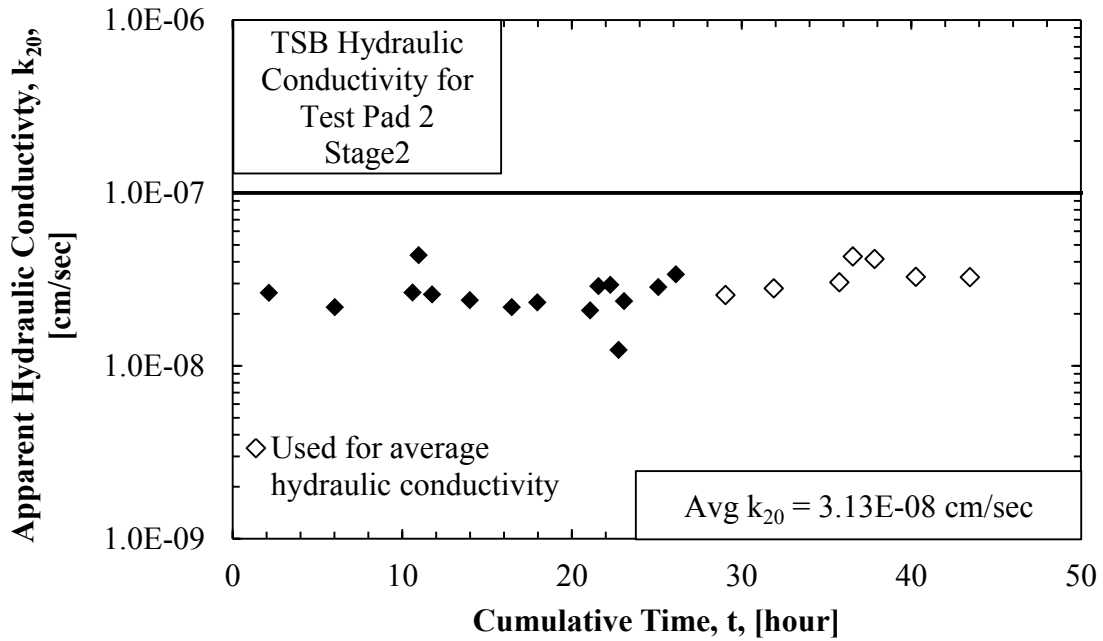


Figure 4.17. Stage 2 apparent hydraulic conductivity data for Test Pad 2.

The k_2/k_1 ratio value is 1.44 resulting in an anisotropy value (m) of 2.39 (as calculated using the Microsoft Excel® Solver function) using the Soil Testing Engineers, Inc. (1983) method and an anisotropy value (m) of 2.42 (as calculated using the Microsoft Excel® Solver

function) using the Boutwell (1992) method. Using the Soil Testing Engineers, Inc. (1983) method a vertical hydraulic conductivity value ($k_{v,20^{\circ}\text{C}}$) of 9.11×10^{-9} cm/sec and a horizontal hydraulic conductivity value ($k_{h,20^{\circ}\text{C}}$) of 5.21×10^{-8} cm/sec was obtained. Using the Boutwell (1992) method a vertical hydraulic conductivity value ($k_{v,20^{\circ}\text{C}}$) of 9.41×10^{-9} cm/sec and a horizontal hydraulic conductivity value ($k_{h,20^{\circ}\text{C}}$) of 5.51×10^{-8} cm/sec was obtained.

The initial hydraulic conductivity data in Figure 4.16 has an increasing trend instead of the expected decreasing trend. When Stage 1 TSB testing was began on Test Pad 2, the standpipe was mistakenly overfilled with an initial water level at 25-centimeters, 10 centimeters over the critical height of 15-centimeters as previously mentioned in Section 3.6.1. The high hydraulic gradient may have affected the initial measured hydraulic conductivity data and caused the initial upward trend. The mistake was noticed and corrected after 46 hours of testing. As shown in Figure 4.16, when the initial water level in the standpipe was lowered to 15-centimeters, the data formed a horizontal trend. Due to scatter and uncertainty in the data, any measured hydraulic conductivity with an initial standpipe reading above the 15-centimeter level was not plotted.

4.5.2 Sealed Double Ring Infiltrometer Results for Test Pad 3

As of December 11, 2012, the SDRI testing is still being conducted on Test Pad 3. The SDRI test has been conducted for 1519 hours and the current measured hydraulic conductivity data are presented in Figure 4.18. The hydraulic conductivity has not achieved steady state flow; however, acceptable hydraulic conductivity (less than the regulatory requirement of 1.0×10^{-7} cm/sec) has been observed as the last measured hydraulic conductivity equal to 1.96×10^{-9} cm/sec using the wetting front method. The SDRI data obtained for Test Pad 3 is presented in Appendix B (Tables B.5 and B.6). Data collected from the tensiometers (used to monitor the wetting front movement), as presented in Figure 4.19, were used to calculate the hydraulic gradient (i).

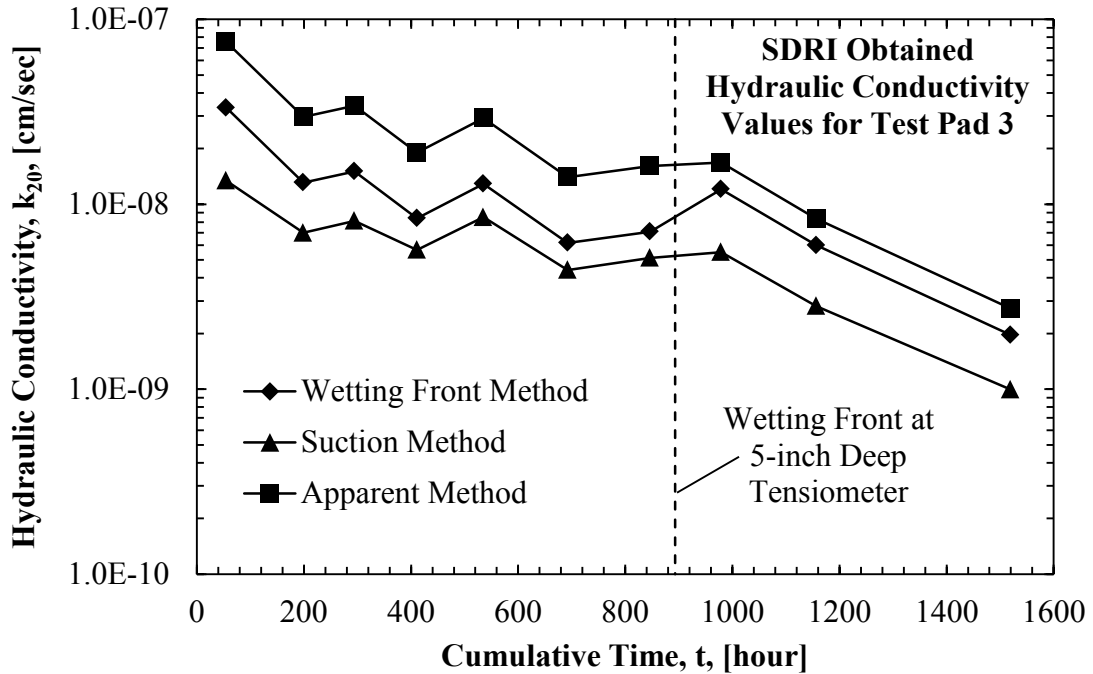


Figure 4.18. SDRI apparent hydraulic conductivity data for Test Pad 3.

In Figure 4.19, at 55 hours, a drop is noticed in all 5 operational tensiometers. The drop was caused by each tensiometer being opened to apply suction to facilitate removal of air bubbles. When the tensiometer cap was opened, the suction was lost and after resealing the cap, the suction slowly restored inside the tensiometer. The broken tensiometer South-23 (as observed immediately after installation) was replaced with a new tensiometer at 752 hours. The wetting front reached the tensiometers with tips located at the 5-inch depth at 893 hours into the SDRI testing.

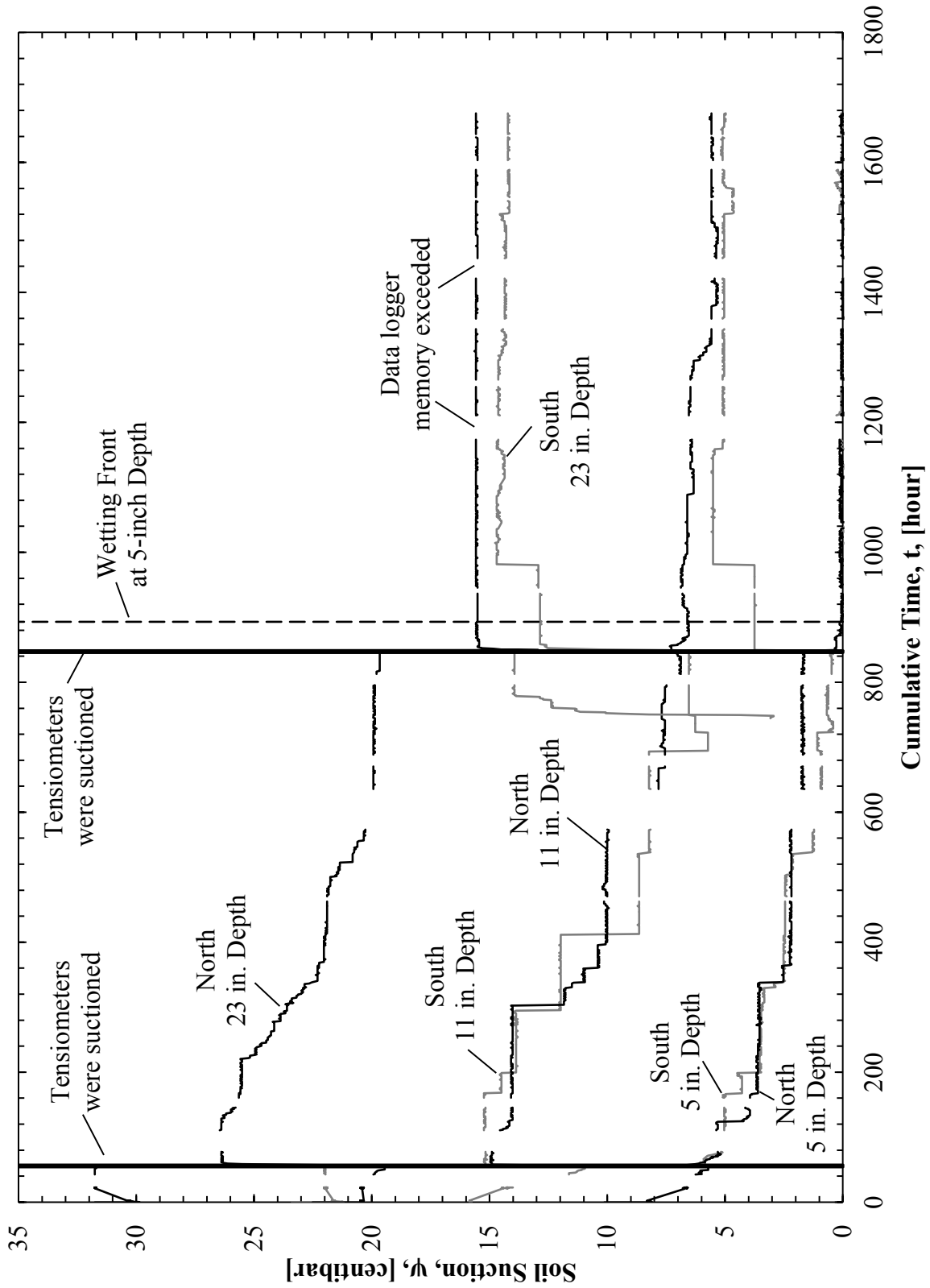


Figure 4.19. Soil suction data collected from Test Pad 3.

Time domain reflectometry (TDR) probes were used to monitor volumetric moisture content (with readings collected every hour). A typical plot of collected TDR data (data collected from South TRD probe at 14-inch depth) is presented in Figure 4.20. Gaps are noticed between portions of the collected data. These gaps are caused by the older data on the memory of the data logger being automatically overwritten to store new data (i.e. the data were not downloaded from the data collector fast enough). Therefore, whenever the data logger was filled, the old data was lost and a gap was created within the database. A volumetric moisture content range of 33 to 37 percent was calculated from TDR data using the equation presented in Topp et al. (1980). This range closely matches the volumetric moisture content range of 34 to 36 percent determined from phase diagrams created using the average of the nuclear density data collected from Lifts 2, 3, and 4 of Test Pad 3.

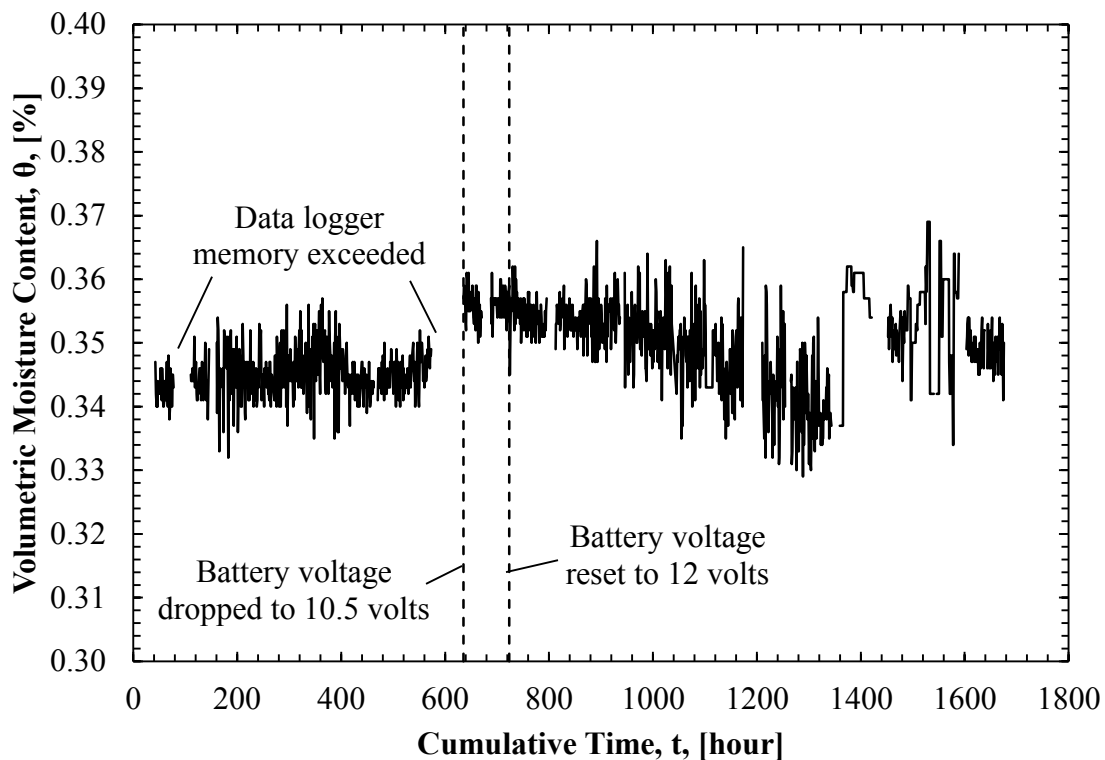


Figure 4.20. TDR data collected from South TRD probe located 14 inches below the soil surface.

A moving average trendline over six data points was used to notice trends in the data. An example of the moving average trend line is presented in Figure 4.21. As shown in Figure 4.21, the volumetric moisture content remains constant until 573 hours and then it shifts upward by 2.5 percent at 635 hours. Between 573 hours and 635 hours, the memory of the data logger was exceeded and the collected data were lost. At 635 hours, a drop of 1.5 volts (from 12 volts to 10.5 volts) was noticed in the battery meter. The drop was caused by the power supply being disturbed and the supplied voltage level being unknowingly reduced. The change in supplied voltage level affected the measurements being recorded by the data logger and caused the shift in data. At 723 hours, the change in voltage was discovered when the power supply was turned off to replace the malfunctioning tensiometer; therefore when the power supply was turned back on, the supplied voltage was readjusted to 12 volts. The shift in the collected TDR data was not noticed in the tensiometer data because the supplied voltage (and therefore change in voltage) is automatically accounted for by obtaining the data from the data collector while processing the tensiometer data.

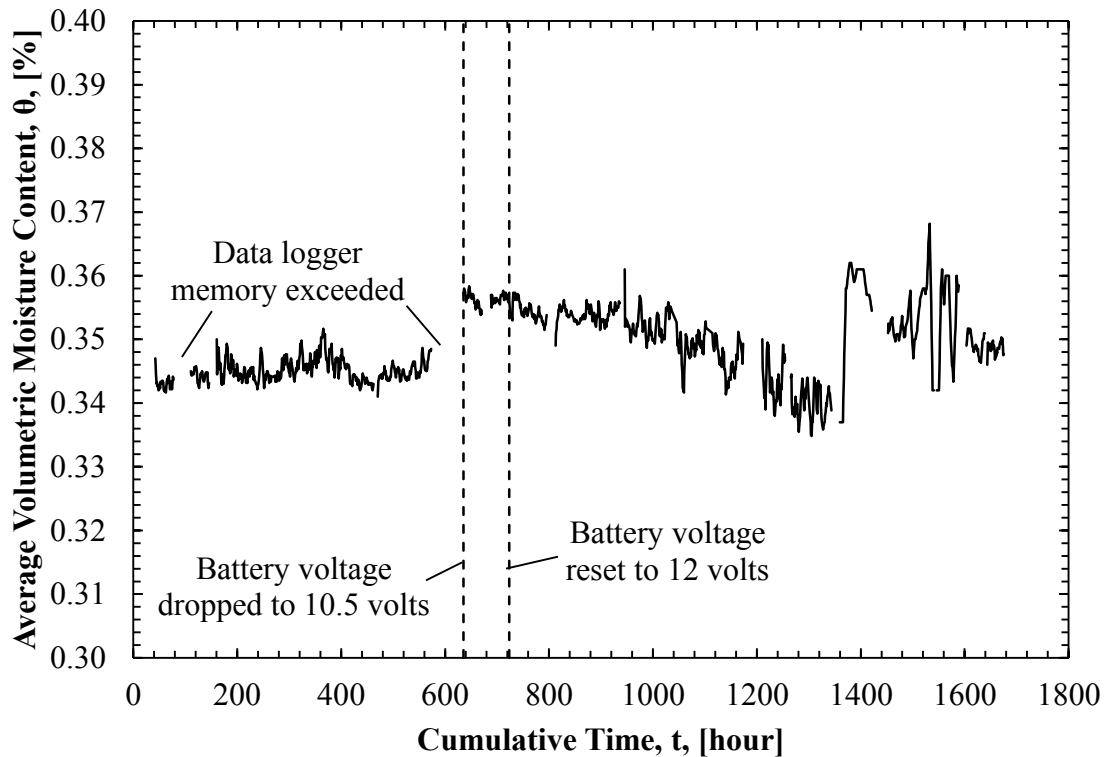


Figure 4.21. Moving average for TDR data collected from South TRD probe located 14 inches below the soil surface.

Based on the steady trend in the data, the moisture content in the soil is not changing significantly. After the jump, the data has a steady horizontal trend and then begins to decrease. The decreasing trend in the data indicates the soil is drying which is expected from the soil in Lift 2, as the wetting front has not yet reached the lift and the soil is drying from the bottom of the liner (because the bottom of the liner is open to the atmosphere). Average data from all of the TDR probes are presented in Figure 4.22 and data from each of the individual TDR probes are presented in Appendix B (Figure B.1 through Figure B.12).

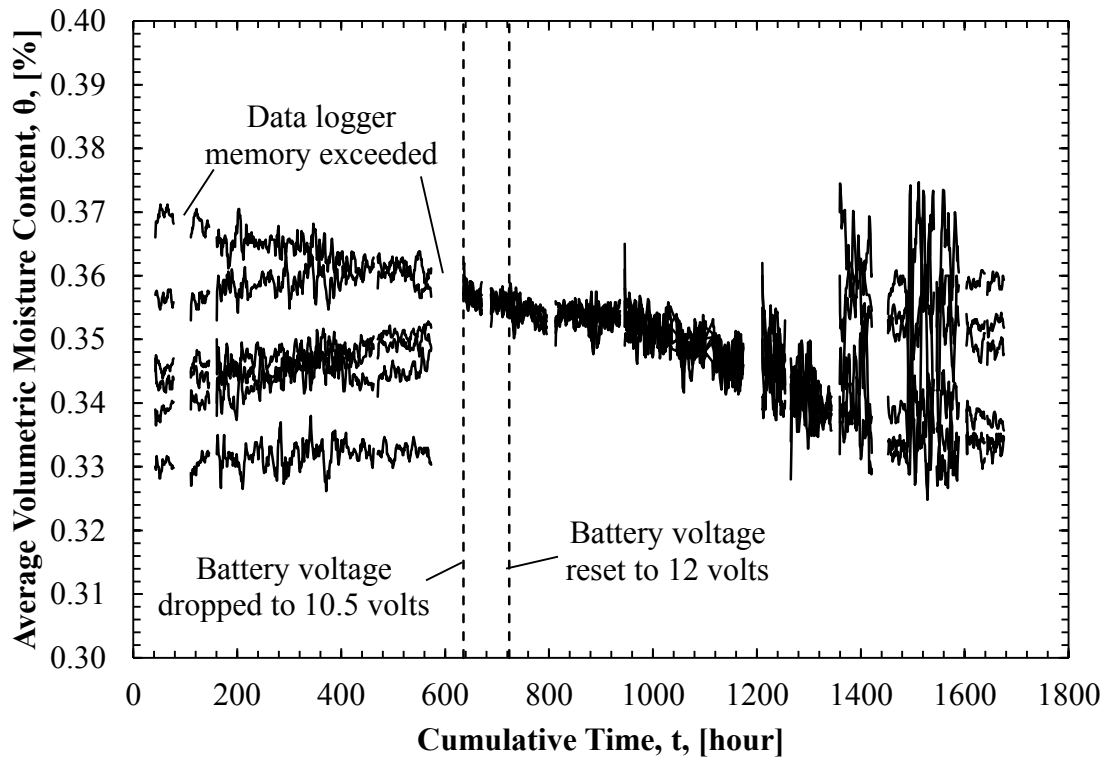


Figure 4.22. Moving average for each individual TDR data collected from Test Pad 3.

A plot of the averaged (smoothed) TDR data from the South TRD probe at 2-inch depth is presented in Figure 4.23. An initial increasing trend is observed as expected due to increased saturation as the wetting front moves through the soil. The expected trend is for the measured volumetric moisture content to increase until the soil around the probe becomes fully saturated, and then the measured volumetric moisture content will remain constant. However, the observed trend is increasing measured volumetric moisture content, then a peak is reached, and a decreasing trend in measured volumetric moisture content is observed. Even though the soil might be fully saturated, the decreasing trend in volumetric moisture content is possibly caused by the soil consolidating, and thereby decreasing in volumetric moisture content.

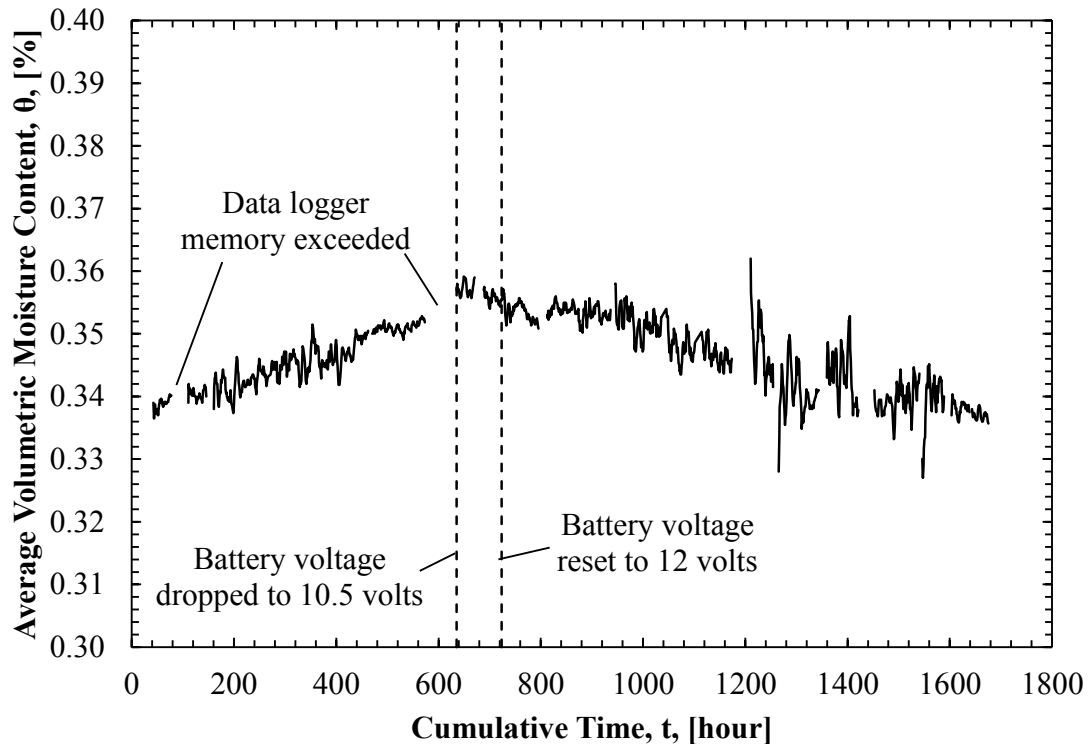


Figure 4.23. Moving average for TDR data collected from South TRD probe at 2-inch depth.

4.6 Laboratory Testing Results

The measured values for laboratory vertical and horizontal hydraulic obtained from samples collected from Test Pads 1 and 2 were used to validate values obtained from the TSB field results. Additionally, the measured values for laboratory vertical hydraulic conductivity obtained from using hand carved and Shelby tube samples from Lifts 1, 2, 3, and 4 collected from Test Pads 1 and 2 were compared to evaluate the effects of sample acquisition. Soil parameters of each of the samples on which laboratory hydraulic conductivity was measured were collected before and after testing to determine changes in soil parameters during testing. Results from soil index testing (e.g. specific gravity, particle size, percent passing No. 200 sieve, Atterberg limits) were used to classify the soil and to ensure that soil properties (e.g. soil gradation and Atterberg limits) were consistent amongst the various compacted test pads.

4.6.1 Hydraulic Conductivity, Dry Unit Weight, and Measured Moisture Content Results for Samples Collected from Test Pad 1

A summary of the initial and final soil parameter data (e.g. moisture content, unit weight, saturation, void ratio, and porosity) as measured from subsamples of the Southeast Shelby tube sample (SE-ST-TP1) and the West and East hand carved samples (W-HC-TP1 and E-HC-TP1) collected from Test Pad 1 are presented in Appendix C for completeness (Table C.1 through Table C.6). Also for completeness, plots of hydraulic conductivity and inflow/outflow ratio as a function of the number of pore volumes of flow for each SE-ST-TP1, W-HC-TP1, and E-HC-TP1 subsamples are presented in Figure C.1 through Figure C.14, Figure C.15 through Figure C.22, and Figure C.23 through Figure C.28, respectively.

The SE-ST-TP1 sample lost moisture between sampling and laboratory testing due to not being stored in the environmental chamber. The initial moisture content of the first sample tested, SE-ST-TP1 Lift 4, was 18.9 percent which was close to the average in-situ moisture content (21.1 percent) measured during construction of the test pad. However, the initial moisture content for subsequent samples from SE-ST-TP1 ranged from 15.2 to 16.6 percent which indicates that moisture was lost from the soil. Additionally, changes in the physical appearance of the soil provide insight that the soil lost moisture after it was sampled from the test pad. The initial moisture content for samples W-HC-TP1 and E-HC-TP1, which were stored in the environmental chamber until testing, ranged from 18.9 to 19.7 percent indicating no significant loss in moisture.

The loss of pressure to the panel board in September, 2011, caused fluctuations in the measured hydraulic conductivity. As seen in Figure 4.24, the measured hydraulic conductivity shifted by one order of magnitude when pressure was not applied (due to malfunction of the compressor for one week). Readings were recorded approximately once per day to allow for a

considerable amount of flow through the soil sample (with a change in head height ranging between 0.5 and 1.5 centimeters). However, occasionally readings were not collected for several days due to research not being conducted (e.g. researches being away from the laboratory for the weekend). Spaces between the measured hydraulic conductivities (i.e. from 1.0 to 1.4 pore volumes of flow as shown in Figure 4.24) are extended periods of time between readings. The extended time in between readings did not affect the calculated hydraulic conductivity as noticed from the continuous trend. During these extended periods, the samples were allowed to equilibrate (i.e. flow was allowed to continue unmeasured until readings could be collected again).

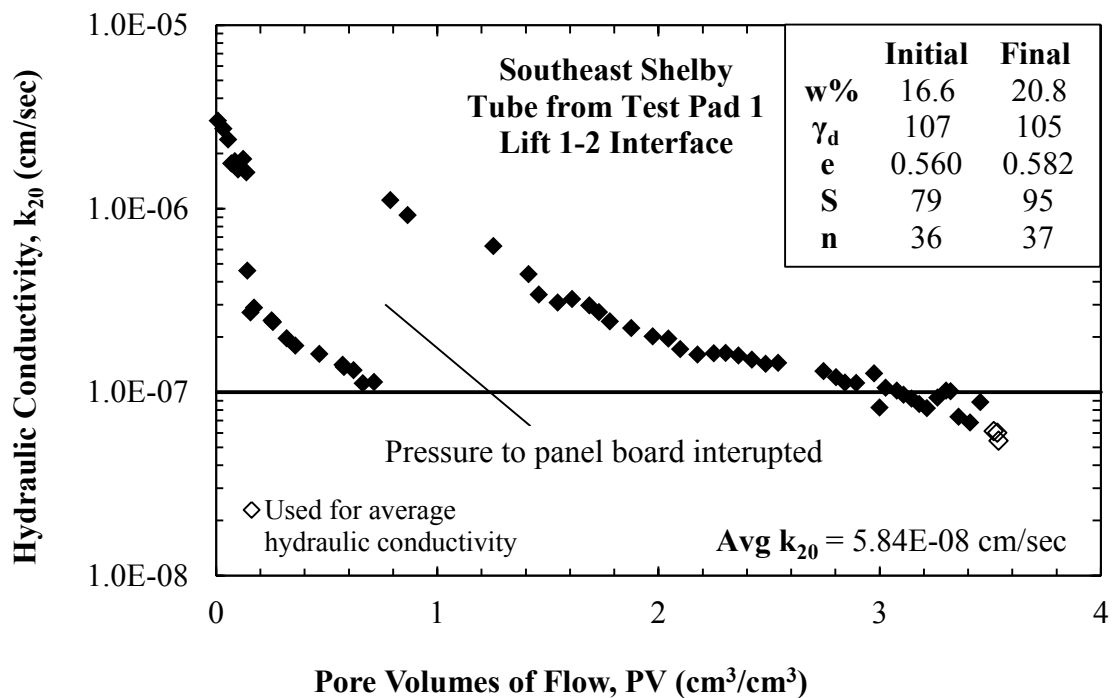


Figure 4.24. Vertical hydraulic conductivity data for SE-ST-TP1 Lift 1-2 Interface.

A plot of vertical hydraulic conductivity with depth for the SE-ST-TP1 is presented in Figure 4.25. The value of vertical hydraulic conductivity linearly increase with depth until the interface between Lifts 2 and 3; at the interface, the hydraulic conductivity suddenly decreases

and then the values again increase in a linear fashion. The interface between Lifts 2 and 3 is where construction of the test pad was paused at the end of the work day and resumed during the next work day.

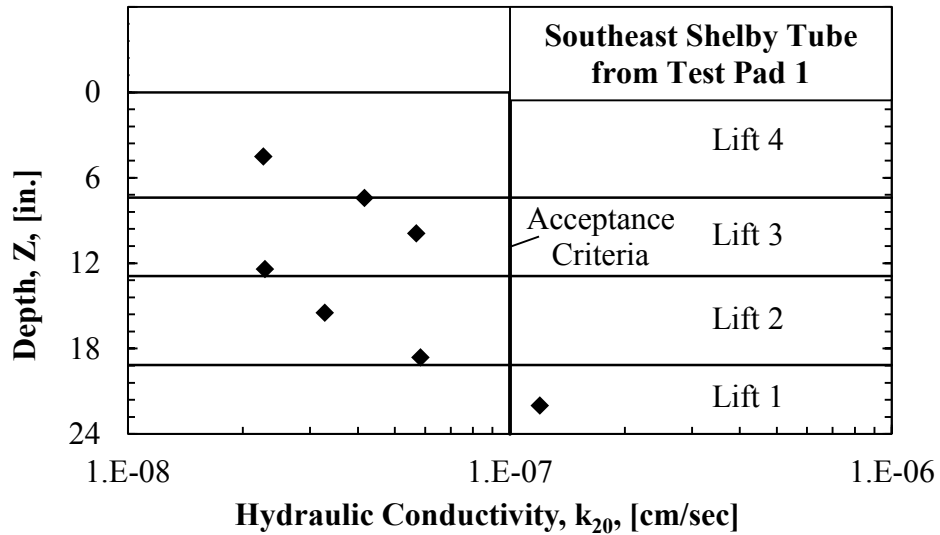


Figure 4.25. Summary plot of vertical hydraulic conductivity values obtained from the SE-ST-TP1 sample.

The compaction effort applied to each lift may not have fully penetrated the entire lift because the hydraulic conductivity increases with depth within each lift. The loss in compaction effort is attributed to the loose lift thickness being too thick for the selected compactor and/or the size of soil clods being too large for even compaction effort across the pad.

A plot of measured vertical and horizontal hydraulic conductivity values (as obtained using the flexible wall hydraulic conductivity device) with depth for both hand carved samples is presented in Figure 4.26. There is no noticeable trend amongst the vertical hydraulic conductivity samples. However, the vertical samples from Lifts 2 and 4 began producing air bubbles during hydraulic conductivity testing. It is believed that the air bubbles were caused by microorganisms developing in the soil samples because all of the cell connections were checked and no signs of water leakage from the cell were noticed. The production of the air bubbles

caused a steep decrease in hydraulic conductivity of the soil as well as drop in the inflow to outflow ratio. Because the air bubbles occupied excess volume in the tail water plumbing, it is likely that the collected tail water measurements became inaccurate when the production of the air bubbles began. The other two vertical samples, Lifts 1 and 3, did not produce air bubbles and yielded hydraulic conductivities that were an order of magnitude higher than the Lifts 2 and 4 values.

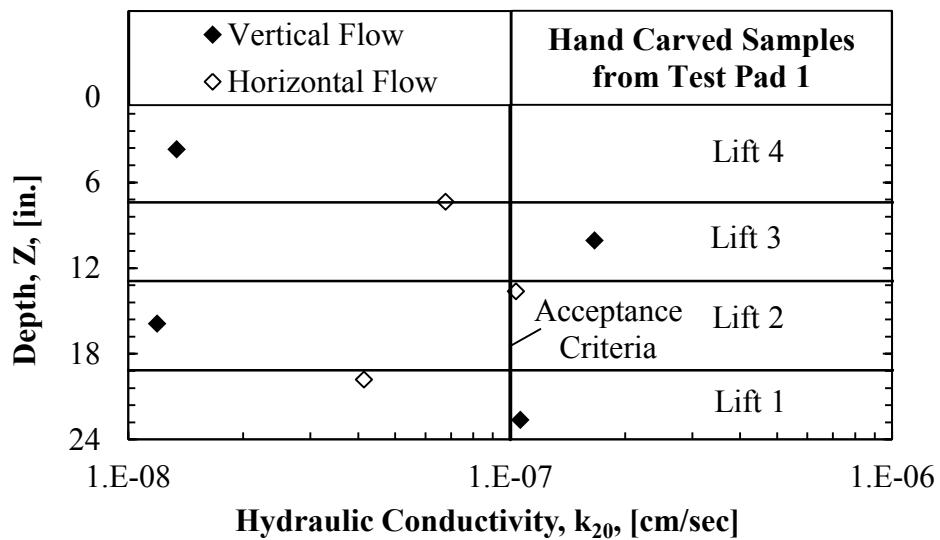


Figure 4.26. Summary plot of vertical and horizontal hydraulic conductivity values obtained from W-HC-TP1 and E-HC-TP1 samples.

The measured dry unit weight and moisture content results obtained from each hydraulic conductivity subsample obtained the SE-ST-TP1 and HC-TP1 samples are presented in Figure 4.27 and Figure 4.28, respectively. Closed symbols denote soil properties obtained before hydraulic conductivity testing and open symbols denote soil properties obtained after hydraulic conductivity testing. A shift in moisture content was caused by the sample becoming more saturated during the testing. Additionally, there was some change in dry unit weight which is confirmed by a change in void ratio. Six of the samples from SE-ST-TP1 plotted outside of the ZOA; however, of the six samples, acceptable hydraulic conductivities (less than 1×10^{-7} cm/sec)

were measured for five of the samples. Unit weights with acceptable hydraulic conductivities (less than 1.0×10^{-7} cm/sec) plotting outside the ZOA may indicate that the ZOA is conservative. Soil properties obtained before hydraulic conductivity testing for four of the HC-TP1 samples and soil properties obtained after hydraulic conductivity testing for all of the samples dictated that the samples should be located within the ZOA. Two of the HC-TP1 samples, W-HC-TP1 Lift 1 and W-HC-TP1 Lift 3, did not possess an acceptable vertical hydraulic conductivity value even though they plotted within the ZOA indicating that the ZOA may be unconservative. The higher vertical hydraulic conductivity values may indicate that macro-structure is present in the large subsamples (hand carved samples) but not the small subsamples (Shelby tube samples) and that the Shelby tube samples were compressed during sampling resulting in a lower void ratio and therefore a lower hydraulic conductivity value.

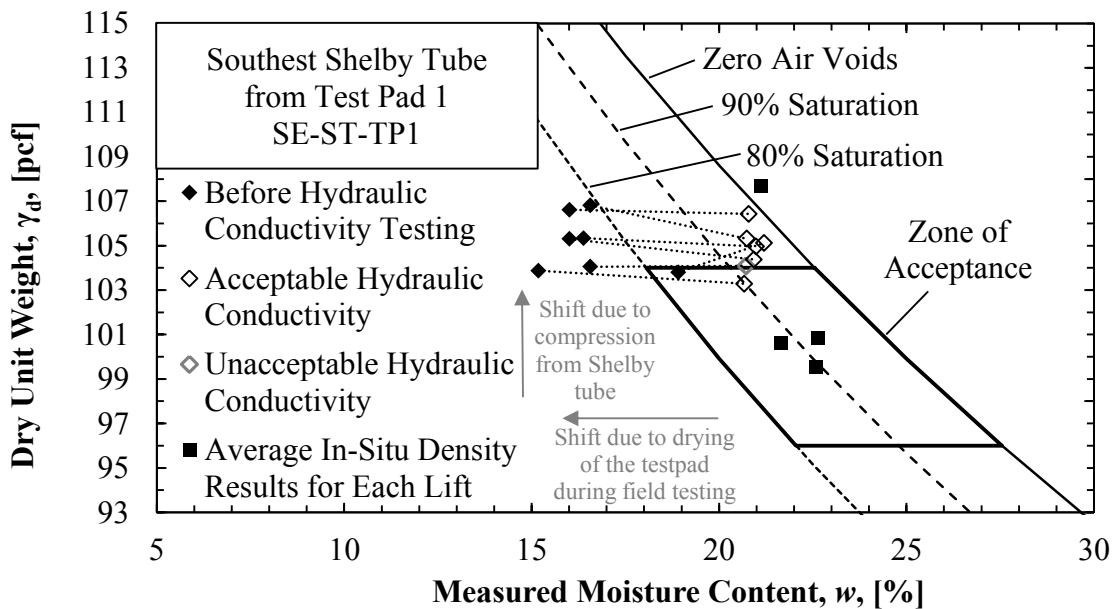


Figure 4.27. Dry unit weight and moisture content results for SE-ST-TP1 before and after laboratory hydraulic conductivity testing.

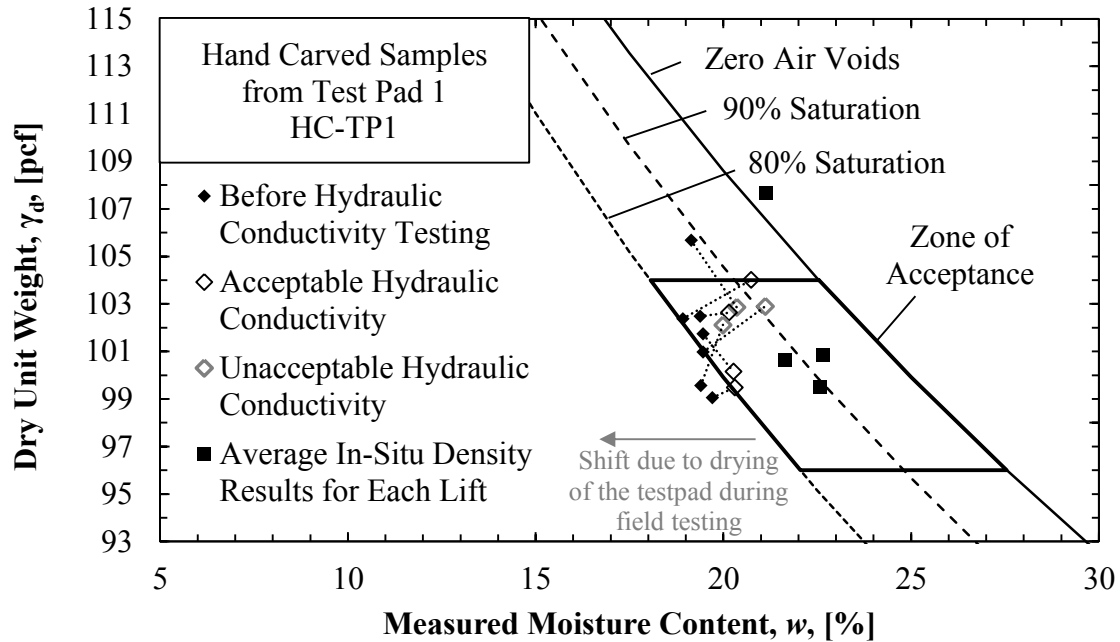


Figure 4.28. Dry unit weight and moisture content results for HC-TP1 before and after laboratory hydraulic conductivity testing.

As shown in Figure 4.27 and Figure 4.28, the unit weights from the Shelby tube subsamples were consecutively higher than the hand carved subsamples. Because both samples were collected from the same test pad, the measured unit weights should match the unit weight measurements collected from the nuclear density gauge testing during soil placement (a direct comparison between the moisture content values cannot be obtained because the obtained moisture content values for the laboratory samples should be less than the nuclear density gauge measurements because of drying during in-situ hydraulic conductivity testing and delays prior to testing the samples in the laboratory). The higher unit weights noticed in the Shelby tube subsamples are caused by the soil compressing as the Shelby tube is pushed into the test pad. The compressing of the soil within the tube during sampling is confirmed by the recovered length of soil in the Shelby tube being less than the actual length pushed.

4.6.2 Hydraulic Conductivity, Dry Unit Weight, and Measured Moisture Content Results for Samples Collected from Test Pad 2

A summary of the initial and final soil parameter data as measured from subsamples of the Southeast Shelby tube sample (SE-ST-TP2) and the West and East hand carved samples (W-HC-TP2 and E-HC-TP2) collected from Test Pad 2 are presented in Appendix C for completeness (Table C.7 through Table C.12). Also for completeness, plots of hydraulic conductivity and inflow/outflow ratio as a function of the number of pore volumes of flow for each SE-ST-TP2, W-HC-TP2, and E-HC-TP2 subsamples are presented in Figure C.29 through Figure C.42, Figure C.43 through Figure C.50, and Figure C.51 through Figure C.56, respectively.

A summary of vertical hydraulic conductivity values obtained from CT-ST-TP2 as a function of depth is presented in Figure 4.29. The measured vertical hydraulic conductivity values (obtained from the flexible wall hydraulic conductivity test) are similar, ranging from 1.19×10^{-8} to 2.04×10^{-8} cm/sec. The similarity of the hydraulic conductivity values may indicate an even compaction was achieved throughout each lift in Test Pad 2. The values of vertical hydraulic conductivity changes uniformly with depth with higher values of hydraulic conductivity at the top and bottom of the test pad as compared to the values obtained for the samples collected from the middle of the test pad. The higher hydraulic conductivity values may indicate that the top and bottom of the test pad were susceptible to moisture loss (e.g. evaporation and drainage) because these portions of the test pad were more exposed to atmospheric conditions. However, the moisture loss theory is not confirmed by the initial moisture content measured from each sample at the beginning of the hydraulic conductivity testing. The initial moisture content throughout the lift was consistent with a range of 18.2 to

18.8 percent with the exception of Lift 1 sample in CT-ST-TP2 and Lift 3-4 Interface sample in CT-ST-TP2 with initial moisture contents of 19.4 and 17.6 percent, respectively.

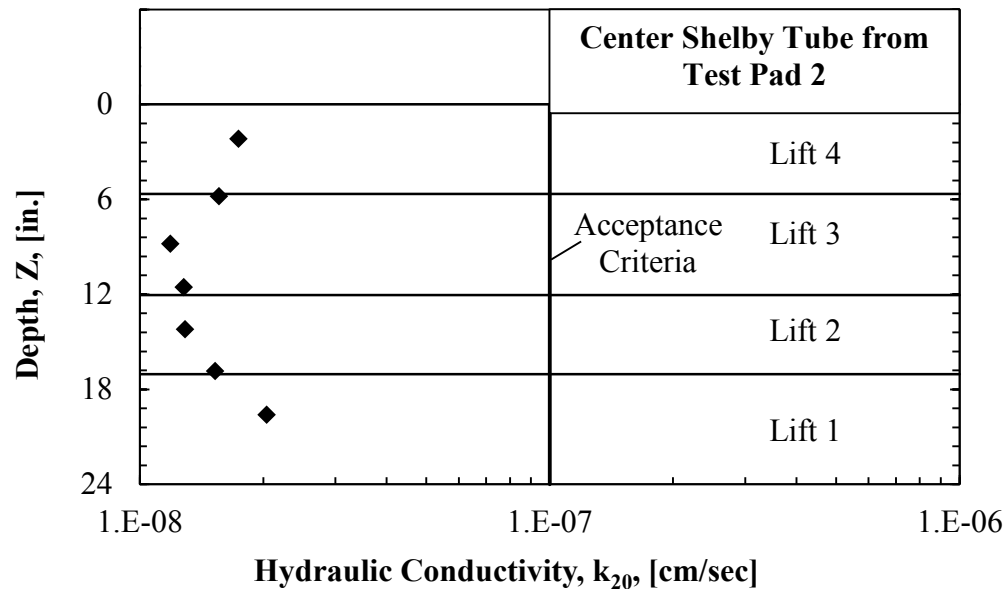


Figure 4.29. Summary plot of vertical hydraulic conductivity values as a function of depth as obtained from the CT-ST-TP2 sample.

A summary of vertical and horizontal hydraulic conductivity values as a function of depth for the HC-TP2 is presented in Figure 4.30. Vertical hydraulic conductivity values are presented as closed symbols and horizontal hydraulic conductivity values are presented as open symbols. HC-TP2 has a larger range of vertical hydraulic conductivity than CT-ST-TP2 with a range of 1.71×10^{-8} to 4.30×10^{-8} cm/sec. The change in vertical hydraulic conductivity with depth of HC-TP2 followed the same trend as observed for the samples obtained from CT-ST-TP2; the vertical hydraulic conductivity values of samples obtained from Lifts 1 and 4 of W-HC-TP2 are higher than the vertical hydraulic conductivity values of samples obtained from Lifts 2 and 3 of W-HC-TP2. The horizontal hydraulic conductivity values range from 3.80×10^{-8} to 7.45×10^{-8} cm/sec with a decreasing linear trend with depth.

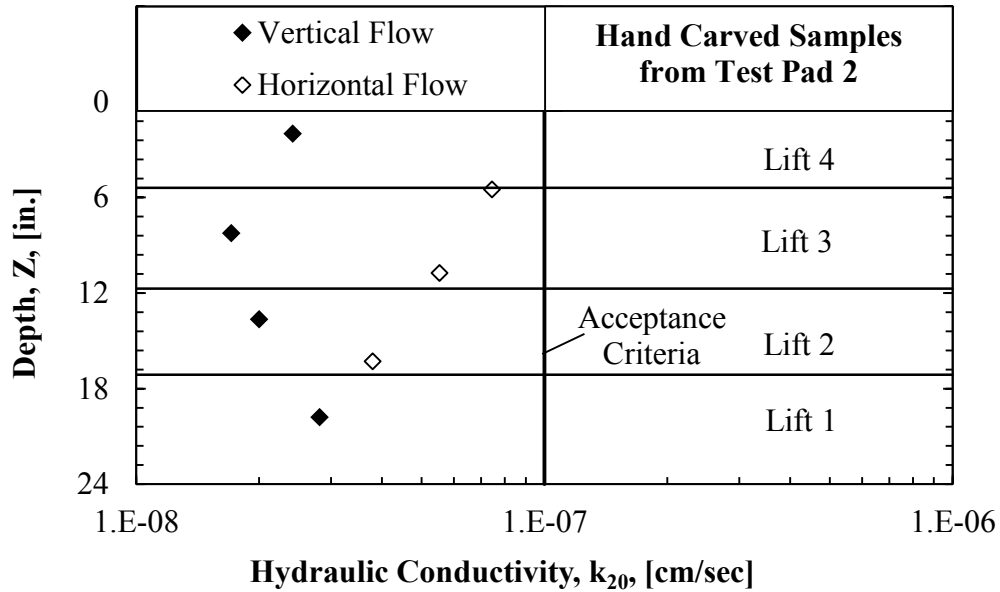


Figure 4.30. Summary plot of vertical and horizontal hydraulic conductivity values as a function of depth as obtained from HC-TP2 samples.

The unit weight measurement results for each hydraulic conductivity sample from CT-ST-TP2 and HC-TP2 are presented in Figure 4.31 and Figure 4.32, respectively. Closed symbols denote soil properties obtained before hydraulic conductivity testing and open symbols denote soil properties obtained after hydraulic conductivity testing. In a similar fashion to Test Pad 1, the saturation and unit weight of the samples, on which hydraulic conductivity testing was being performed, changed during flexible wall hydraulic conductivity testing. Uniform dry unit weight and moisture content values were observed for the CT-ST-TP2 samples after hydraulic conductivity testing as observed in Figure 4.31. All of the dry unit weight and moisture content combination values obtained from CT-ST-TP2, before and after hydraulic conductivity testing, plotted outside of the ZOA; however, acceptable hydraulic conductivity values (less than 1×10^{-7} cm/sec) were measured for all of the CT-ST-TP2 samples. Values for dry unit weight and moisture content combinations for the vertical hydraulic conductivity subsamples from W-HC-TP2 plotted within the ZOA before and after testing, and acceptable values of vertical hydraulic

conductivity (less than 1.0×10^{-7} cm/sec) were measured for the subsamples. As with Test Pad 1, the dry unit weight and corresponding moisture content values measured for the hand carved subsamples collected from Test Pad 2 were comparable to the in-situ dry unit weight and corresponding moisture content values measured during test pad placement. However, as with Test Pad 1, dry unit weight measurements obtained from the Shelby tube subsamples collected from Test Pad 2 were higher than the in-situ dry unit weight measurements obtained during test pad placement, indicating that pushing Shelby tube into the test pad causes the soil to compress during sampling.

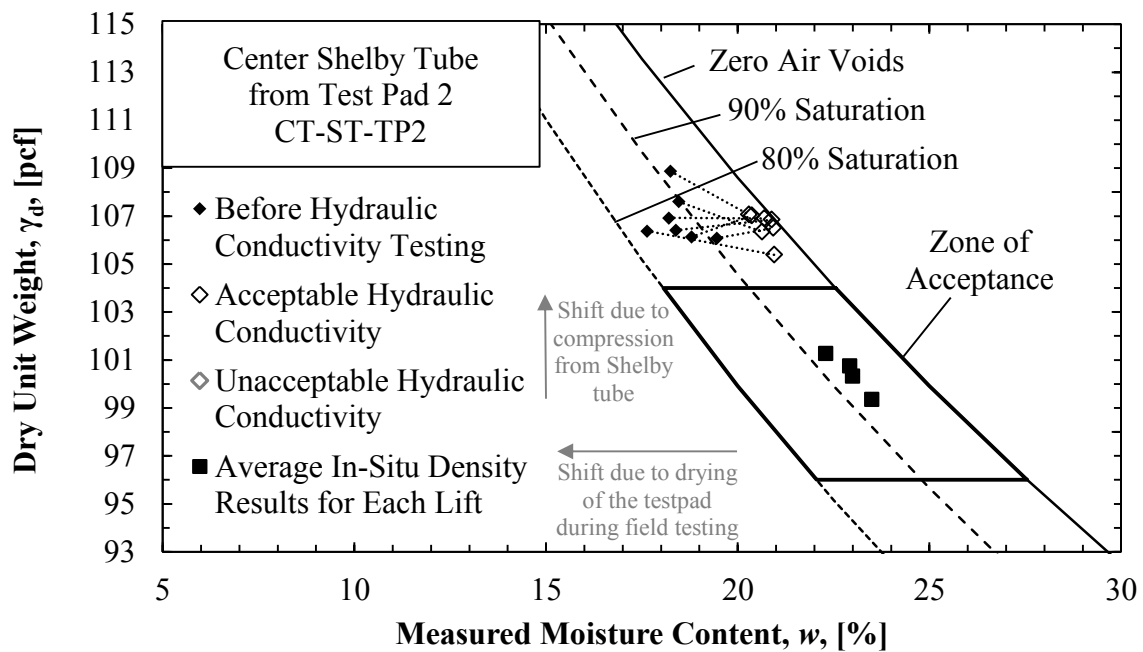


Figure 4.31. Dry unit weight and moisture content results for CT-ST-TP2 before and after laboratory hydraulic conductivity testing.

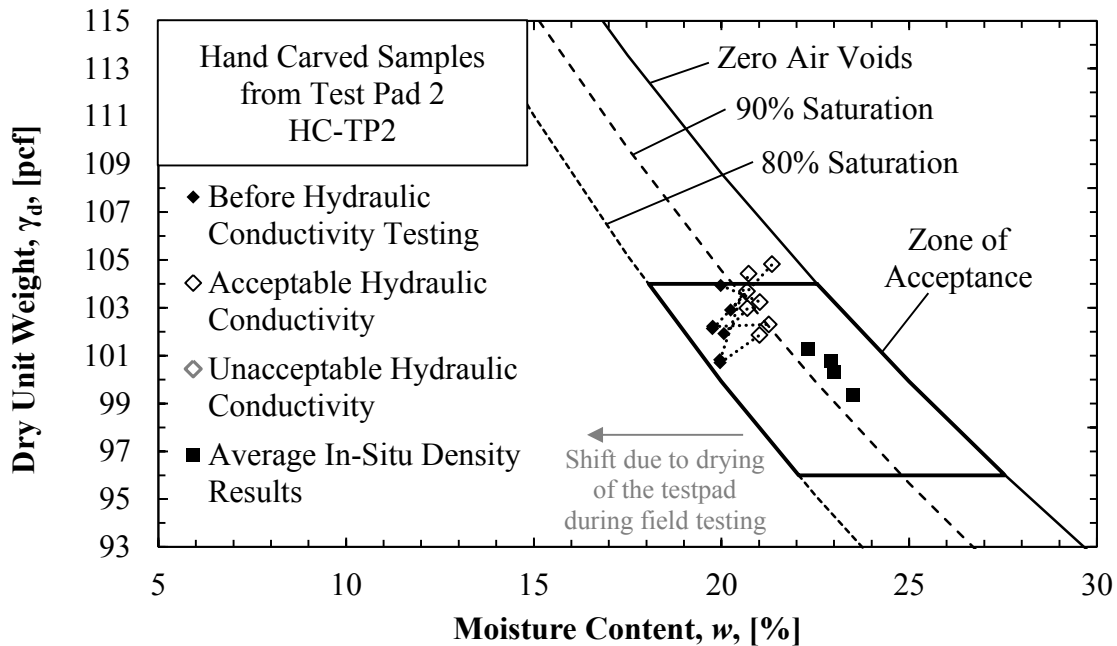


Figure 4.32. Dry unit weight and moisture content results for HC-TP2 before and after laboratory hydraulic conductivity testing.

4.6.3 Soil Index Testing Results for Samples Collected from Test Pads 1 and 2

Soil index testing was conducted on subsamples obtained from Shelby tube samples (from SW-ST-TP1 and SW-ST-TP2) and from the cuttings obtained from the TSB borehole from Test Pad 2. Summaries of the index properties from SW-ST-TP1, SW-ST-TP2, and TSB borehole cuttings from Test Pad 2 are presented in Appendix D in Table D.1 through Table D.3, respectively, for completeness. The average laboratory measured specific gravity for the soil was 2.67 (2.60-2.71). A sample of the data for particle size analysis obtained from percent passing the No. 200 sieve and hydrometer testing are presented in Figure 4.33. The results obtained from particle size analysis conducted on subsamples from SW-ST-TP1, SW-ST-TP2, and TSB borehole cuttings from Test Pad 2 are presented in Figure D.1 through Figure D.16, for completeness. The average percent fines is 87.5 percent (based on the percent passing the No. 200 sieve). From the percent passing the No. 200 sieve and hydrometer analysis, the soil has a clay fraction of 27.3 percent. The results of the Atterberg limits tests are presented in Figure 4.34

through Figure 4.36 for Tests Pad 1, 2 (Shelby tube), and 2 (TSB boring), respectively. The corresponding results of the liquid limit tests are presented in Figure D.17 through Figure D.32, for completeness. The average liquid limit and plastic limit of the soil were 36 and 17, respectively, with a plasticity index of 19. The average laboratory measured activity for the soil was 0.70 (0.63-0.78).

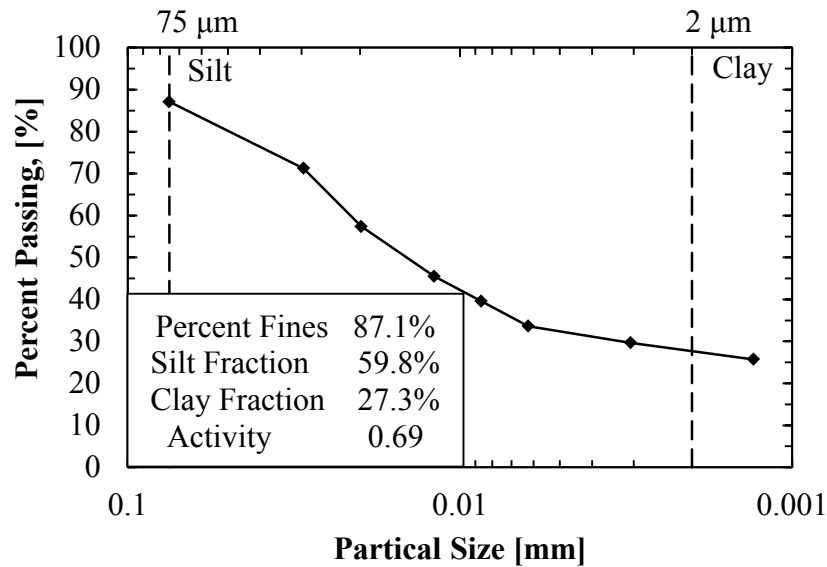


Figure 4.33 Hydrometer results from Test Pad 1 Southwest Shelby Tube Lift 1 sample (SW-ST-TP1).

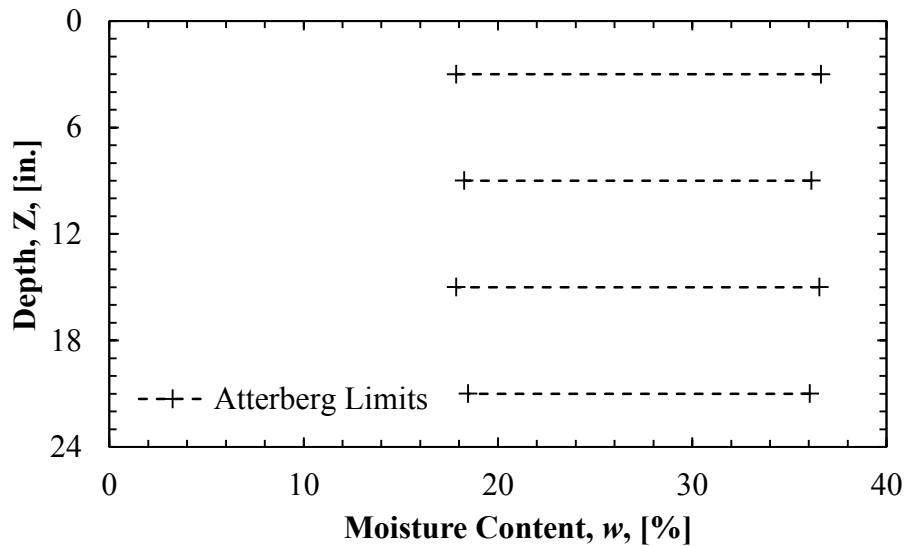


Figure 4.34. Summary of Atterberg limit results from samples obtained from Test Pad 1 Southwest Shelby Tube (SW-ST-TP1).

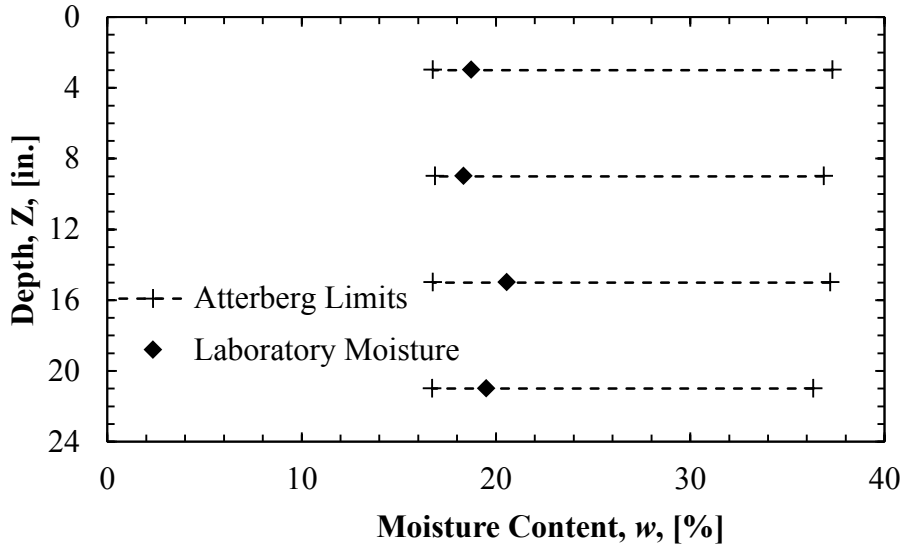


Figure 4.35. Summary of Atterberg limit results and in-situ moisture content from samples obtained from Test Pad 2 Southwest Shelby Tube (SW-ST-TP2).

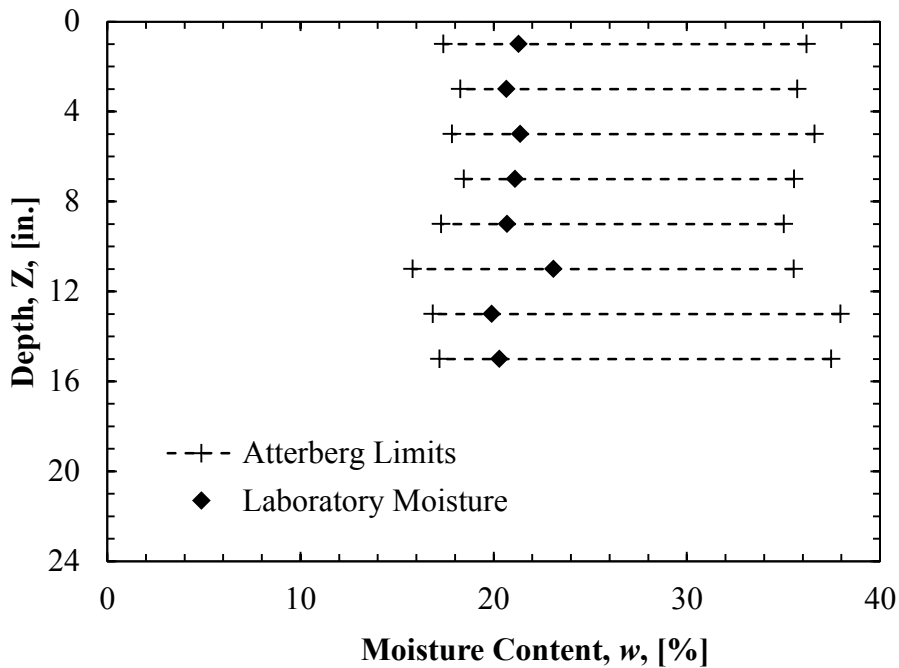


Figure 4.36. Summary of Atterberg limit results and in-situ moisture content from samples obtained from TSB Test Pad 2 cuttings (SW-TSB-TP2).

The collected laboratory index properties were used to classify the soil using the Unified Soil Classification System (USCS) method (ASTM D2487, 2012) and the American Association of State Highway and Transportation Officials (AASHTO) classification method (ASTM D3282,

2012). Using the USCS method, the soil classifies as lean clay (CL). Using the AASHTO method, the soil classifies as A-6(12).

4.7 Discussion of Testing Techniques Comparisons

Values obtained for hydraulic conductivity from the two field testing methods (sealed double ring infiltrometer [SDRI] and two stage borehole [TSB]) were compared to each other and to the values obtained from laboratory measurements (hand carved and Shelby tube samples). Specifically, the laboratory results were used to validate the accuracy of the field obtained values for vertical and horizontal hydraulic conductivity as is commonly completed in practice. Additionally, the laboratory results were used to determine if there is a difference between small diameter Shelby tube samples and large diameter hand carved samples. The two in-situ hydraulic conductivity testing techniques were compared against each other to determine the difference in the obtained vertical hydraulic conductivity measurements.

Additionally, the dry unit weight and moisture content values obtained from the nuclear density gauge were compared to dry unit weight and moisture content values obtained from Shelby tube and hand carved samples used for laboratory hydraulic conductivity testing. The comparisons between the dry unit weight and moisture content values were used to determine the amount of compression and drying of the soil sample during sample acquisition and prior to. Compression of the soil samples was also evaluated using the recovery length data from the collected Shelby tubes by comparing the recovered to the pushed lengths. The volumetric moisture content measurements obtained from the time domain reflectometry (TDR) probes in Test Pad 3 were compared to the gravimetric moisture content measurements obtained from the nuclear density testing from Test Pad 3 to determine the amount of drying while the test pad was in place.

4.7.1 Discussion on Comparisons between the Hydraulic Conductivity Values Obtained from Shelby Tube and Hand Carved Samples

A comparison of the vertical hydraulic conductivity values obtained for Lifts 1, 2, 3, and 4, as obtained from testing on subsamples from SE-ST-TP1 and CT-ST-TP2, and the vertical hydraulic conductivity of Lifts 1, 2, 3, and 4 as obtained from testing on subsamples from W-HC-TP1 and W-HC-TP2, respectively, are presented in Figure 4.37 and Figure 4.38, respectively. Due to problems occurring during the laboratory hydraulic conductivity testing of Test Pad 1, as discussed in Section 3.8.1, Figure 4.37 was presented only for completeness. Only samples from Test Pad 2 were used to evaluate Shelby tube and hand carved results because they are believed to be more reliable. As shown in Figure 4.38, lower hydraulic conductivity values were consistently measured in the Shelby tube samples than in the hand carved samples. The ratio of Shelby tube hydraulic conductivity compared to hand carved hydraulic conductivity for Lifts 1, 2, 3, and 4 yielded a linear trend with an average ratio of 0.70.

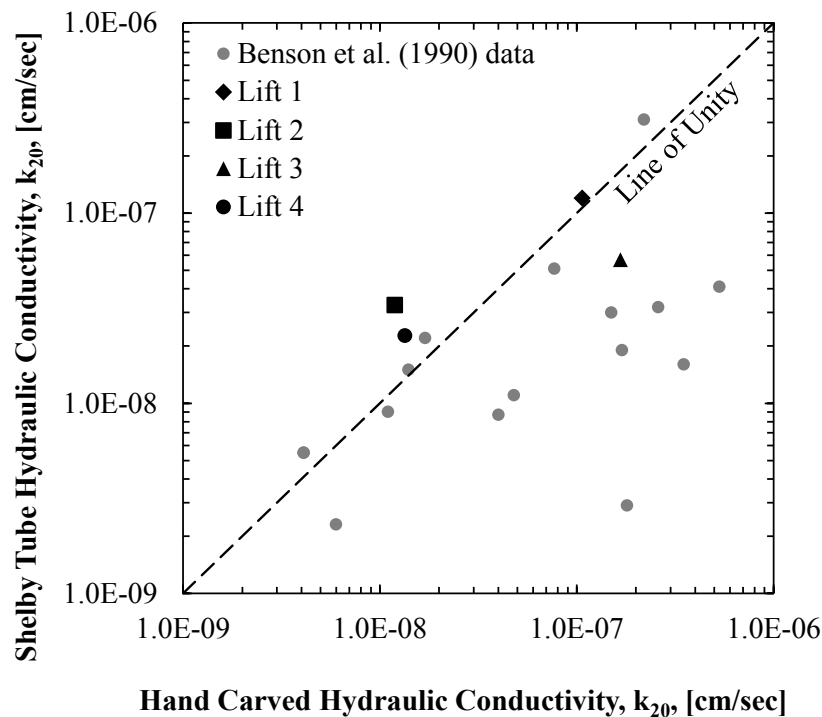


Figure 4.37. Comparison between vertical hydraulic conductivity of Shelby tube samples and hand carved samples from Test Pad 1.

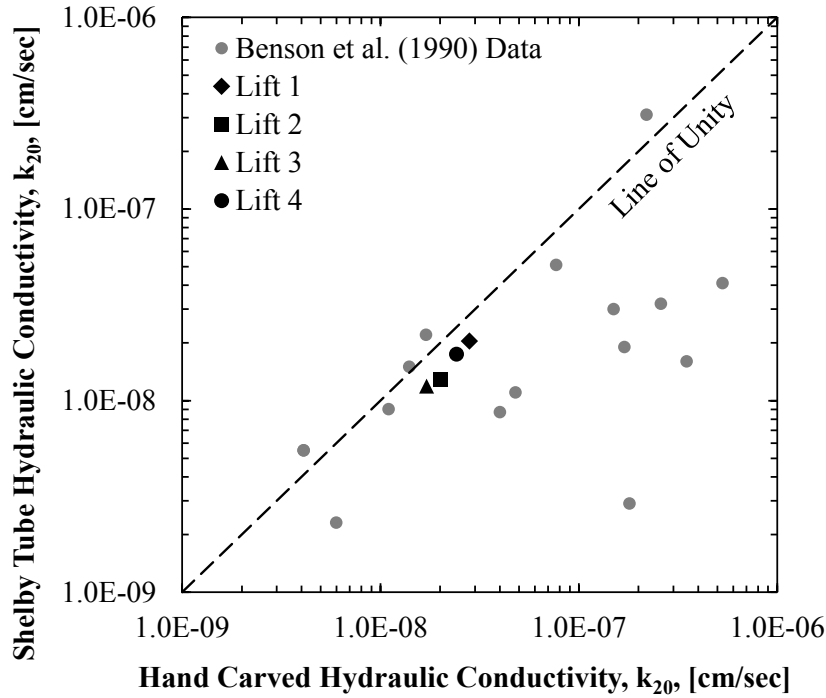


Figure 4.38. Comparison between vertical hydraulic conductivity of Shelby tube samples and hand carved samples from Test Pad 2.

4.7.2 Discussion on the Comparisons between the Laboratory and Field (TSB) Hydraulic Conductivity Results

A comparison between laboratory hydraulic conductivity values (Shelby tube and hand carved) and field hydraulic conductivity values for Test Pads 1 and 2 are presented in Figure 4.39 and Figure 4.40, respectively. The hydraulic conductivity of Lift 3 and the Lift 2-3 Interface were selected for analysis because those are the zones that are directly measured by the TSB test. Due to problems occurring during the laboratory hydraulic conductivity testing of Test Pad 1, as discussed in Section 3.8.1, only samples from Test Pad 2 were used to compare the results obtained from laboratory and field (TSB) analyses. For Test Pad 2, the vertical hydraulic conductivity values measured on Lifts 3 from CT-ST-TP2 and Lift 3 from W-HC-TP2 was plotted against the vertical hydraulic conductivity as measured using the TSB testing device. Similarly, the horizontal hydraulic conductivity values measured on the Lift 2-3 Interface from E-HC-TP2 was plotted against the horizontal hydraulic conductivity using from the TSB test. All

three comparisons for Test Pad 2 plotted near the line of unity indicating that the laboratory hydraulic conductivity is comparable to field hydraulic conductivity. This relationship agrees with the relationship presented in Benson et al. (1999) as previously discussed in Section 2.11. Because the SDRI testing is currently being conducted and therefore Test Pad 3 has not been sampled, comparisons between field and laboratory data for Test Pad 3 cannot be made.

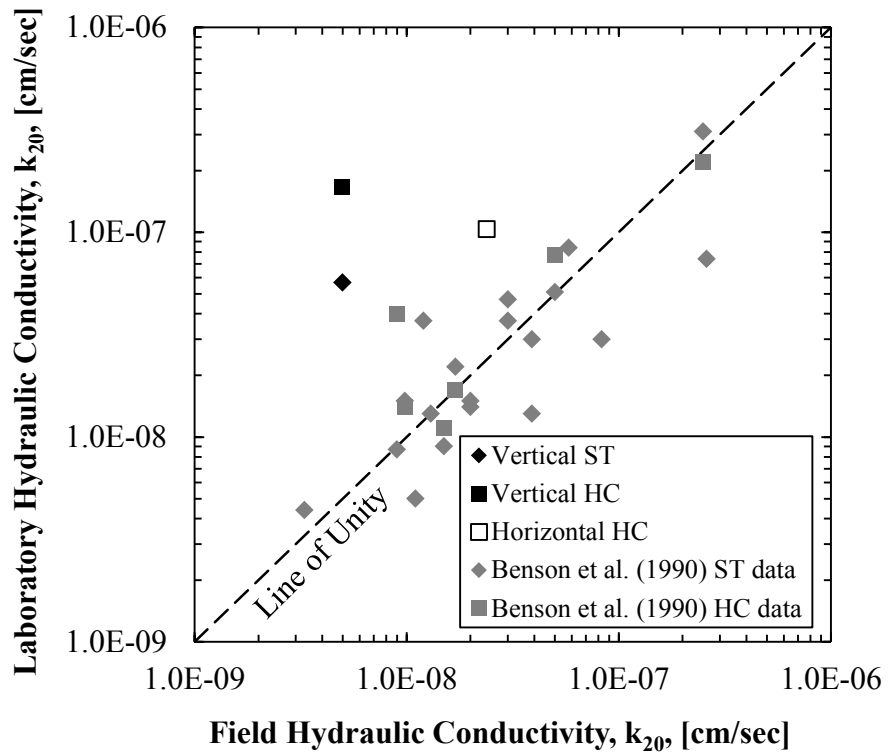


Figure 4.39. Comparison between laboratory hydraulic conductivity and two stage field hydraulic conductivity for Test Pad 1.

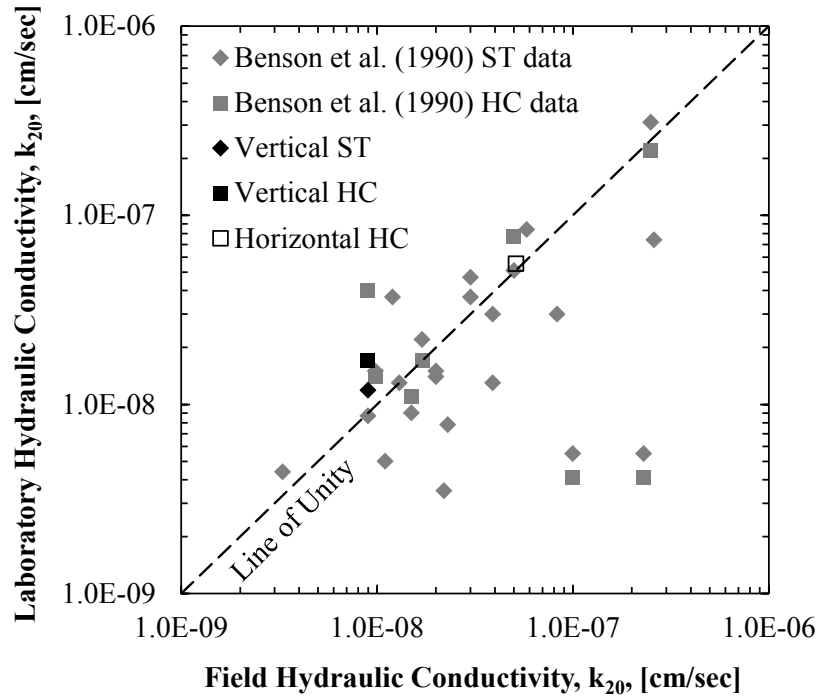


Figure 4.40. Comparison between laboratory hydraulic conductivity and two stage borehole field hydraulic conductivity for Test Pad 2.

4.7.3 Discussion on the Comparisons between Field (TSB) and Field (SDRI) Hydraulic Conductivity Results

A comparison between the vertical hydraulic conductivity values from Test Pads 1 and 2 obtained using the TSB methodology and vertical hydraulic conductivity values from Test Pad 3 obtained using the SDRI methodology is presented in Figure 4.41. The vertical hydraulic conductivity results obtained from SDRI testing are comparable (within half an order of magnitude) with the vertical hydraulic conductivity results obtained from TSB testing. This comparison is consistent with literature and demonstrates that either test (SDRI or TSB) may be used for in-situ hydraulic conductivity testing when good compaction techniques are utilized. However, the TSB test is recommended for in-situ hydraulic conductivity testing because of lower material cost, easier installation, and quicker testing time as compared to the SDRI test. Although the vertical hydraulic conductivity results were comparable, it is not a direct comparison between the two test methods because the SDRI test targets the top two inches of

soil located in Lift 4 and the TSB test targets the soil in the center of Lift 3. Additionally, the three tests were conducted on three separate test pads, each having different molding soil conditions and therefore different soil structure.

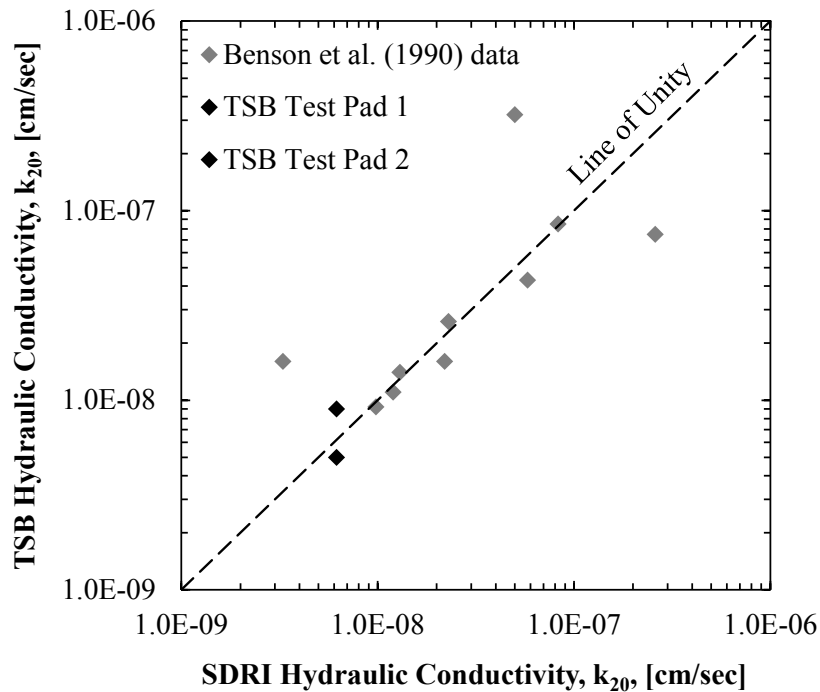


Figure 4.41. TSB vertical hydraulic conductivity from Test Pads 1 and 2 compared to SDRI hydraulic conductivity from Test Pad 3.

4.7.4 Discussion on the Comparisons between Laboratory and Nuclear Density Gauge Dry Unit Weight Results

Comparisons between the dry unit weight values from Test Pads 1 and 2 obtained from laboratory Shelby tube and hand carved samples, respectively, and the average dry unit weight values obtained from nuclear density gauge measurements in Test Pads 1 and 2 are presented in Figure 4.42 and Figure 4.43. Except for one point obtained from Lift 1 of Test Pad 1, the average dry unit weight values obtained from the Shelby tube samples are consistently higher (greater than 2 pcf difference) than the average dry unit weight values obtained from the nuclear density gauge. However, the average dry unit weight values obtained from the hand carved samples are comparable (within 2 pcf difference) with the average dry unit weight values obtained from the

nuclear density gauge. The higher dry unit weight measurements obtained from the Shelby tube samples may indicate that compression of the soil results from pushing the Shelby tube into the soil.

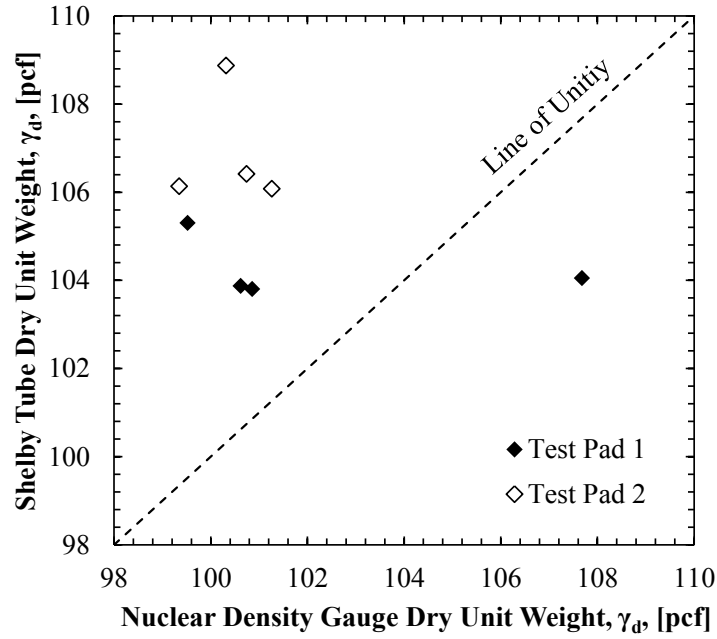


Figure 4.42. Comparison between Shelby tube dry unit weight measurements and nuclear density gauge dry unit weight measurements from Test Pads 1 and 2.

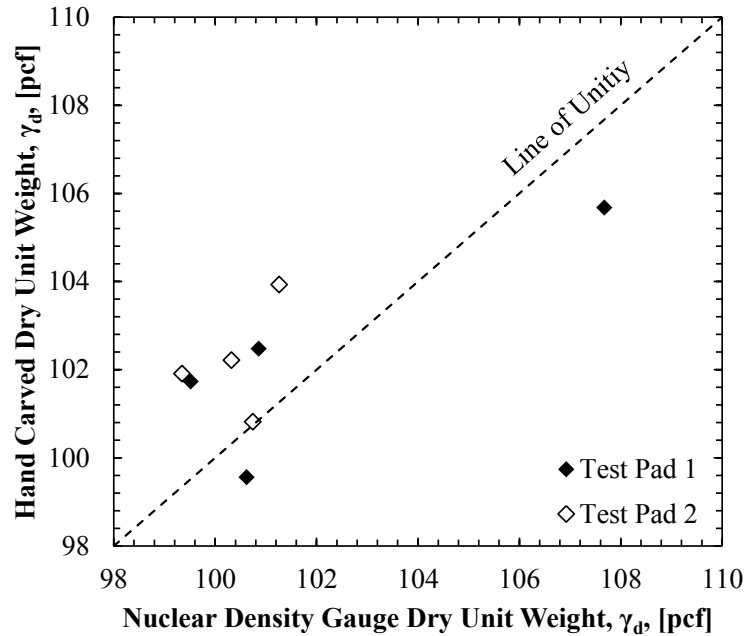


Figure 4.43. Comparison between hand carved dry unit weight measurements and nuclear density gauge dry unit weight measurements from Test Pads 1 and 2.

4.7.5 Discussion on the Comparisons between Shelby Tube and Hand Carved Dry Unit Weight Results

A comparison between the dry unit weight values obtained from Shelby tube samples and dry unit weight values obtained from hand carved samples is presented in Figure 4.44. All but one point fell below the line of unity. The dry unit weight values obtained from the laboratory Shelby tube samples were consistently higher (greater than 2 pcf difference) than the dry unit weight values obtained from the laboratory hand carved samples.

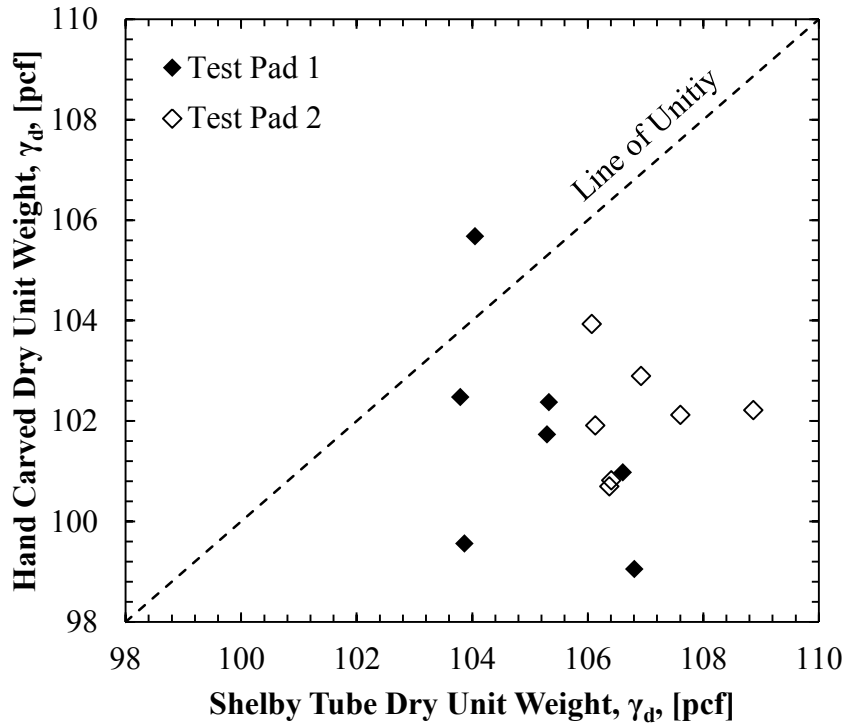


Figure 4.44. Comparison between hand carved dry unit weight measurements and Shelby tube dry unit weight measurements from Test Pads 1 and 2.

4.7.6 Discussion on the Comparisons between Laboratory and Nuclear Density Gauge Moisture Content Results

Comparisons between the average moisture content values obtained from laboratory Shelby tube and hand carved samples, respectively, and the average moisture content values from the nuclear density gauge are presented in Figure 4.45 and Figure 4.46. As shown in both figures, the measured moisture content values from the Shelby tube and hand carved samples are consistently lower than the measured in-situ (nuclear density gauge) moisture content values. The lower moisture content values may indicate that the soil dried, or lost moisture, between time of placement of the test pad and time of laboratory testing.

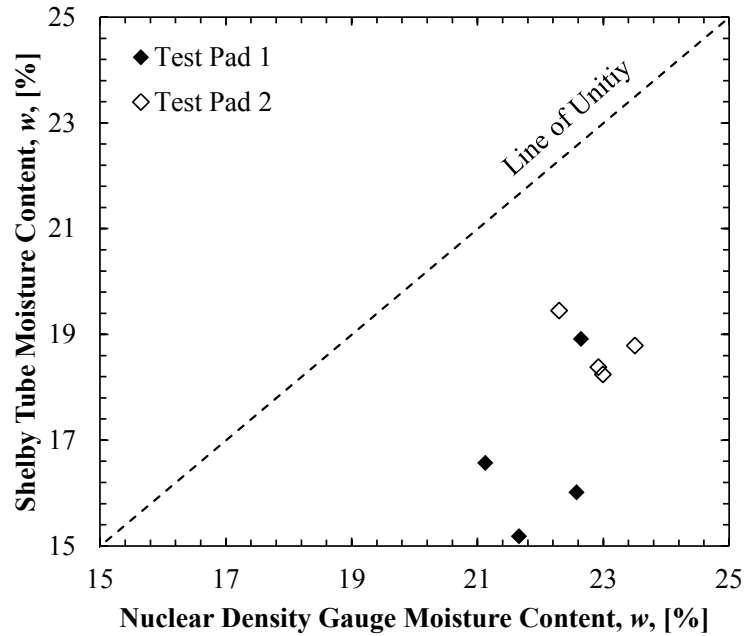


Figure 4.45. Comparison between Shelby tube moisture content measurements and nuclear density gauge moisture content measurements from Test Pads 1 and 2.

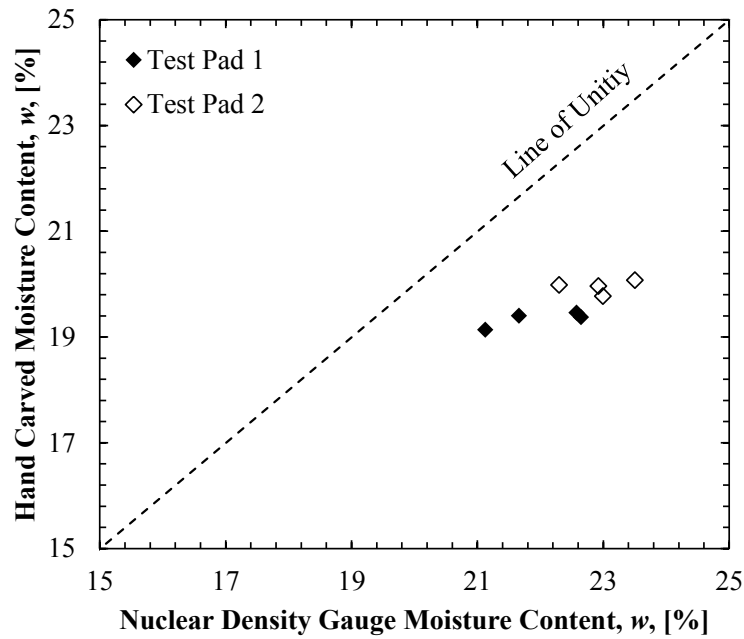


Figure 4.46. Comparison between hand carved moisture content measurements and nuclear density gauge moisture content measurements from Test Pads 1 and 2.

4.7.7 Discussion on the Comparisons between Hand Carved and Shelby Tube Moisture Content Results

A comparison of moisture content values obtained from the hand carved samples and moisture content values obtained from the Shelby tube samples is presented in Figure 4.47. As mentioned previously, the Shelby tube from Test Pad 1 (SE-ST-TP1) was not stored in the environmental chamber before hydraulic conductivity testing commenced. Therefore, the SE-ST-TP1 was susceptible to drying which does not yield an accurate field moisture content and may cause change in the soil parameters (including the hydraulic conductivity of the soil). As shown in Figure 4.47, considerable drying (approximately 2.5 to 3.5 percent difference in moisture content) was observed in the Shelby tube samples as compared to the hand carved samples collected from Test Pad 1. Less drying (within two percent difference in moisture content) was observed in the Shelby tube samples as compared to the hand carved samples collected from Test Pad 2. The hand carved samples stored in the environmental chamber had relatively consistent moisture content values while the Shelby tube samples stored either outside of the environmental chamber (Test Pad 1) or inside the environmental chamber (Test Pad 2) had varying moisture content. While both Shelby tube and hand carved samples were susceptible to condensation or evaporation in and out of the environmental chamber, the consistent moisture content obtained from the hand carved samples is believed to be a function of both overall sample size and the moisture content test sample size.

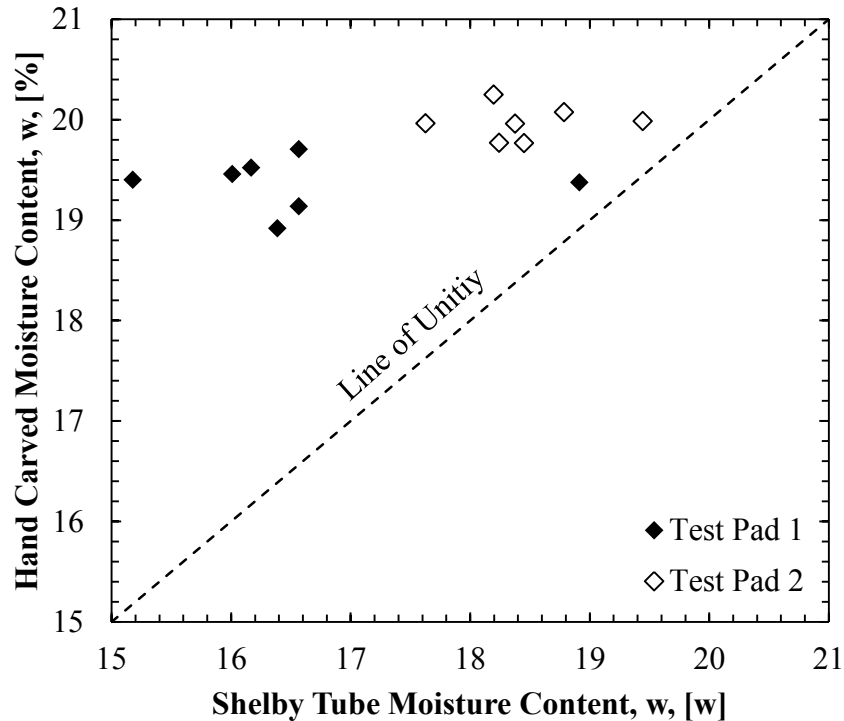


Figure 4.47. Comparison between hand carved moisture content measurements and Shelby tube moisture content measurements from Test Pads 1 and 2.

The moisture content values obtained from the hand carved samples remained consistent for both Test Pads 1 and 2 while the moisture content values obtained from the Shelby tube samples for Test Pad 2 varied. Although the hand carved samples from Test Pads 1 and 2 and the Shelby tube samples from Test Pad 2 were stored in the environmental chamber, the samples were subjected to fluctuations in temperature inside of the environmental chamber. As shown in Figure 4.47, the Shelby tube samples were more susceptible to the temperature variations than the hand carved samples because of overall all samples size. Additionally, the moisture content samples for the hand covered samples were larger (over 100 grams) than the moisture content samples used for the Shelby tube samples (approximately 50 grams). Because of the sample sizes, the Shelby tube moisture content samples could have dried significantly before being measured, thereby causing varied measured moisture content values for the Shelby tube samples.

4.7.8 Discussion on the Comparisons between Shelby Tube Recovery and Push Lengths Results

Compression of the soil caused by pushing Shelby tubes was also determined by analyzing the recovered length to pushed length of the Shelby tube. A comparison of the recovered length and the pushed length of the Shelby tubes collected from Test Pads 1 and 2 is presented in Figure 4.48. One Shelby tube, SW-ST-TP1, had a recovery length to pushed length ratio greater than one (1.02) indicating that some expansion of the soil occurred during sample acquisition due to suction forces being developed during Shelby tube extraction. The other three Shelby tubes had recovery length to pushed length ratios of less than one (0.82 to 0.89) indicating that the soil was compressed during sample acquisition. The low recovery ratios in the Shelby tubes collected from Test Pad 2 may be attributed to rocking of the Shelby tubes during sample acquisition and higher moisture content causing increased adhesion of the soil to the Shelby tube which causes increased compression.

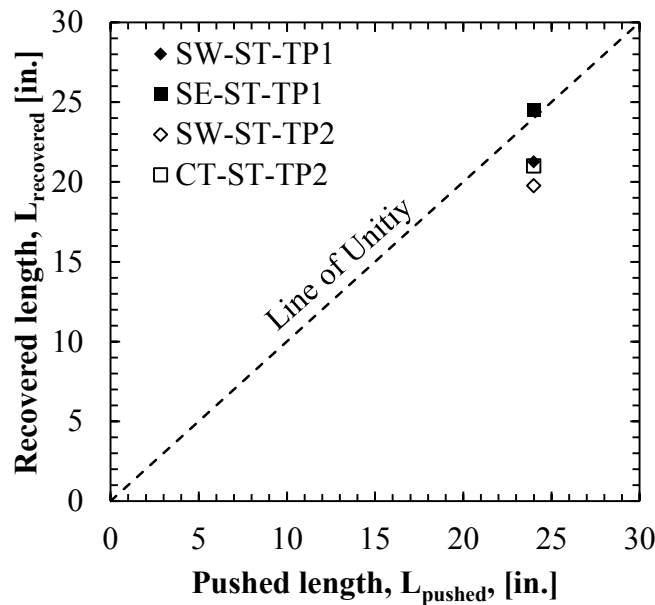


Figure 4.48. Recovered length compared to the pushed length for Shelby tube sample acquisition.

4.7.9 Discussion on the Comparisons between TDR Probe and Nuclear Density Gauge Moisture Content Results

To compare the volumetric moisture content values obtained from the TDR probes to the average gravimetric moisture content values obtained from the nuclear density gauge, the volumetric moisture content was converted to gravimetric moisture content. The unit weight of water and the average total unit weight value obtained from the nuclear density gauge were utilized for this conversion. A comparison of the gravimetric moisture content values calculated from the measurements obtained from the TDR probes and the gravimetric moisture content measurements obtained using the nuclear density gauge is presented in Figure 4.49. The moisture content measurements plot near the line of unity (typically within one percent moisture) indicating that little drying occurred between time of placement of Test Pad 3 and time of commencement of the SDRI test due to the small time frame (approximately two months).

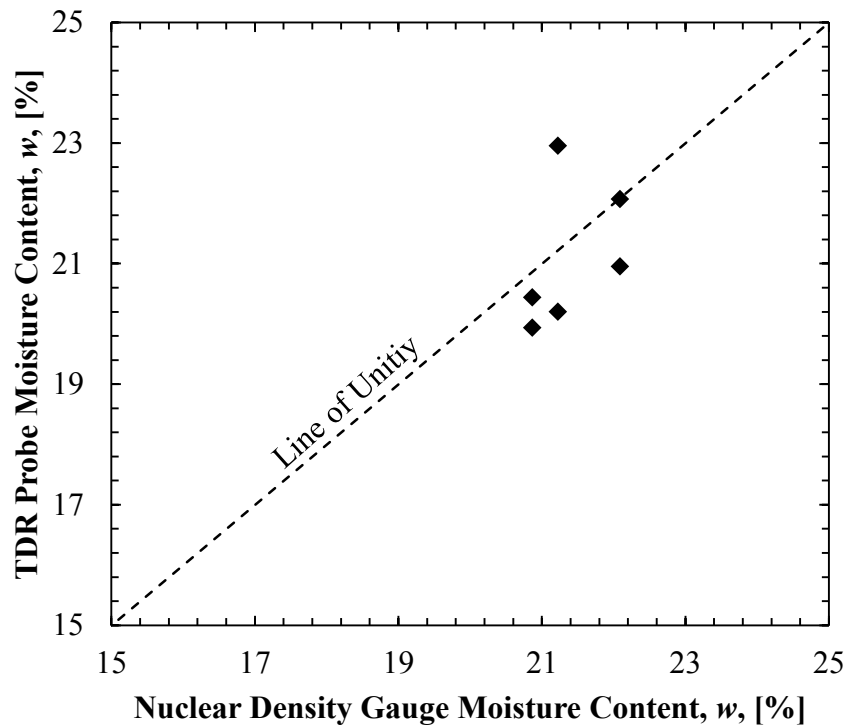


Figure 4.49. Comparison between TDR probe gravimetric moisture content measurements and nuclear density gauge moisture content measurements from Test Pad 3.

4.8 Conclusion

The dataset provided in ASTM D6391 (2010) was analyzed using data reduction methods presented by Soil Testing Engineers, Inc. [STEI] (1983), Daniel (1989), Boutwell (1992), Boutwell and Tsai (1992), Trautwein and Boutwell (1994), ASTM D6391 (2012) Method A, Chapuis (1989), Chiasson (2005), and ASTM D6391 (2012) Method B. Comparing the hydraulic conductivity of Stage 1 amongst the various methods, a similar hydraulic conductivity was calculated using the time lag equation methods. A hydraulic conductivity one order of magnitude higher than the time lag equation methods was calculated using the velocity method and a hydraulic conductivity three orders of magnitude higher than the time lag equation methods was calculated using the Z-t methods.

A Daniel and Benson (1990) zone of acceptance (ZOA) and an APCEC (2007) ZOA were developed and compared. Nuclear density measurements collected during test pad construction were plotted against the Daniel and Benson (1990) ZOA to determine lift acceptance. The values for apparent hydraulic conductivities were measured from in-situ hydraulic conductivity (TSB) testing conducted on the test pads and the corresponding values for vertical and horizontal hydraulic conductivities were calculated. Laboratory testing results obtained from flexible wall hydraulic conductivity testing on samples exhumed from the liner (Test Pads 1 and 2) were used to validate the in-situ hydraulic conductivity measured in the test pads. Additionally, the unit weight and moisture content of each hydraulic conductivity sample were measured to determine changes in the soil properties during testing and the causes for the change. Soil index tests were used to determine the characteristics of the soil (i.e. specific gravity, particle size, percent passing No. 200 sieve, Atterberg limits), to verify the soils in each the pads were similar, and to classify the soil. Because the results of the index testing were

similar, the results of the different hydraulic conductivity testing techniques were then compared to determine correlations between the various testing procedures.

For samples collected from the same test pad, higher values of unit weight were obtained from Shelby tube samples than from the hand carved samples attained from the same pad. This indicates that the Shelby tube compresses the soil, thereby increasing the unit weight of the soil, when pushed to obtain an “undisturbed” soil sample. Additionally, while all laboratory samples demonstrated some degree of drying, more drying was observed in Shelby tube soil samples not stored in the environmental chamber before the commencement of the laboratory testing as compared to the soil samples that were stored in the environmental chamber prior to commencement of the laboratory testing.

If laboratory testing is required for field construction verification, it is recommended that hand carved samples be obtained from the field test pad instead of Shelby tube samples. As mentioned previously, pushing a Shelby tube causes compression in the soil and thereby changes the soil parameters, specifically unit weight and hydraulic conductivity. Additionally, due to the small sample sizes, Shelby tube samples are more susceptible to evaporation and condensation while in storage and while preparing the soil sample for laboratory testing and collecting a sample for a moisture content test. Hand carved samples are recommended for laboratory testing due to the large sample size, which makes the sample less susceptible to moisture changes in storage or during laboratory preparation. Additionally, hand carved sample acquisition causes less disturbance to the soil sample and thereby does not change the soil parameters significantly.

In Test Pad 1, the laboratory measured vertical hydraulic conductivity values obtained from testing conducted on the Shelby tubes samples were comparable to the vertical hydraulic conductivity values obtained from testing conducted on the hand carved samples. Lower

hydraulic conductivity values (one half to one order of magnitude) were measured in-situ (using TSB permeameter) than in the laboratory (using values from testing conducted on the Shelby tube and hand carved samples obtained at the same depth as the depth of the bottom of the TSB permeameter). In Test Pad 2, the vertical hydraulic conductivity values obtained from laboratory testing conducted on both Shelby tube and hand carved samples were similar (within half an order of magnitude) with consistently lower values of hydraulic conductivity being obtained from the Shelby tube samples.

In Test Pad 2, lower values of hydraulic conductivity were measured in-situ (using TSB testing) than in laboratory testing. However, the ratio of the laboratory hydraulic conductivity to field hydraulic conductivity values for Test Pad 2 was approximately unity (i.e. the comparison points plot near the line of unity). A higher value of vertical hydraulic conductivity was obtained from the sealed double ring infiltrometer (SDRI) test conducted on Test Pad 3 than from the TSB test conducted on Test Pad 1 and a lower vertical hydraulic conductivity value was obtained from the SDRI test conducted on Test Pad 3 than from the TSB test conducted on Test Pad 2. A half order of magnitude difference was observed between the three values of in-situ vertical hydraulic conductivity measured within Test Pads 1 (TSB), 2 (TSB), and 3 (SDRI).

The dry unit weight measurements obtained from the Shelby tube samples were higher than the dry unit weight measurements obtained from the hand carved samples. Therefore, pushing of the Shelby tube causes compression of the soil and may change the soil structure. Compression caused by pushing the Shelby tubes into the soil is also confirmed by the Shelby tube samples of Test Pad 2 having a lower hydraulic conductivity of the hand carved samples from Test Pad 2 and by the recovery ratio being less than one.

The moisture content values obtained from laboratory samples were lower than the moisture content values obtained from the nuclear density gage during test pad placement for both Test Pads 1 and 2. Most of the moisture loss occurred within the soil liner between test pad deconstruction and laboratory testing. However, some of the moisture loss occurred during TSB testing. Nuclear density testing should have been conducted after in-situ hydraulic conductivity testing at the time of deconstruction of the test pad to verify the loss of moisture. This moisture loss may have been associated either with evaporation at the base of the test pad (bottom of Lift 1) or due to the plastic cover pulling water out of the soil and forming condensation at the top of the test pad (top of Lift 4). Comparing the TDR probe and nuclear density gauge measurements from Test Pad 3 indicates that little drying has occurred between placement of Test Pad 3 and the start of the SDRI test associated with a short time period between test pad placement with nuclear density measurements and the TDR probe measurements at the beginning of the SDRI test.

Chapter 5: Observations, Conclusions, and Recommendations

5.1 Introduction

Based on a review of each of the two stage borehole (TSB) data reduction methods found in the literature and the observed results from this study, a recommended methodology to process and analyze data is presented in this chapter. Conclusions derived from results obtained from the field and laboratory hydraulic conductivity testing techniques employed as part of this research project are presented. Recommendations are also provided for additional avenues of research that were not addressed in this study in relation to both in-situ and laboratory hydraulic conductivity testing.

5.2 Observations

- By analyzing the time lag data reduction methods, it was determined that each time lag procedure presented contained either an incorrect variable definition and/or a typographical error in the equation(s).
- Similar results were obtained from both the STEI (1983) method and the Boutwell (1992) method for determining the anisotropy value.
- The Arkansas Pollution Control and Ecology Commission [APCEC] (2007) zone of acceptance (ZOA) encompassed soil samples with unacceptable hydraulic conductivity values and did not encompass soil samples with acceptable hydraulic conductivity values.
- Three laboratory scale tests pads were constructed by placing soil within a zone of acceptance (placement window) determined using the Daniel and Benson (1990) procedure, as constructed using only the hydraulic conductivity requirement.
- In Test Pad 2, lower but comparable hydraulic conductivity values were obtained from the Shelby tube samples as compared to the hand carved samples. Also in Test Pad 2,

similar hydraulic conductivity values were obtained from the TSB field and the Shelby tube and hand carved measurement for the same target zones.

- Similar hydraulic conductivity values were obtained from the TSB field measurements and the SDRI field measurement.
- The dry unit weight values obtained from the Shelby tube samples were higher than the dry unit weight values obtained from the nuclear density testing performed during test pad placement. However, the dry unit weight values obtained from the hand carved samples were comparable to the dry unit weight values obtained from the nuclear density testing performed during test pad placement.
- Both the Shelby tube samples and the hand carved samples had lower moisture content values than the moisture content values obtained from nuclear density testing performed during test pad placement. The Shelby tube samples from Test Pad 1 were not properly stored after being sampled. Therefore, the samples dried considerably and did not yield accurate field moisture content values. A greater variance of laboratory moisture content measurement values was observed in the Shelby tube samples than in the hand carved samples.

5.3 Conclusions

- The ASTM D6391 (2012) Method A method for reducing TSB data contains no errors in the equations. However, one definition error is presented in the text but is later corrected for in the sample calculations presented in ASTM D6391 (2012).
- Based on the reported data, the APCEC (2007) ZOA is unconservative with respect to hydraulic conductivity performance as obtained from laboratory testing on laboratory compacted soils.

- Test pads may be constructed at any time during the year inside the test pad box at the Engineering Research Center if the soil is properly moisture conditioned and placed within the ZOA placement window.
- Similar hydraulic conductivity values may be obtained using laboratory testing techniques on Shelby tube and hand carved samples and field testing techniques using the TSB and SDRI methodologies.
- Based on the reported data, using Shelby tube samplers for sample acquisition causes compression of the soil which increases dry unit weight and lowers hydraulic conductivity.
- Hand carved samples are less susceptible to changes in moisture content caused by evaporation and condensation during environmentally controlled storage due to the large sample size of the hand carved samples as compared to the small size of Shelby tube samples.

5.4 General Recommendations

Recommendations for developing an acceptance criteria are presented. Recommendations are provided for future use of in-situ testing methods. Specifically, a discussion about in-situ testing focusing on the selection of the proper TSB data reduction methods and the selection of the proper in-situ testing methodology should be utilized are included. Recommendations are also provided for improvements to the SDRI testing methodology as presented in this document.

5.4.1 Recommendations on Development of an Acceptance Criteria

The Arkansas Pollution Control and Ecology Commission [APCEC] (2007) method for developing a zone of acceptance (ZOA) that is used as a acceptance criterion for a municipal solid waste or hazardous waste landfill liner is not recommended based on the results reported in

this document. This method does not correlate the unit weight and moisture content to a required hydraulic conductivity. Instead, the Daniel and Benson (1990) method for developing a zone of acceptance is recommended because it correlates unit weight and moisture content to required hydraulic conductivity. The Daniel and Benson (1990) method uses laboratory results (obtained from Proctor and flexible wall hydraulic conductivity testing) to develop an acceptance criterion that is then used to ensure that the values of hydraulic conductivity obtained in the laboratory are duplicated in the field.

5.4.2 Recommendations on How to Reduce Two Stage Borehole Data

Data obtained from two stage borehole (TSB) testing conducted in accordance with ASTM D6391 (2012) with a falling head should be reduced using a combination of the ASTM D6391 (2012) Method A and the Soil Testing Engineers, Inc. (1983) method. The ASTM D6391 (2012) Method A method is used to calculate the value of apparent hydraulic conductivity for Stage 1 and Stage 2 (k_1 and k_2 , respectively). The height of head used in the ASTM D6391 (2012) Method A should be defined as the lesser of the difference between the water level in the standpipe to the elevation of the water table (or permeable surface) or to 20 internal casing diameters below the bottom of the casing. The k_2/k_1 ratio and the length (L) to Stage 2 extension diameter (D_2) ratio (L/D) are used in Equation 5.1 from the STEI (1983) method to calculate the anisotropy value (m). It is recommended that the STEI (1983) method be used due to the relative ease of use compared to the Boutwell (1992) method. The anisotropy value can be evaluated numerically using Microsoft Excel® Solver to obtain the m value. The m value is then used to solve for the vertical hydraulic conductivity (k_v) and horizontal hydraulic conductivity (k_h) with respect to k_1 as presented in Equation 5.2 and Equation 5.3, respectively.

$$\frac{k_2}{k_1} = m \frac{\ln\left[\frac{L}{D} + \sqrt{1 + \left(\frac{L}{D}\right)^2}\right]}{\ln\left[\frac{mL}{D} + \sqrt{1 + \left(\frac{mL}{D}\right)^2}\right]} \quad (\text{Soil Testing Engineers, Inc., 1983}) \quad \text{Equation 5.1}$$

$$k_h = mk_1 \quad (\text{Soil Testing Engineers, Inc., 1983}) \quad \text{Equation 5.2}$$

$$k_v = \frac{1}{m} k_1 \quad (\text{Soil Testing Engineers, Inc., 1983}) \quad \text{Equation 5.3}$$

Where: k = Hydraulic conductivity

m = Anisotropy value

L = Length of Stage 2 extension below casing

D = Diameter of Stage 2 extension

5.4.3 Recommendations on In-Situ Hydraulic Conductivity Testing and Sampling Soil Specimens for Laboratory Testing

TSB and SDRI testing are both viable options for conducting in-situ hydraulic conductivity testing. The SDRI test is advantageous and covers a large test area that allows the assessment of the micro- and macro-void soil structure on liner performance. However, the cost of materials and lengthy installation and testing times does not always make the SDRI test ideal for test pad verification measurements. Instead, TSB testing may be conducted more quickly and more economically with similar results. Because of the smaller testing area, it is recommended that multiple TSB tests (five) be installed and conducted simultaneously. Four of the five tests must meet the regulatory required hydraulic conductivity value.

Although comparable results were obtained between hydraulic conductivity values obtained from the Shelby tube and hand carved samples, the use of a Shelby tube sampler is not ideal for sample acquisition because of the compression caused within the soil. Instead, hand carved samples are superior for obtaining “undisturbed” samples. While it is recommended in literature that hand carved samples (block samples) be at least one-foot in diameter, hand carved

samples with a diameter of ten inches, which are then trimmed to six inches after being transported to the laboratory, may be used to obtain viable results (as demonstrated during this research project). Obtaining hand carved samples provides soil parameter measurements for minimally disturbed samples that compare closely with in-situ vertical and horizontal hydraulic conductivity values.

5.4.4 *Recommendations on SDRI Testing*

To seal the joints of the outer ring, the use of a soft, pliable rubber gasket when a permanent seal (e.g. epoxy) is not desired is recommended. A stiff rubber gasket (as utilized in this project) will not work as it will not mold against the outer ring. This material did not provide a sufficient seal and required the use of an additional sealant (marine epoxy).

An uninterruptable power supply (UPS) should be utilized for the data acquisition devices to ensure that data collection is uninterrupted in the event of a temporary power outage. A UPS will prevent gaps in the collected data and help to ensure that the results are not skewed by missing data. Additionally, a large memory unit capable of storing multiple weeks worth of data should be included in the data acquisition device to increase the time required between data retrieval from the data acquisition device. This measure will also prevent gaps in the collected data by ensuring that older data is not overwritten by newer data.

5.5 *Recommendations for Future Research*

Recommendations are provided for areas of future research. Recommendations on future research directions include continuing the current research at the Engineering Research Center (ERC), incorporating the nuclear density gauge during test pad removal, verifying the accuracy of the nuclear density gauge, evaluating the use of the Mariotte tube in TSB testing, determining if diurnal cycles are present in environmentally controlled testing data, and evaluating the

effectiveness of pushing a Shelby tube in a performance liner. While the majority of the future research recommendations are geared towards use at the ERC, the recommendations may be employed in other areas of research as well.

5.5.1 Recommendations for Continuing the Current Research at the Engineering Research Center

At the time of this document submission, the SDRI test was still being conducted within Test Pad 3. The SDRI test should be continued until the wetting front reaches the bottom of the test pad. Following completion of the test, the SDRI device should be drained and removed. Two Shelby tube samples and two hand carved samples should be collected and the samples should be tested in the laboratory. Determination of hydraulic conductivity and soil index properties should be obtained following the same procedures provided herein. Comparisons between the SDRI obtained field hydraulic conductivity value and the laboratory obtained hydraulic conductivity values for Test Pad 3 should then be obtained.

Test Pad 4 should be constructed following the recommended procedures described herein and a sealed double ring infiltrometer (SDRI) test should be conducted within Test Pad 4. This second SDRI test would be used to verify the first SDRI test and to build a larger database of results obtained from environmentally controlled in-situ hydraulic conductivity testing. Additionally, the second SDRI test should be used to better compare time the domain reflectometry (TDR) data and tensiometer data while measuring the wetting front.

5.5.2 Recommendations for Nuclear Density Testing During Test Pad Removal

As part of removal for Test Pad 3 and subsequent test pads, nuclear density gauge readings should be obtained at various locations and lifts throughout the test pad. The obtained unit weight and moisture content readings can be used for further comparison against the initial nuclear density gauge readings and the laboratory collected unit weight and moisture content

values. A comparison between the nuclear density gauge readings obtained from test pad construction and the nuclear density gauge readings obtained from test pad removal can be made to determine changes in the unit weight and moisture content during in-situ hydraulic conductivity testing. Additionally, a comparison between the nuclear density gauge readings obtained from test pad removal and the unit weight and moisture content values obtained from laboratory testing can be developed to determine changes in soil parameters due to soil sampling and handling.

5.5.3 Recommendation for Verifying the Accuracy of the Nuclear Density Gauge

To verify the accuracy of the nuclear density gauge used for this research project, the nuclear density gauge results should be compared to other in-situ density test results obtained from tests such as the sand cone test or the drive tube test. Due to the large disturbance caused by the sand cone test and the drive tube test, the verification should be conducted during test pad removal. Following completion of the in-situ hydraulic conductivity test, both in-situ density tests, the nuclear density gauge test and the test method selected for verification, should be conducted on the test pad surface. Multiple tests should be conducted at random locations using both methodologies for a better comparison.

5.5.4 Recommendation for Evaluating the Use of Mariotte Tube for Constant Head Two Stage Borehole Testing

The new method for conducting TSB testing using a Mariotte tube to apply a constant head to the permeameter (ASTM D6391, 2012) is suggested for use in Test Pads 5 and 6. The results from the constant head TSB test should then be compared to the results obtained from the falling head TSB tests conducted on Test Pads 1 and 2. Additionally, another suggestion for Test Pad 5 and 6 is to conduct a TSB test with the use of TDR probes and tensiometers. One TSB test should be conducted in the center of the test pad in a similar manner as the tests conducted in

Test Pads 1 and 2. TDR probes should be installed both below the TSB casing and to the side of the TSB Stage 2 extension area. Tensiometers should be installed near the TSB casing. The TDR probes and tensiometers can be used to monitor the vertical and horizontal movement of the wetting front as Stage 1 and Stage 2 of the testing are being conducted.

5.5.5 Recommendation for Determining Diurnal Cycles in Hydraulic Conductivity Testing

Further research should be completed to study the effects of diurnal cycles, or lack thereof, in environmentally controlled compacted clay liners. The results obtained from this research should be compared to results obtained from non-environmentally controlled compacted clay liners like those constructed at the University of Arkansas Cato Springs Research Center (Coffman and Garner, 2012). Specifically, for a direct and accurate comparison, it is recommended that the results from this research project be compared to non-environmentally controlled compacted clay liners constructed from the same soil and construction design and using the same in-situ testing parameters.

5.5.6 Recommendations for Evaluating the Use Shelby Tubes in a Performance Liner

For state agency requirements of pushing a Shelby tube into the performance liner, research should be conducted to determine if the disturbance caused by sample acquisition affects the hydraulic conductivity of the performance liner. After constructing a test pad in the ERC test pad box, a Shelby tube should be pushed into and retrieved from the center of the test pad. The hole created by the Shelby tube sample acquisition should be filled with bentonite using the same technique used on performance liners. Then the SDRI apparatus can be installed around the filled Shelby tube hole and an in-situ hydraulic conductivity test can be conducted directly over the hole. The results from this test should be compared to SDRI results from previous test pads to determine if collecting a Shelby tube sample from the performance liner affects the in-situ hydraulic conductivity. Because of the swelling nature of bentonite, a method of applying

effective stress to the plugged hole (simulating solid waste on top of the hole in an actual liner)
needs to be developed.

References

- Albrecht, K., and Cartwright, K., (1989). "Infiltration and Hydraulic Conductivity of a Compacted Earthen Liner." *Ground Water*, Vol. 27, No. 1, pp. 14-19.
- American Society for Testing and Materials (2012), "Standard Test Method for Amount of Material in Soils Finer than No. 200 (75- μ m) Sieve" Annual Book of ASTM Standards, Designation D 1140, Vol. 4.08, ASTM, West Conshohocken, PA.
- American Society for Testing and Materials (2012), "Standard Test Method for Classification of Soils and Soil-Aggregate Mixtures for Highway Construction Purposes" Annual Book of ASTM Standards, Designation D 3282, Vol. 4.08, ASTM, West Conshohocken, PA.
- American Society for Testing and Materials (2012), "Standard Test Method for Classification of Soils for Engineering Purposes (Unified Soil Classification System)" Annual Book of ASTM Standards, Designation D 2487, Vol. 4.08, ASTM, West Conshohocken, PA.
- American Society for Testing and Materials (2010), "Standard Test Method for Field Measurement of Hydraulic Conductivity Limits of Porous Materials Using Two Stages of Infiltration from a Borehole" Annual Book of ASTM Standards, Designation D 6391, Vol. 4.08, ASTM, West Conshohocken, PA.
- American Society for Testing and Materials (2012), "Standard Test Method for Field Measurement of Hydraulic Conductivity Using Borehole Infiltration" Annual Book of ASTM Standards, Designation D 6391, Vol. 4.08, ASTM, West Conshohocken, PA.
- American Society for Testing and Materials (2012), "Standard Test Method for Field Measurement of Infiltration Rate Using Double-Ring Infiltrometer with Sealed-Inner Ring" Annual Book of ASTM Standards, Designation D 5093, Vol. 4.08, ASTM, West Conshohocken, PA.
- American Society for Testing and Materials (2012), "Standard Test Method for In-Place Density and Water Content of Soil and Soil-Aggregate by Nuclear Methods (Shallow Depth)" Annual Book of ASTM Standards, Designation D 6938, Vol. 4.08, ASTM, West Conshohocken, PA.
- American Society for Testing and Materials (2012), "Standard Test Method for Laboratory Compaction Characteristics of Soil Using Modified Effort (56,000 ft-lbf/ft³(2,700 kN-m/m³))" Annual Book of ASTM Standards, Designation D 1557, Vol. 4.08, ASTM, West Conshohocken, PA.
- American Society for Testing and Materials (2012), "Standard Test Methods for Laboratory Compaction Characteristics of Soil Using Standard Effort (12,400 ft-lbf/ft³(600 kN-m/m³))" Annual Book of ASTM Standards, Designation D 698, Vol. 4.08, ASTM, West Conshohocken, PA.

- American Society for Testing and Materials (2012), “Standard Test Method for Laboratory Determination of Water (Moisture) Content of Soil and Rock by Mass” Annual Book of ASTM Standards, Designation D 2216, Vol. 4.08, ASTM, West Conshohocken, PA.
- American Society for Testing and Materials (2012), “Standard Test Method for Liquid Limit, Plastic Limit, and Plasticity Index of Soils” Annual Book of ASTM Standards, Designation D 4318, Vol. 4.08, ASTM, West Conshohocken, PA
- American Society for Testing and Materials (2012), “Standard Test Method for Measurement of Hydraulic Conductivity of Saturated Porous Materials Using a Flexible Wall Permeameter” Annual Book of ASTM Standards, Designation D 5084, Vol. 4.08, ASTM, West Conshohocken, PA.
- American Society for Testing and Materials (2012), “Standard Test Method for Particle-Size Analysis of Soils” Annual Book of ASTM Standards, Designation D 422, Vol. 4.08, ASTM, West Conshohocken, PA.
- American Society for Testing and Materials (2012), “Standard Test Methods for Specific Gravity of Soil Solids by Water Pycnometer” Annual Book of ASTM Standards, Designation D 854, Vol. 4.08, ASTM, West Conshohocken, PA.
- Arkansas Pollution Control and Ecology Commission, (2007). “Regulation No. 22: Solid Waste Management Rules.” Arkansas Department of Environmental Quality, <<http://www.APCEC.state.ar.us/regs/default.htm>>. Accessed April 4, 2012.
- Benson, C., Daniel, D., and Boutwell, G., (1999). “Field Performance of Compacted Clay Liners.” *Journal of Geotechnical and Geoenvironmental Engineering*, ASCE, Vol. 125, No. 5, pp. 390-403.
- Benson, C., Gunter, J., Boutwell, G., Trautwein, S., and Berzanskis, P., (1997). “Comparison of Four Methods to Assess Hydraulic Conductivity” *Journal of Geotechnical and Geoenvironmental Engineering*, ASCE, Vol. 123, No. 10.
- Benson, C., Hardianto, F., and Motan, E., (1994). “Representative Specimen Size for Hydraulic Conductivity Assessment of Compacted Soil Lines.” *Hydraulic Conductivity and Waste Contaminant Transport in Soil*, STP 1142, D. Daniel and S. Trautwein, eds., ASTM, Philadelphia, pp. 3-29.
- Black, D., and Lee, K., (1973). “Saturating Laboratory Samples by Back Pressure” *Journal of the Soil Mechanics and Foundations Division*, ASCE, Vol. 99, No. SM1, pp. 75-93.
- Boutwell, G., (1992). “The STEI Two-Stage Borehole Field Permeability Test.” *Containment Liner Technology and Subtitle “D”*, Houston Section, ASCE, Houston, TX.
- Boutwell, G. and Tsai, C., (1992). “The Two-Stage Field Permeability Test for Clay Liners.” *Geotechnical News*, C. Shackelford and D. Daniel, eds., pp. 32-34.

- Chapuis, R., (1999). "Borehole variable-head permeability tests in compacted clay liners and covers." *Canadian Geotechnical Journal*, Vol. 36, pp. 39-51.
- Chiasson, P., (2005). "Methods of interpretation of borehole falling-head tests performed in compacted clay liners." *Canadian Geotechnical Journal*, Vol. 42, pp. 79-90.
- Coffman, R., and Garner, C., (2012). Final Report of MBTC-3031 Project. Mack-Blackwell Rural Transportation Center.
- Daniel, D., (1984). "Predicting Hydraulic Conductivity of Clay Liners." *Journal of Geotechnical Engineering*, ASCE, Vol. 110, No. 2, pp. 285-300.
- Daniel, D., (1989). "In Situ Hydraulic Conductivity Tests for Compacted Clay." *Journal of Geotechnical Engineering*, ASCE, Vol. 115, No. 9, pp. 1205-1226.
- Daniel, D., (1994). "State-of-the-Art: Laboratory Hydraulic Conductivity Tests for Saturated Soils." *Hydraulic Conductivity and Waste Contaminant Transport in Soil*, STP 1142, D. Daniel and S. Trautwein, eds., ASTM, Philadelphia, pp. 30-78.
- Daniel, D. and Benson, C., (1990). "Water Content-Density Criteria for Compacted Soil Liners." *Journal of Geotechnical Engineering*, ASCE, Vol. 116, No. 12, pp. 1811-1830.
- Daniel, D., and Trautwein, S., (1986). "Field Permeability Test for Earthen Liners." *Proceedings of In Situ '86*, Blacksburg, Va., pp. 146-160.
- Day, S., and Daniel, D., (1985). "Hydraulic Conductivity of Two Clay Prototype Clay Liners." *Journal of Geotechnical Engineering*, ASCE, Vol. 111, No. 8, pp. 957-970.
- Elshury, B., Sraders, G., Anderson, D., Rehage, J., Sai, J., and Daniel, D., (1990). "Field and Laboratory Testing of a Compacted Soil Liner." Report available from the Environmental Protection Agency.
- Herkelrath, W., Hamburg, S., and Murphy, F., (1991). "Automatic, real-time monitoring of soil moisture in a remote field area with time domain reflectometry." *Water Resources Research*. Vol. 27, No. 5, pp. 857-864.
- Hvorslev, J., (1951). "Time Lag and Soil Permeability in Ground Water Observations." Bulletin No. 36, USA/COE WES Vicksburg, MS.
- Irrrometer, (2012). Irrrometer-E gauge and probe documentation. Irrrometer website. <<http://www.irrometer.com/pdf/instruction%20manuals/IRRROMETERS/755%20E%20GaugeVACUUM%20hi%20Web4.pdf>>. Accessed June, 2012.
- Ledieu, J., De Ridder, P., De Clerck, P., and Dautrebande, S., (1986). "A method of measuring soil moisture by time-domain reflectometry." *Journal of Hydrology*, Vol. 88, pp. 319-328.

- Lambe, T., (1954). "The Permeability of Fine-Grained Soils." Symposium on Permeability of Soils, STP 163, ASTM, Philadelphia, pp. 56-67.
- Maldonado, C., and Coffman, R., (2012). "Hydraulic Conductivity of Environmentally Controlled Landfill Liner Test Pad." ASCE Geotechnical Special Publication No. 225, Proc. GeoCongress 2012: State of the Art and Practice in Geotechnical Engineering, Oakland, California, March, pp. 3593-3602.
- Neupane, D., Bowders, J., Loehr, J., Bouazza, A., and Trautwein, S., (2005). "Sealed Double-Ring Infiltrometers for Estimating Very Low Hydraulic Conductivities." Geotechnical Testing Journal, Vol. 28, No. 3.
- Ridley, A., Marsland F., and Patel A., (1998) "Tensiometers: their design and use for civil engineering purposes." Geotechnical Site Characterisation: Proc. 1st International Conference on Site Characterisation, Atlanta, USA. (Ed. P.K.Robertson & P.W.Mayne), Vol 2, pp. 851-856.
- Sai, J. and Anderson, D. (1990). "Field Hydraulic Conductivity Tests for Compacted Soil Liners." Geotechnical Testing Journal, Vol. 13, No. 3, pp. 215-225.
- Siddiqui, S., Drnevich, V., and Deschamps, R., (2000). "Time domain reflectometry development for use in Geotechnical Engineering." Geotechnical Testing Journal, Vol. 23, No. 1, pp. 9-20.
- Soil Testing Engineers, Inc. (1983). *STEI Two-Stage Field Permeability Test*. Soil Testing Engineers, Inc., Baton Rouge, LA.
- Take, W., and Bolton, M., (2003) "Tensiometer saturation and the reliable measurement of soil suction," *Géotechnique*, Vol. 53, No. 2, pp. 159 - 172.
- Trast, J., and Benson, C., (1995). "Estimating Field Hydraulic Conductivity of Compacted Clay." *Journal of Geotechnical and Engineering*, ASCE,
- Trautwein, S. and Boutwell, G. (1994). "In situ hydraulic conductivity tests for compacted soil liners and caps." *Hydraulic Conductivity and Waste Contaminant Transport in Soil*, STP 1142, D. Daniel and S. Trautwein, eds., ASTM, Philadelphia, pp. 184-223.
- Trautwein Soil Testing Equipment Company (1987). "Installation and operating instructions for the sealed double-ring infiltrometer." Trautwein Soil Testing Equipment Company, Houston, TX.
- Topp, G., Davis, J., and Annan, A., (1980). "Electromagnetic determination of soil water content: measurements in coaxial transmission lines." *Water Resources Research*, Vol. 16, No. 3, pp. 574-582.
- United States Bureau of Reclamation, (1974) The Earth Manual, Second Edition, pp. 573-578.

Appendix A. Results for Zone of Acceptance Laboratory Testing

Table A.1. Summary of Proctor data/initial data for laboratory testing (flexible wall hydraulic conductivity testing) on the Proctor samples.

Compaction Effort	Sample Number	Water Content w [%]	Dry Unit Weight γ_d [pcf]	Void Ratio e	Saturation S [%]	Porosity n [%]
Standard Energy	1	9.1	101	0.649	38	39
	2	14.4	110	0.517	74	34
	3	19.6	106	0.580	90	37
	4	23.6	98	0.696	90	41
	5	12.3	106	0.575	57	36
	6	17.8	108	Not used for flexible wall testing		
	7	16.5	110	Not used for flexible wall testing		
75% of Standard Energy	1	17.4	108	0.540	86	35
	2	21.0	103	0.613	91	38
	3	24.7	97	0.723	91	42
	4	13.8	108	0.549	67	35
	5	11.1	102	0.637	47	39
	6	25.0	97	Not used for flexible wall testing		
50% of Standard Energy	1	18.6	107	0.557	89	36
	2	20.9	104	0.605	92	38
	3	21.9	101	0.648	90	39
	4	16.0	104	0.611	70	38
	5	22.3	101	Not used for flexible wall testing		

Table A.2. Summary final data obtained from laboratory testing (flexible wall hydraulic conductivity testing) on the Proctor samples.

Compaction Effort	Sample Number	Hydraulic Conductivity	Water Content	Water Content	Water Content	Dry Unit Weight	Void Ratio	Saturation	Porosity	
		k_{20} [cm/sec]	w_{top} [%]	w_{mid} [%]	w_{bot} [%]	γ_d [pcf]	e	S [%]	n [%]	
Standard Energy	1	5.90E-05	24.0	24.1	25.6	96	0.745	88	43	
	2	2.38E-06	18.5	18.7	20.0	107	0.559	91	36	
	3	2.07E-07	19.8	19.2	19.7	107	0.565	92	36	
	4	4.03E-08	23.0	24.9	23.0	101	0.654	96	40	
	5	1.41E-05	19.9	19.9	22.3	103	0.624	89	38	
	6	Not used for flexible wall testing								
	7	Not used for flexible wall testing								
75% of Standard Energy	1	2.15E-07	19.6	19.2	19.5	108	0.548	95	35	
	2	3.09E-08	19.7	19.0	19.7	107	0.562	92	36	
	3	7.53E-08	21.6	23.1	23.4	98	0.693	87	41	
	4	5.51E-06	18.9	20.0	21.6	105	0.593	91	37	
	5	6.75E-05	21.2	20.8	21.4	99	0.684	82	41	
	6	Not used for flexible wall testing								
50% of Standard Energy	1	2.14E-07	19.1	19.7	18.9	107	0.557	92	36	
	2	6.63E-08	21.3	20.3	20.4	98	0.693	80	41	
	3	6.03E-08	20.4	20.2	19.8	104	0.603	89	38	
	4	2.42E-05	20.4	19.5	18.9	102	0.630	83	39	
	5	Not used for flexible wall testing								

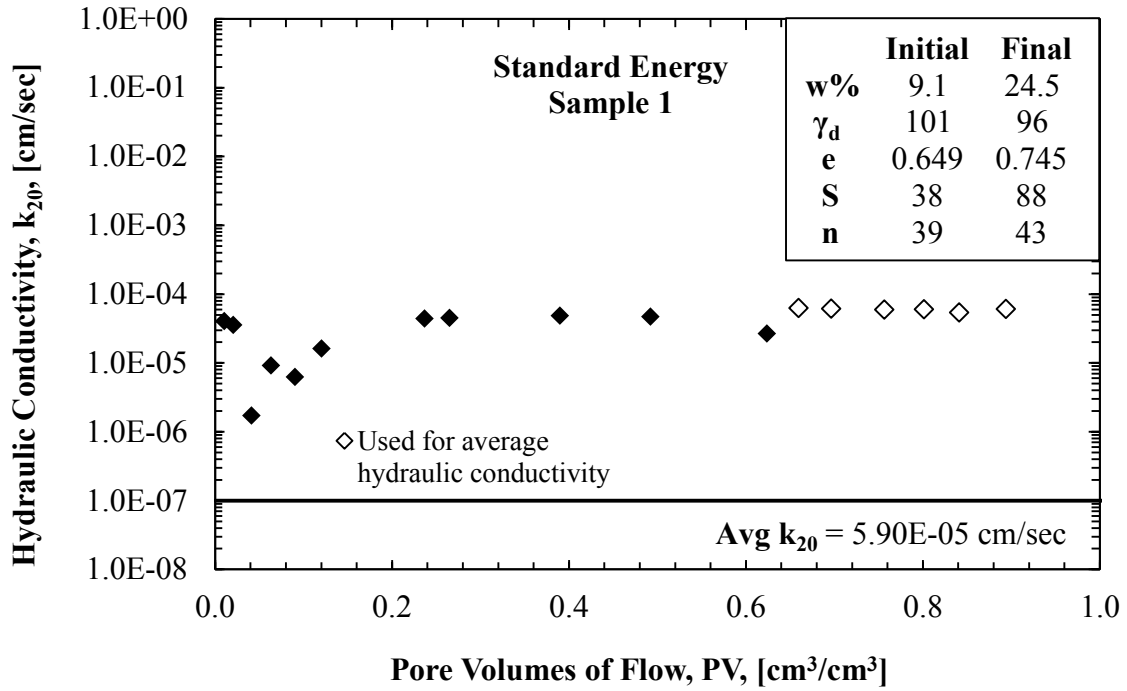


Figure A.1. Vertical hydraulic conductivity data for Standard Energy Sample 1.

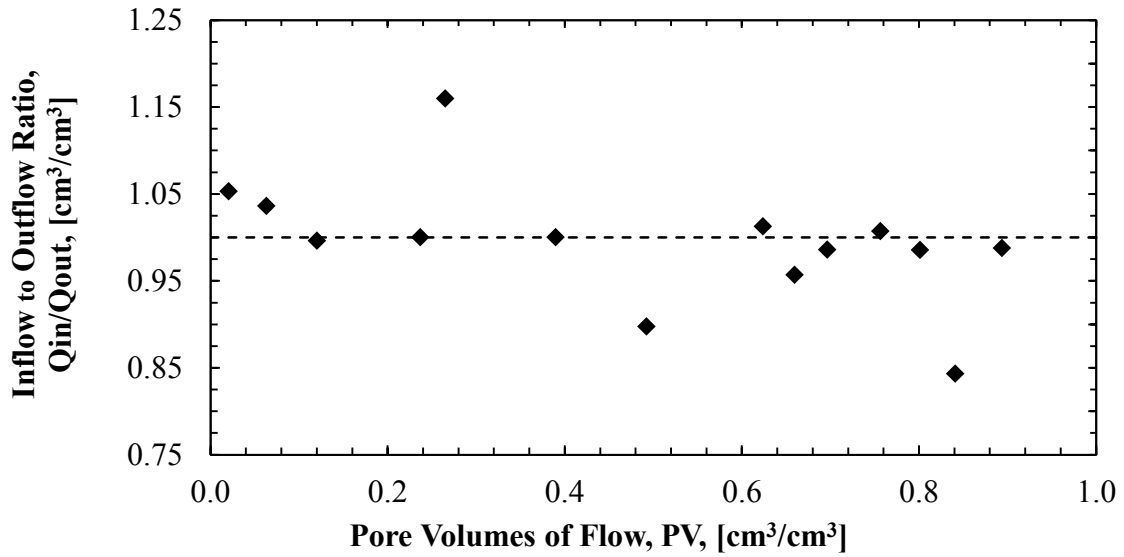


Figure A.2. Inflow to outflow ratio data for Standard Energy Sample 1.

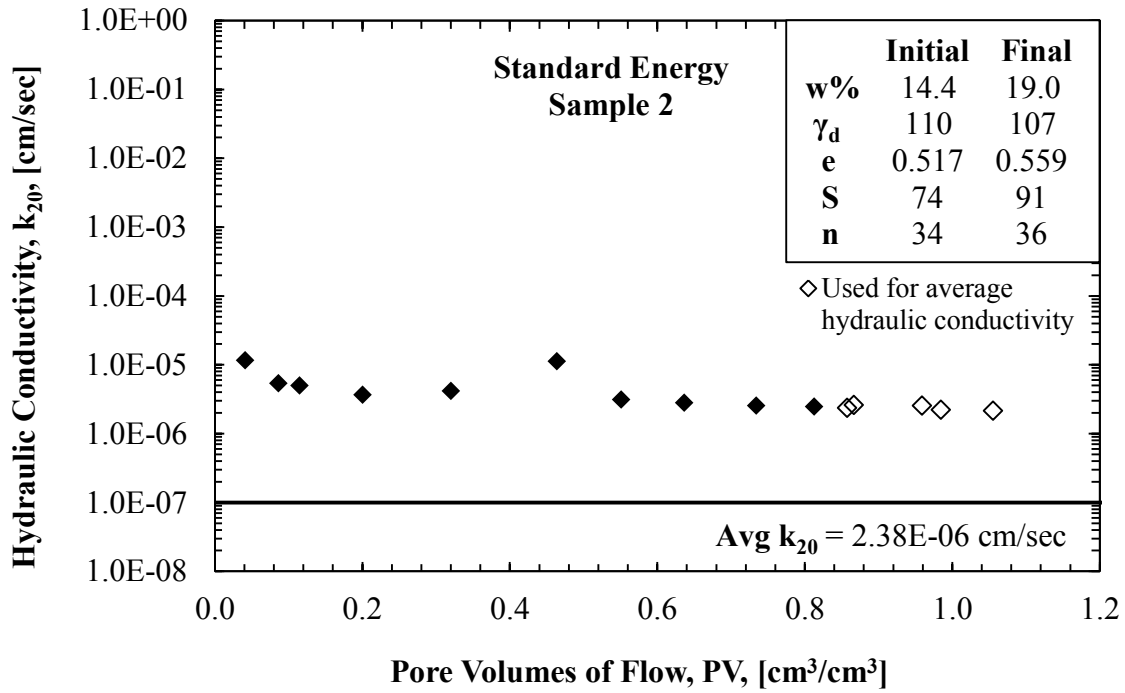


Figure A.3. Vertical hydraulic conductivity data for Standard Energy Sample 2.

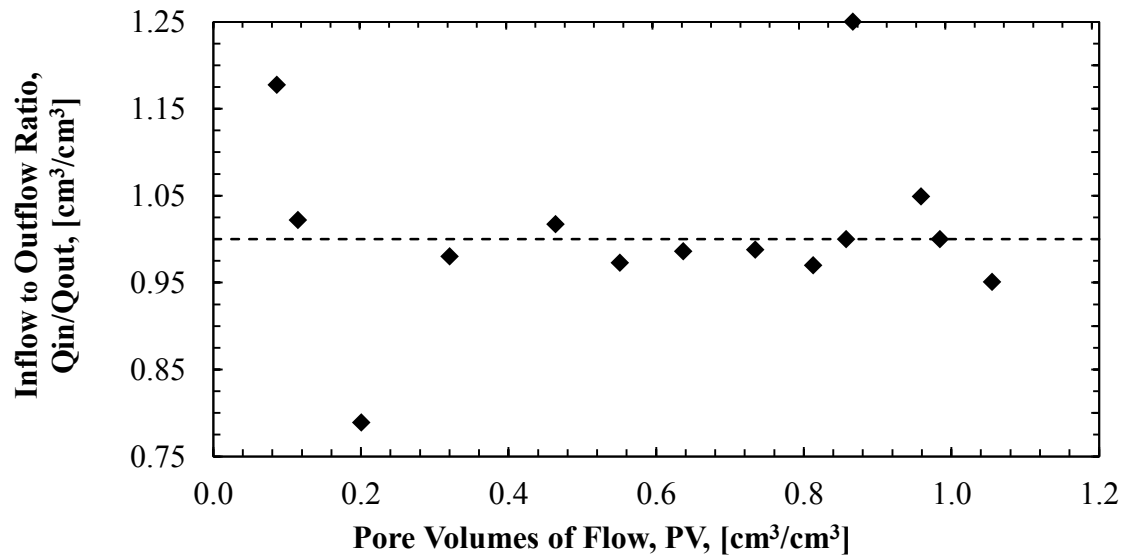


Figure A.4. Inflow to outflow ratio data for Standard Energy Sample 2.

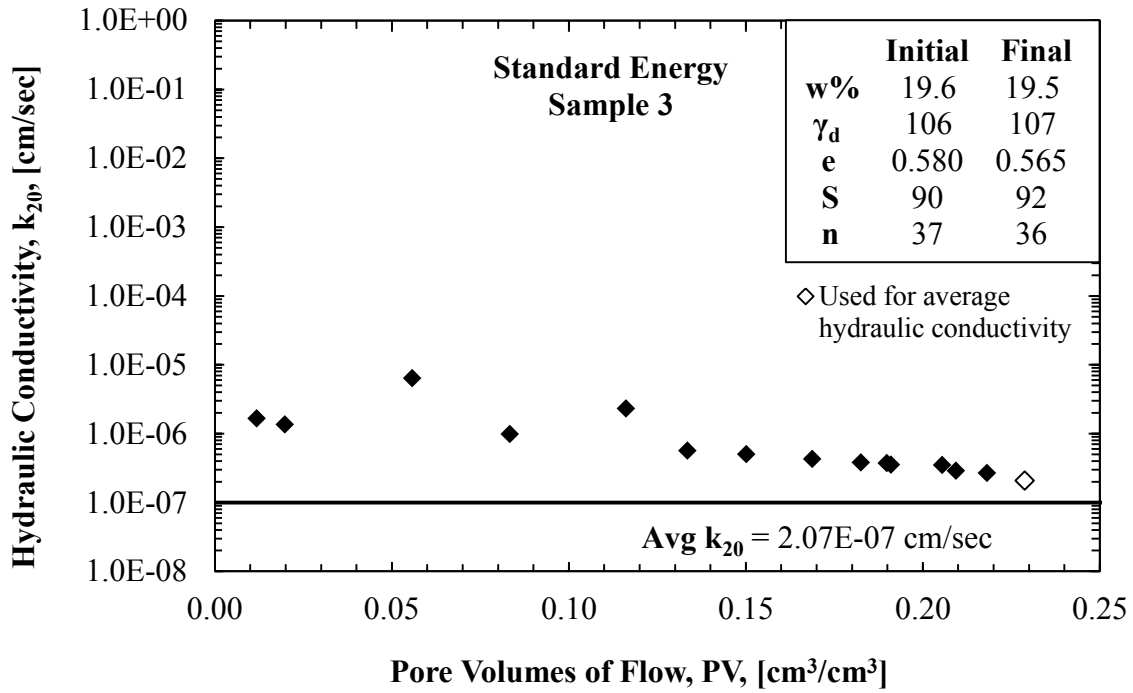


Figure A.5. Vertical hydraulic conductivity data for Standard Energy Sample 3.

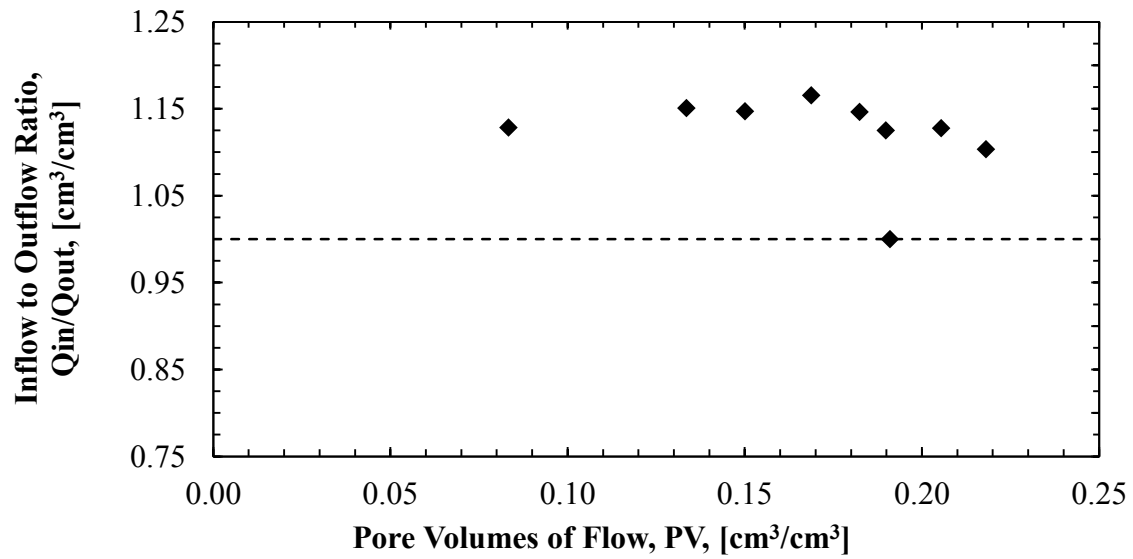


Figure A.6. Inflow to outflow ratio data for Standard Energy Sample 3.

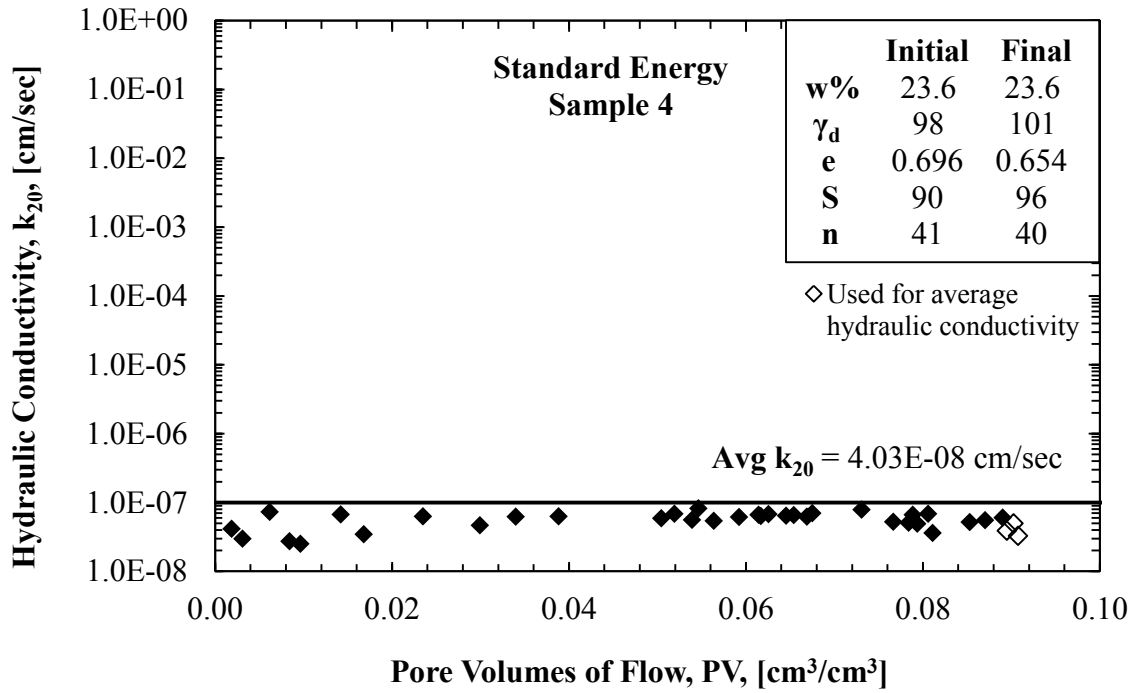


Figure A.7. Vertical hydraulic conductivity data for Standard Energy Sample 4.

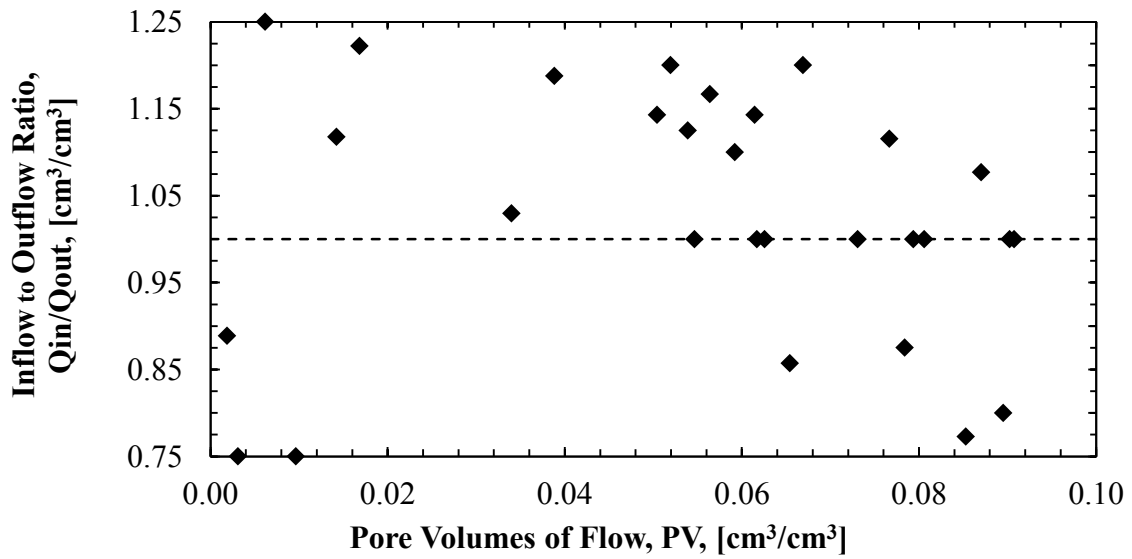


Figure A.8. Inflow to outflow ratio data for Standard Energy Sample 4.

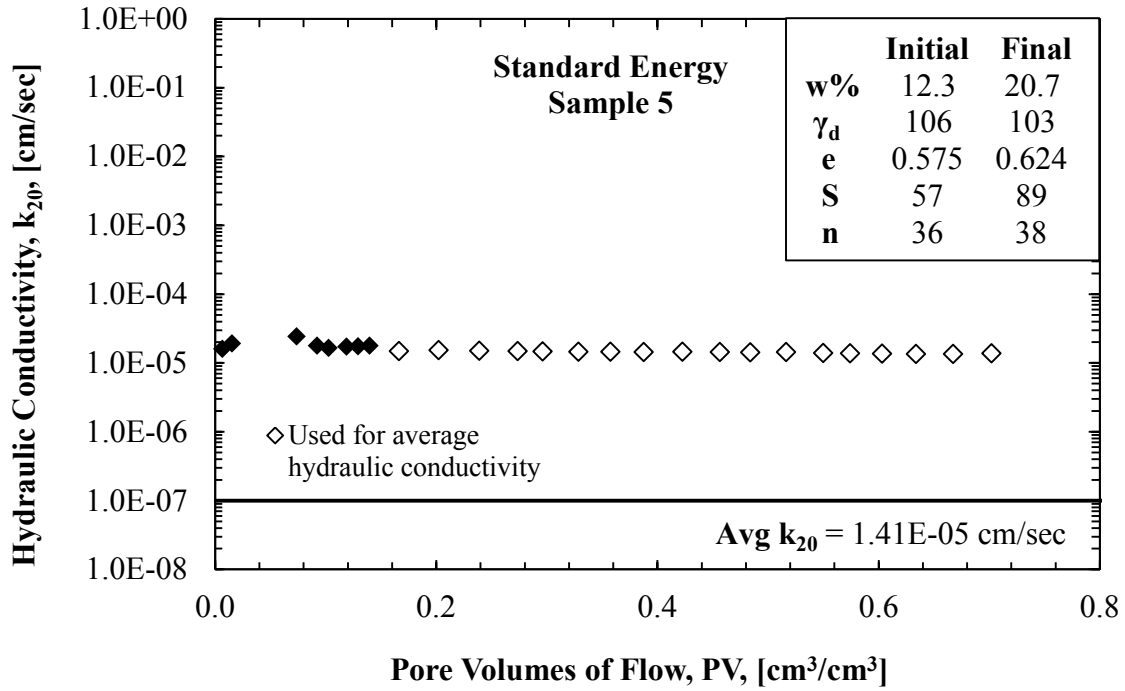


Figure A.9. Vertical hydraulic conductivity data for Standard Energy Sample 5.

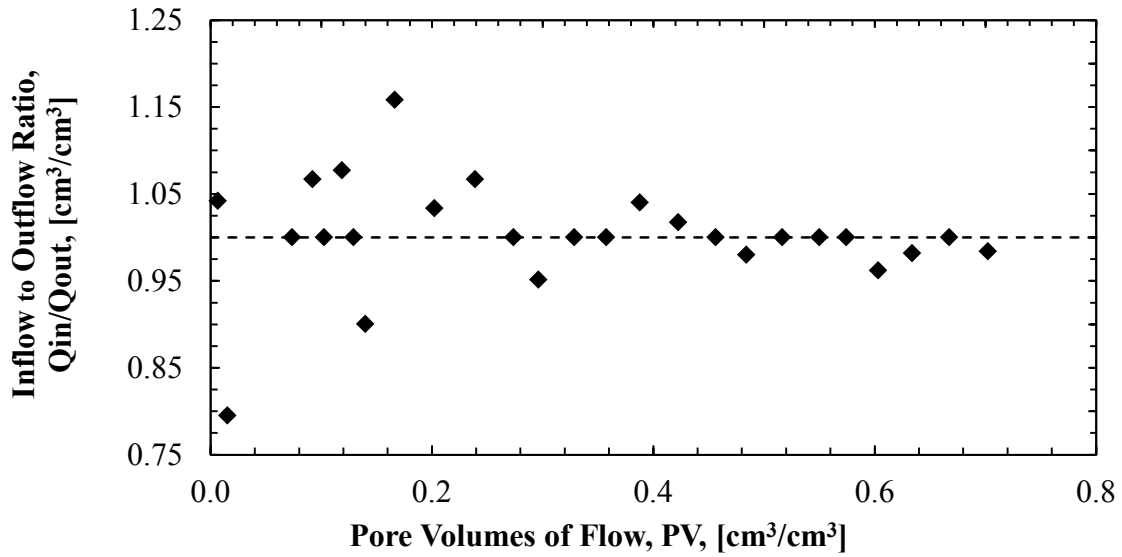


Figure A.10. Inflow to outflow ratio data for Standard Energy Sample 5.

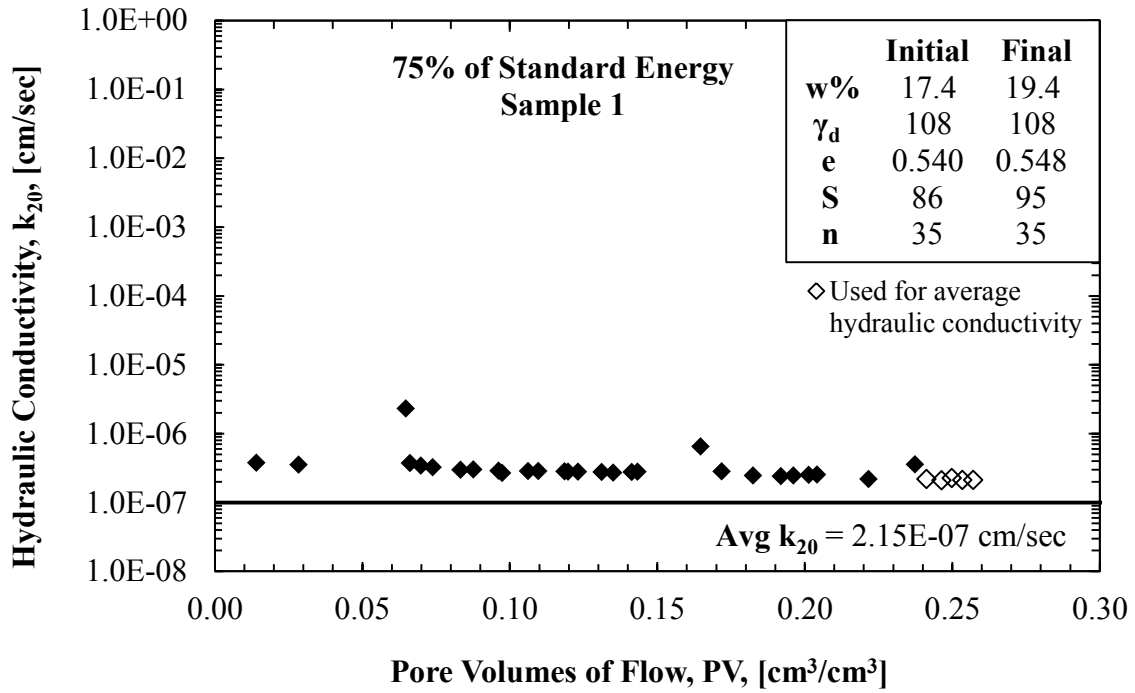


Figure A.11. Vertical hydraulic conductivity data for 75-percent of Standard Energy Sample 1.

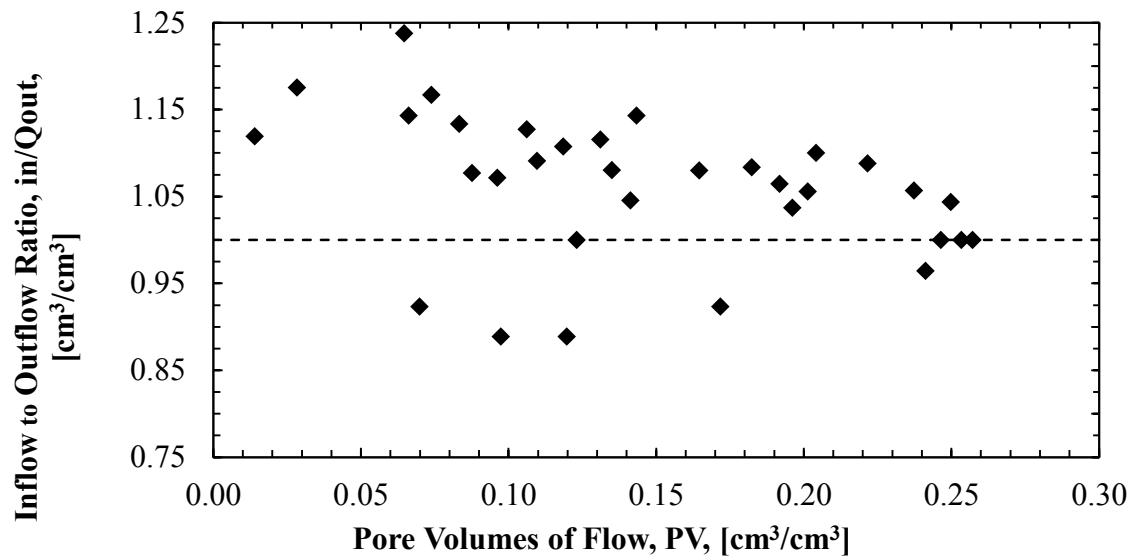


Figure A.12. Inflow to outflow ratio data for 75-percent of Standard Energy Sample 1.

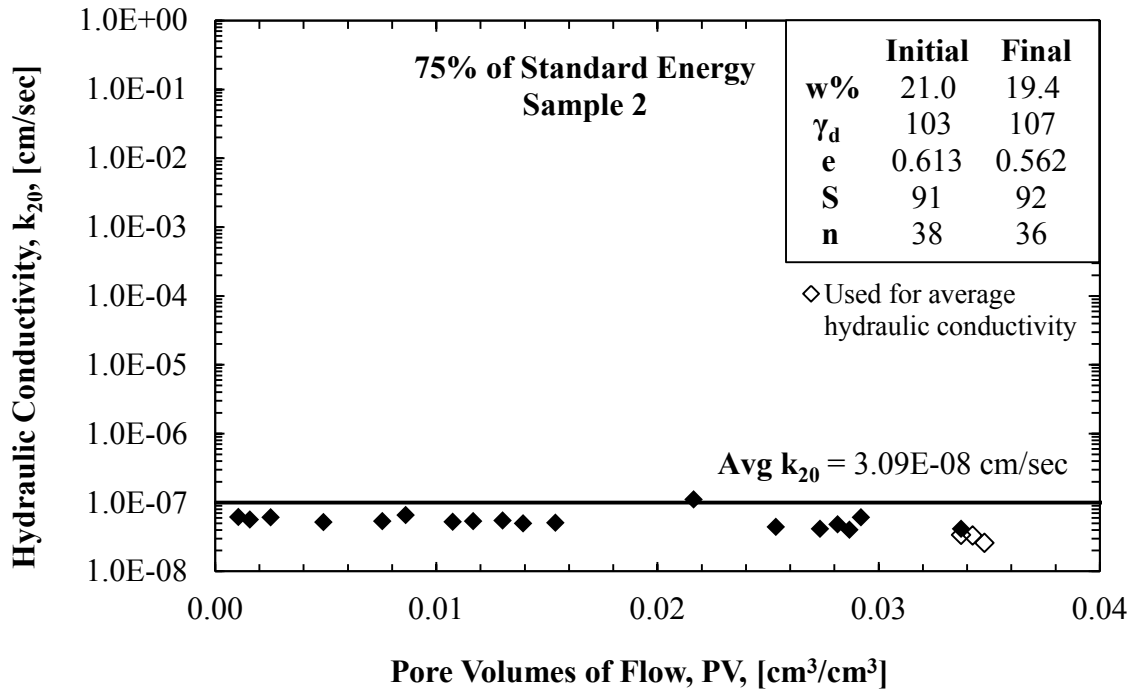


Figure A.13. Vertical hydraulic conductivity data for 75-percent of Standard Energy Sample 2.

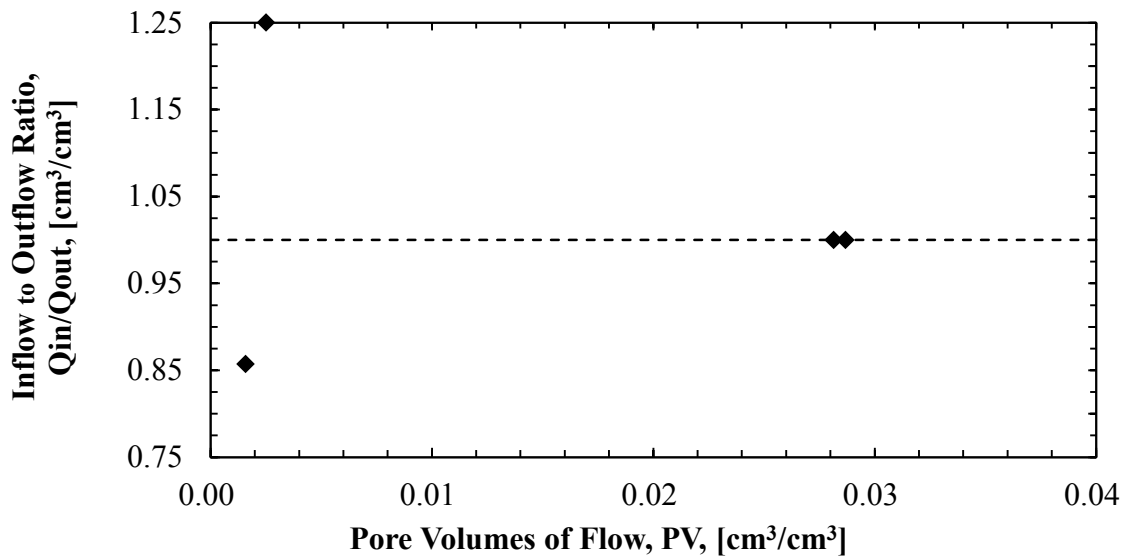


Figure A.14. Inflow to outflow ratio data for 75-percent of Standard Energy Sample 2.

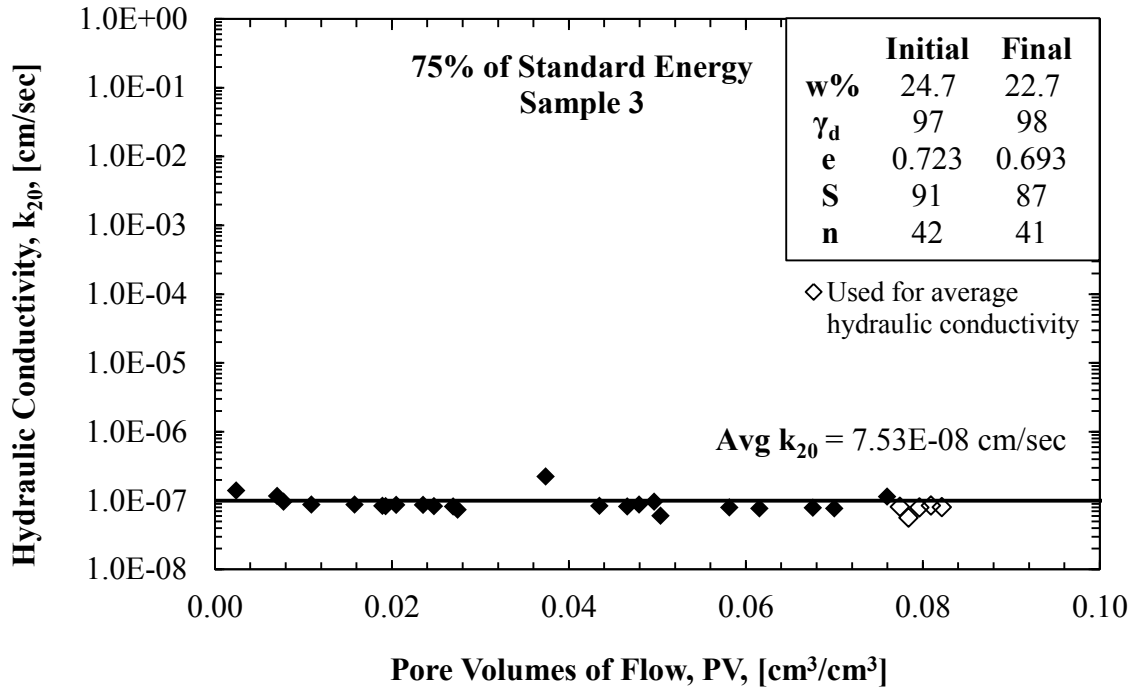


Figure A.15. Vertical hydraulic conductivity data for 75-percent of Standard Energy Sample 3.

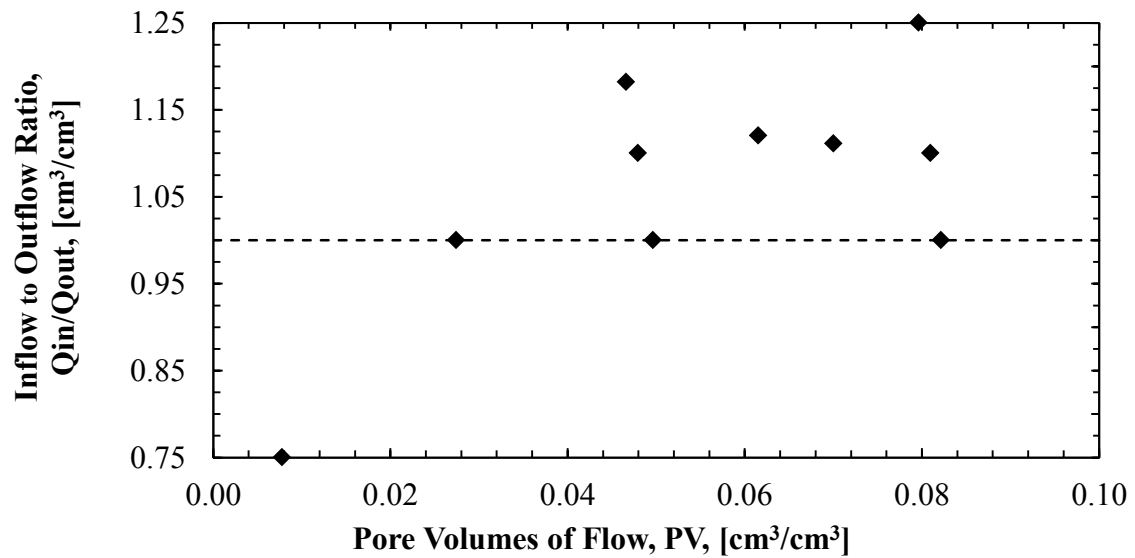


Figure A.16. Inflow to outflow ratio data for 75-percent of Standard Energy Sample 3.

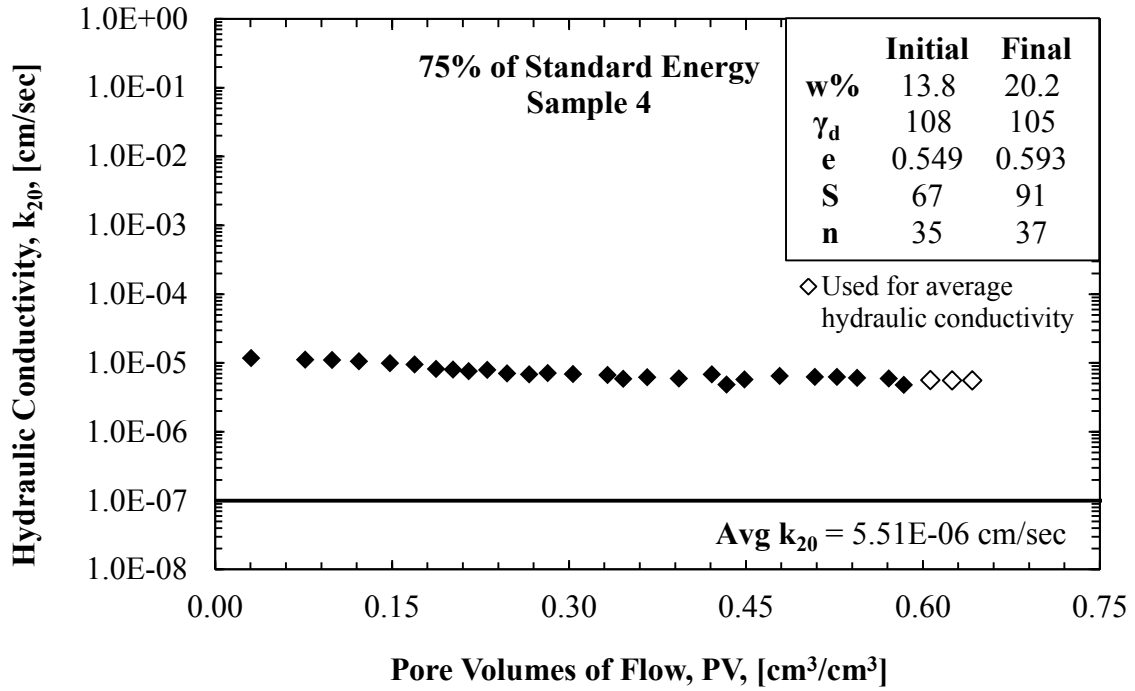


Figure A.17. Vertical hydraulic conductivity data for 75-percent of Standard Energy Sample 4.

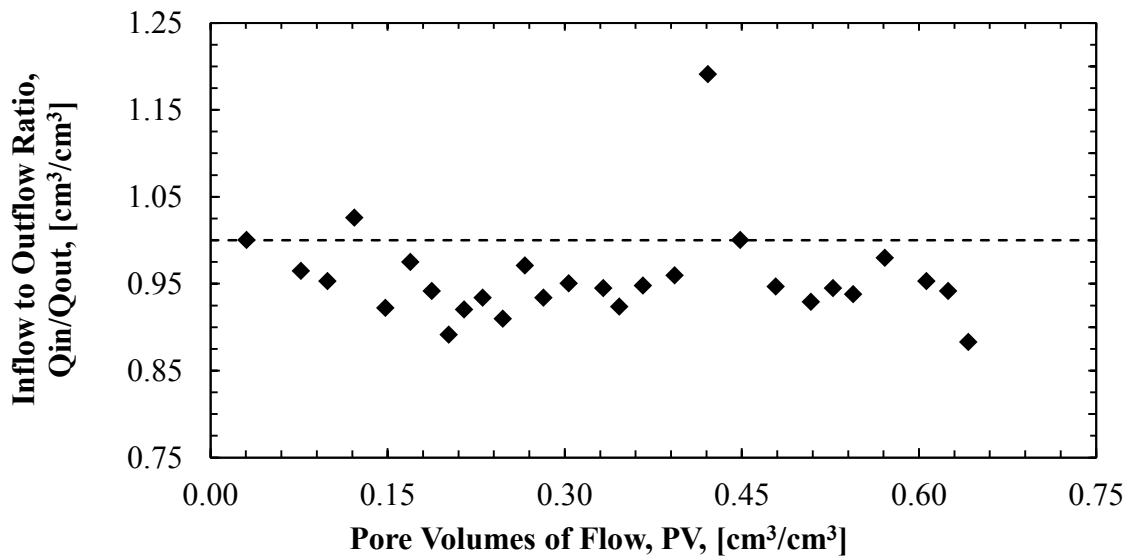


Figure A.18. Inflow to outflow ratio data for 75-percent of Standard Energy Sample 4.

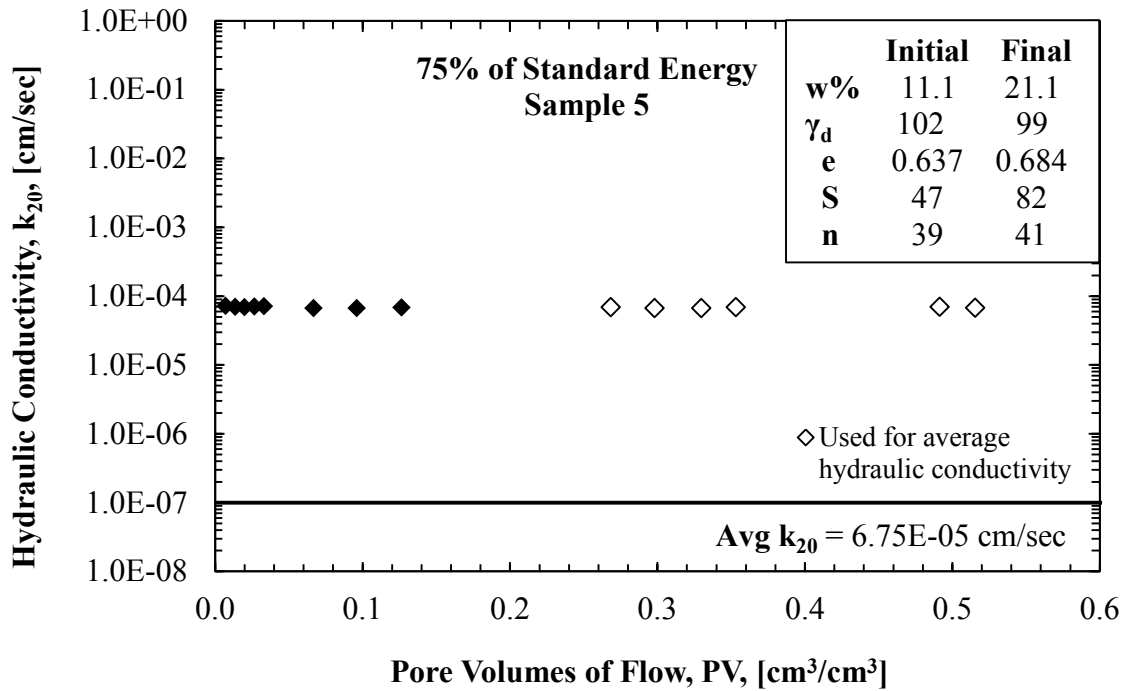


Figure A.19. Vertical hydraulic conductivity data for 75-percent of Standard Energy Sample 5.

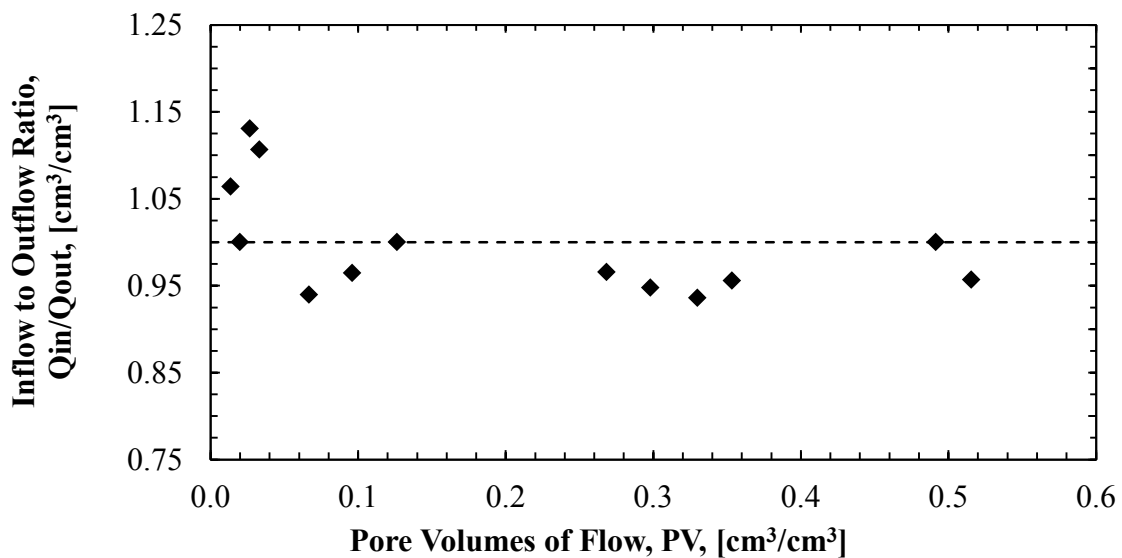


Figure A.20. Inflow to outflow ratio data for 75-percent of Standard Energy Sample 5.

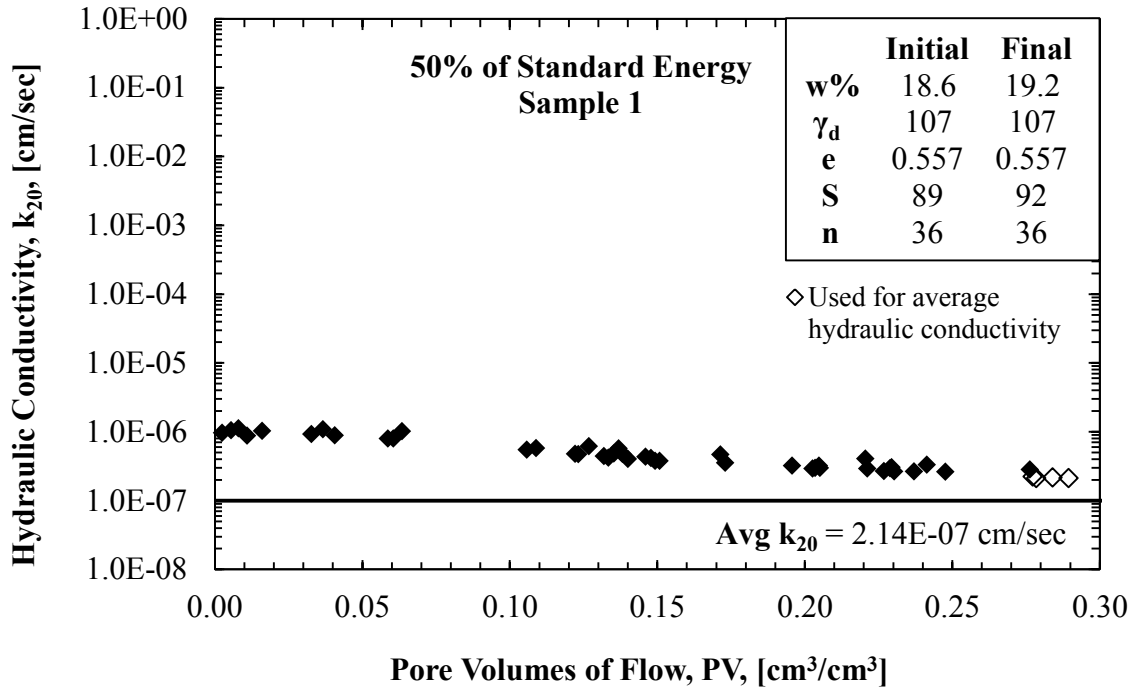


Figure A.21. Vertical hydraulic conductivity data for 50-percent of Standard Energy Sample 1.

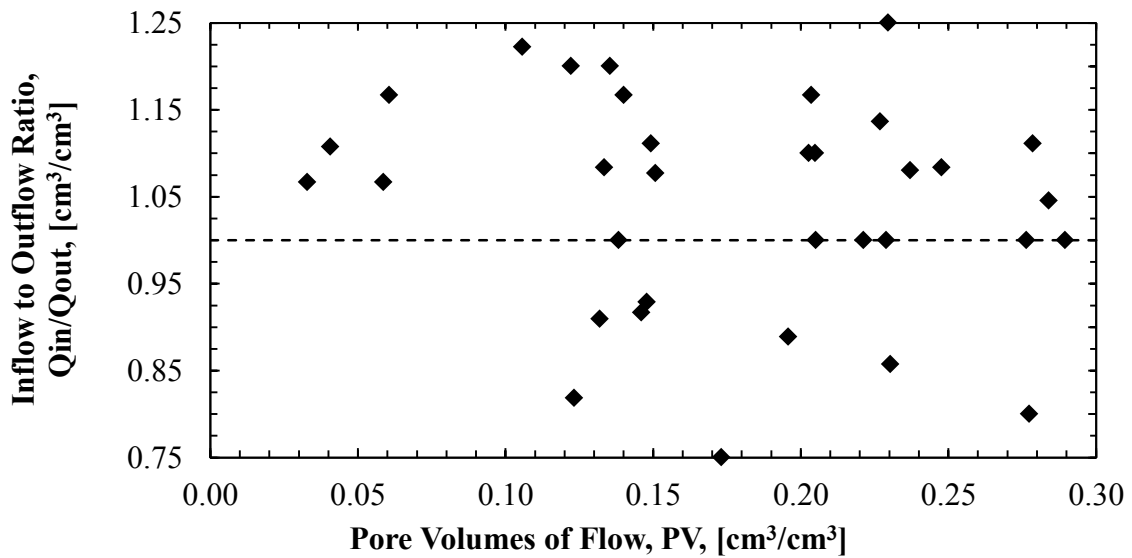


Figure A.22. Inflow to outflow ratio data for 50-percent of Standard Energy Sample 1.

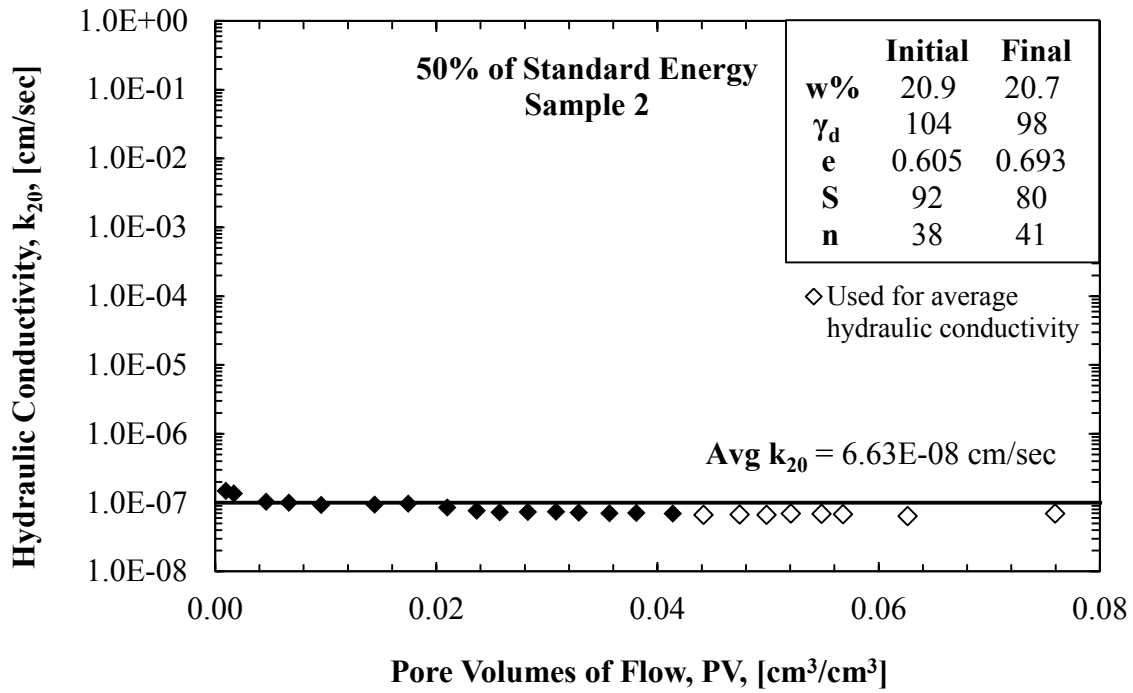


Figure A.23. Vertical hydraulic conductivity data for 50-percent of Standard Energy Sample 2.

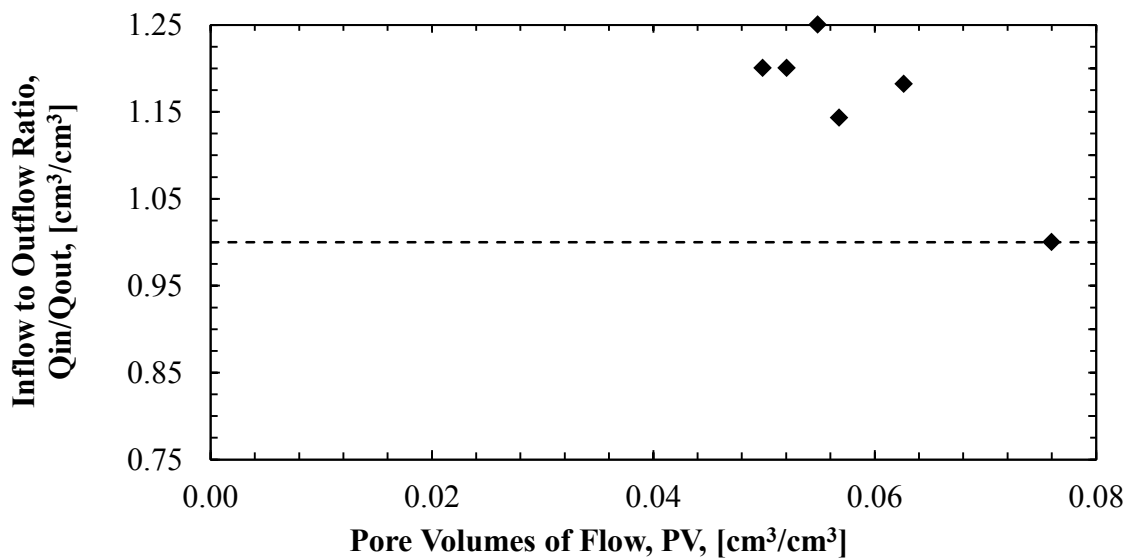


Figure A.24. Inflow to outflow ratio data for 50-percent of Standard Energy Sample 2.

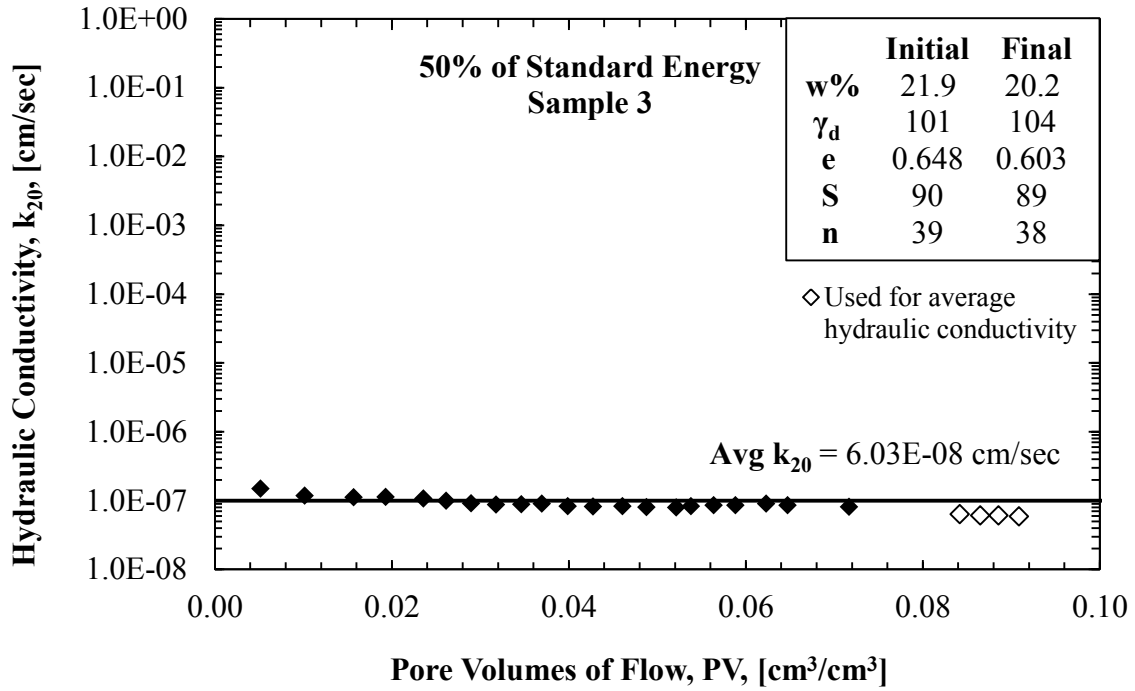


Figure A.25. Vertical hydraulic conductivity data for 50-percent of Standard Energy Sample 3 (previously presented as Figure 4.5).

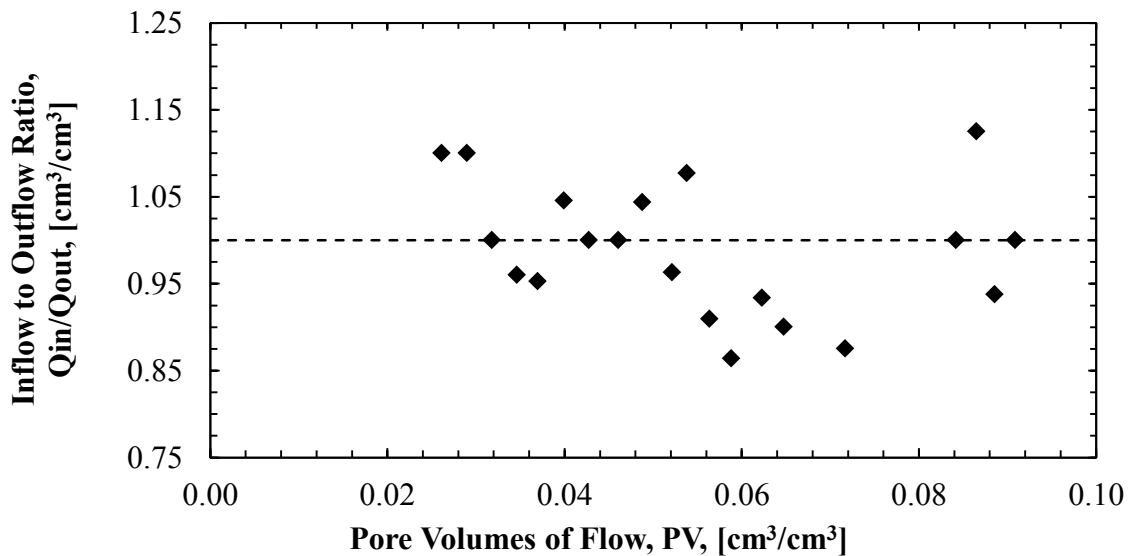


Figure A.26. Inflow to outflow ratio data for 50-percent of Standard Energy Sample 3 (previously presented as Figure 4.6).

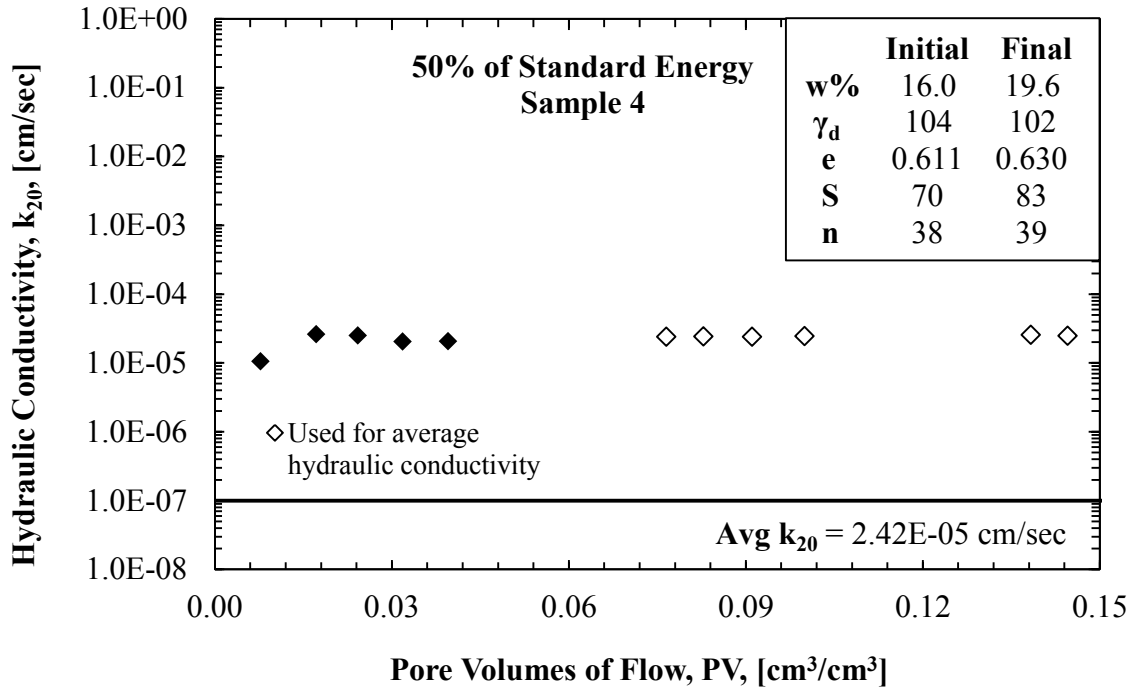


Figure A.27. Vertical hydraulic conductivity data for 50-percent of Standard Energy Sample 4.

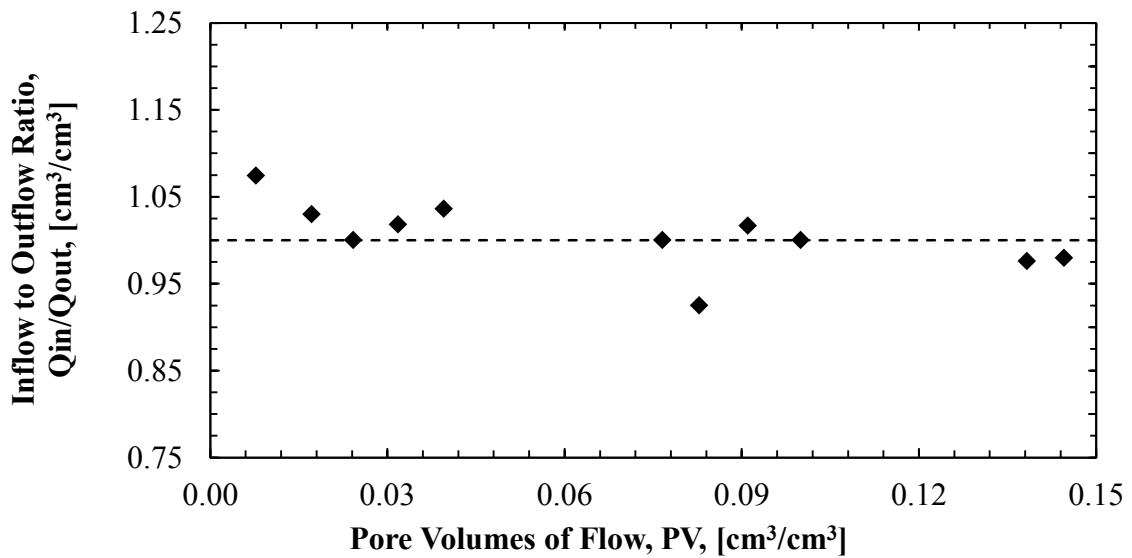


Figure A.28. Inflow to outflow ratio data for 50-percent Reduced Energy Sample 4.

Appendix B. Results Obtained from Field Testing Conducted on Test Pads 1, 2, and 3

Table B.1. Summary of TSB data for Stage 1 conducted on Test Pad 1.

DATE	CLOCK TIME	STOP WATCH TIME	R [cm]	TEG [cm]	Temp _{water} [°C]	Time [sec]	Temp Corr Factor	Initial Head [cm]	Corrected Final Head [cm]	Hydraulic Conductivity [cm/sec]	Cumm. Time [sec]	Cumm. Time [hour]	Time [hour]	k1*t [cm/sec]
5-Jul	16:15	0:00:00	209	107	29.1				92.02					
6-Jul	16:35	25:19:13	119	72	28.7	91153	0.8153	92.02	86.52	7.49E-09	91153	25.3		
	16:37	0:00:00	209	104	28.6			86.52	92.02		91153	25.3		
	18:15	1:37:52	204	103	28.8	5872	0.8189	92.02	91.62	8.26E-09	97025	27.0		
	18:17	0:00:00	204	103	28.8			91.62	91.52		97025	27.0		
7-Jul	13:40	19:23:45	141	90	27.5	69825	0.8288	91.52	86.52	9.07E-09	166850	46.3		
	13:44	0:00:00	206	107	27.5			86.52	91.72		166850	46.3		
	16:52	3:07:43	192	107	28.1	11263	0.8352	91.72	90.32	1.55E-08	178113	49.5		
	16:53	0:00:00	210	107	28.1			90.32	92.12		178113	49.5		
8-Jul	11:42	18:49:22	148	107	26.5	67762	0.8445	92.12	85.92	1.18E-08	245875	68.3		
	11:44	0:00:00	207	107	26.5			85.92	91.82		245875	68.3		
9-Jul	20:28	32:43:50	109	91	30.8	117830	0.8198	91.82	83.62	8.85E-09	363705	101.0		
	20:31	0:00:00	215	108	30.8			83.62	92.62		363705	101.0		
10-Jul	18:25	21:53:48	147	102	29.3	78828	0.7952	92.62	86.42	9.50E-09	442533	122.9		
	18:28	0:00:00	211	102	29.3			86.42	92.22		442533	122.9		
11-Jul	10:56	16:28:33	161	98	28.6	59313	0.8144	92.22	87.62	9.55E-09	501846	139.4		
	10:59	0:00:00	207	115	28.6			87.62	91.82		501846	139.4		
	16:08	5:09:15	192	113	30.2	18555	0.8065	91.82	90.52	8.43E-09	520401	144.6		
	16:09	0:00:00	201	113	30.2			90.52	91.22		520401	144.6		
12-Jul	10:49	18:40:25	145	109	28.5	67225	0.8074	91.22	86.02	9.58E-09	587626	163.2		
	10:51	0:00:00	207	109	28.5			86.02	91.82		587626	163.2		
	14:49	3:57:56	194	109	29.0	14276	0.8180	91.82	90.52	1.11E-08	601902	167.2		
	14:51	0:00:00	194	109	29.0			90.52	90.52		601902	167.2		
	16:51	2:00:00	190	109	29.8	7200	0.8065	90.52	90.12	6.74E-09	609102	169.2		
	16:53	0:00:00	190	109	29.8			90.12	90.12		609102	169.2		
13-Jul	11:10	18:17:00	156	107	29.2	65820	0.8048	90.12	86.92	6.01E-09	674922	187.5		
	11:12	0:00:00	205	107	29.2			86.92	91.62		674922	187.5		
14-Jul	10:31	23:18:51	137	105	28.7	83931	0.8144	91.62	85.02	9.86E-09	758853	210.8		
	10:32	0:00:00	210	105	28.7			85.02	92.12		758853	210.8		
	14:40	4:07:45	196	104	29.0	14865	0.8162	92.12	90.82	1.06E-08	773718	214.9		
	14:41	0:00:00	211	104	29.0			90.82	92.22		773718	214.9		

Table B.1. Summary of TSB data for Stage 1 conducted on Test Pad 1 (continued).

DATE	CLOCK TIME	STOP WATCH TIME	R [cm]	TEG [cm]	Temp _{water} [°C]	Time [sec]	Temp Corr Factor	Initial Head [cm]	Corrected Final Head [cm]	Hydraulic Conductivity [cm/sec]	Cumm. Time [sec]	Cumm. Time [hour]	Time [hour]	k _i *t [cm/sec]
15-Jul	11:06	20:25:08	152	102	28.4	73508	0.8189066	92.22	86.52	9.66182E-09	847226	235.3		
	11:08	0:00:00	212	102	28.4			86.52	92.32		847226	235.3		
	14:53	3:44:43	200	102	28.7	13483	0.8216	92.32	91.12	1.08E-08	860709	239.1		
	14:55	0:00:00	214	102	28.7			91.12	92.52		860709	239.1		
18-Jul	11:12	20:17:06	2	83	26.7	245826	0.8371	92.52	73.22	1.08E-08	1106535	307.4		
	11:17	0:00:00	208	103	26.7			73.22	91.92		1106535	307.4		
	18:24	7:07:06	187	101	29.1	25626	0.8334	91.92	90.02	9.23E-09	1132161	314.5		
	18:25	0:00:00	209	101	29.1			90.02	92.02		1132161	314.5		
19-Jul	11:54	16:29:00	157	99	27.8	59340	0.8234	92.02	87.02	1.05E-08	1191501	331.0		
	11:56	0:00:00	221	114	27.8			87.02	93.22		1191501	331.0		
	19:45	8:49:00	196	113	28.8	31740	0.8261	93.22	90.82	9.23E-09	1223241	339.8		
	19:46	0:00:00	214	113	28.8			90.82	92.52		1223241	339.8		
20-Jul	11:06	15:19:56	166	112	28.1	55196	0.8234	92.52	87.82	1.06E-08	1278437	355.1		
	11:08	0:00:00	211	112	28.1			87.82	92.22		1278437	355.1		
	16:38	5:30:00	196	112	29.3	19800	0.8189	92.22	90.72	9.22E-09	1298237	360.6		
	16:39	0:00:00	224	112	29.3			90.72	93.52		1298237	360.6		
21-Jul	10:37	17:58:02	168	110	28.1	64682	0.8189	93.52	88.12	1.02E-08	1362919	378.6	18.0	1.84E-07
	10:39	0:00:00	216	110	28.1			88.12	92.72		1362919	378.6		
22-Jul	10:10	23:30:55	141	108	26.8	84655	0.8417	92.72	85.42	1.11E-08	1447574	402.1	23.5	2.61E-07
	10:13	0:00:00	226	123	26.8			85.42	93.72		1447574	402.1		
23-Jul	15:58	5:44:58	133	120	27.6	107098	0.8464	93.72	84.72	1.08E-08	1554672	431.9	29.7	3.23E-07
	15:59	0:00:00	222	120	27.6			84.72	93.32		1554672	431.9		
25-Jul	10:38	18:38:59	86	113	26.3	153539	0.8511	93.32	80.42	1.12E-08	1708211	474.5	42.6	4.78E-07
	10:39	0:00:00	216	113	26.3			80.42	92.72		1708211	474.5		
	16:14	5:34:58	198	112	27.3	20098	0.8540	92.72	91.02	1.07E-08	1728309	480.1	5.6	5.97E-08
	16:15	0:00:00	207	112	27.3			91.02	91.82		1728309	480.1		
26-Jul	10:44	18:29:10	151	112	27.8	66550	0.8399	91.82	86.22	1.08E-08	1794859	498.6	18.5	2.00E-07

Table B.2. Summary of TSB data for Stage 2 conducted on Test Pad 2.

DATE	CLOCK TIME	STOP WATCH TIME	R [cm]	TEG [cm]	Temp _{water} [°C]	Time [sec]	Temp Corr Factor	Initial Head [cm]	Corrected Final Head [cm]	Hydraulic Conductivity [cm/sec]	Cumm. Time [sec]	Cumm. Time [hour]	Time [hour]	k ₂ *t [cm ² /sec]
26-Jul	11:59	0:00:00	210	141	28.1				92.12					
	12:59	1:00:07	170	141	28.3	3607	0.8279	92.12	88.12	4.87E-08	3607	1.0		
	13:04	0:00:00	222	141	28.3			88.12	93.32		3607	1.0		
	15:04	2:00:00	180	141	27.8	7200	0.8307	93.32	89.12	2.54E-08	10807	3.0		
	13:05	0:00:00	221	141	27.8			89.12	93.22		10807	3.0		
	16:00	0:55:00	202	141	28.8	3300	0.8261	93.22	91.32	2.46E-08	14107	3.9		
	16:00	0:00:00	202	141	28.8			91.32	91.32		14107	3.9		
	17:38	1:38:41	173	141	28.8	5921	0.8171	91.32	88.42	2.13E-08	20028	5.6		
	10:38	0:00:00	221	139	28.1			88.42	93.22		20028	5.6		
	12:25	1:47:00	195	139	28.4	6420	0.8270	93.22	90.62	1.74E-08	26448	7.3		
12:26	0:00:00	231	139	28.4			90.62	94.22		26448	7.3			
14:39	2:11:00	202	138	29.0	7860	0.8189	94.22	91.42	1.50E-08	34308	9.5	2.18	3.28E-08	
14:40	0:00:00	202	138	29.0			91.42	91.32		34308	9.5			
15:48	1:08:00	188	139	29.5	4080	0.8091	91.32	89.82	1.57E-08	38388	10.7	1.13	1.78E-08	
16:04	0:00:00	184	139	29.5			89.82	89.52		38388	10.7			
17:08	1:04:00	171	139	30.0	3840	0.8004	89.52	88.22	1.46E-08	42228	11.7	1.07	1.55E-08	
10:43	0:00:00	216	137	28.4			88.22	92.72		42228	11.7			
12:10	1:27:00	196	137	28.3	5220	0.8252	92.72	90.72	1.65E-08	47448	13.2	1.45	2.39E-08	
12:12	0:00:00	218	137	28.3			90.72	92.92		47448	13.2			
14:33	2:21:00	190	137	28.8	8460	0.8216	92.92	90.12	1.42E-08	55908	15.5	2.35	3.34E-08	
14:34	0:00:00	190	137	28.8			90.12	90.12		55908	15.5			
15:59	1:25:00	173	138	29.2	5100	0.8136	90.12	88.32	1.54E-08	61008	16.9	1.42	2.18E-08	
15:59	0:00:00	173	138	29.2			88.32	88.42		61008	16.9			
17:29	1:30:00	157	137	29.9	5400	0.8039	88.42	86.92	1.22E-08	66408	18.4	1.50	1.82E-08	
17:30	0:00:00	157	137	29.9			86.92	86.82		66408	18.4			
18:15	0:44:00	148	138	28.2	2640	0.8127	86.82	85.82	1.70E-08	69048	19.2	0.73	1.25E-08	
11:18	0:00:00	204	134	28.1			85.82	91.52		69048	19.2			
13:26	2:07:00	171	134	28.1	7620	0.8297	91.52	88.22	1.91E-08	76668	21.3	2.12	4.04E-08	
13:26	0:00:00	171	134	28.1			88.22	88.22		76668	21.3			
15:25	1:59:00	153	134	29.2	7140	0.8198	88.22	86.42	1.13E-08	83808	23.3	1.98	2.24E-08	

Table B.3. Summary of TSB data for Stage 1 conducted on Test Pad 2.

DATE	CLOCK TIME	STOP WATCH TIME	R [cm]	TEG [cm]	Temp _{water} [°C]	Time [sec]	Temp Corr Factor	Initial Head [cm]	Corrected Final Head [cm]	Hydraulic Conductivity [cm/sec]	Cumm. Time [sec]	Cumm. Time [hour]	Time [hour]	k1*t [cm/sec]
8-Jan-12	12:52	27:50:00	157	100	21.8				86.82					
10-Jan-12	9:47	72:45:00	59	100	22.6	161700	0.9488	86.82	77.02	9.55E-09	161700	44.9		
28-Feb-12	15:50	23:38:00	143	100	22.6			77.02	85.42		161700	44.9		
	16:23	24:11:00	141	100	22.6	1980	0.9399	85.42	85.22	1.51E-08	163680	45.5		
29-Feb-12	15:02	22:37:00	144	100	22.7			85.22	85.52		163680	45.5		
	15:59	23:35:00	140	100	22.6	3480	0.9388	85.52	85.12	1.72E-08	167160	46.4		
4-Mar-12	18:43	0:00:00	150	100	22.9			85.12	86.12		167160	46.4		
5-Mar-12	7:44	13:01:30	79	100	23.2	46890	0.9301	86.12	79.02	2.32E-08	214050	59.5		
	21:00	26:17:00	32	100	22.8	47730	0.9312	79.02	74.32	1.63E-08	261780	72.7		
	21:02	0:00:00	157	100	22.8			74.32	86.82		261780	72.7		
6-Mar-12	20:19	23:17:00	64	100	22.8	83820	0.9355	86.82	77.52	1.72E-08	345600	96.0		
8-Mar-12	7:57	0:00:00	147	100	23.0			77.52	85.82		345600	96.0		
	15:57	8:00:00	99	100	23.0	28800	0.9312	85.82	81.02	2.53E-08	374400	104.0		
9-Mar-12	9:39	25:42:00	21	100	23.0	63720	0.9312	81.02	73.22	2.01E-08	438120	121.7		
	9:42	0:00:00	151	112	23.1			73.22	86.22		438120	121.7		
10-Mar-12	15:18	29:36:00	29	103	23.4	106560	0.9258	86.22	74.92	1.66E-08	544680	151.3		
	15:20	0:00:00	150	103	23.4			74.92	86.12		544680	151.3		
11-Mar-12	21:09	28:49:30	38	107	23.1	103770	0.9258	86.12	74.52	1.75E-08	648450	180.1		
	21:11	0:00:00	147	107	23.1			74.52	85.82		648450	180.1		
12-Mar-12	20:51	23:40:30	41	103	23.0	85230	0.9301	85.82	75.62	1.88E-08	733680	203.8		
	20:53	0:00:00	150	103	23.0			75.62	86.12		733680	203.8		
13-Mar-12	7:56	11:03:00	93	100	23.3	39780	0.9279	86.12	80.72	2.05E-08	773460	214.9	11.05	2.27E-07
3-Apr-12	8:22	0:00:00	151	112	22.9			80.72	86.22		773460	214.9		
	19:09	10:47:00	91	108	22.8	38820	0.9344	86.22	80.62	2.20E-08	812280	225.6	10.78	2.37E-07
	19:12	0:00:00	157	108	22.8			80.62	86.82		812280	225.6		
4-Apr-12	19:03	23:51:00	40	106	23.0	85860	0.9333	86.82	75.32	2.10E-08	898140	249.5	23.85	5.01E-07
	19:04	0:00:00	149	106	23.0			75.32	86.02		898140	249.5		
5-Apr-12	20:01	12:56:00	78	104	23.0	46560	0.9312	86.02	79.12	2.27E-08	944700	262.4	12.93	2.94E-07

Table B.4. Summary of TSB data for Stage 2 conducted on Test Pad 2.

CLOCK TIME	STOP WATCH TIME	R [cm]	TEG [cm]	Temp _{water} [°C]		Time [sec]	Temp Corr Factor	Initial Head [cm]	Corrected Final Head [cm]	Hydraulic Conductivity [cm/sec]	Cumm. Time [sec]	Cumm. Time [hour]	Time [hour]	k ₂ *t [cm/sec]
15:17	0:00:00	148	108	22.8				85.92						
17:25	2:08:00	110	108	22.6	0.9377	7680	0.9377	85.92	82.12	2.64E-08	7680	2.1		
21:19	6:02:00	57	109	22.5	0.9410	14040	0.9410	82.12	76.72	2.18E-08	21720	6.0		
12:23	0:00:00	149	96	22.9				76.72	86.02		21720	6.0		
16:58	4:34:00	68	95	22.6	0.9366	16440	0.9366	86.02	78.02	2.66E-08	38160	10.6		
13:43	0:00:00	149	100	22.8				78.02	86.02		38160	10.6		
14:05	0:22:00	138	100	22.7	0.9366	1320	0.9366	86.02	84.92	4.36E-08	39480	11.0		
14:53	1:10:00	123	99	22.8	0.9366	2880	0.9366	84.92	83.52	2.58E-08	42360	11.8		
17:06	3:23:00	88	98	22.8	0.9355	7980	0.9355	83.52	80.02	2.40E-08	50340	14.0		
19:35	5:51:30	54	97	22.7	0.9366	8910	0.9366	80.02	76.62	2.18E-08	59250	16.5		
14:34	0:00:00	153	109	22.9				76.62	86.42		59250	16.5		
16:04	1:30:00	128	108	22.8	0.9344	5400	0.9344	86.42	84.02	2.33E-08	64650	18.0		
19:11	4:37:00	86	108	22.7	0.9366	11220	0.9366	84.02	79.72	2.09E-08	75870	21.1		
15:19	0:00:00	152	108	22.8				79.72	86.32		75870	21.1		
15:49	0:30:00	142	108	22.8	0.9355	1800	0.9355	86.32	85.32	2.89E-08	77670	21.6		
16:31	1:12:00	130	110	22.7	0.9366	2520	0.9366	85.32	83.92	2.94E-08	80190	22.3		
17:00	1:41:00	124	110	22.5	0.9399	1740	0.9399	83.92	83.52	1.23E-08	81930	22.8		
17:19	2:00:00	119	110	22.7	0.9399	1140	0.9399	83.52	83.02	2.36E-08	83070	23.1		
16:54	0:00:00	153	112	22.7				83.02	86.42		83070	23.1		
18:55	2:01:00	113	111	22.7	0.9377	7260	0.9377	86.42	82.52	2.85E-08	90330	25.1		
20:36	0:00:00	150	105	22.6				82.52	86.12		90330	25.1		
21:39	1:02:30	127	106	22.7	0.9388	3750	0.9388	86.12	83.72	3.38E-08	94080	26.1		
12:35	3:58:00	77	106	22.7	0.9377	10530	0.9377	83.72	78.82	2.57E-08	104610	29.1	2.93	7.50E-08
15:26	6:49:00	30	108	22.8	0.9366	10260	0.9366	78.82	73.92	2.80E-08	114870	31.9	2.85	7.98E-08
8:39	0:00:00	155	100	22.8				73.92	86.62		114870	31.9		
12:31	3:52:00	76	99	22.6	0.9377	13920	0.9377	86.62	78.82	3.04E-08	128790	35.8	3.87	1.17E-07
15:32	0:00:00	151	102	22.8				78.82	86.22		128790	35.8		
16:19	0:47:00	128	102	22.8	0.9355	2820	0.9355	86.22	83.92	4.28E-08	131610	36.6	0.78	3.36E-08
9:16	0:00:00	147	117	22.8				83.92	85.82		131610	36.6		
10:33	1:17:00	110	116	22.8	0.9355	4620	0.9355	85.82	82.22	4.14E-08	136230	37.8	1.28	5.32E-08
12:59	3:43:00	59	115	22.8	0.9355	8760	0.9355	82.22	77.12	3.27E-08	144990	40.3	2.43	7.95E-08
13:00	0:00:00	157	113	23.2				77.12	86.82		144990	40.3		
16:11	3:11:00	84	110	23.0	0.9290	11460	0.9290	86.82	79.82	3.25E-08	156450	43.5	3.18	1.04E-07

Table B.5. Summary of raw data obtained from SDRI test conducted on Test Pad 3.

Start Time t_1	End Time t_2	Initial Wt. of Bag W_1	Final Wt. of Bag W_2	Initial Temp T_1	Final Temp T_2	Initial Water Ht. h_1	Final Water Ht. h_2	North Tensiometers		
								1	2	3
[date]	[date]	[grams]	[grams]	[°C]	[°C]	[in.]	[in.]	[centibar]	[centibar]	[centibar]
10/9/2012 12:30 PM	10/11/2012 7:20 PM	3585.0	3494.9	23.5	23.5	12	12	6.26		
10/11/2012 7:30 PM	10/17/2012 7:20 PM	3393.8	3300.8	23.5	23.5	12	12	3.67		
10/17/2012 7:25 PM	10/21/2012 7:10 PM	3300.1	3229.1	23.5	23.3	12	11.875	3.60		
10/21/2012 7:20 PM	10/26/2012 4:00 PM	3229.1	3181.0	23.3	23.2	12	11.875	2.04		
10/26/2012 4:10 PM	10/31/2012 8:10 PM	3143.2	3064.5	23.2	23.5	12	11.75	2.18		
10/31/2012 8:15 PM	11/7/2012 9:35 AM	3030.0	2983.1	23.5	21.5	12	12	1.70		
11/7/2012 9:40 AM	11/13/2012 7:40 PM	2969.4	2916.6	21.5	23.5	12	12	1.63		
11/13/2012 7:45 PM	11/19/2012 8:15 AM	2916.6	2870.2	23.5	19.7	12	12	0.00	6.81	
11/19/2012 8:20 AM	11/26/2012 6:05 PM	2870.2	2840.8	19.7	19.2	12	12	0.00	6.47	
12/4/2012 12:00 PM	12/11/2012 8:45 PM	2833.8	2823.9	21.5	20.1	12	12	0.00	5.58	

Table B.6. Summary of reduced data obtained from SDRI test conducted on Test Pad 3.

Infiltration Rate	Temp. Corr. Factor	6" depth	12" depth	18" depth	Wetting Front Depth	Apparent Method	Wetting Front Method	Suction Method	Apparent Method	Wetting Front Method	Suction Method	Apparent Method	Wetting Front Method	Suction Method
i	Rt	Tensiometers			z	Hydraulic Gradient, i			Hydraulic Conductivity, k			Corr. Hydraulic Conductivity, k ₂₀		
[cm/sec]		[cm]	[cm]	[cm]	[cm]	[cm/cm]	[cm/cm]	[cm/cm]	[cm/sec]	[cm/sec]	[cm/sec]	[cm/sec]	[cm/sec]	[cm/sec]
1.23E-07	0.920	63.8	0.0	0.0	12.7	1.5	3.40	8.42	8.18E-08	3.61E-08	1.46E-08	7.53E-08	3.32E-08	1.34E-08
4.83E-08	0.920	37.4	0.0	0.0	12.7	1.5	3.40	6.35	3.22E-08	1.42E-08	7.61E-09	2.97E-08	1.31E-08	7.01E-09
5.54E-08	0.923	36.7	0.0	0.0	12.7	1.5	3.40	6.29	3.70E-08	1.63E-08	8.81E-09	3.41E-08	1.50E-08	8.13E-09
3.08E-08	0.926	20.8	0.0	0.0	12.7	1.5	3.40	5.04	2.05E-08	9.06E-09	6.12E-09	1.90E-08	8.39E-09	5.66E-09
4.74E-08	0.924	22.2	0.0	0.0	12.7	1.5	3.40	5.15	3.16E-08	1.40E-08	9.22E-09	2.92E-08	1.29E-08	8.51E-09
2.23E-08	0.942	17.3	0.0	0.0	12.7	1.5	3.40	4.76	1.49E-08	6.55E-09	4.68E-09	1.40E-08	6.17E-09	4.41E-09
2.56E-08	0.942	16.6	0.0	0.0	12.7	1.5	3.40	4.71	1.71E-08	7.54E-09	5.44E-09	1.61E-08	7.10E-09	5.13E-09
2.62E-08	0.962	0.0	69.4	0.0	27.94	1.5	2.09	4.58	1.75E-08	1.25E-08	5.72E-09	1.68E-08	1.20E-08	5.51E-09
1.24E-08	1.014	0.0	65.9	0.0	27.94	1.5	2.09	4.45	8.24E-09	5.91E-09	2.78E-09	8.36E-09	5.99E-09	2.82E-09
4.19E-09	0.981	0.0	56.9	0.0	27.94	1.5	2.09	4.13	2.79E-09	2.00E-09	1.01E-09	2.74E-09	1.96E-09	9.95E-10

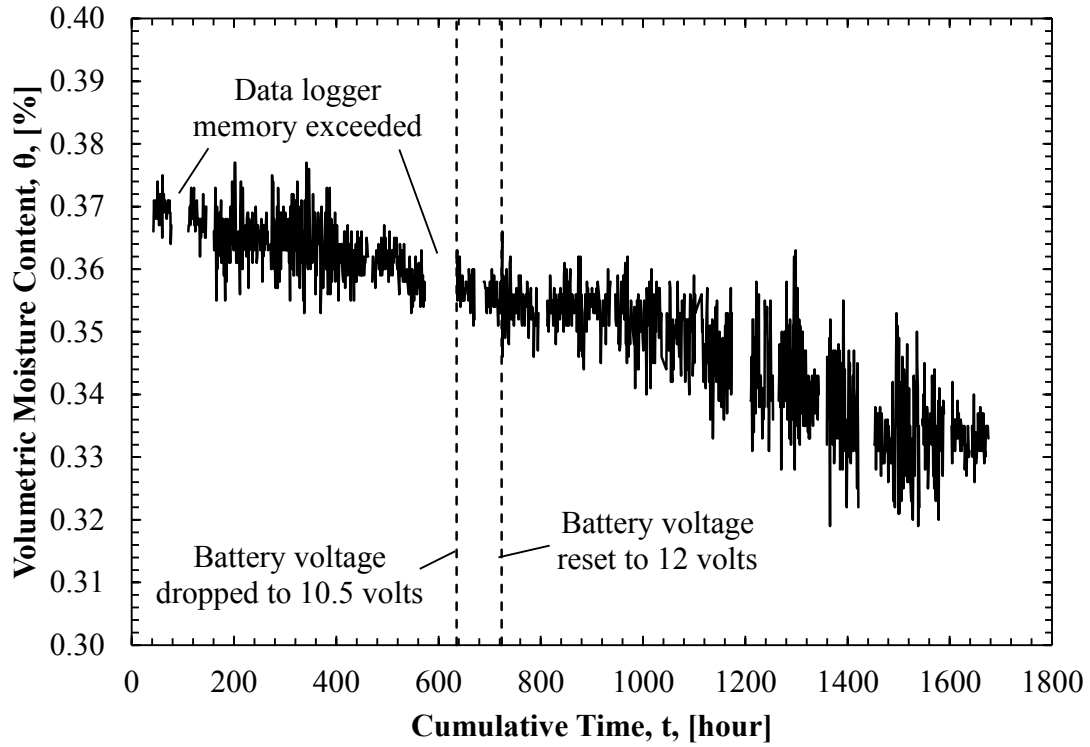


Figure B.1. TDR data collected from North TRD probe at 2-inch depth.

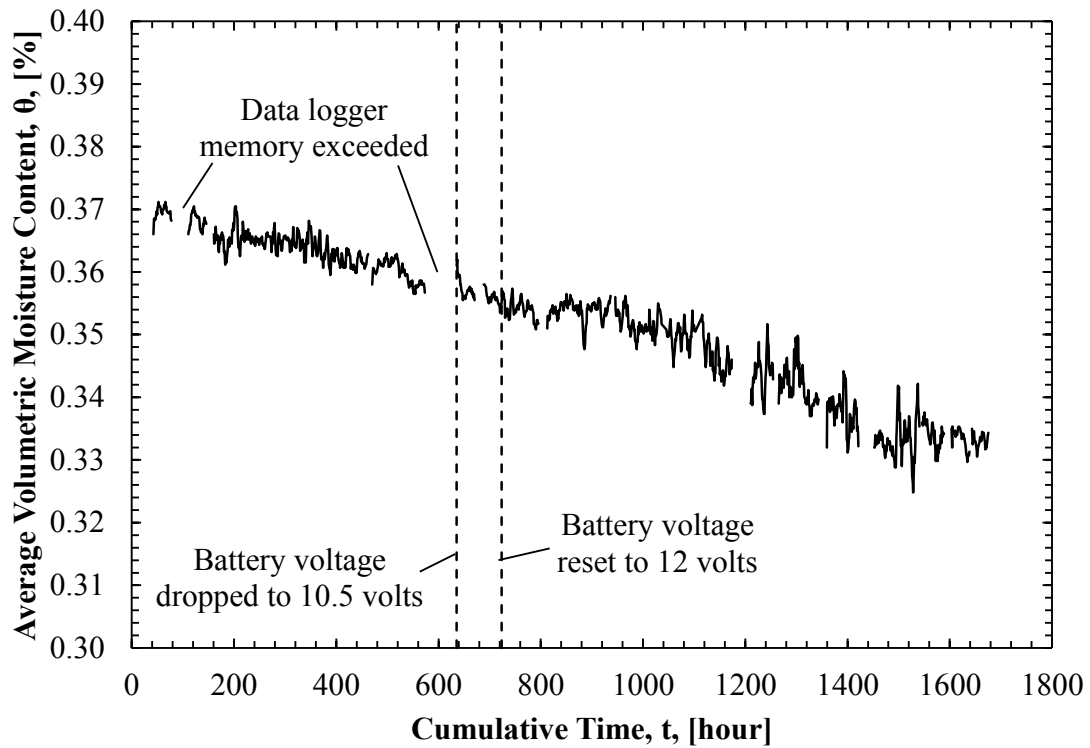


Figure B.2. Moving average for TDR data collected from North TRD probe at 2-inch depth.

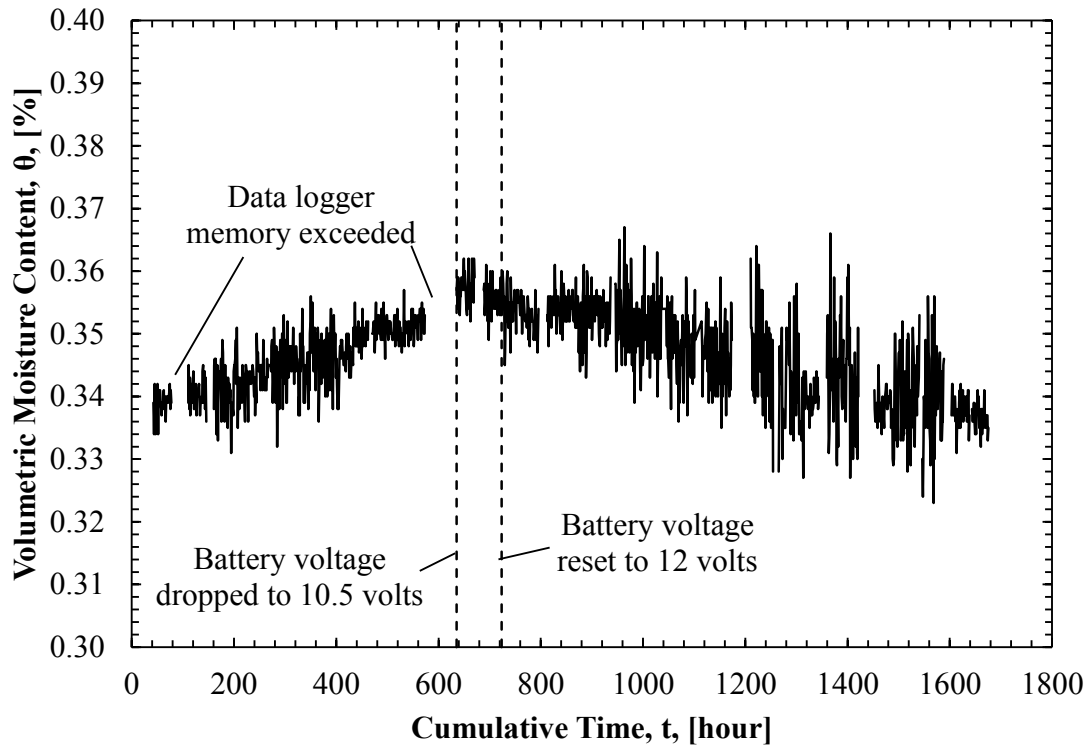


Figure B.3. TDR data collected from South TRD probe at 2-inch depth.

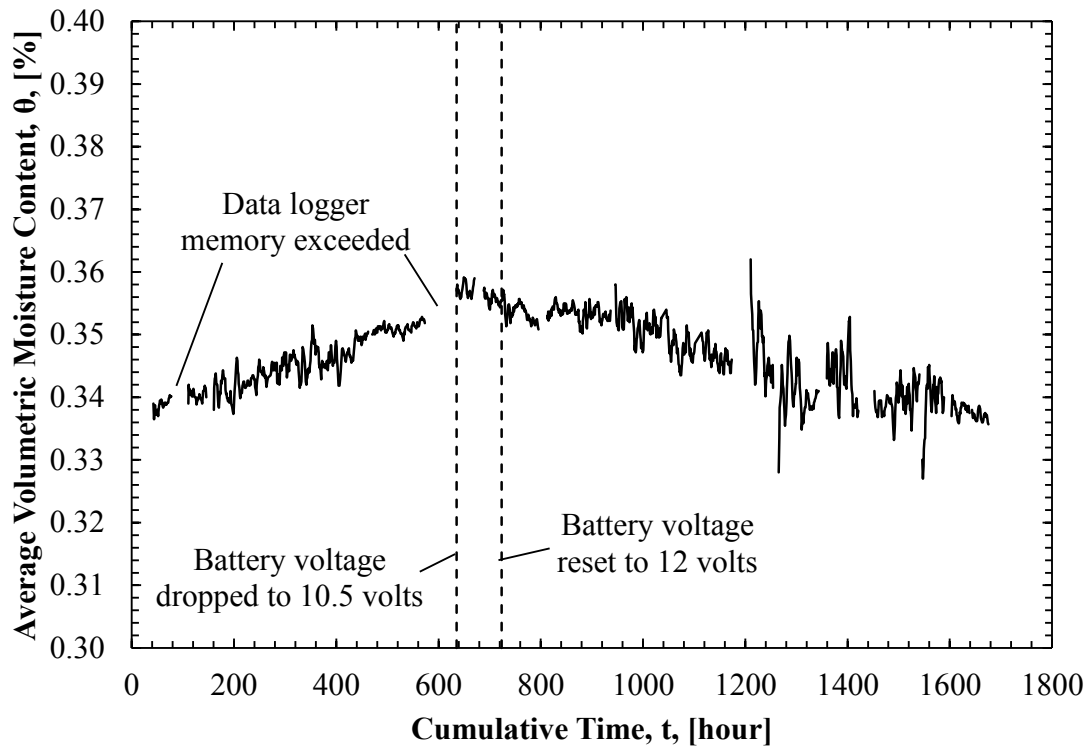


Figure B.4. Moving average for TDR data collected from South TRD probe at 2-inch depth (previously presented as Figure 4.23).

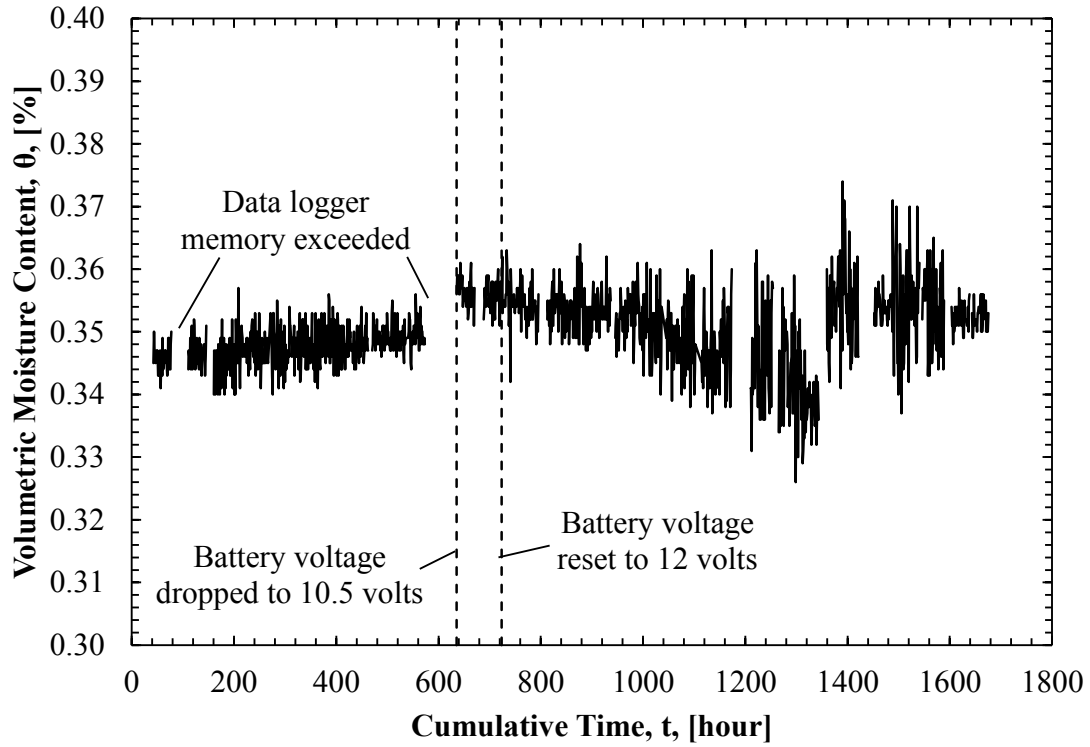


Figure B.5. TDR data collected from North TRD probe at 8-inch depth.

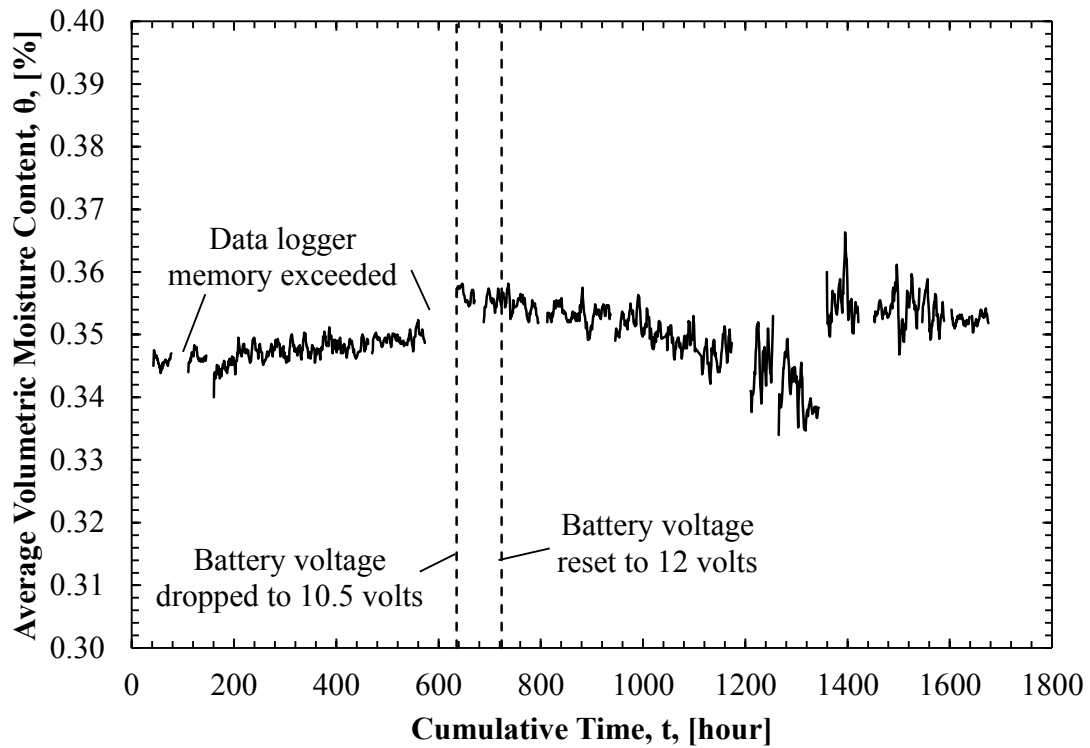


Figure B.6. Moving average for TDR data collected from North TRD probe at 8-inch depth.

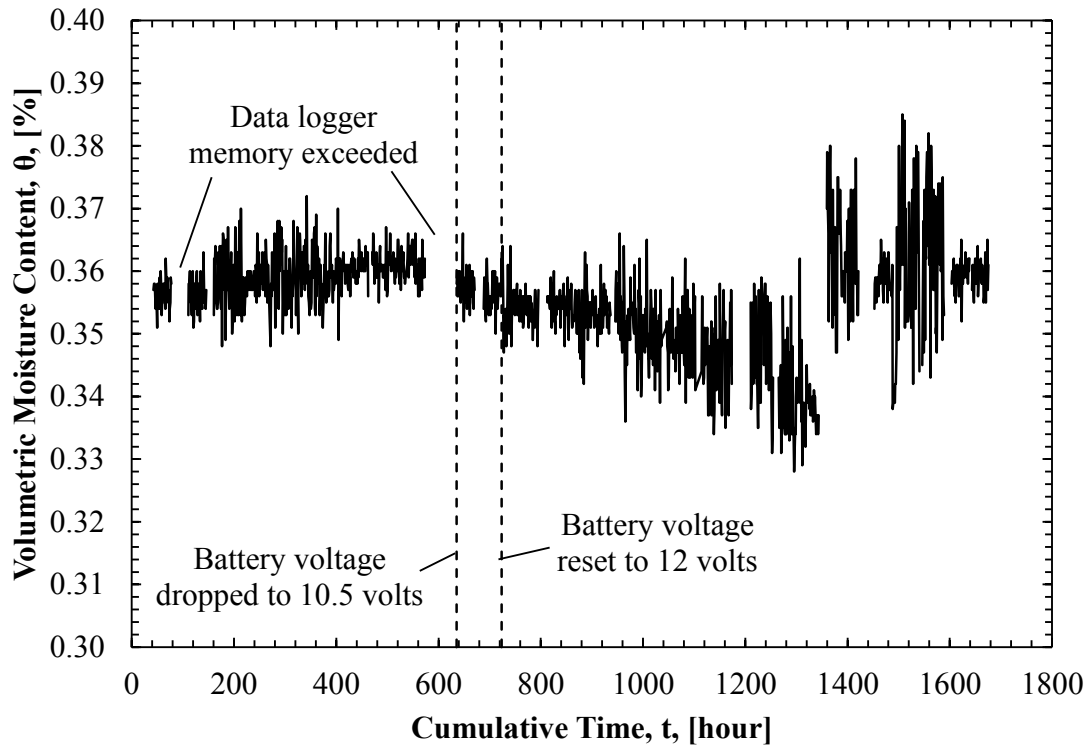


Figure B.7. TDR data collected from South TRD probe at 8-inch depth.

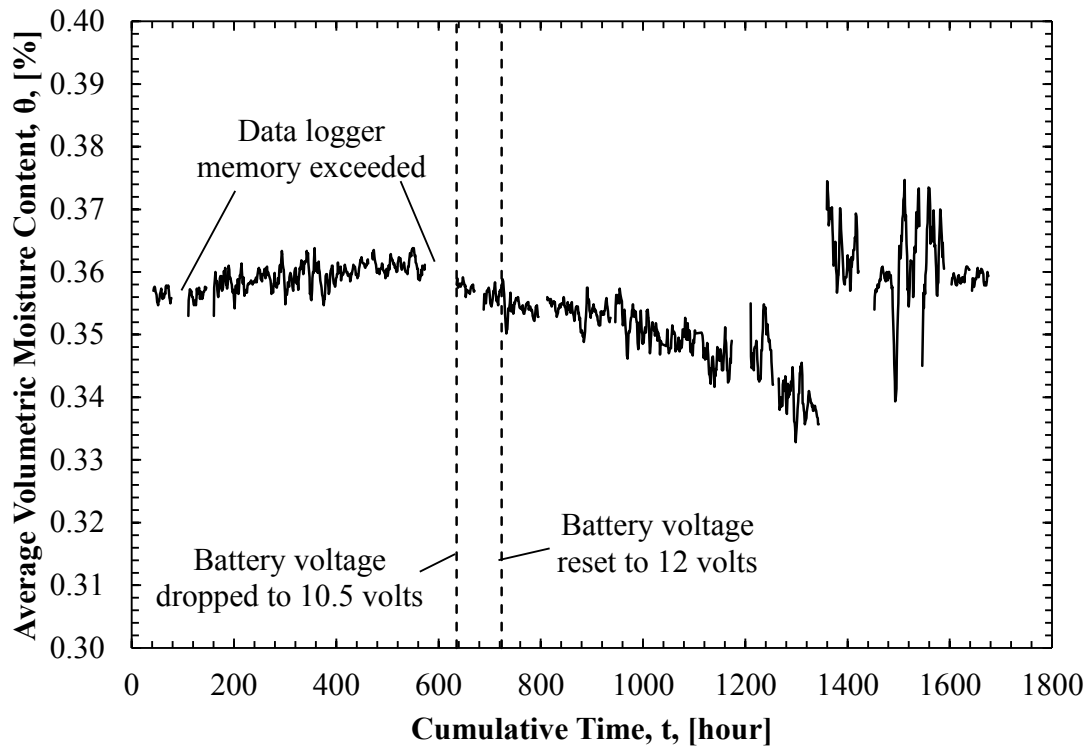


Figure B.8. Moving average for TDR data collected from South TRD probe at 8-inch depth.

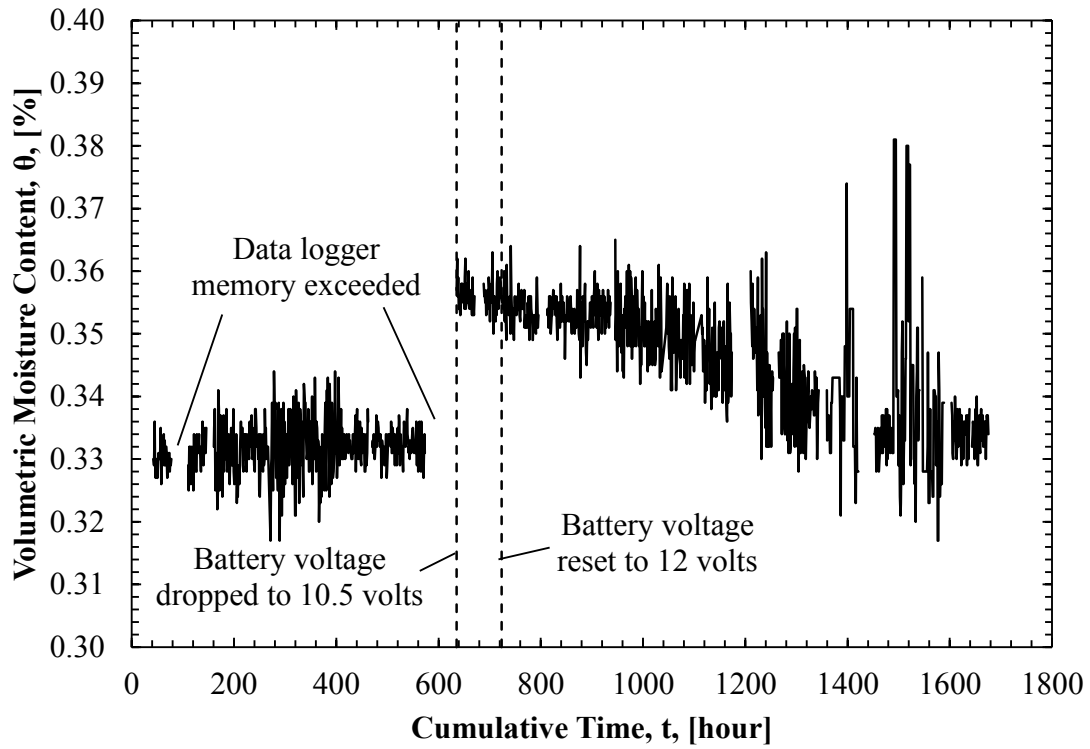


Figure B.9. TDR data collected from North TRD probe at 14-inch depth.

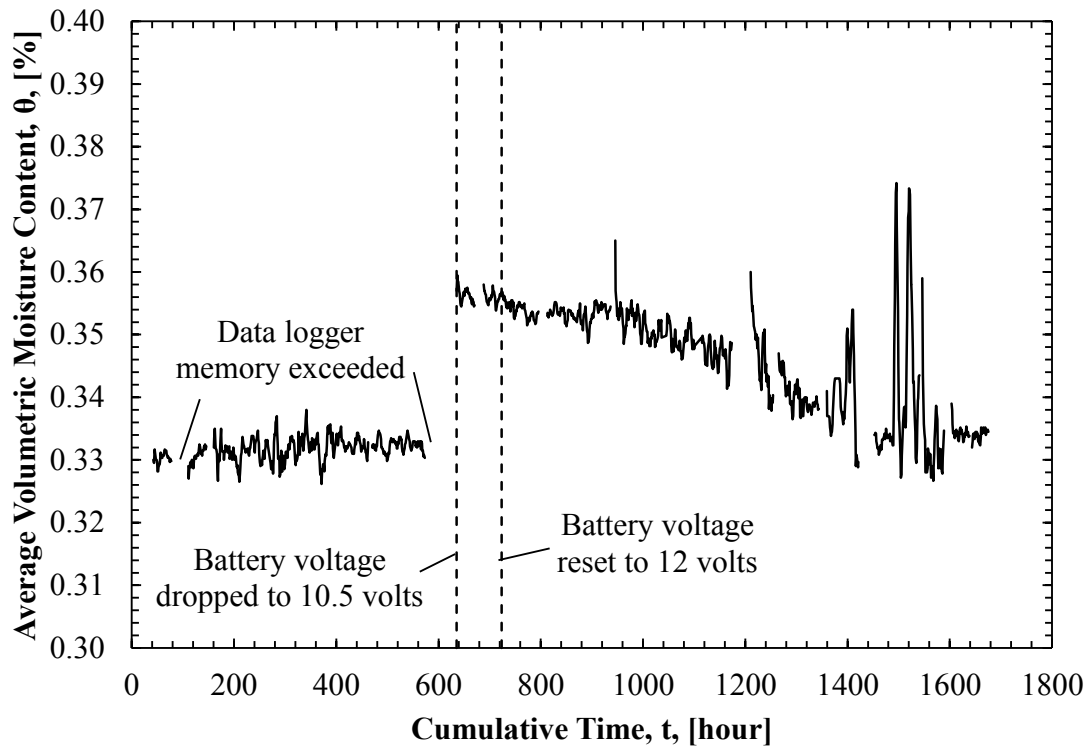


Figure B.10. Moving average for TDR data collected from North TRD probe at 14-inch depth.

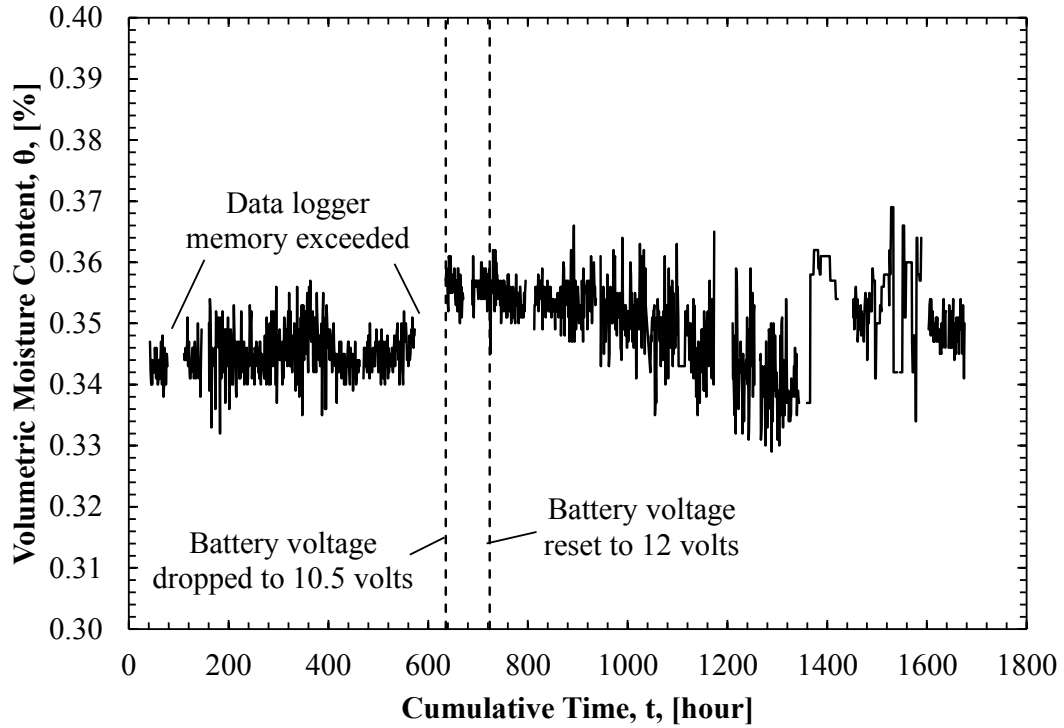


Figure B.11. TDR data collected from South TRD probe at 14-inch depth (previously presented as Figure 4.20).

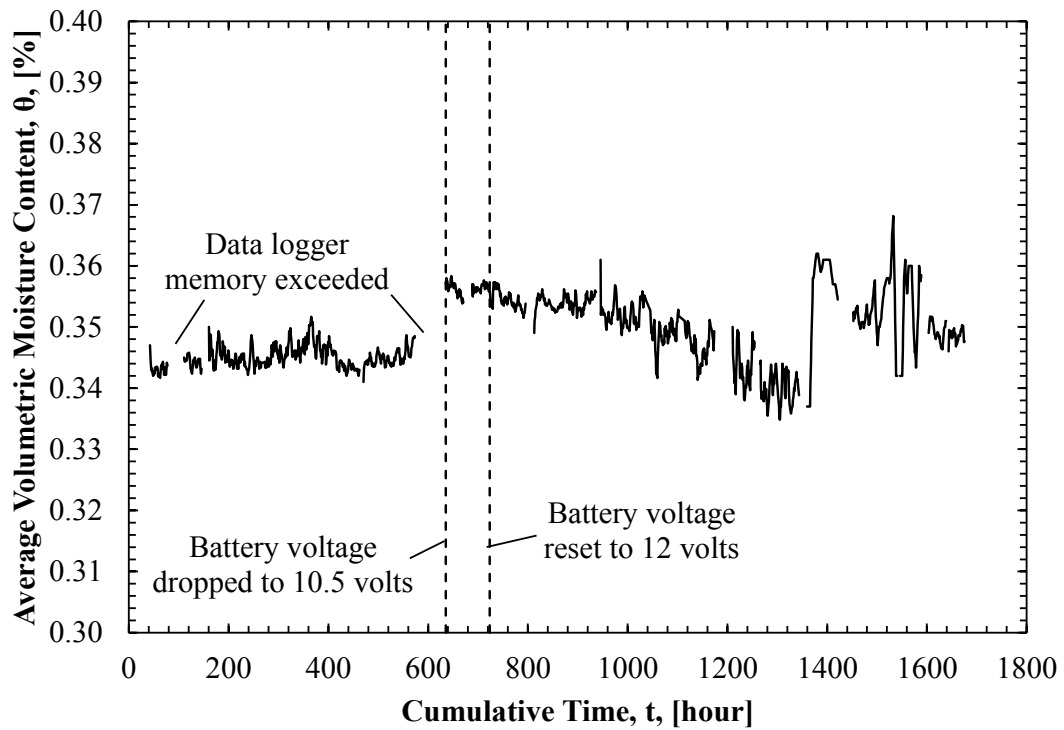


Figure B.12. Moving average for TDR data collected from South TRD probe at 14-inch depth (previously presented as Figure 4.21).

Appendix C. Laboratory Flexible Wall Hydraulic Conductivity for Test Pads 1 and 2

Table C.1. Summary of initial data for SE-ST-TP1.

Lift	Water Content w [%]	Dry Unit Weight γ_d [pcf]	Void Ratio e	Saturation S [%]	Porosity n [%]
1	16.6	104	0.601	74	38
1-2	16.0	111	0.500	86	33
2	16.0	105	0.582	73	37
2-3	16.0	107	0.563	76	36
3	15.2	104	0.604	67	38
3-4	16.4	105	0.582	75	37
4	18.9	104	0.605	83	38

Table C.2. Summary of initial data for W-HC-TP1.

Lift	Water Content w [%]	Dry Unit Weight γ_d [pcf]	Void Ratio e	Saturation S [%]	Porosity n [%]
1	19.1	106	0.577	89	37
2	19.5	102	0.639	81	39
3	19.4	100	0.674	77	40
4	19.4	102	0.627	83	39

Table C.3. Summary of initial data for E-HC-TP1.

Lift Interface	Water Content w [%]	Dry Unit Weight γ_d [pcf]	Void Ratio e	Saturation S [%]	Porosity n [%]
1-2	19.7	99	0.683	77	41
2-3	19.5	101	0.651	80	39
3-4	18.9	102	0.628	80	39

Table C.4. Summary of final data for SE-ST-TP1.

Lift	Hydraulic Conductivity k [cm/sec]	Water Content W _{top} [%]	Water Content W _{mid} [%]	Water Content W _{bot} [%]	Dry Unit Weight γ _d [pcf]	Void Ratio e	Saturation S [%]	Porosity n [%]
1	1.20E-07	20.8	20.5	20.8	104	0.601	92	38
1-2	5.64E-08	20.3	20.7	21.3	105	0.582	95	37
2	3.28E-08	20.8	20.9	21.1	104	0.596	94	37
2-3	2.29E-08	21.6	20.8	19.9	106	0.565	98	36
3	5.69E-08	20.9	21.0	20.1	103	0.613	90	38
3-4	4.16E-08	20.4	20.4	22.2	105	0.587	95	37
4	2.27E-08	20.7	21.5	21.4	105	0.585	97	37

Table C.5. Summary of final data for W-HC-TP1.

Lift	Hydraulic Conductivity k ₂₀ [cm/sec]	Water Content W _{top} [%]	Water Content W _{mid} [%]	Water Content W _{bot} [%]	Dry Unit Weight γ _d [pcf]	Void Ratio e	Saturation S [%]	Porosity n [%]
1	1.07E-07	20.0	20.2	20.9	103	0.620	88	38
2	1.19E-08	20.2	20.4	20.2	100	0.664	81	40
3	1.67E-07	19.8	19.9	20.2	102	0.632	84	39
4	1.34E-08	20.1	20.1	20.2	103	0.624	86	38

Table C.6. Summary of final data for E-HC-TP1.

Lift Interface	Hydraulic Conductivity k ₂₀ [cm/sec]	Water Content W _{top} [%]	Water Content W _{mid} [%]	Water Content W _{bot} [%]	Dry Unit Weight γ _d [pcf]	Void Ratio e	Saturation S [%]	Porosity n [%]
1-2	6.78E-08	20.5	20.0	20.4	99	0.676	80	40
2-3	1.04E-07	21.1	21.1	0.0	103	0.620	91	38
3-4	4.15E-08	20.6	20.9	20.8	104	0.603	92	38

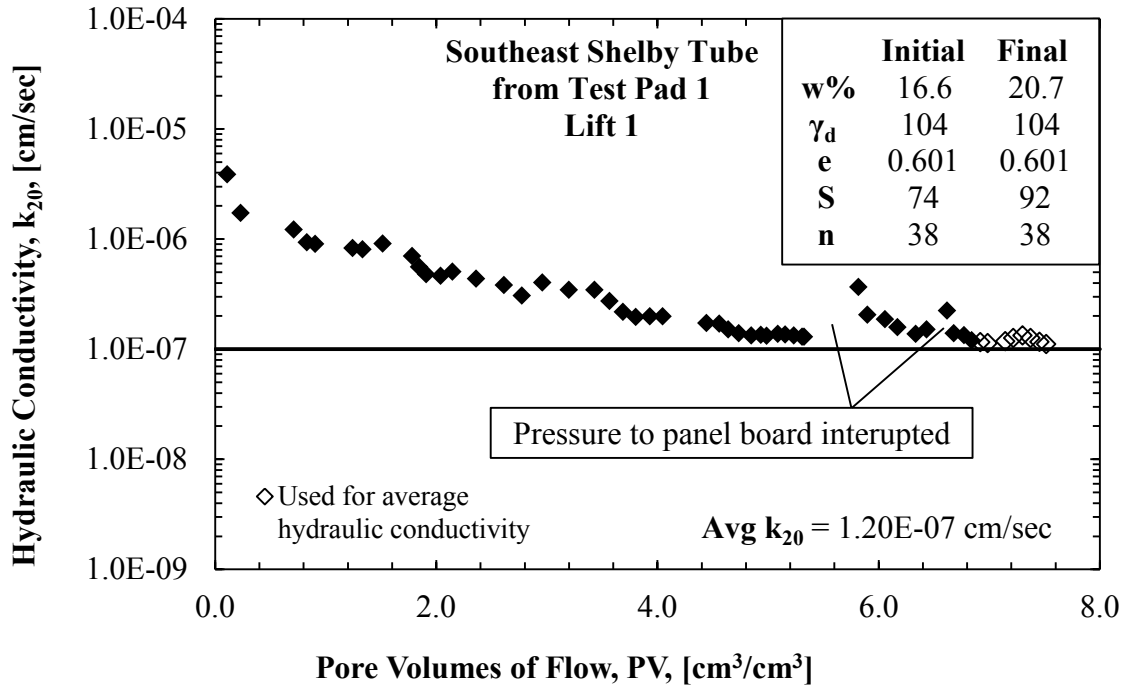


Figure C.1. Vertical hydraulic conductivity data for SE-ST-TP1 Lift 1.

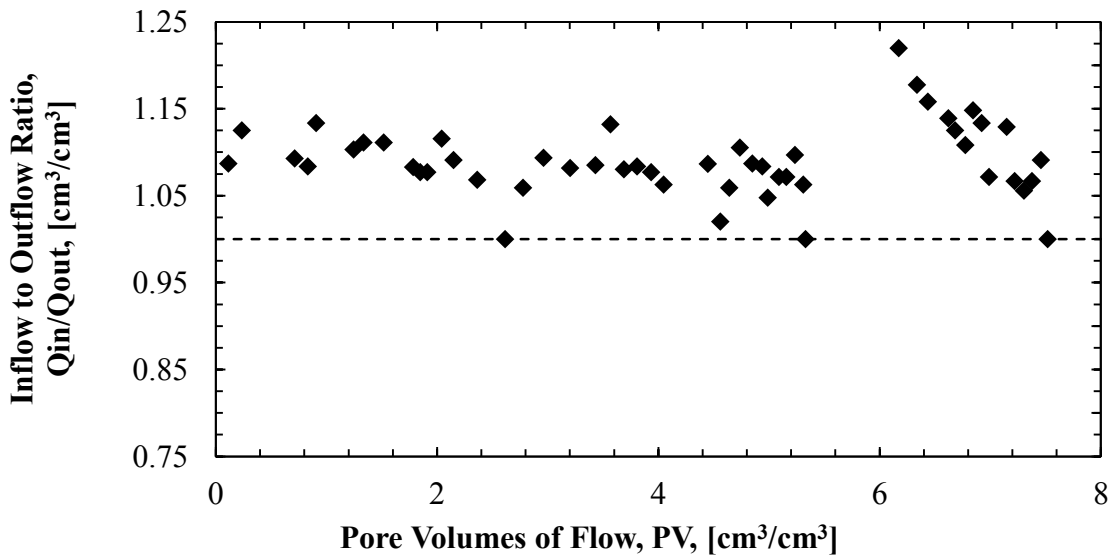


Figure C.2. Inflow to outflow data for SE-ST-TP1 Lift 1.

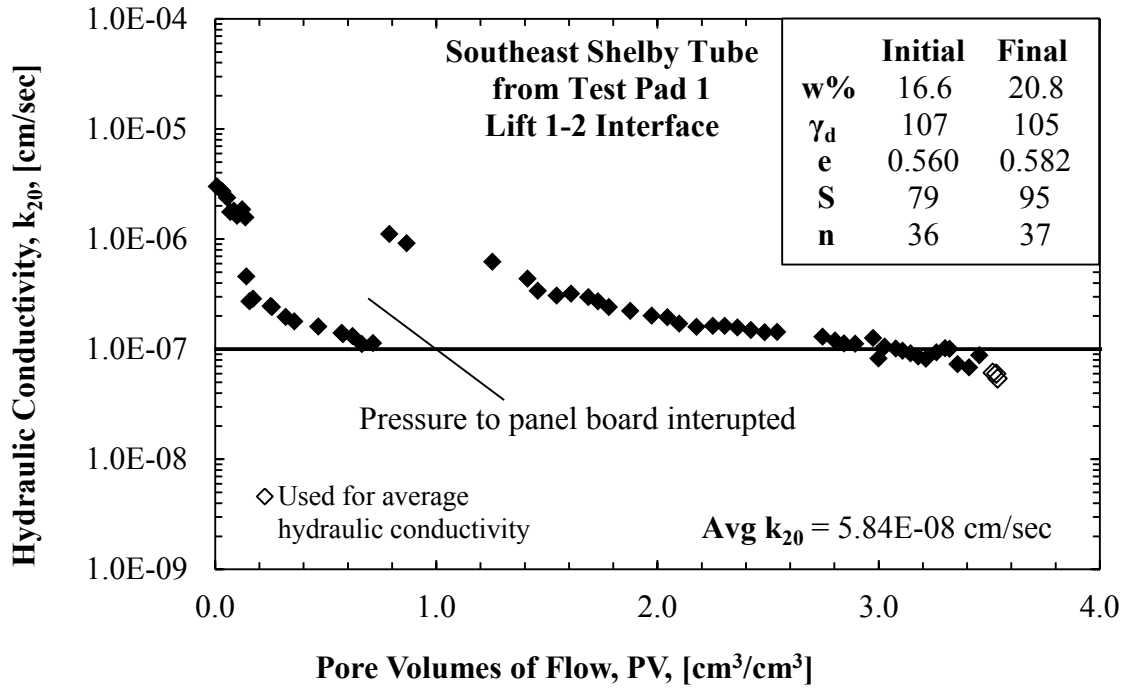


Figure C.3. Vertical hydraulic conductivity data for SE-ST-TP1 Lift 1-2 interface (previously presented as Figure 4.24).

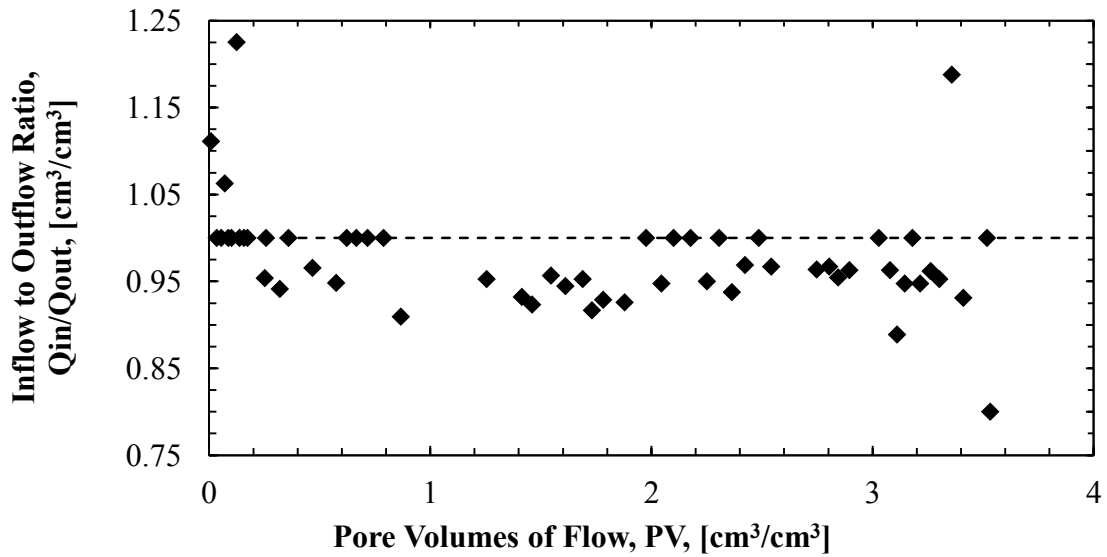


Figure C.4. Inflow to outflow data for SE-ST-TP1 Lift 1-2 interface.

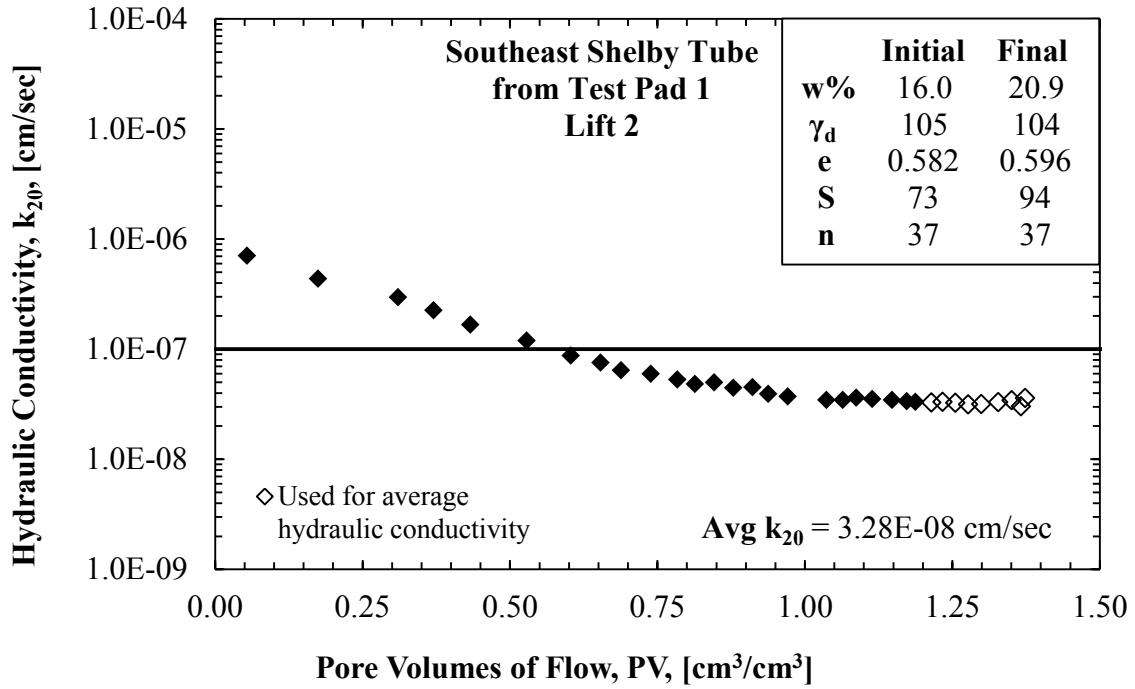


Figure C.5. Vertical hydraulic conductivity data for SE-ST-TP1 Lift 2.

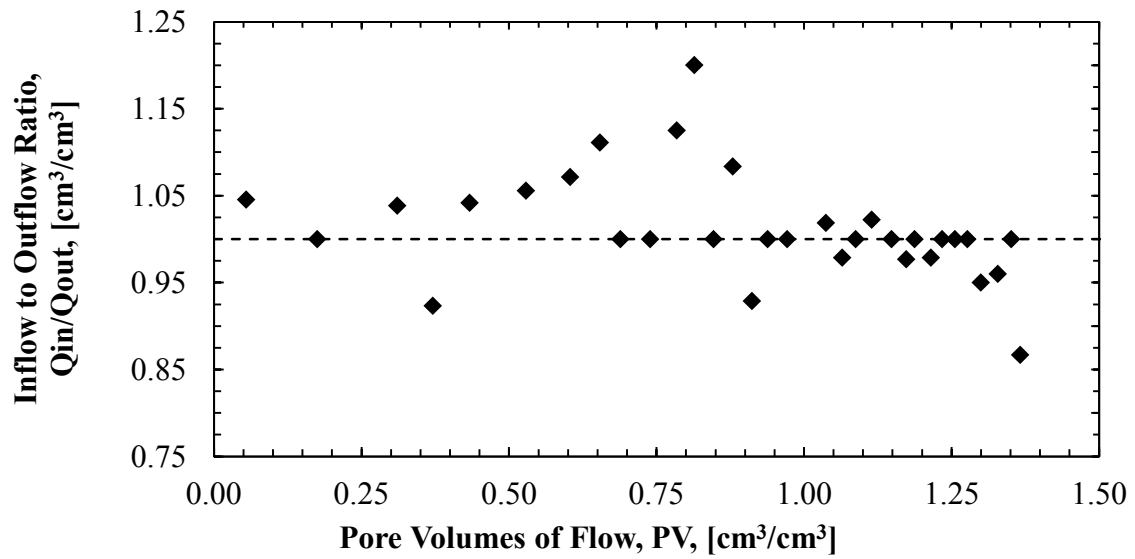


Figure C.6. Inflow to outflow data for SE-ST-TP1 Lift 2.

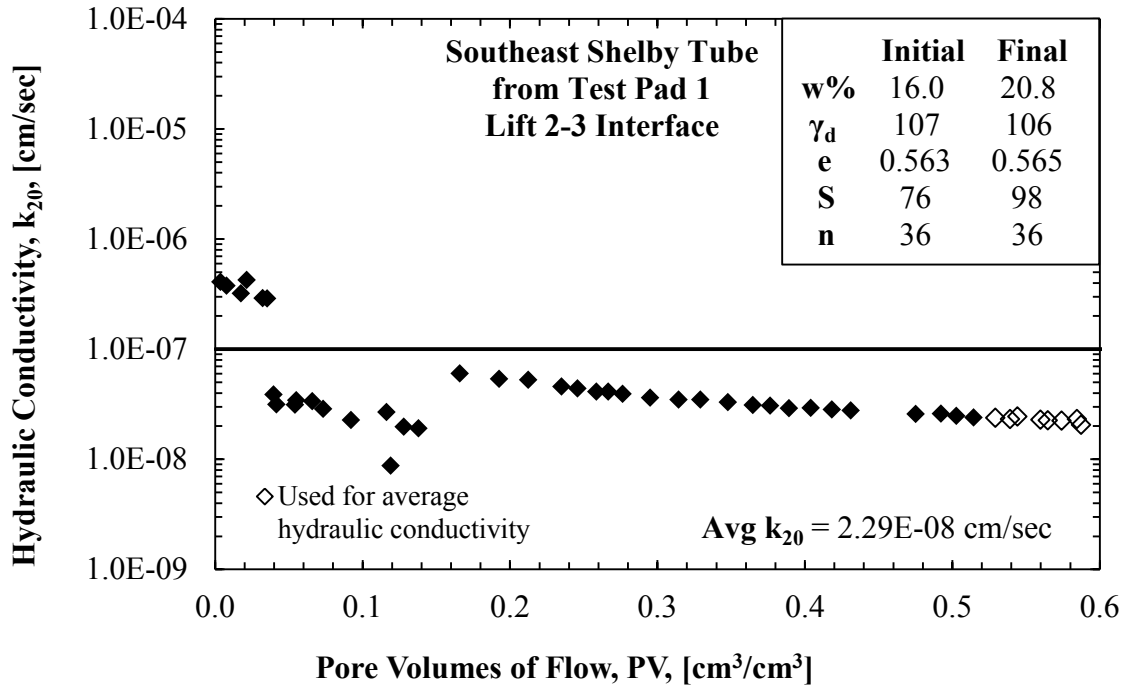


Figure C.7. Vertical hydraulic conductivity data for SE-ST-TP1 Lift 2-3 interface.

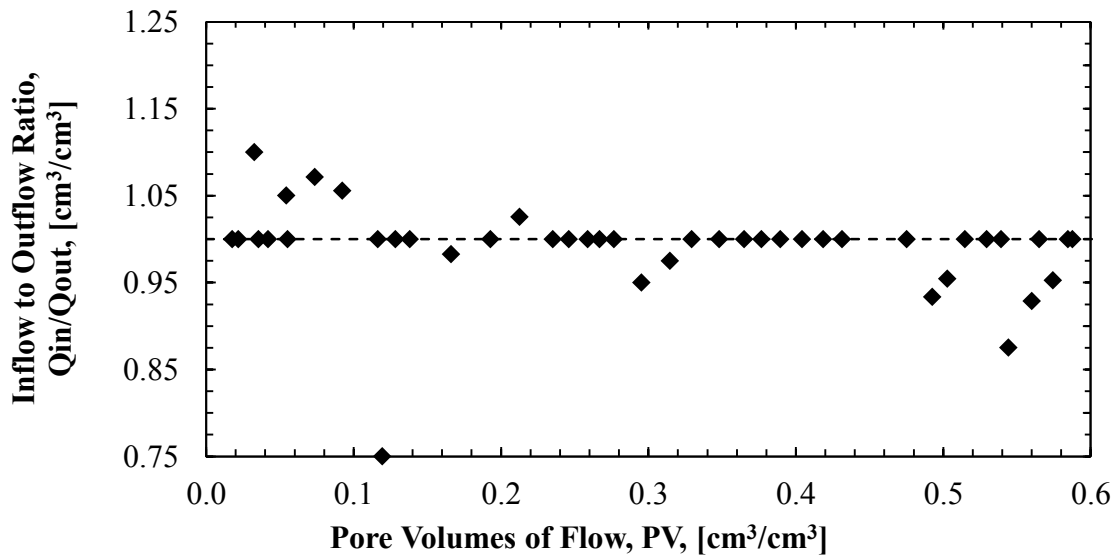


Figure C.8. Inflow to outflow data for SE-ST-TP1 Lift 2-3 interface.

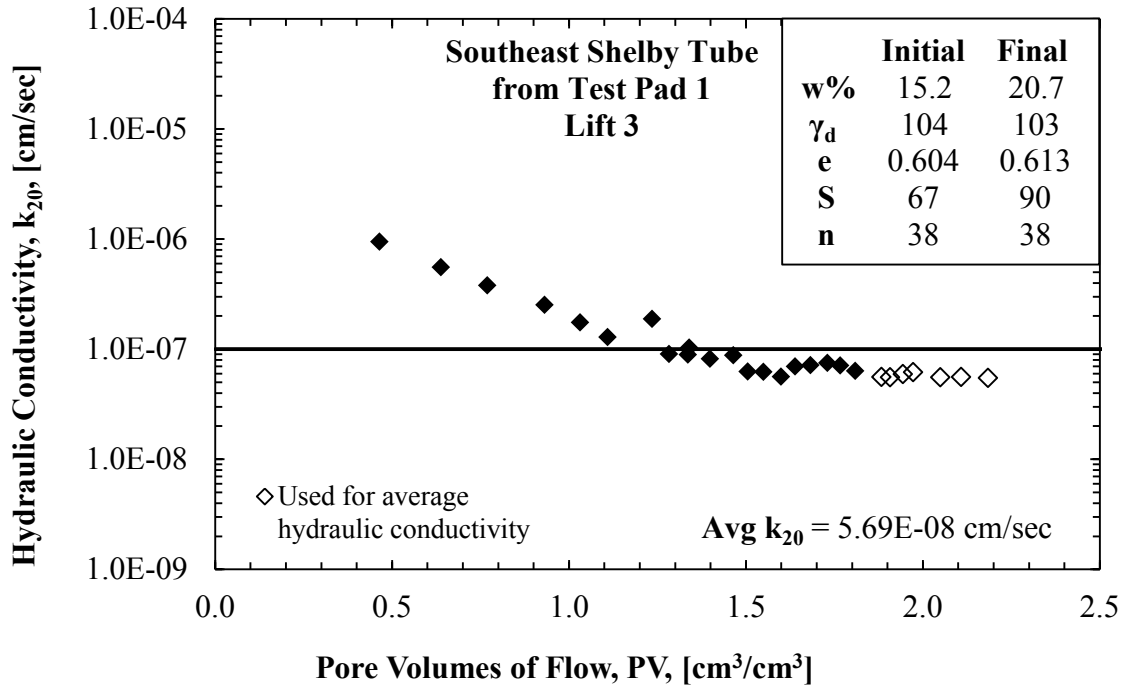


Figure C.9. Vertical hydraulic conductivity data for SE-ST-TP1 Lift 3.

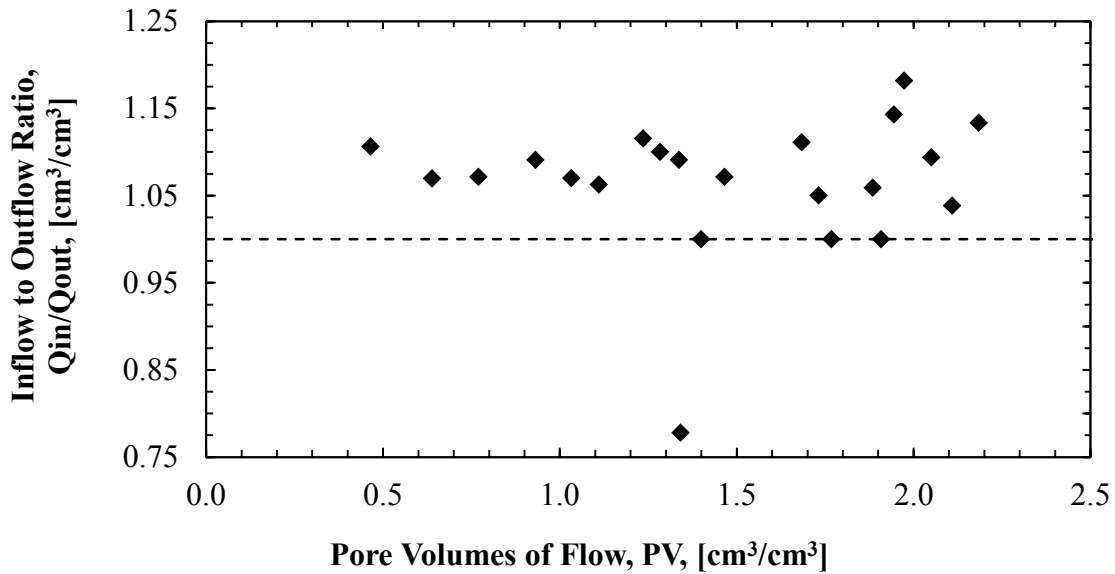


Figure C.10. Inflow to outflow data for SE-ST-TP1 Lift 3.

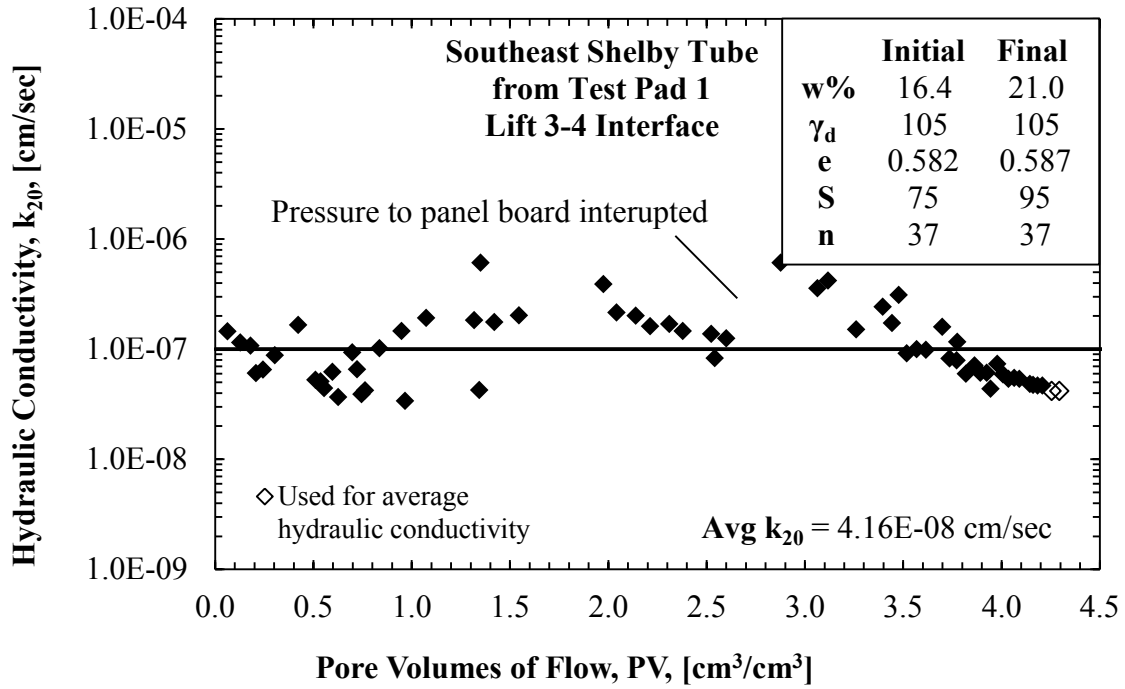


Figure C.11. Vertical hydraulic conductivity data for SE-ST-TP1 Lift 3-4 interface.

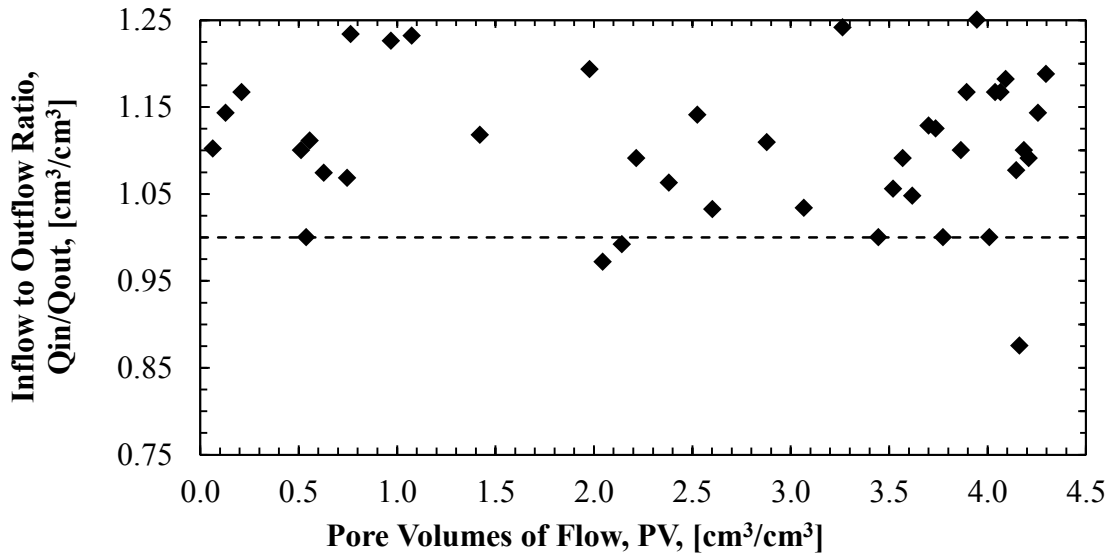


Figure C.12. Inflow to outflow data for SE-ST-TP1 Lift 3-4 interface.

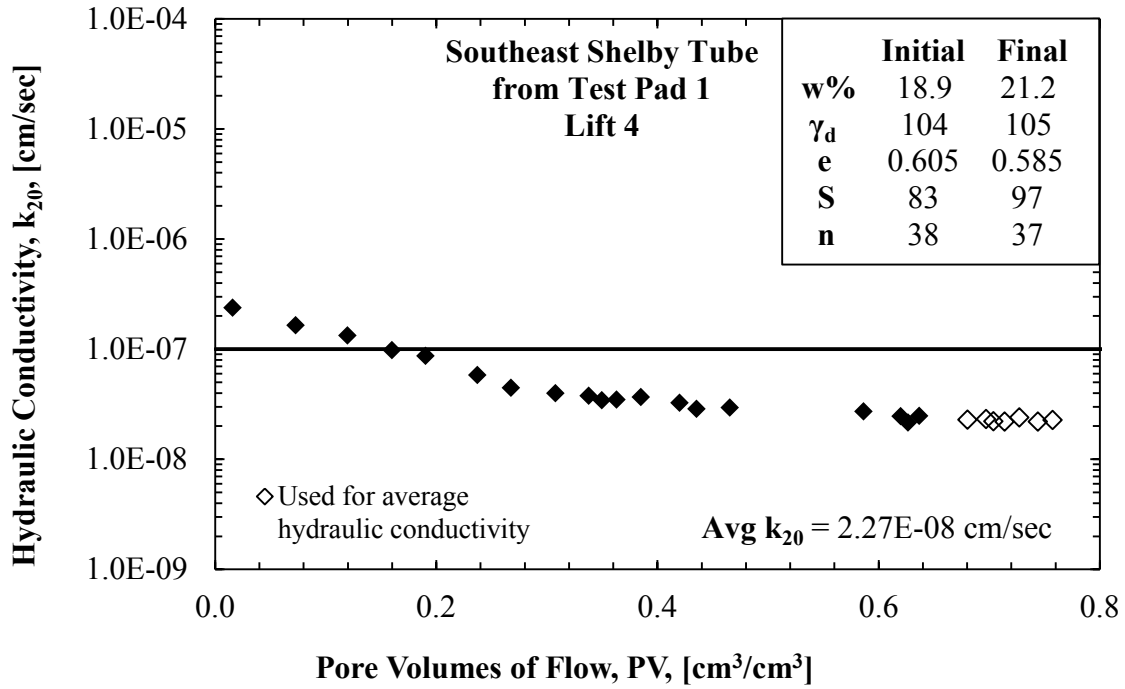


Figure C.13. Vertical hydraulic conductivity data for SE-ST-TP1 Lift 4.

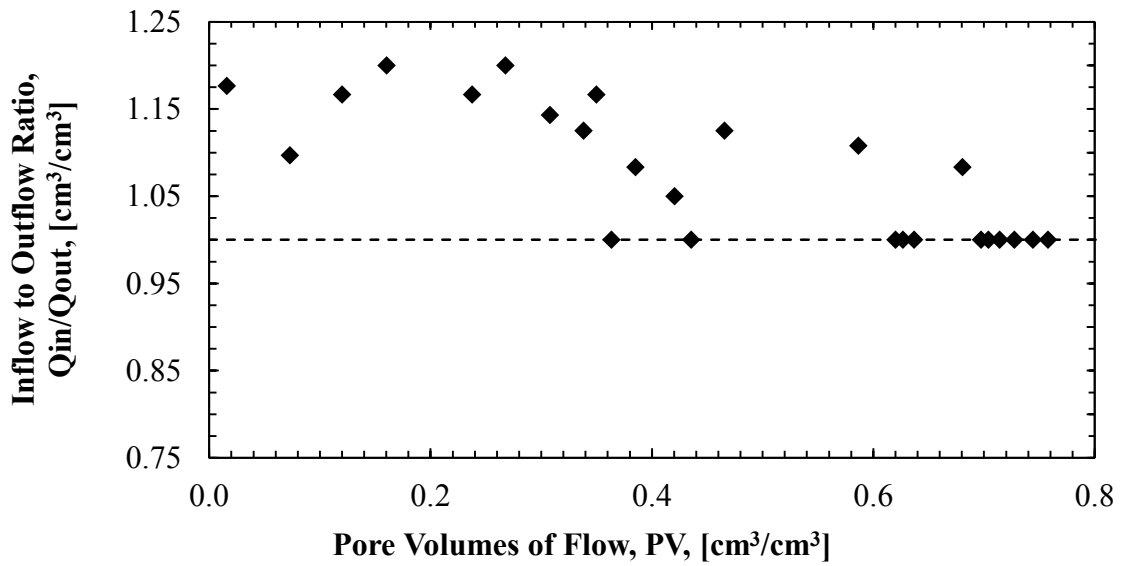


Figure C.14. Inflow to outflow data for SE-ST-TP1 Lift 4.

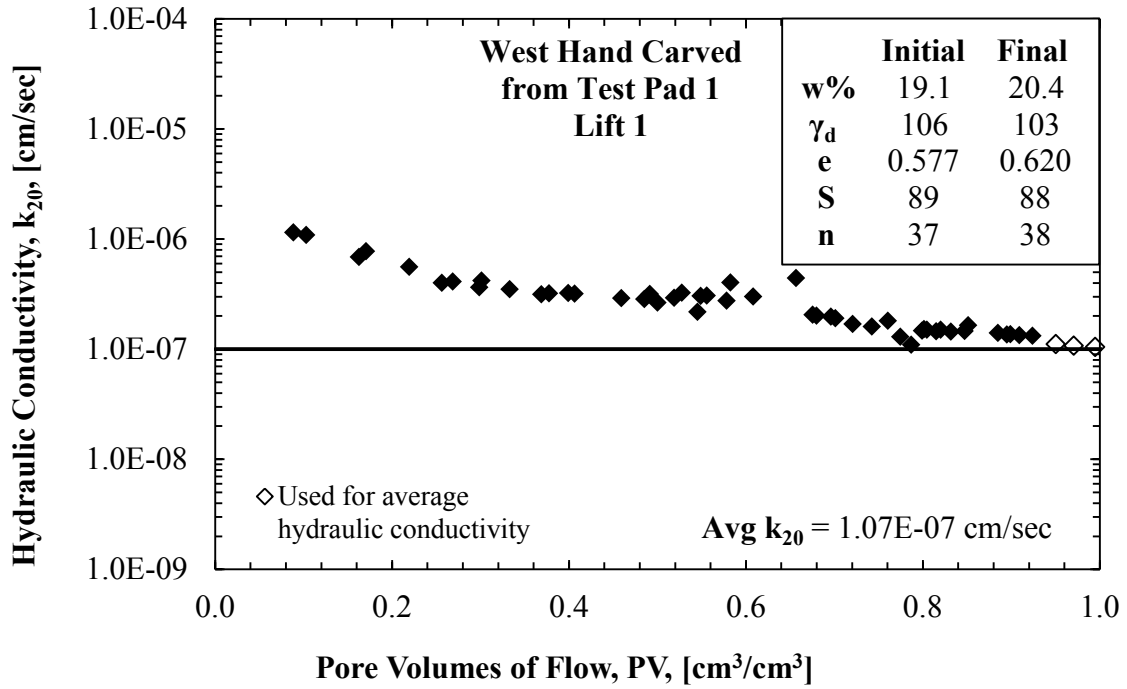


Figure C.15. Vertical hydraulic conductivity data for W-HC-TP1 Lift 1.

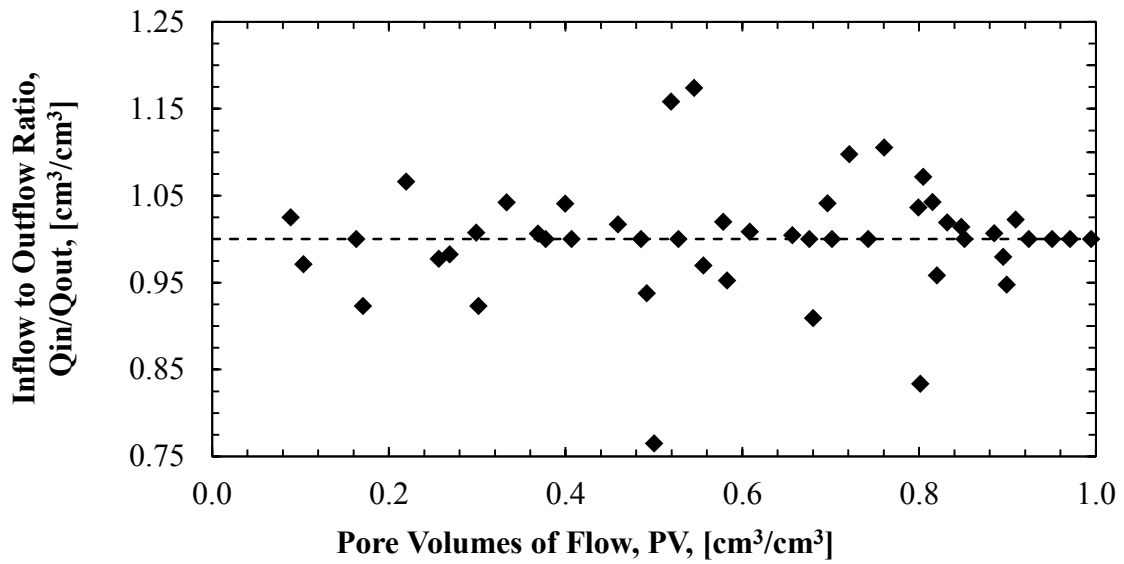


Figure C.16. Inflow to outflow data for W-HC-TP1 Lift 1.

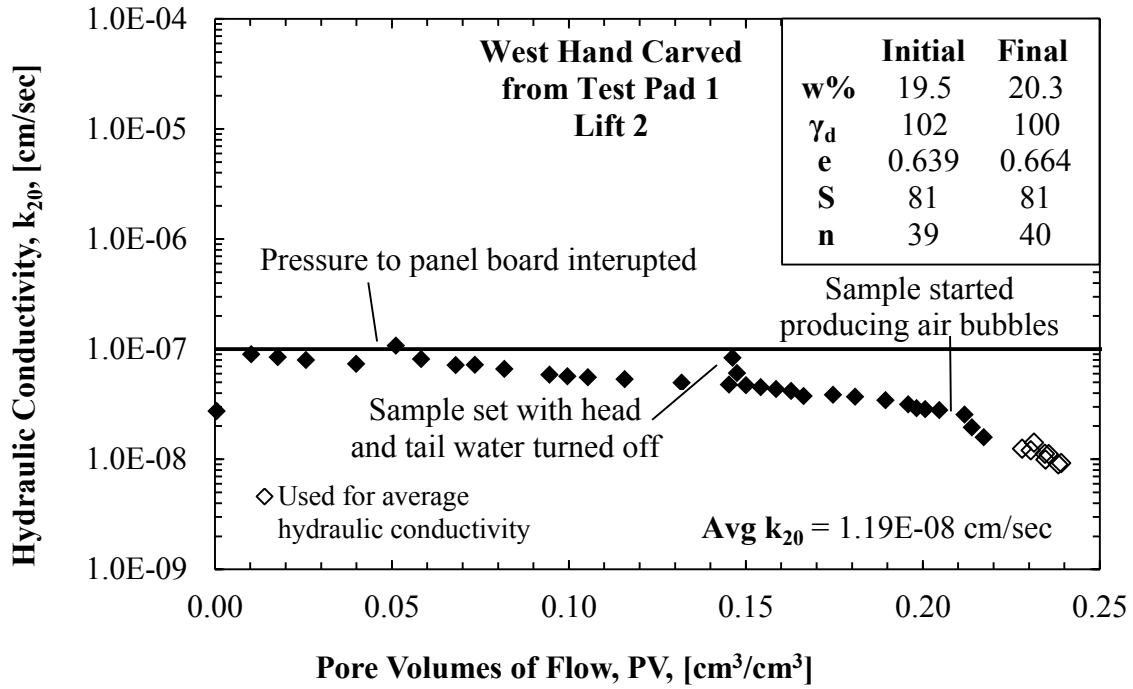


Figure C.17. Vertical hydraulic conductivity data for W-HC-TP1 Lift 2.

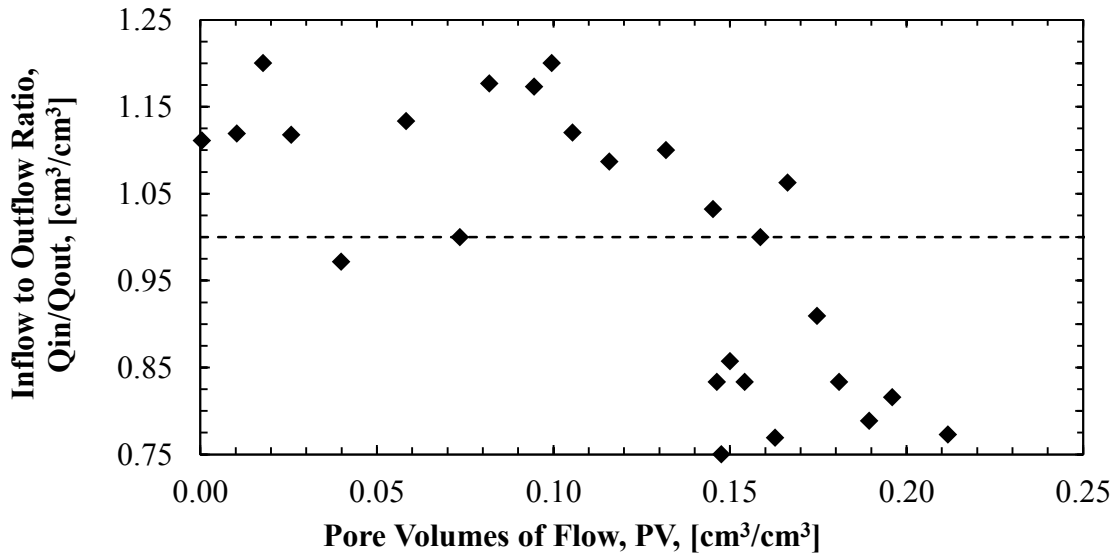


Figure C.18. Inflow to outflow data for W-HC-TP1 Lift 2.

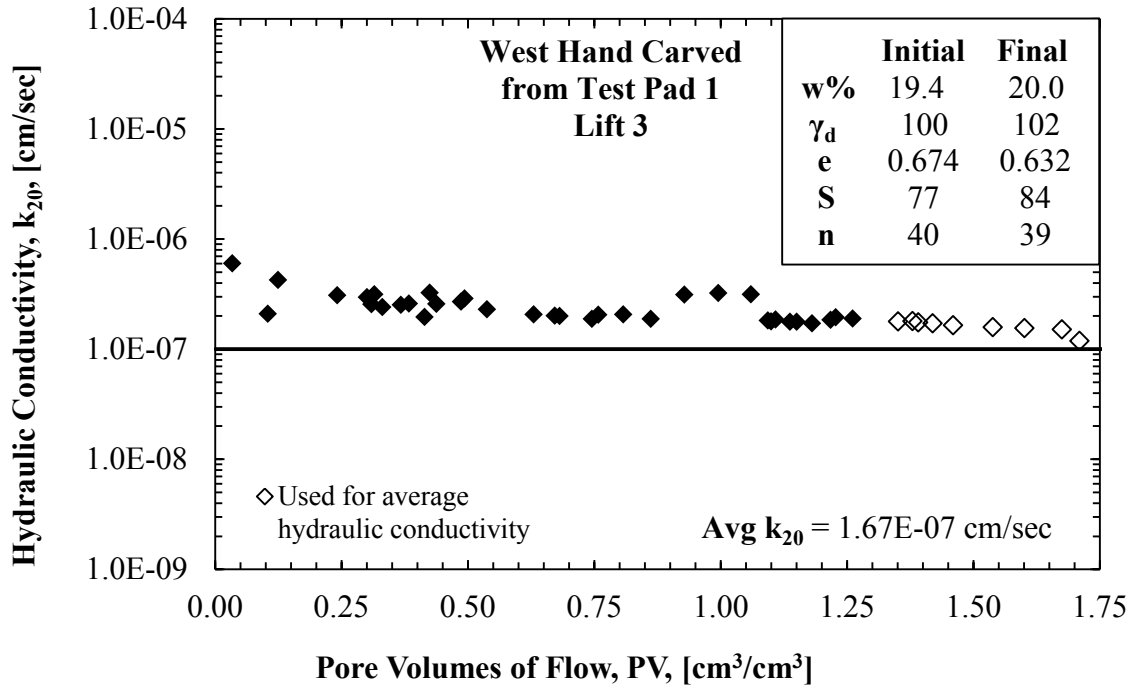


Figure C.19. Vertical hydraulic conductivity data for W-HC-TP1 Lift 3.

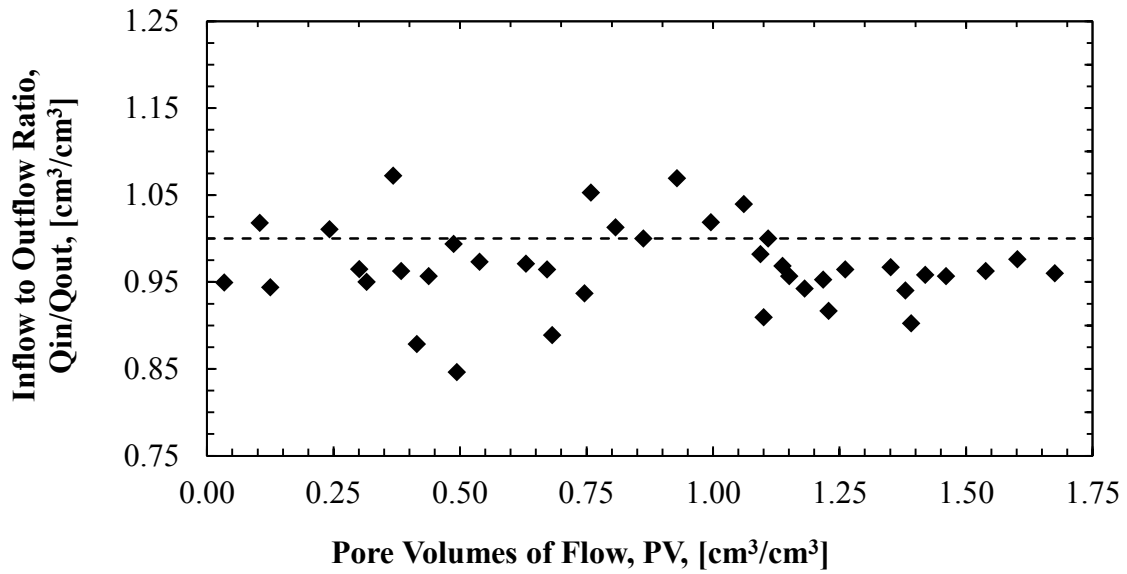


Figure C.20. Inflow to outflow data for W-HC-TP1 Lift 3.

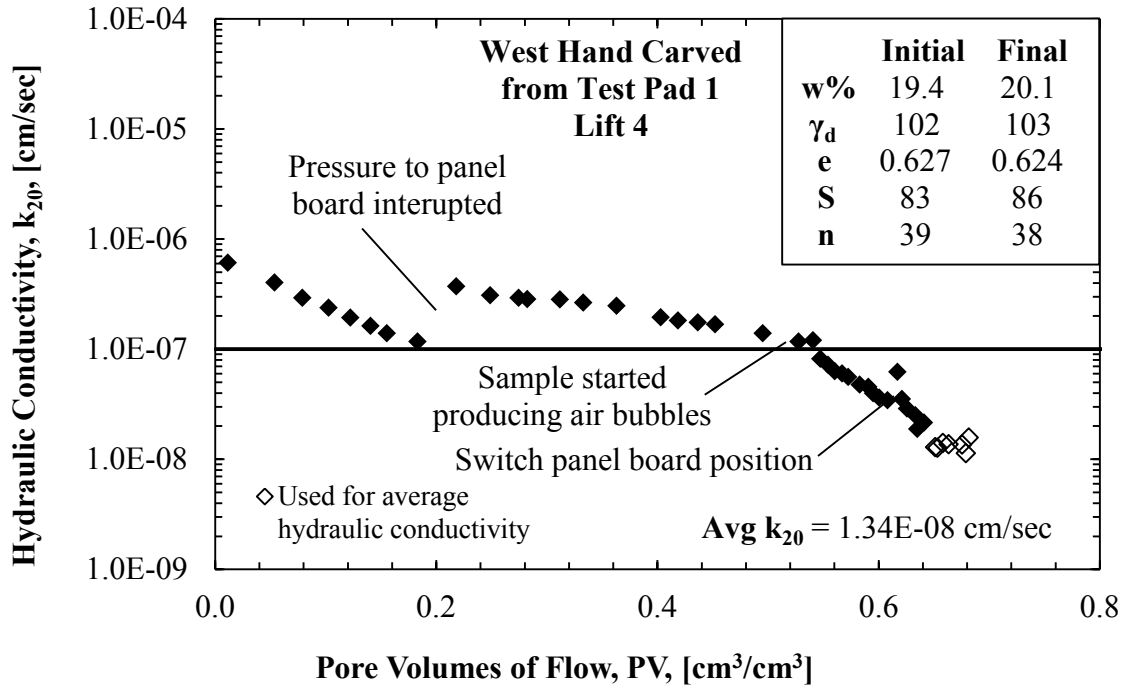


Figure C.21. Vertical hydraulic conductivity data for W-HC-TP1 Lift 4.

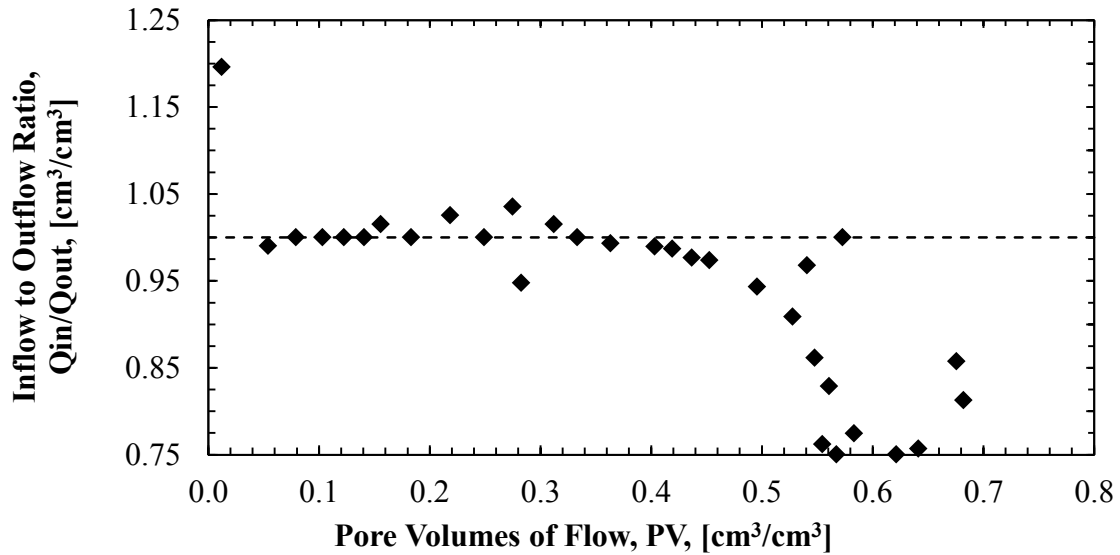


Figure C.22. Inflow to outflow data for W-HC-TP1 Lift 4.

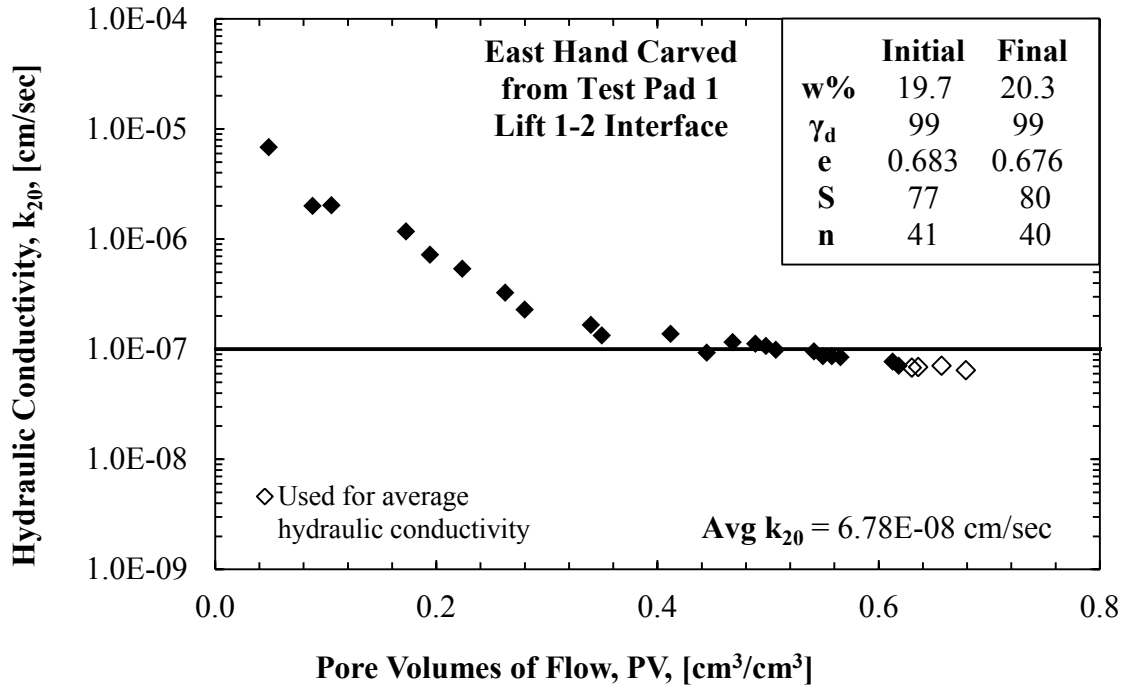


Figure C.23. Horizontal hydraulic conductivity data for E-HC-TP1 Lift 1-2 Interface.

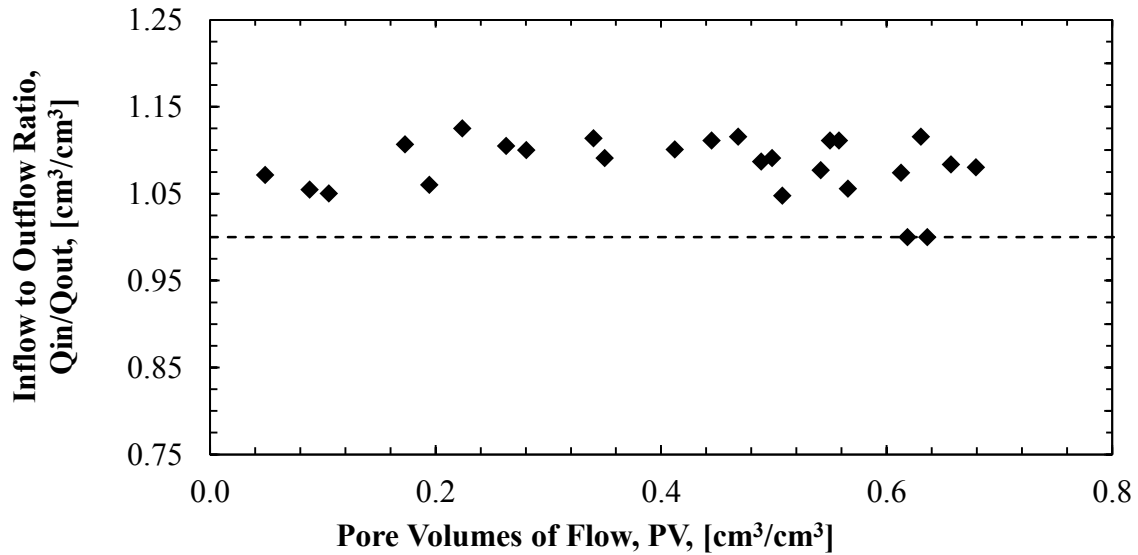


Figure C.24. Inflow to outflow data for E-HC-TP1 Lift 1-2 Interface.

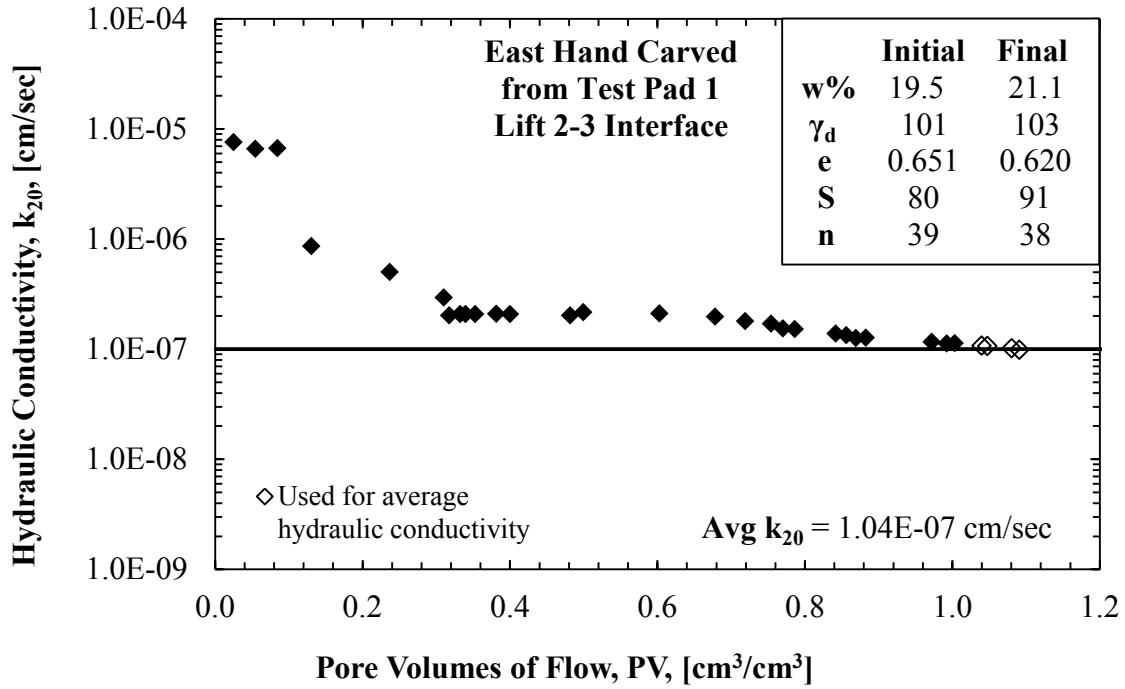


Figure C.25. Horizontal hydraulic conductivity data for E-HC-TP1 Lift 2-3 Interface.

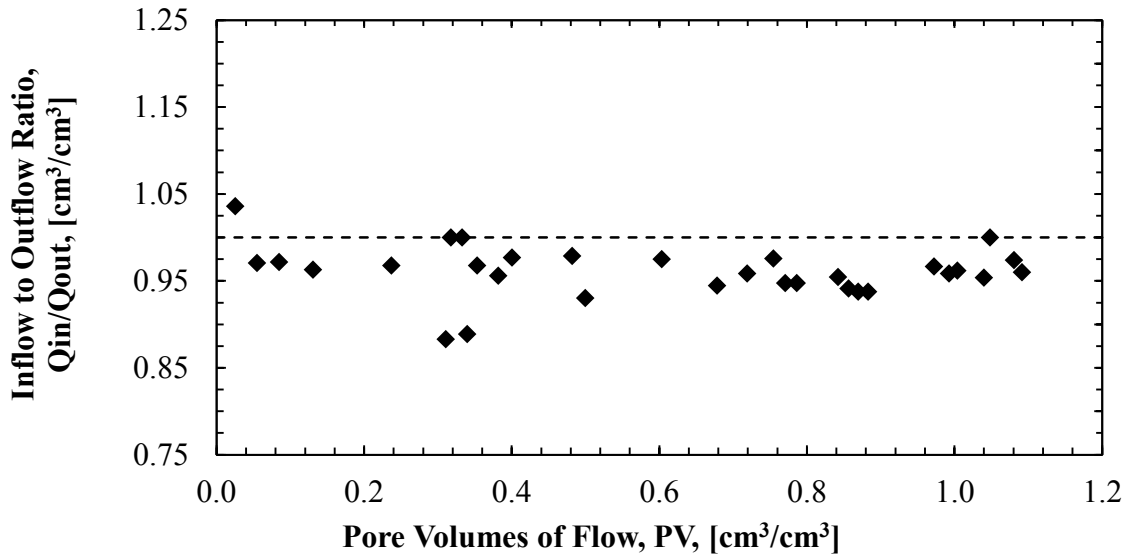


Figure C.26. Inflow to outflow data for E-HC-TP1 Lift 2-3 Interface.

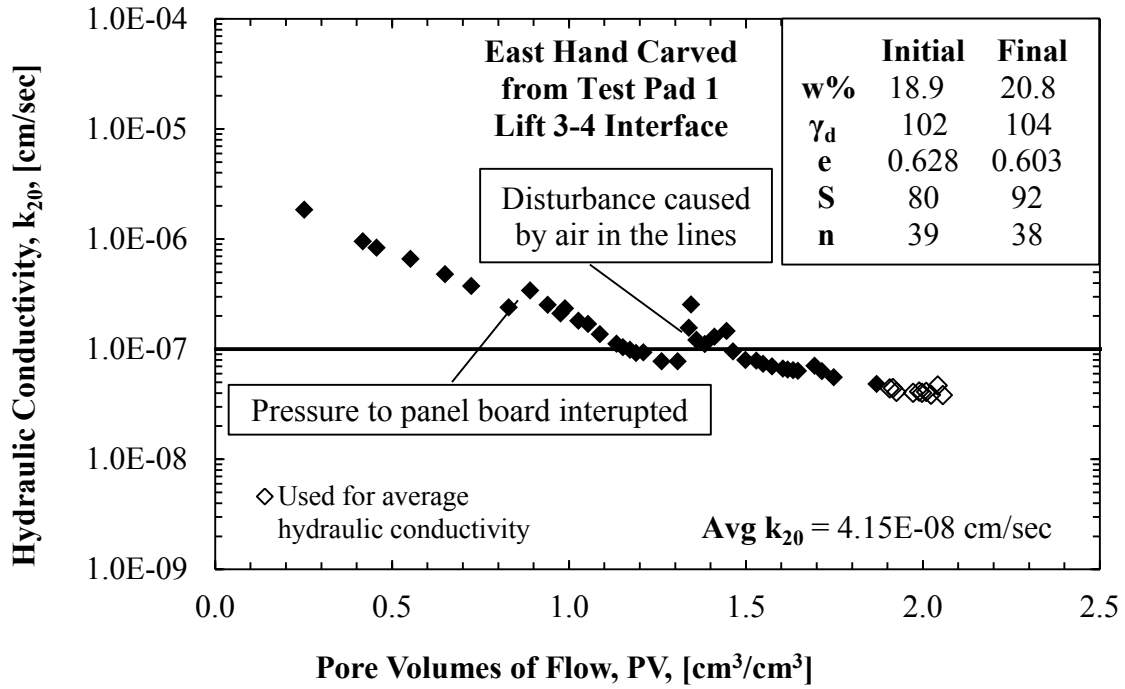


Figure C.27. Horizontal hydraulic conductivity data for E-HC-TP1 Lift 3-4 Interface.

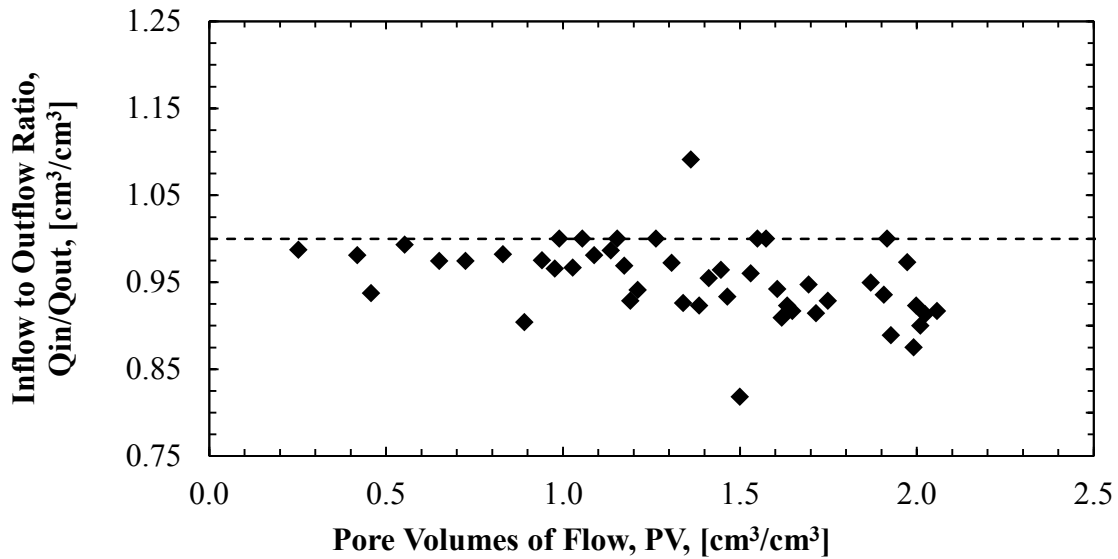


Figure C.28. Inflow to outflow data for E-HC-TP1 Lift 3-4 Interface.

Table C.7. Summary of initial data for CT-ST-TP2.

Lift	Water Content w [%]	Dry Unit Weight γ_d [pcf]	Void Ratio e	Saturation S [%]	Porosity n [%]
1	19.4	106	0.571	91	36
1-2	18.2	107	0.559	87	36
2	18.2	109	0.531	92	35
2-3	18.5	108	0.549	90	35
3	18.8	106	0.570	88	36
3-4	17.6	106	0.567	83	36
4	18.4	106	0.566	87	36

Table C.8. Summary of initial data for W-HC-TP2.

Lift	Water Content w [%]	Dry Unit Weight γ_d [pcf]	Void Ratio e	Saturation S [%]	Porosity n [%]
1	20.0	104	0.604	88	38
2	19.8	102	0.631	84	39
3	20.1	102	0.636	84	39
4	20.0	101	0.653	82	40

Table C.9. Summary of initial data for E-HC-TP2.

Lift Interface	Water Content w [%]	Dry Unit Weight γ_d [pcf]	Void Ratio e	Saturation S [%]	Porosity n [%]
1-2	20.2	103	0.620	87	38
2-3	19.8	102	0.632	83	39
3-4	20.0	101	0.655	81	40

Table C.10. Summary of final data for CT-ST-TP2.

Lift	Hydraulic Conductivity k_{20} [cm/sec]	Water Content w_{top} [%]	Water Content w_{mid} [%]	Water Content w_{bot} [%]	Dry Unit Weight γ_d [pcf]	Void Ratio e	Saturation S [%]	Porosity n [%]
1	2.04E-08	20.9	20.9	21.0	107	0.565	99	36
1-2	1.53E-08	20.7	21.0	20.4	107	0.559	99	36
2	1.29E-08	20.0	20.2	20.7	107	0.557	97	36
2-3	1.28E-08	20.6	20.5	20.8	106	0.567	97	36
3	1.19E-08	20.9	20.1	20.0	107	0.557	98	36
3-4	1.56E-08	21.1	21.0	20.7	105	0.582	96	37
4	1.74E-08	20.8	21.0	20.8	107	0.560	100	36

Table C.11. Summary of final data for W-HC-TP2.

Lift	Hydraulic Conductivity k_{20} [cm/sec]	Water Content w_{top} [%]	Water Content w_{mid} [%]	Water Content w_{bot} [%]	Dry Unit Weight γ_d [pcf]	Void Ratio e	Saturation S [%]	Porosity n [%]
1	2.81E-08	21.2	20.8	21.1	103	0.615	91	38
2	2.00E-08	21.9	20.9	21.0	102	0.629	90	39
3	1.71E-08	20.7	20.5	20.8	103	0.619	89	38
4	2.42E-08	20.0	21.2	21.0	104	0.596	93	37

Table C.12. Summary of final data for E-HC-TP2.

Lift Interface	Hydraulic Conductivity k_{20} [cm/sec]	Water Content w_{top} [%]	Water Content w_{mid} [%]	Water Content w_{bot} [%]	Dry Unit Weight γ_d [pcf]	Void Ratio e	Saturation S [%]	Porosity n [%]
1-2	3.80E-08	20.0	20.8	21.2	104	0.607	91	38
2-3	5.53E-08	21.2	21.3	21.6	105	0.590	97	37
3-4	7.45E-08	21.3	21.0	20.7	102	0.637	88	39

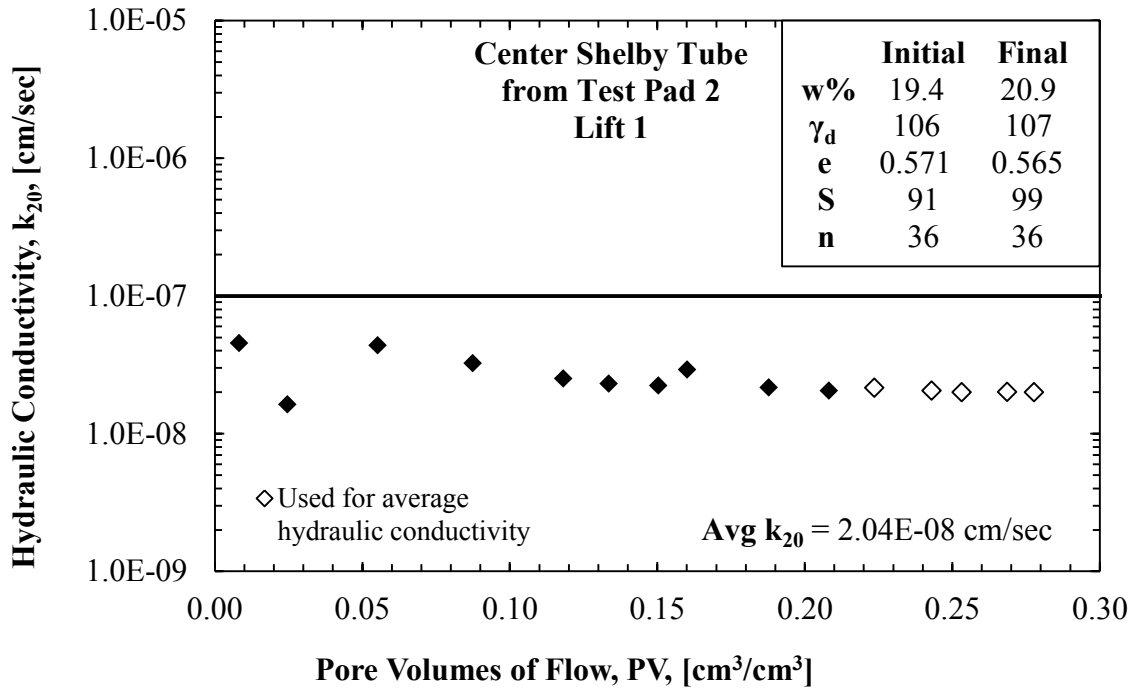


Figure C.29. Vertical hydraulic conductivity data for CT-ST-TP1 Lift 1.

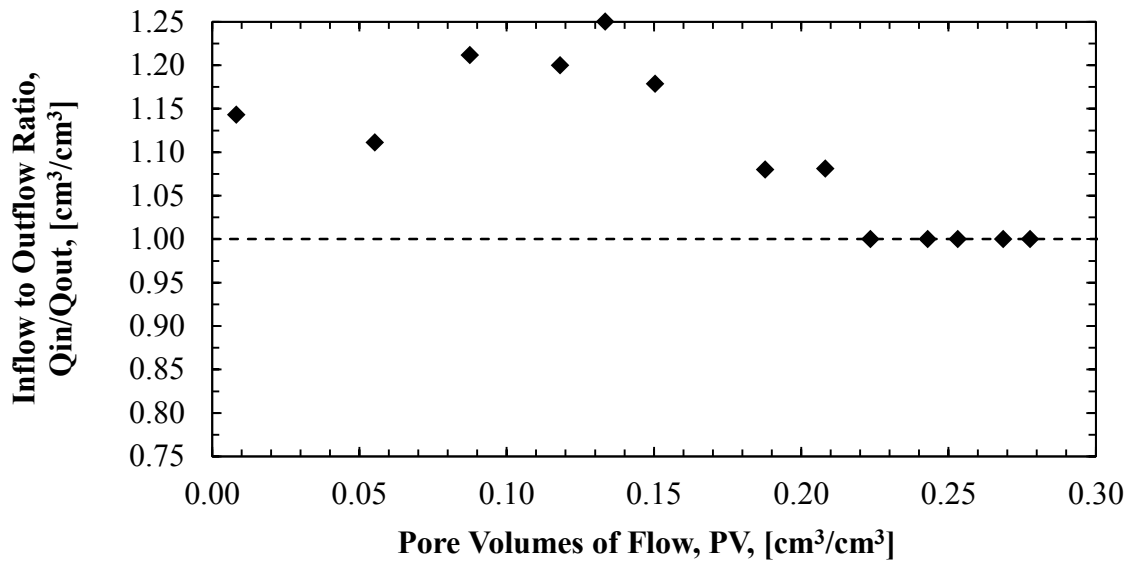


Figure C.30. Inflow to outflow data for CT-ST-TP2 Lift 1.

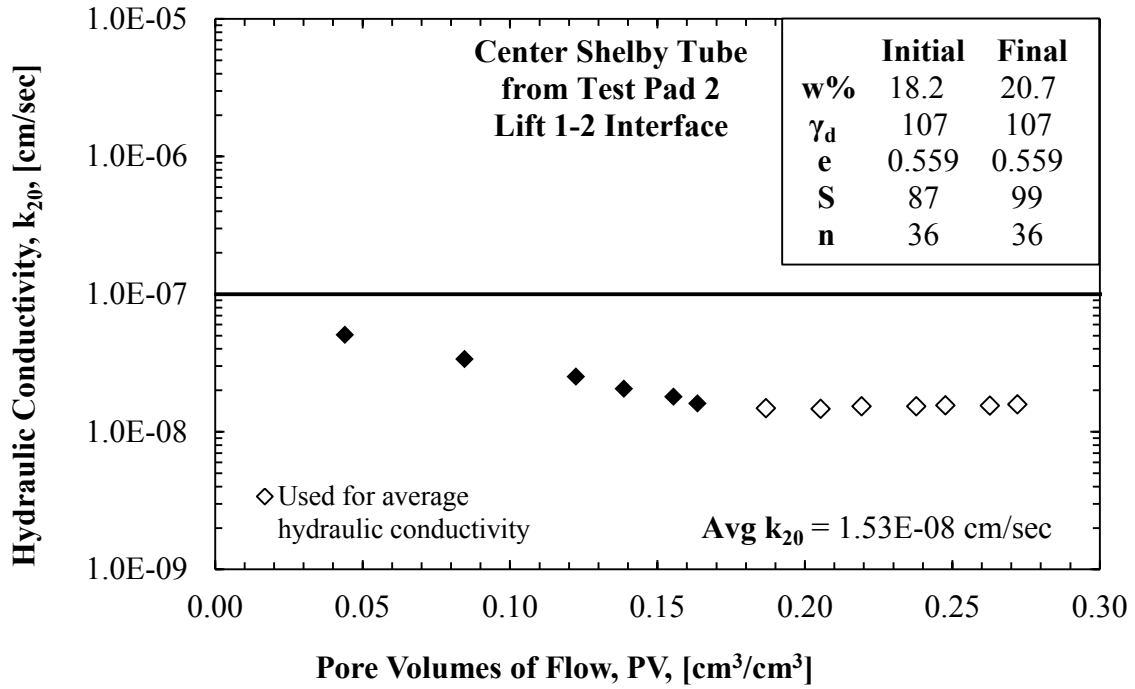


Figure C.31. Vertical hydraulic conductivity data for CT-ST-TP2 Lift 1-2 interface.

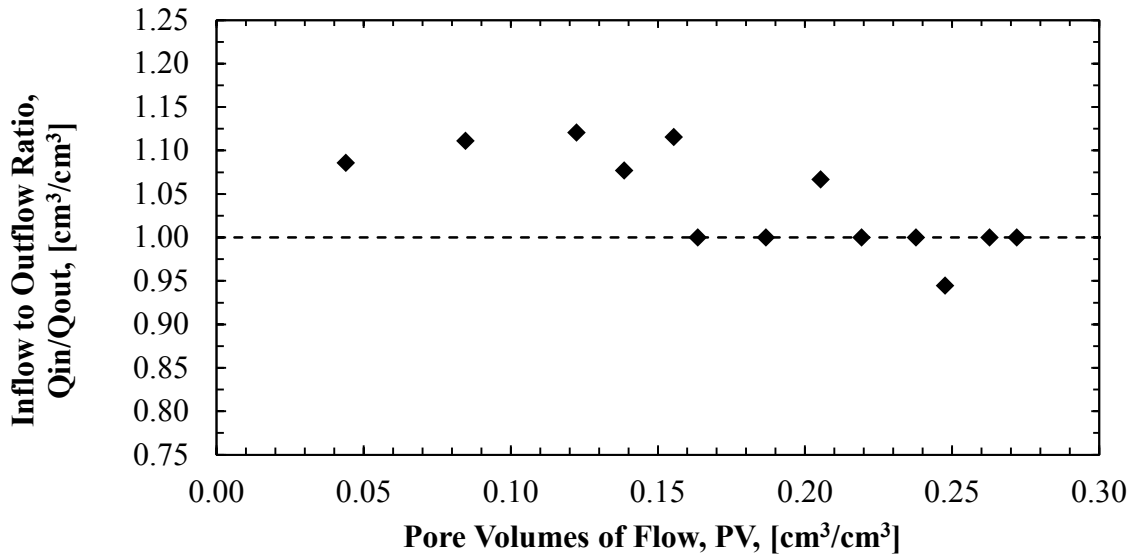


Figure C.32. Inflow to outflow data for CT-ST-TP2 Lift 1-2 interface.

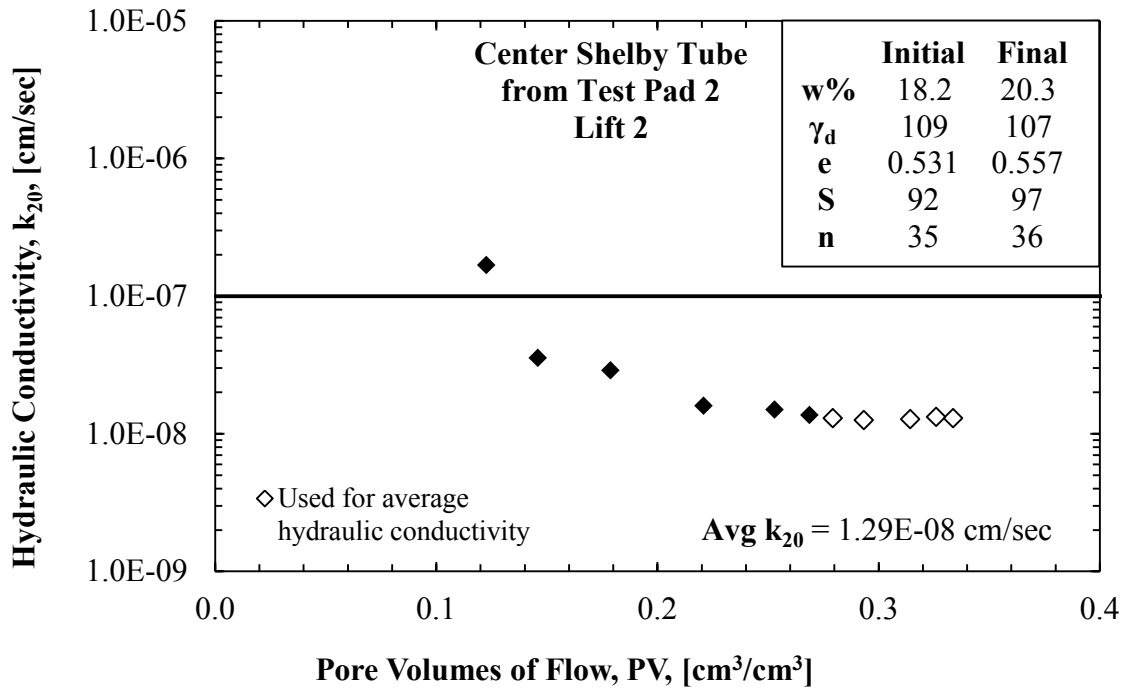


Figure C.33. Vertical hydraulic conductivity data for CT-ST-TP2 Lift 2.

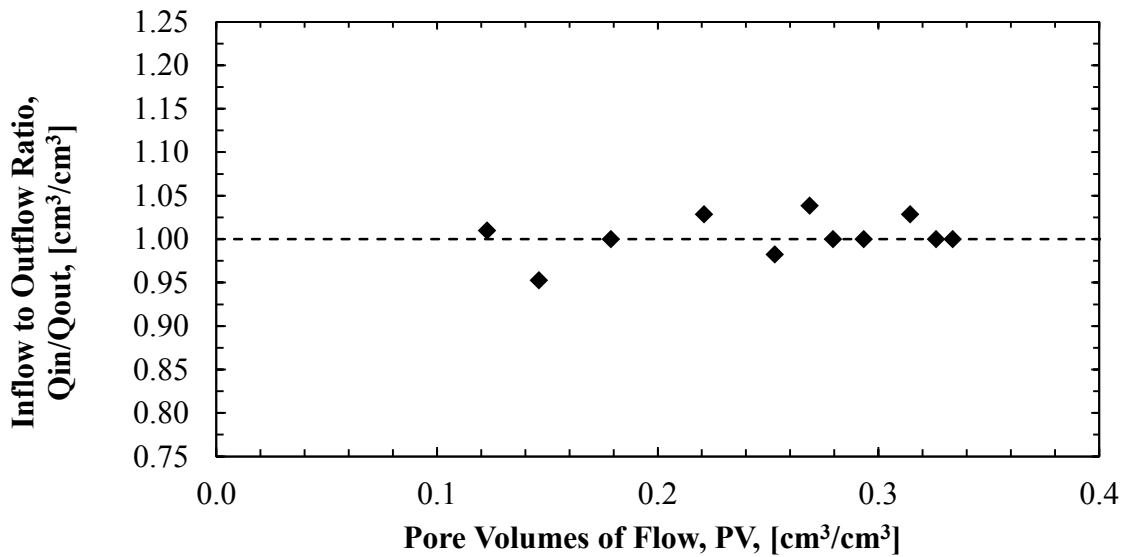


Figure C.34. Inflow to outflow data for CT-ST-TP2 Lift 2.

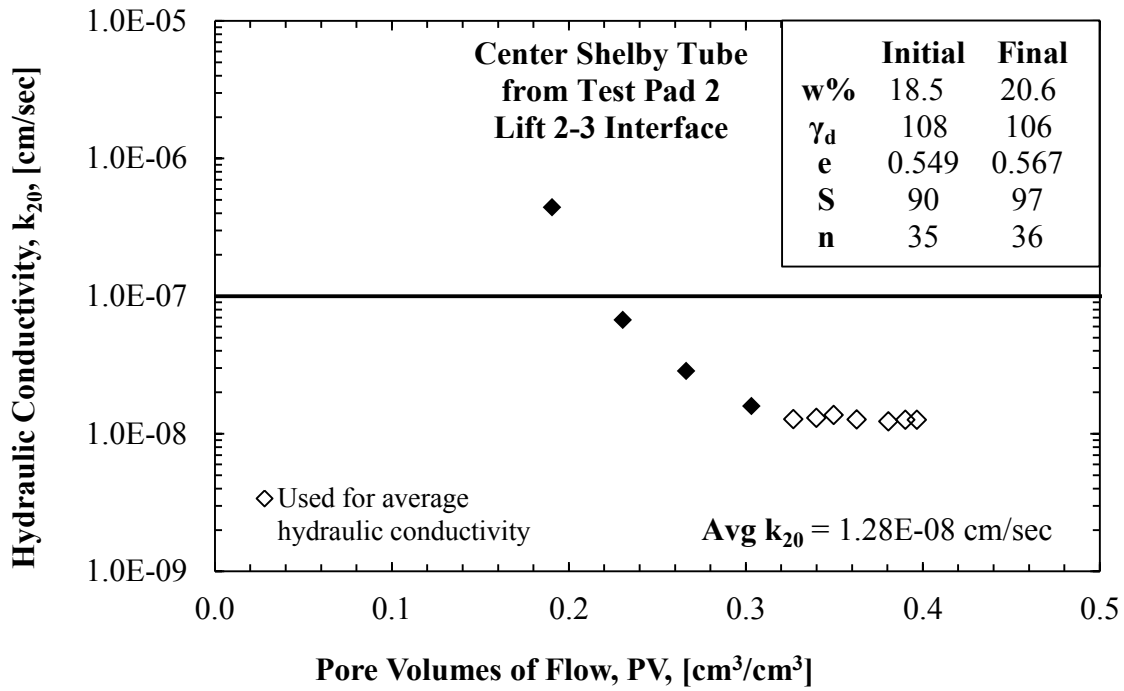


Figure C.35. Vertical hydraulic conductivity data for CT-ST-TP2 Lift 2-3 interface.

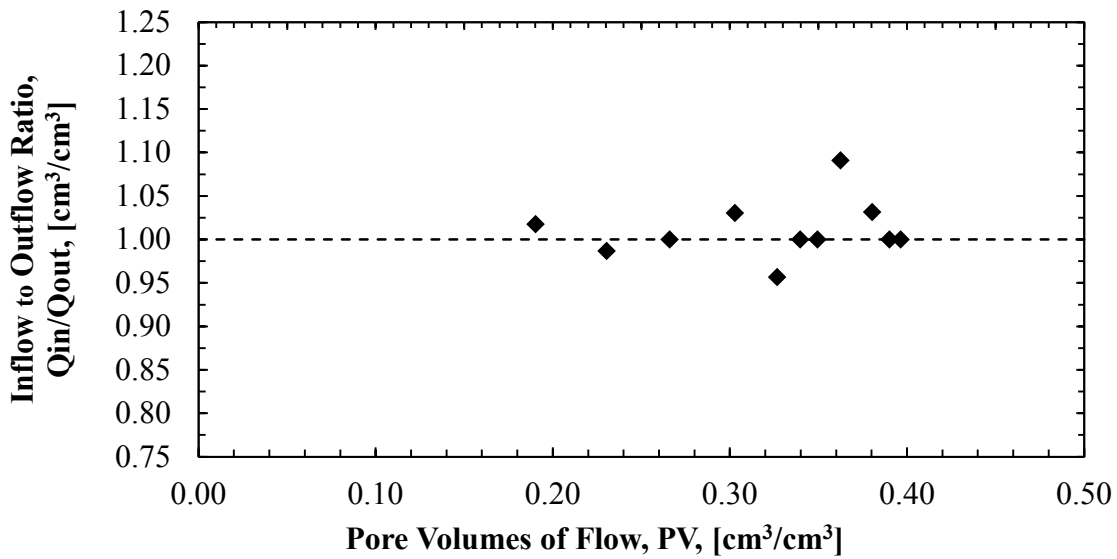


Figure C.36. Inflow to outflow data for CT-ST-TP2 Lift 2-3 interface.

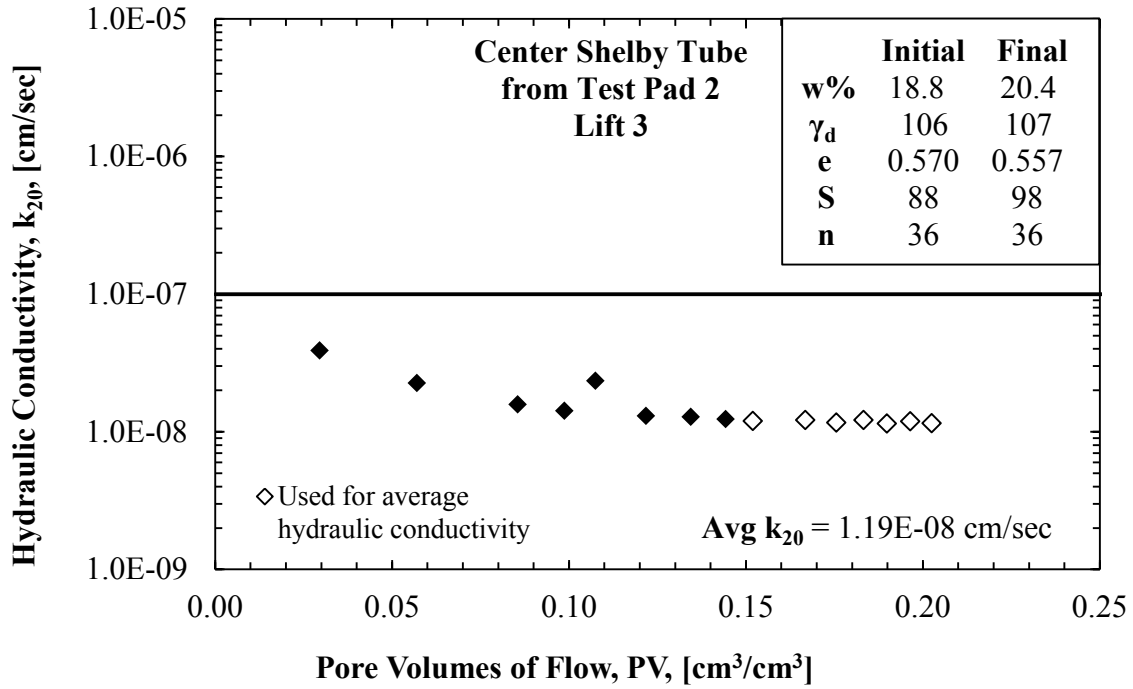


Figure C.37. Vertical hydraulic conductivity data for CT-ST-TP2 Lift 3.

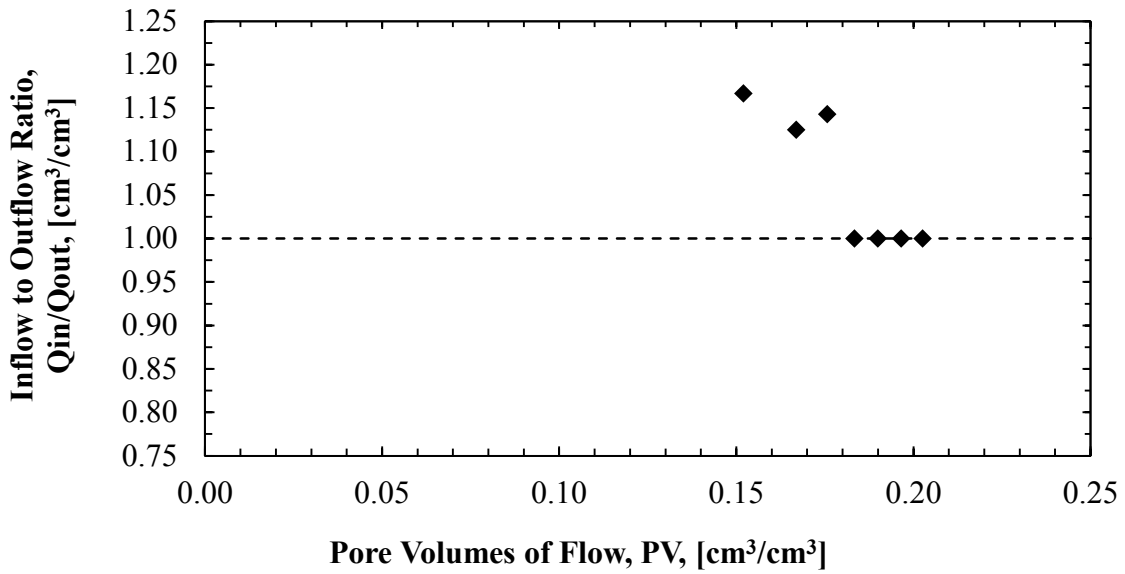


Figure C.38. Inflow to outflow data for CT-ST-TP2 Lift 3.

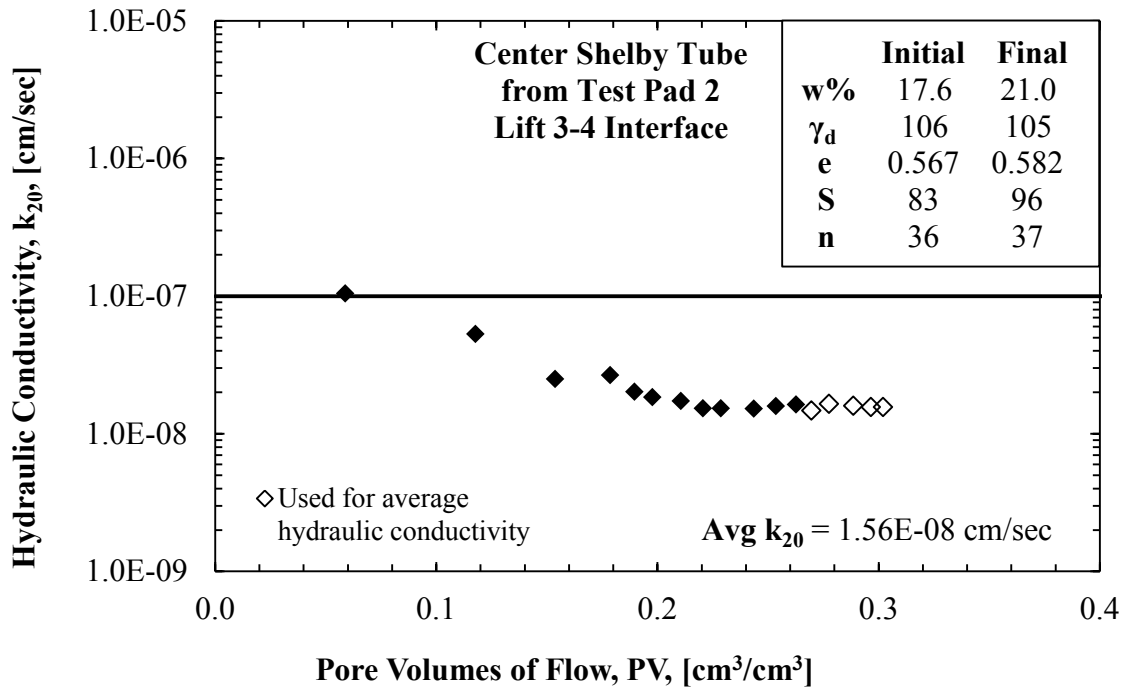


Figure C.39. Vertical hydraulic conductivity data for CT-ST-TP2 Lift 3-4 interface.

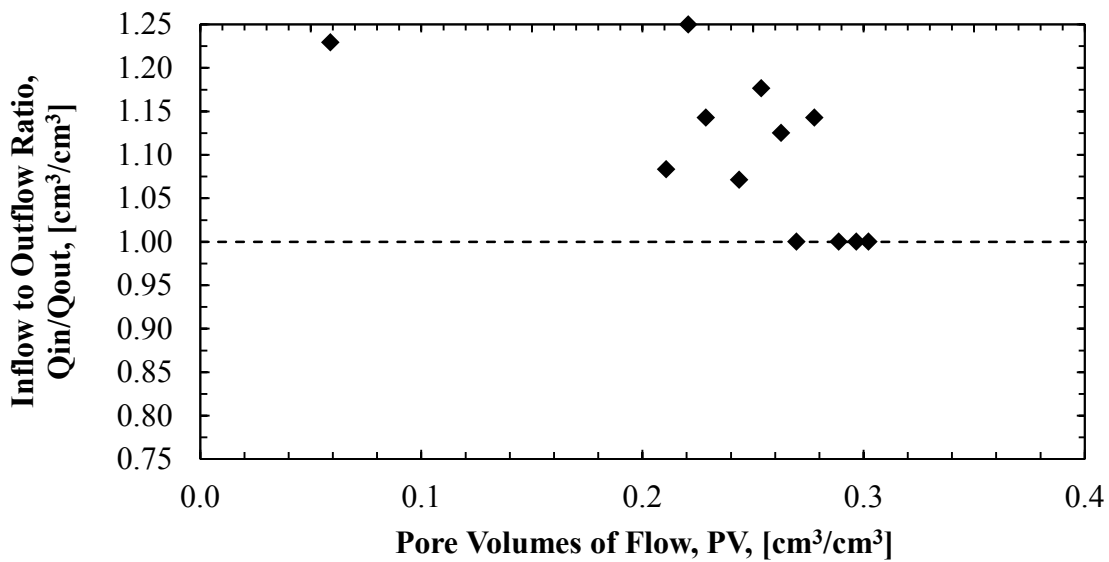


Figure C.40. Inflow to outflow data for CT-ST-TP2 Lift 3-4 interface.

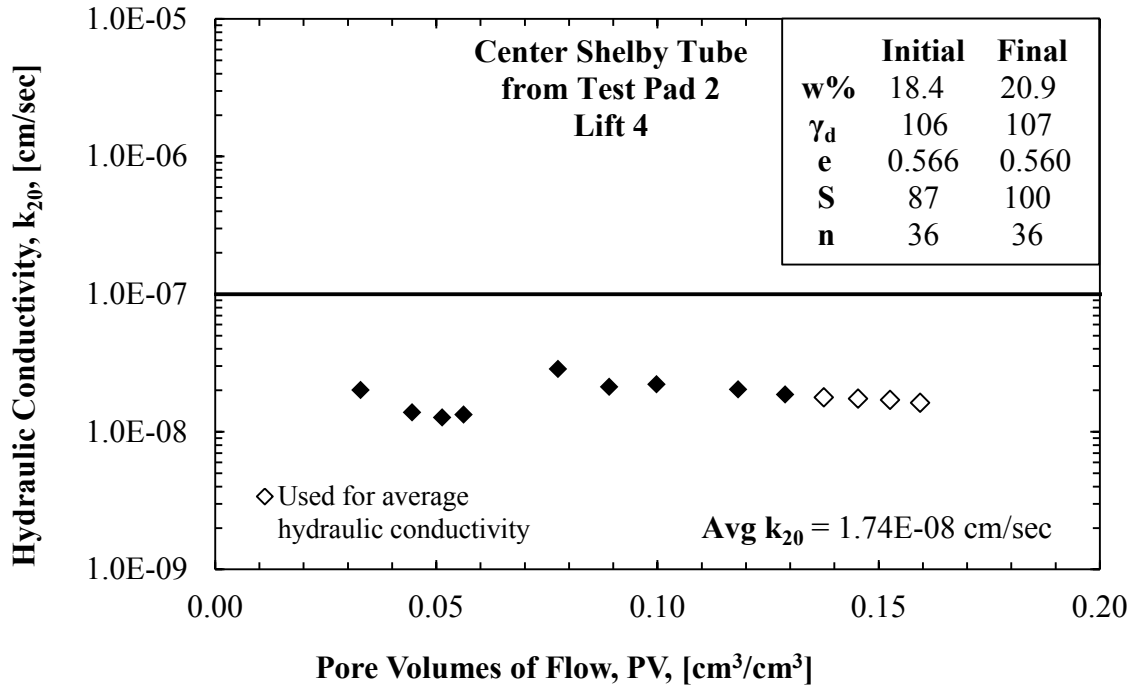


Figure C.41. Vertical hydraulic conductivity data for CT-ST-TP2 Lift 4.

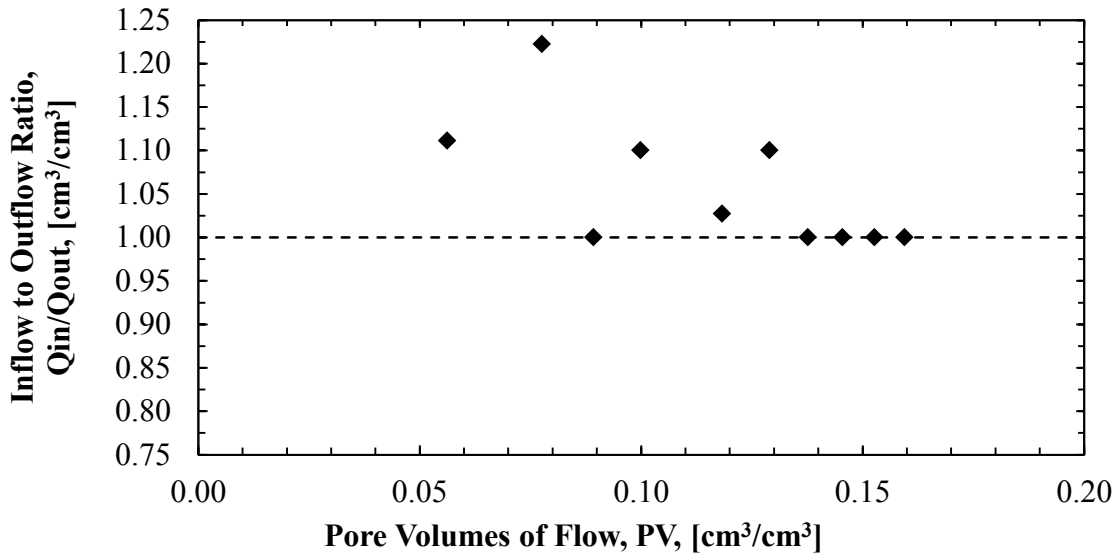


Figure C.42. Inflow to outflow data for CT-ST-TP2 Lift 4.

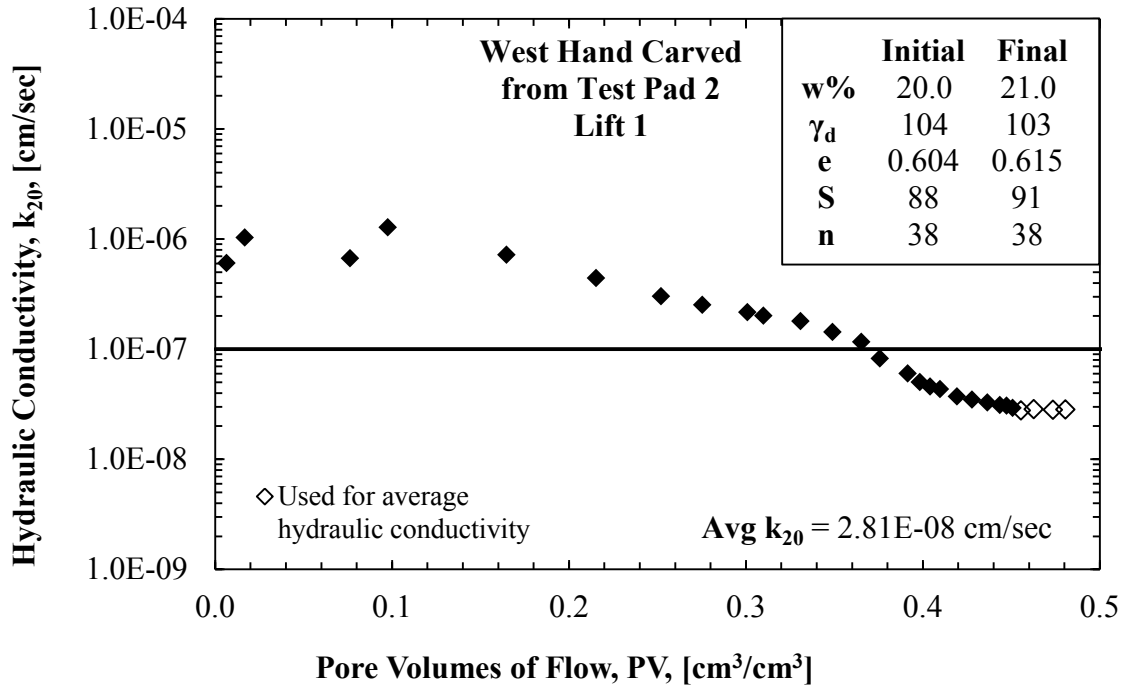


Figure C.43. Vertical hydraulic conductivity data for W-HC-TP2 Lift 1.

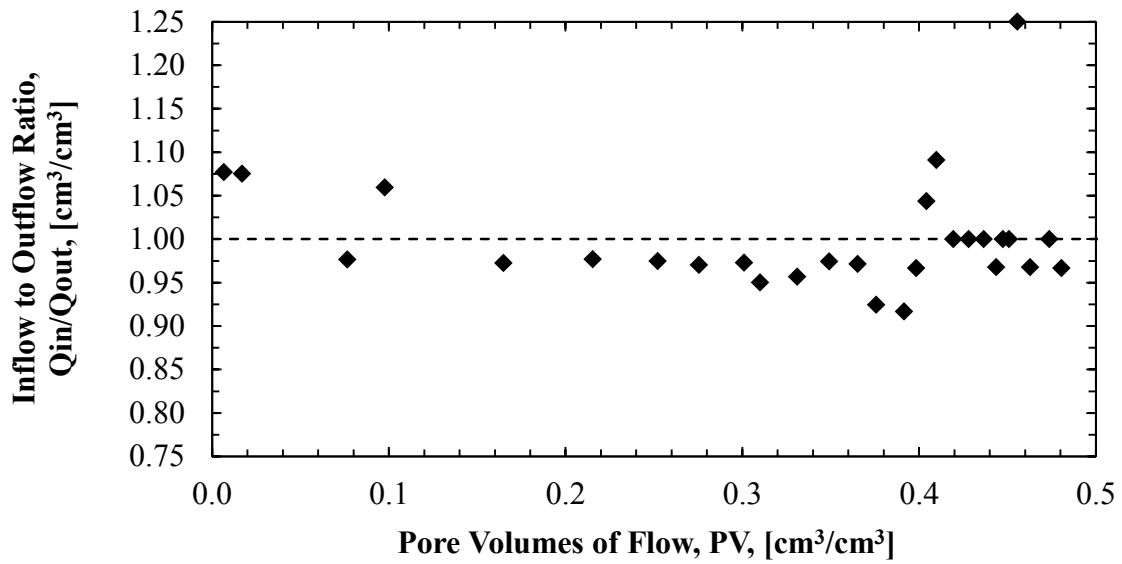


Figure C.44. Inflow to outflow data for W-HC-TP2 Lift 1.

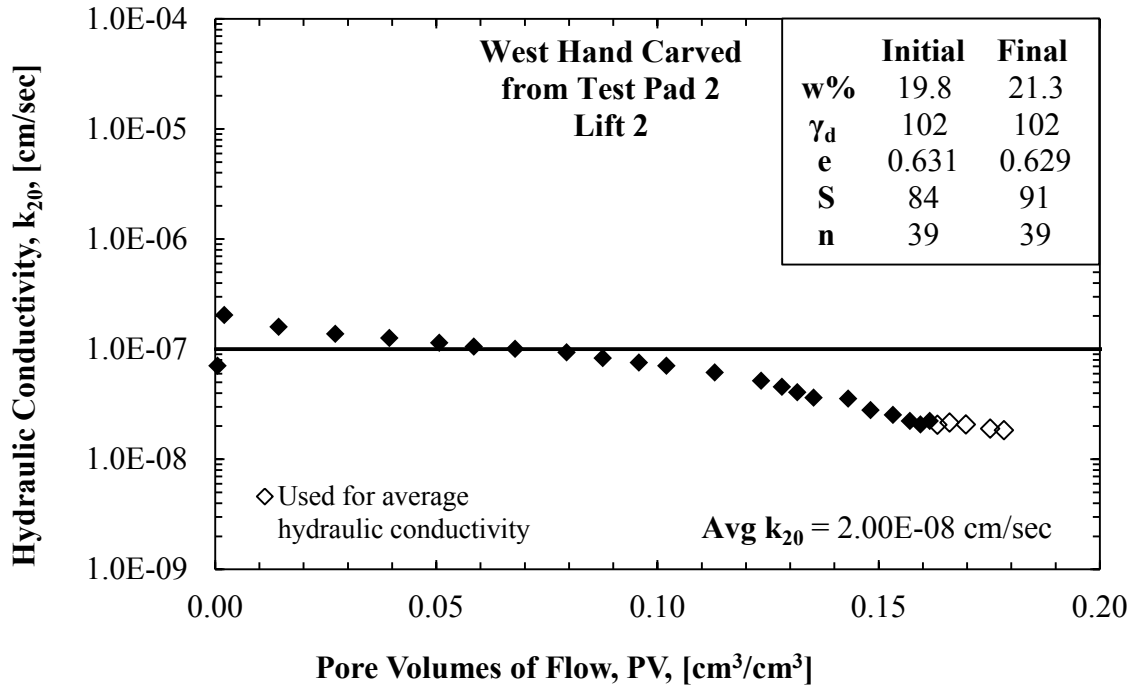


Figure C.45. Vertical hydraulic conductivity data for W-HC-TP2 Lift 2.

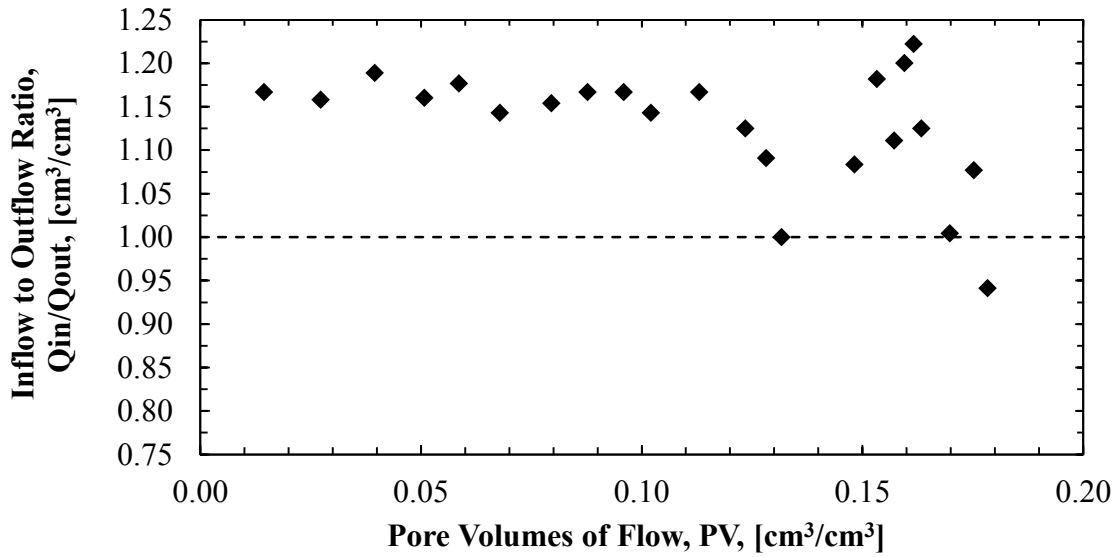


Figure C.46. Inflow to outflow data for W-HC-TP2 Lift 2.

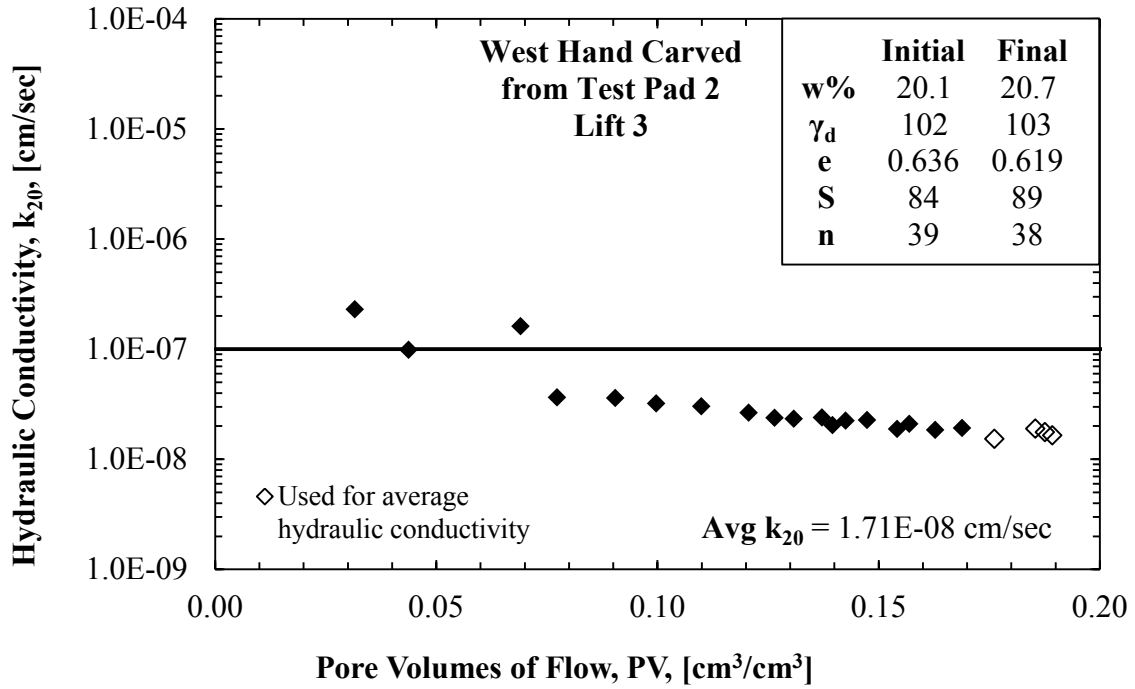


Figure C.47. Vertical hydraulic conductivity data for W-HC-TP2 Lift 3.

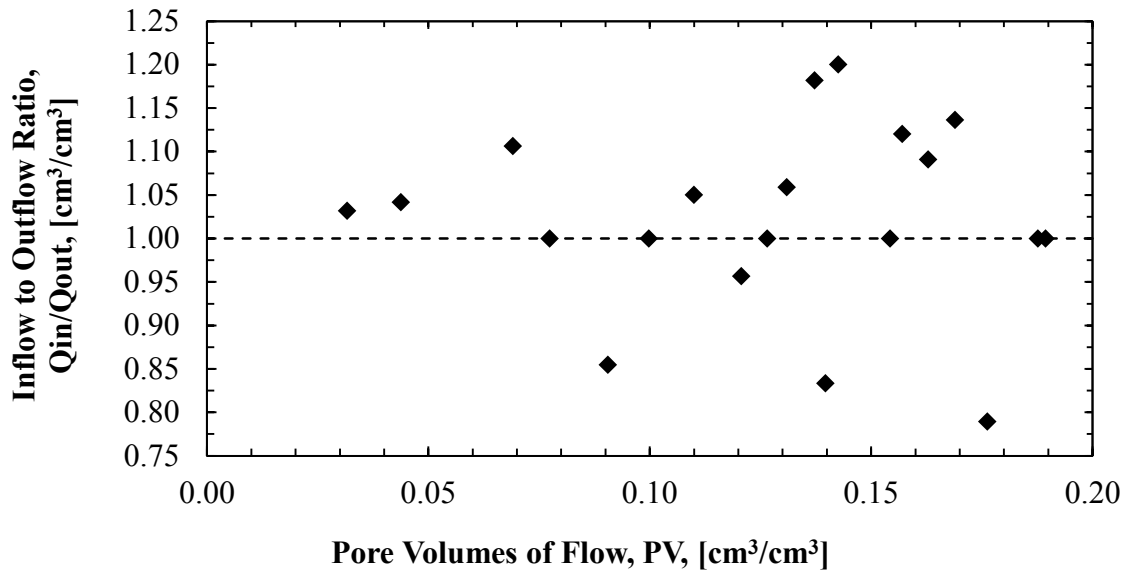


Figure C.48. Inflow to outflow data for W-HC-TP2 Lift 3.

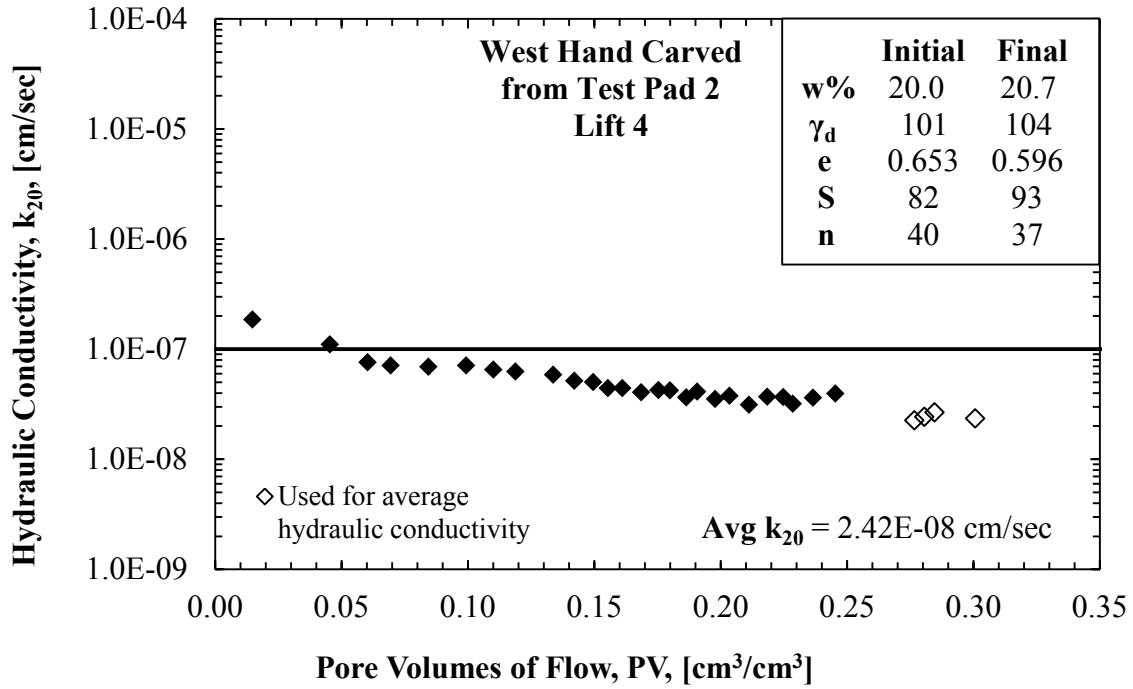


Figure C.49. Vertical hydraulic conductivity data for W-HC-TP2 Lift 4.

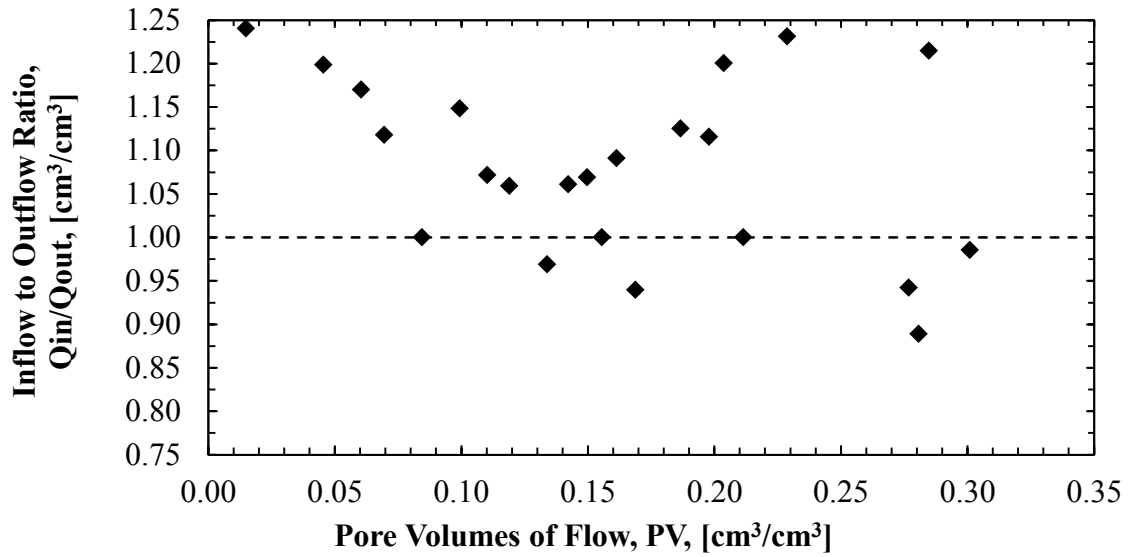


Figure C.50. Inflow to outflow data for W-HC-TP2 Lift 4.

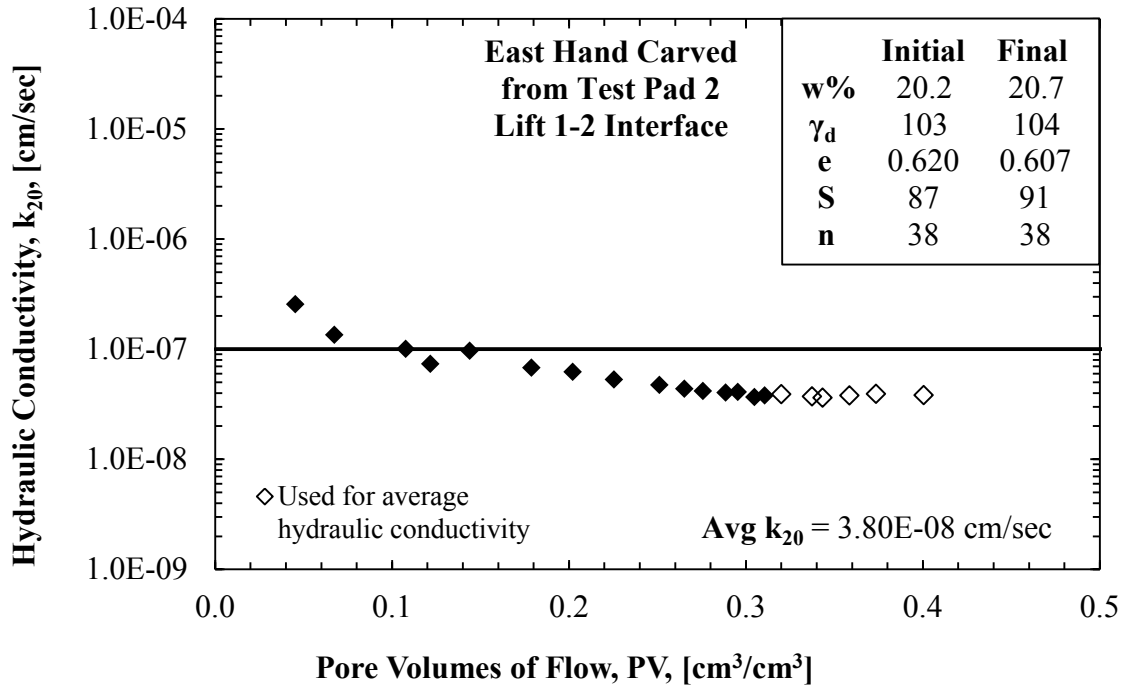


Figure C.51. Horizontal hydraulic conductivity data for E-HC-TP2 Lift 1-2 Interface.

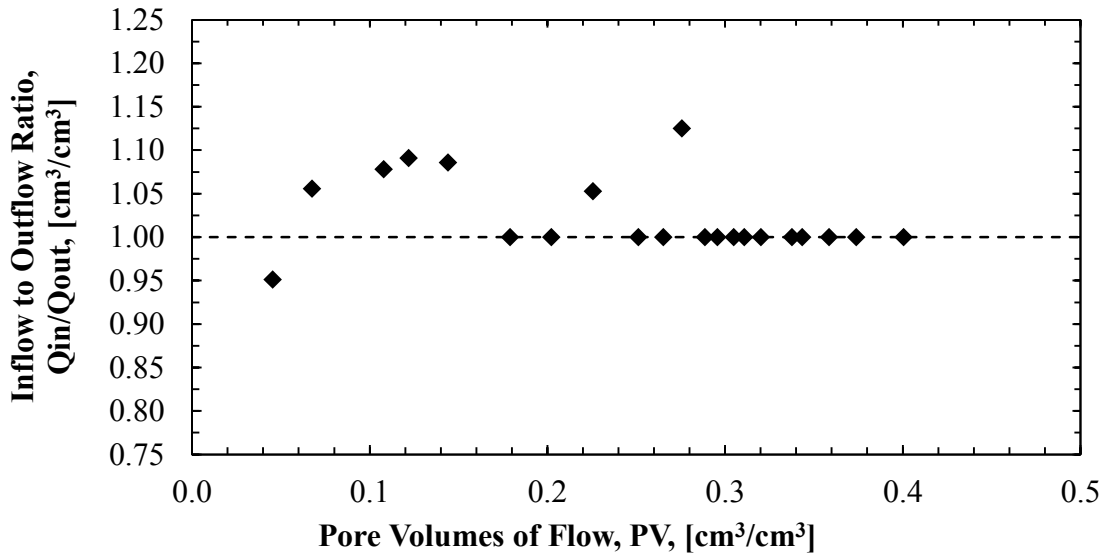


Figure C.52. Inflow to outflow data for E-HC-TP2 Lift 1-2 Interface.

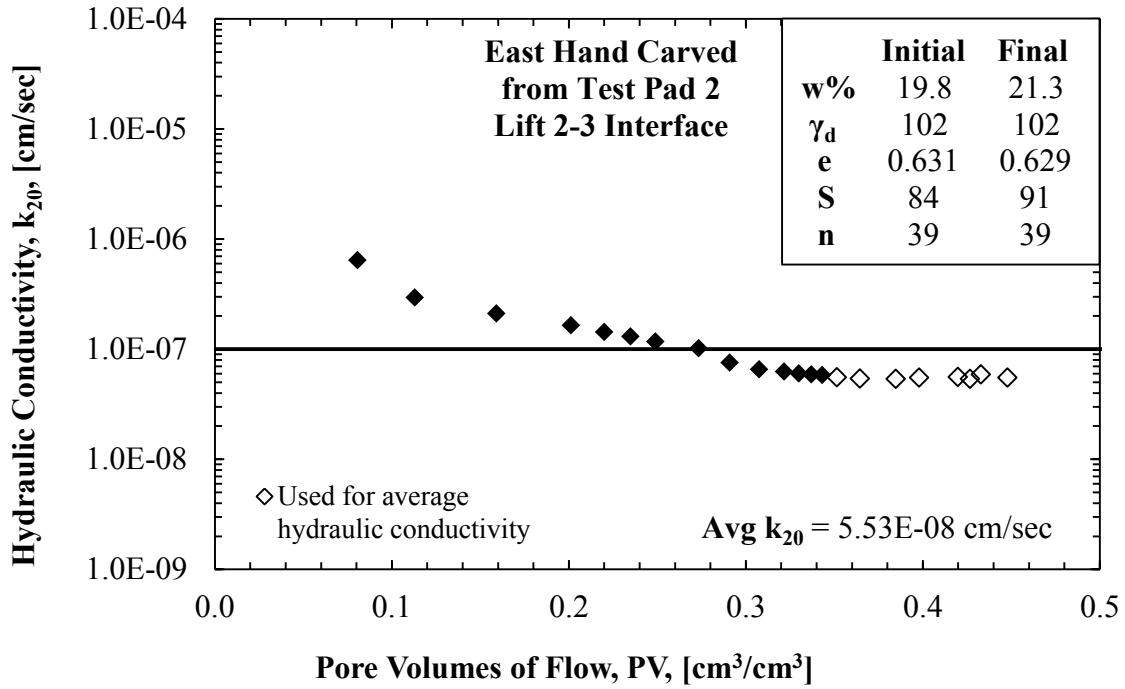


Figure C.53. Horizontal hydraulic conductivity data for E-HC-TP2 Lift 2-3 Interface.

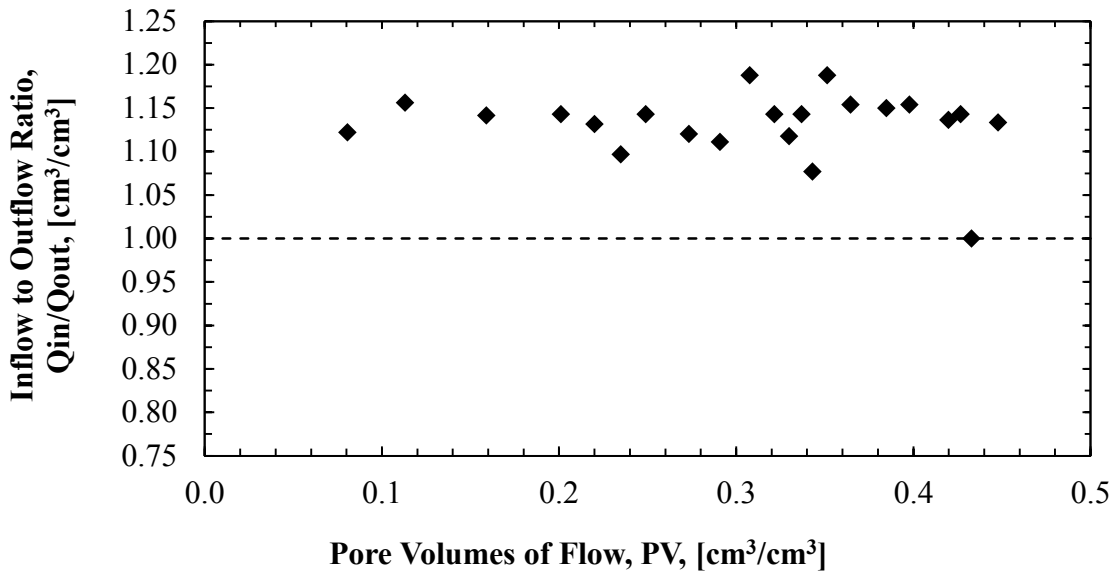


Figure C.54. Inflow to outflow data for E-HC-TP2 Lift 2-3 Interface.

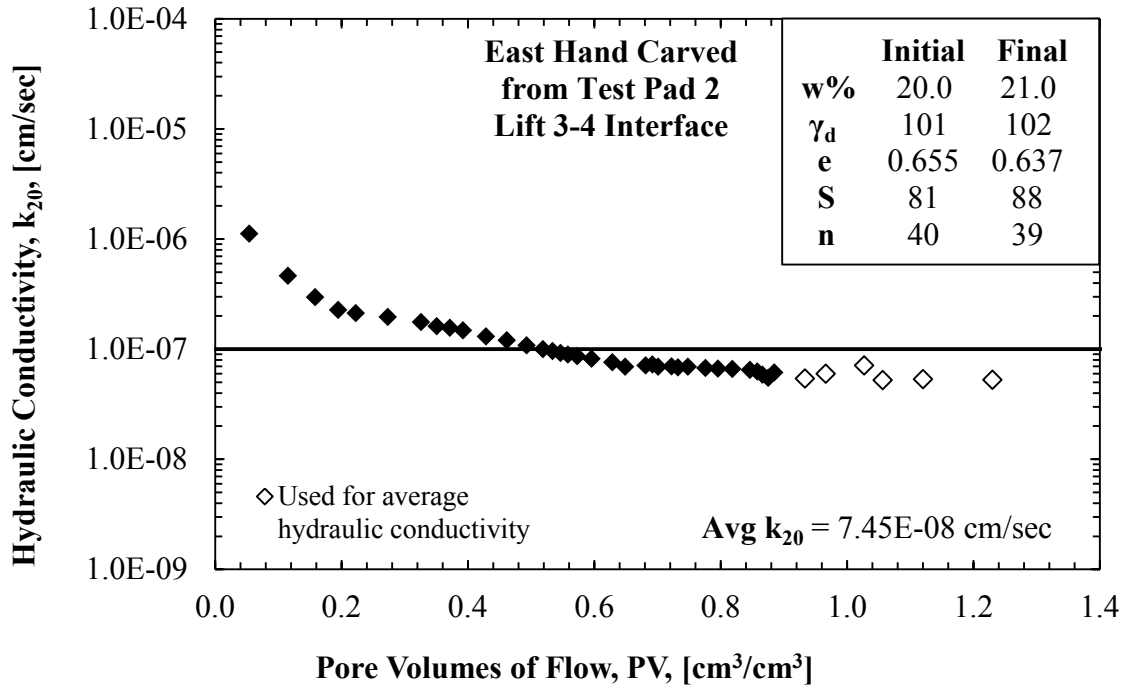


Figure C.55. Horizontal hydraulic conductivity data for E-HC-TP2 Lift 3-4 Interface.

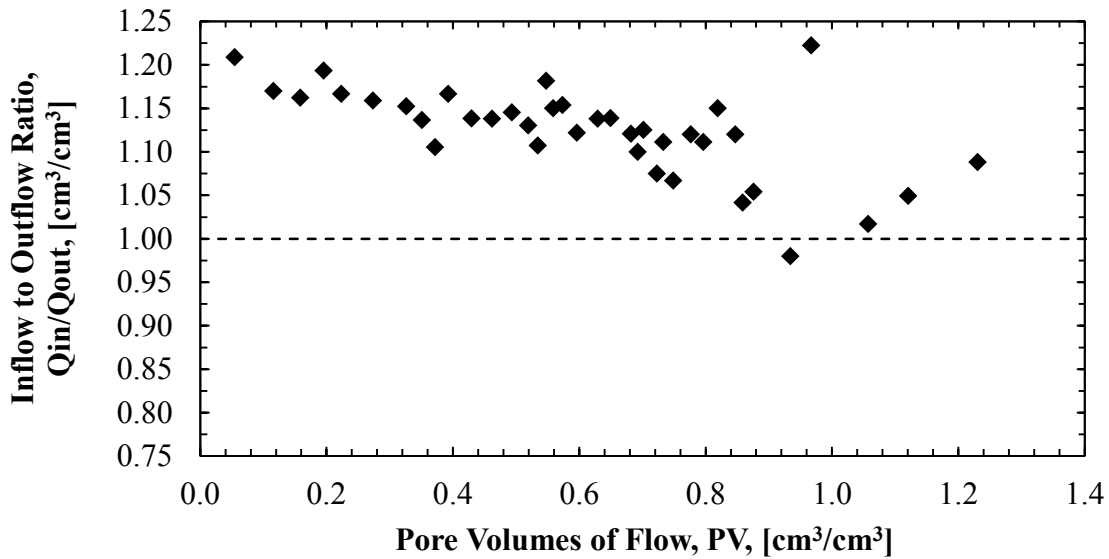


Figure C.56. Inflow to outflow data for E-HC-TP2 Lift 3-4 Interface.

Appendix D. Results for Soil Index Testing

Table D.1. Summary of soil index properties for SW-ST-TP1.

Lift	Specific Gravity	Percent Fines	Clay Fraction	Activity
1	2.68	87.1	27.3	0.69
2	2.66	88.0	27.6	0.65
3	2.68	88.4	27.1	0.69
4	2.66	87.1	27.8	0.63
Average	2.67	87.6	27.5	0.66

Table D.2. Summary of soil index properties for SW-ST-TP2.

Lift	Specific Gravity	Percent Fines	Clay Fraction	Activity
Lift 1	2.68	86.8	25.9	0.76
Lift 2	2.69	87.7	27.6	0.74
Lift 3	2.68	86.1	25.9	0.77
Lift 4	2.70	88.6	26.6	0.77
Average	2.69	87.3	26.5	0.76

Table D.3. Summary of soil index properties for TSB Test Pad 2 cuttings.

Depth	Specific Gravity	Percent Fines	Clay Fraction	Activity
0-2"	2.67	87.1	27.6	0.69
2-4"	2.68	87.9	27.8	0.65
4-6"	2.65	87.2	29.4	0.65
6-8"	2.66	88.0	27.8	0.65
8-10"	2.65	86.9	27.5	0.65
10-12"	2.71	87.9	28.1	0.71
12-14"	2.69	88.0	26.9	0.78
14-16"	2.67	88.0	26.1	0.77
Average	2.67	87.6	27.7	0.69

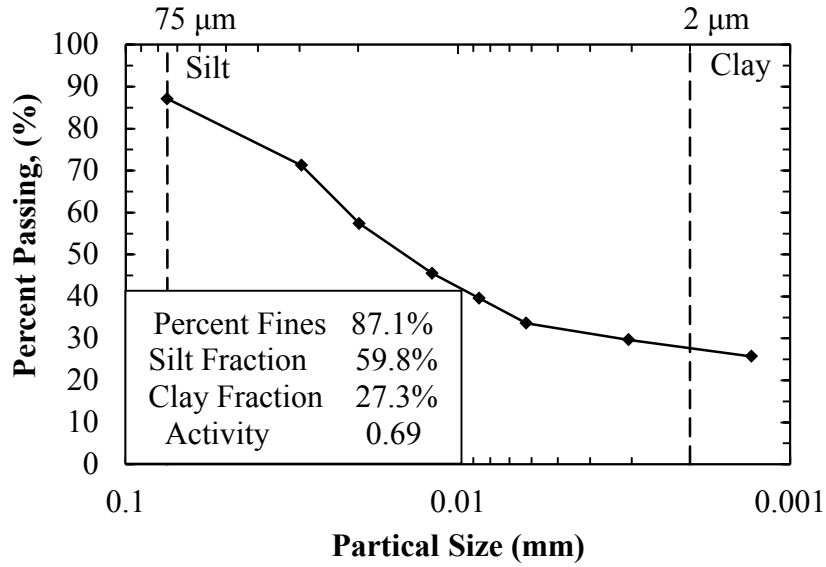


Figure D.1 Hydrometer results from Test Pad 1 Southwest Shelby Tube Lift 1 sample (SW ST-TP1) [previously presented as Figure 4.33].

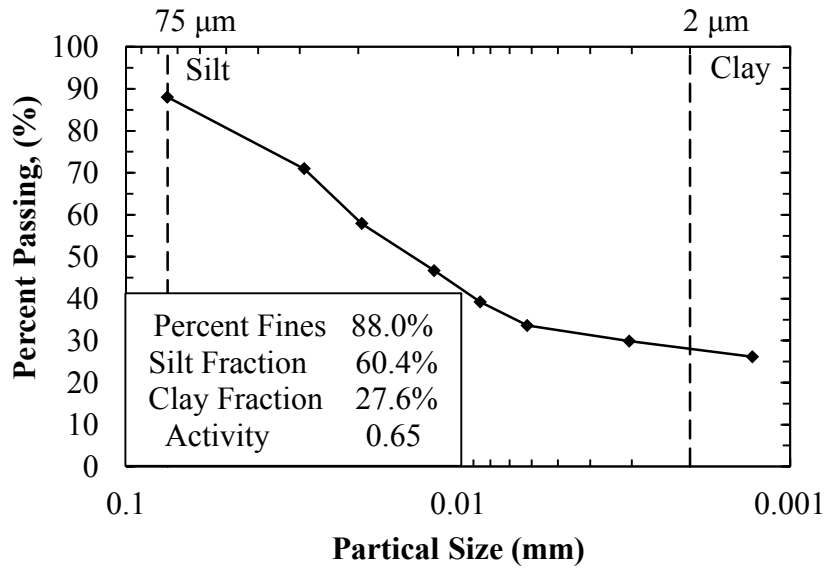


Figure D.2. Hydrometer results from Test Pad 1 Southwest Shelby Tube Lift 2 sample (SW ST-TP1).

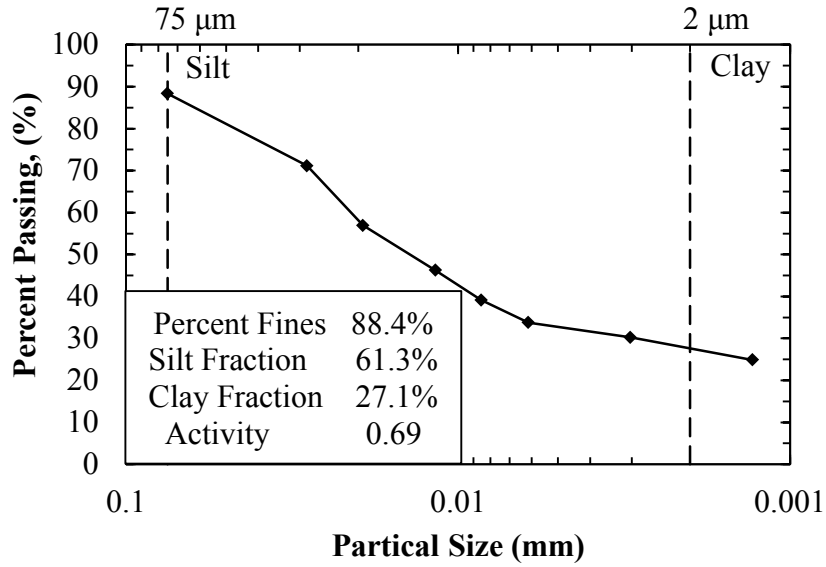


Figure D.3. Hydrometer results from Test Pad 1 Southwest Shelby Tube Lift 3 sample (SW ST-TP1).

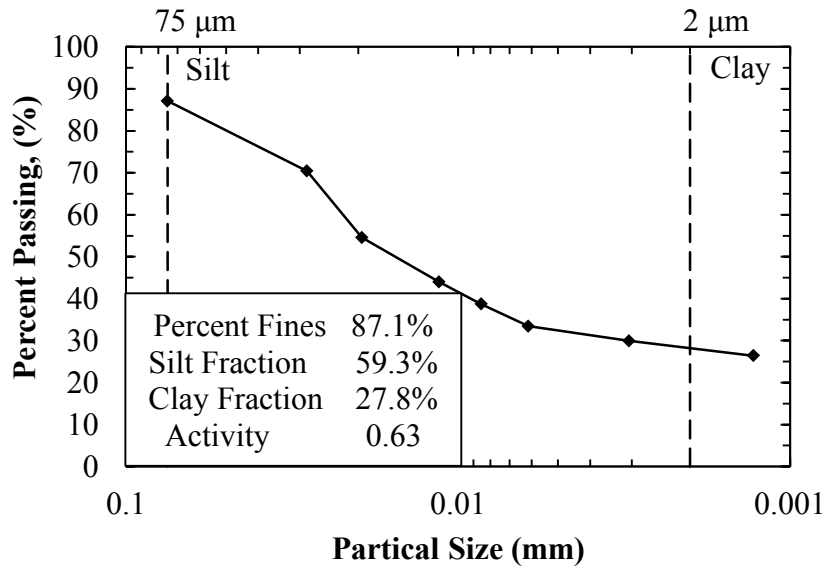


Figure D.4. Hydrometer results from Test Pad 1 Southwest Shelby Tube Lift 4 sample (SW ST-TP1).

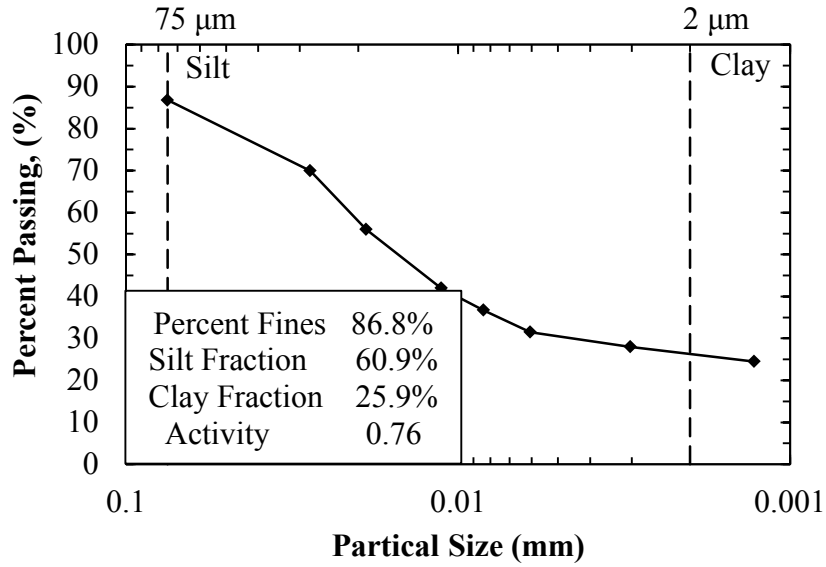


Figure D.5. Hydrometer results from Test Pad 2 Southwest Shelby Tube Lift 1 sample (SW ST-TP2).

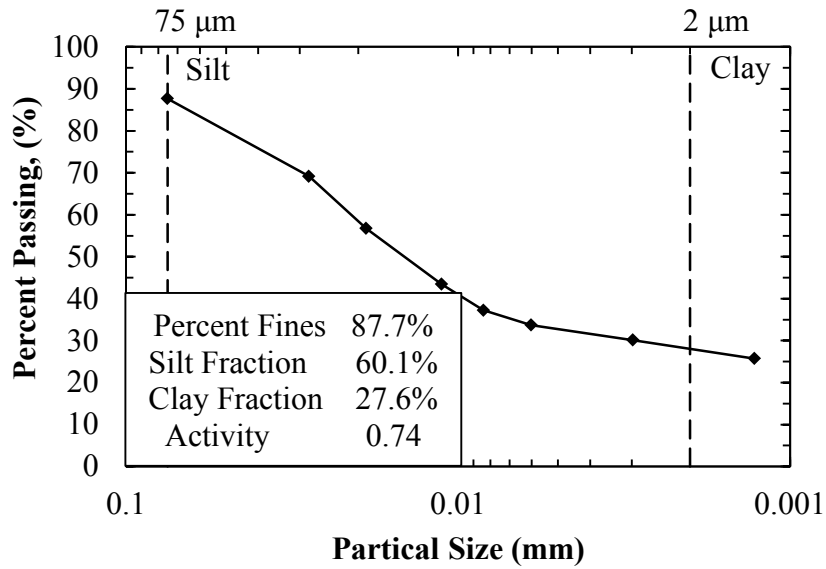


Figure D.6. Hydrometer results from Test Pad 2 Southwest Shelby Tube Lift 2 sample (SW ST-TP2).

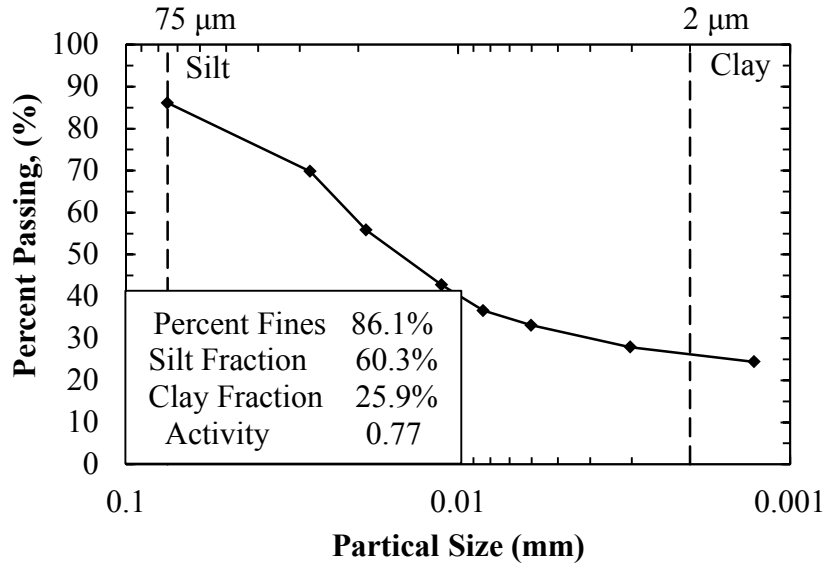


Figure D.7. Hydrometer results from Test Pad 2 Southwest Shelby Tube Lift 3 sample (SW ST-TP2).

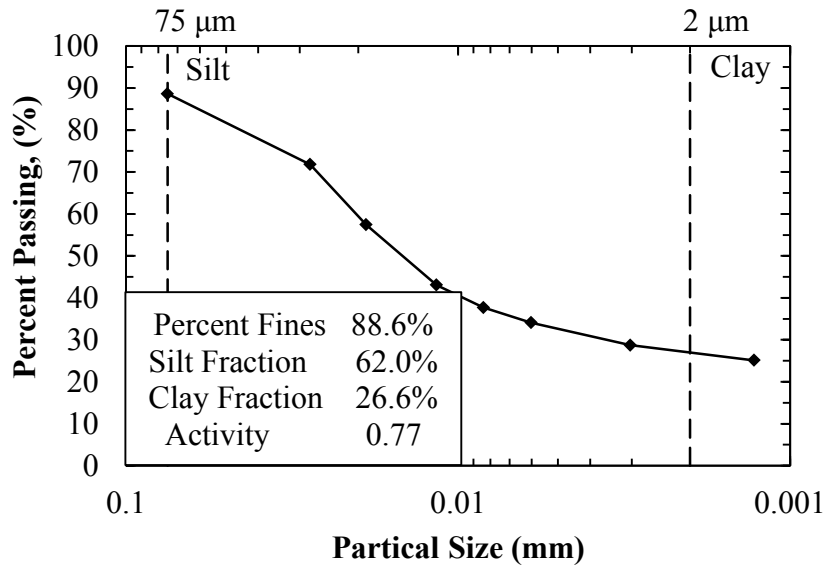


Figure D.8. Hydrometer results from Test Pad 2 Southwest Shelby Tube Lift 4 sample (SW ST-TP2).

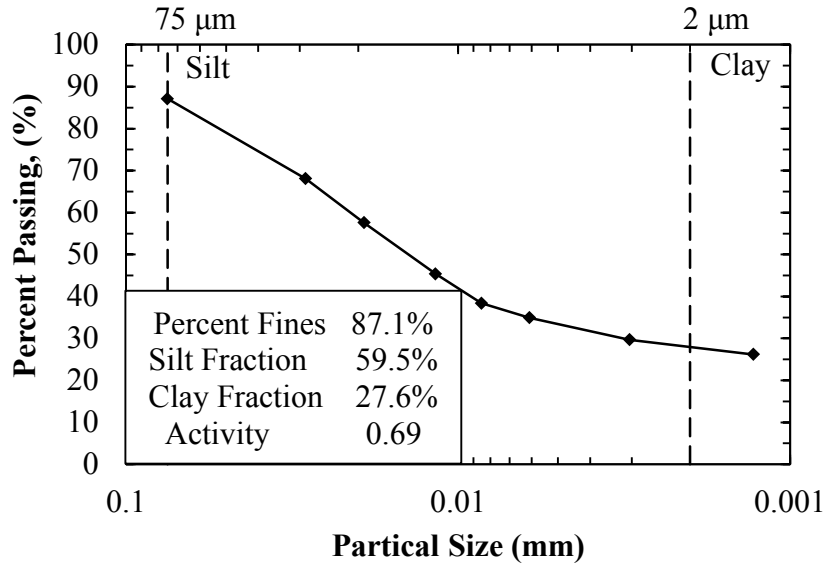


Figure D.9. Hydrometer results for sample from Test Pad 2 TSB borehole (0-2in.) obtained prior to TSB testing.

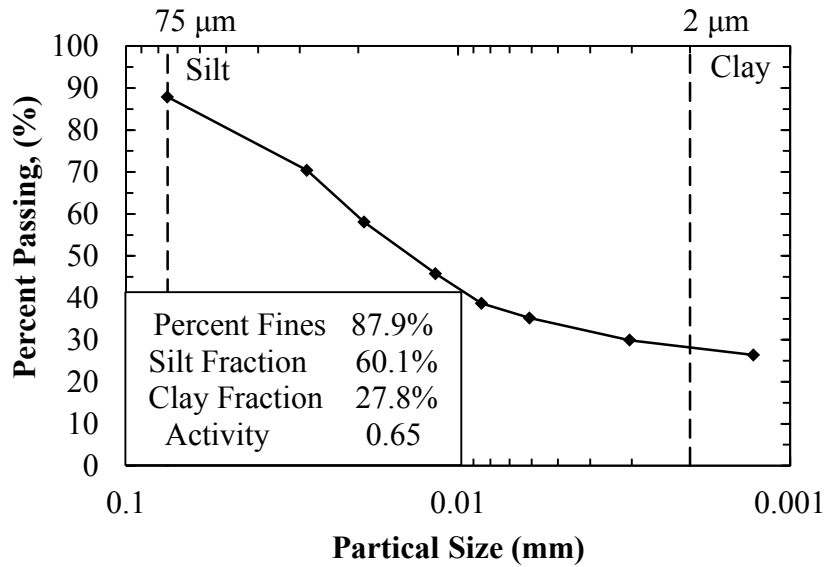


Figure D.10. Hydrometer results for sample from Test Pad 2 TSB borehole (2-4in.) obtained prior to TSB testing.

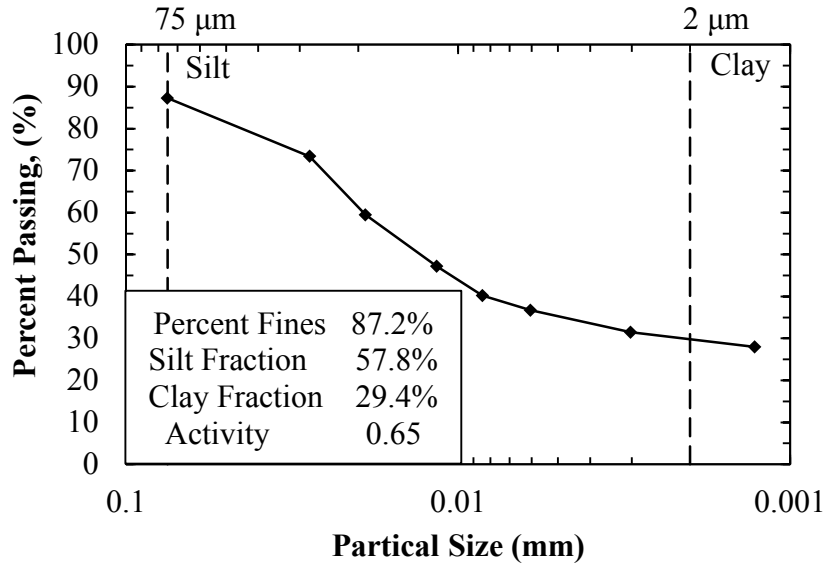


Figure D.11. Hydrometer results for sample from Test Pad 2 TSB borehole (4-6in.) obtained prior to TSB testing.

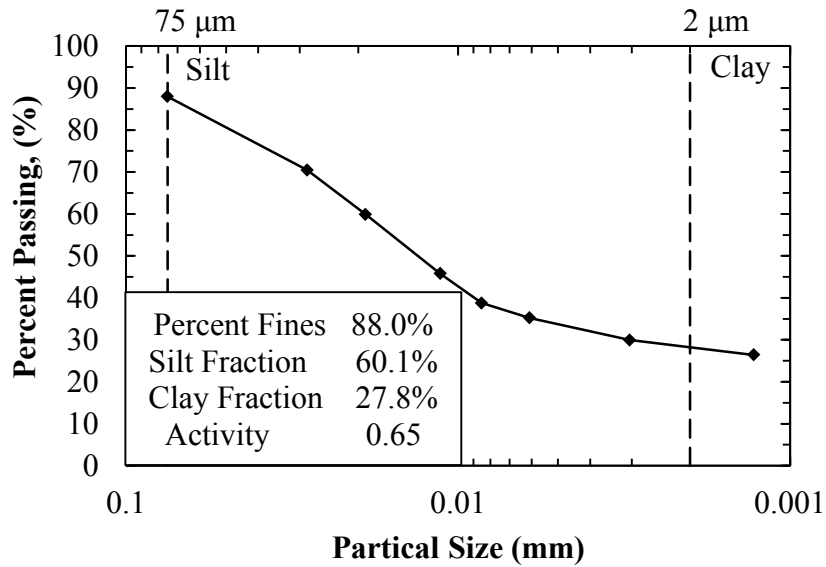


Figure D.12. Hydrometer results for sample from Test Pad 2 TSB borehole (6-8in.) obtained prior to TSB testing.

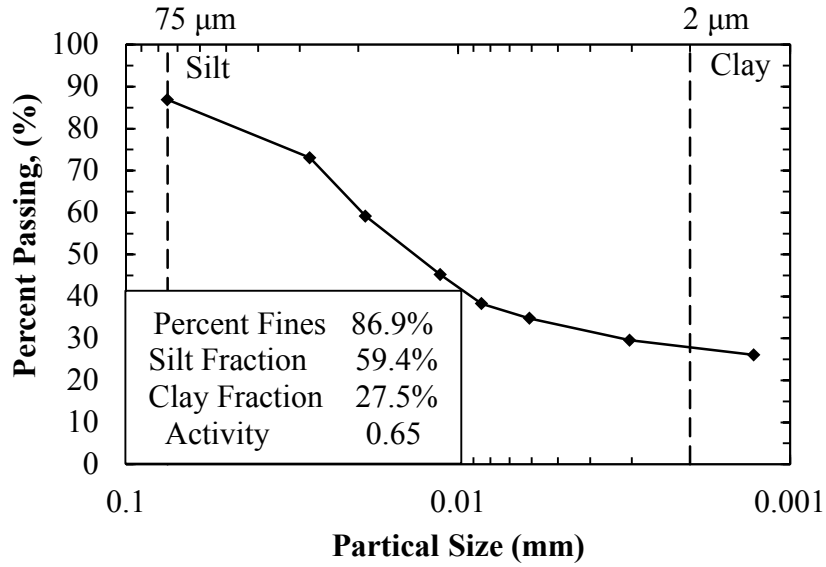


Figure D.13. Hydrometer results for sample from Test Pad 2 TSB borehole (8-10in.) obtained prior to TSB testing.

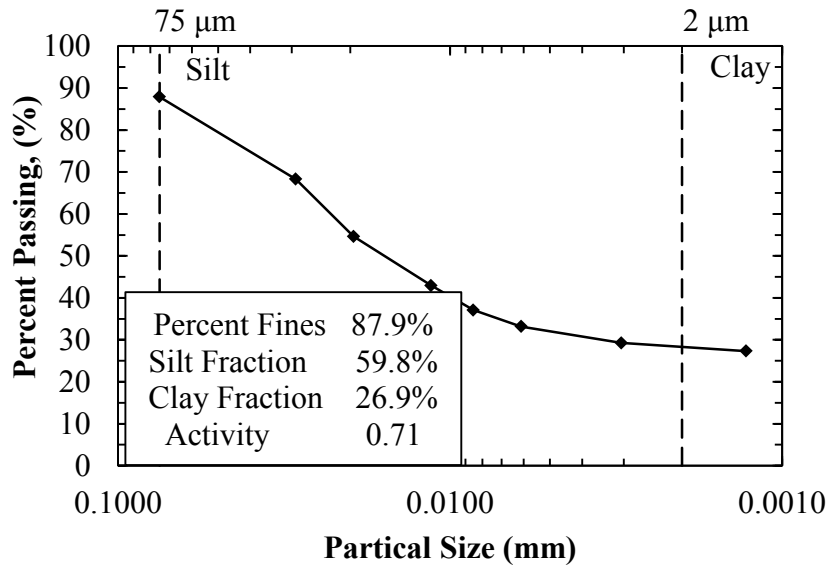


Figure D.14. Hydrometer results for sample from Test Pad 2 TSB borehole (10-12in.) obtained after Stage 1 of TSB testing.

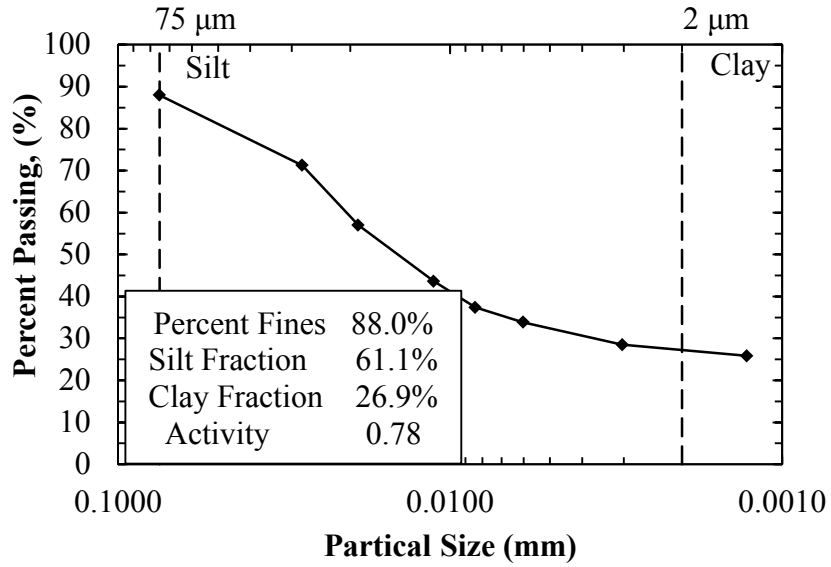


Figure D.15. Hydrometer results for sample from Test Pad 2 TSB borehole (12-14in.) obtained after Stage 1 of TSB testing.

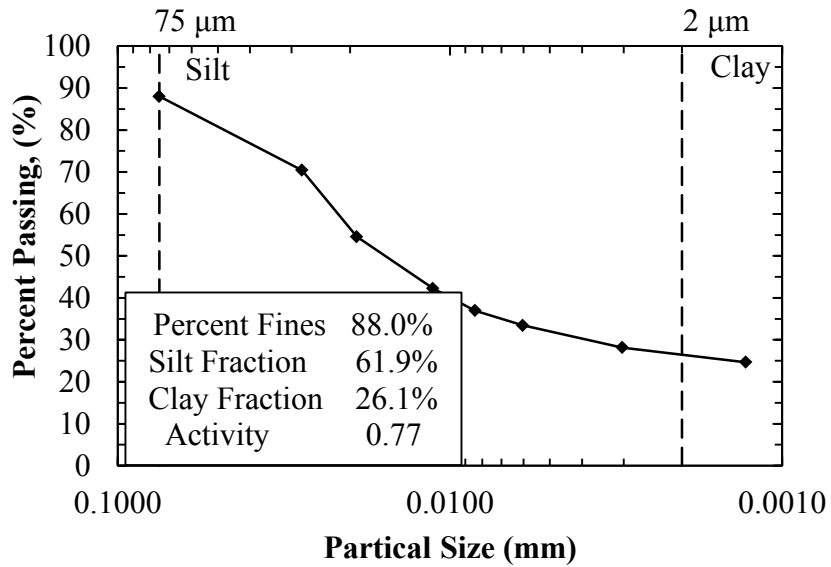


Figure D.16. Hydrometer results for sample from Test Pad 2 TSB borehole (14-16in.) obtained after Stage 1 of TSB testing.

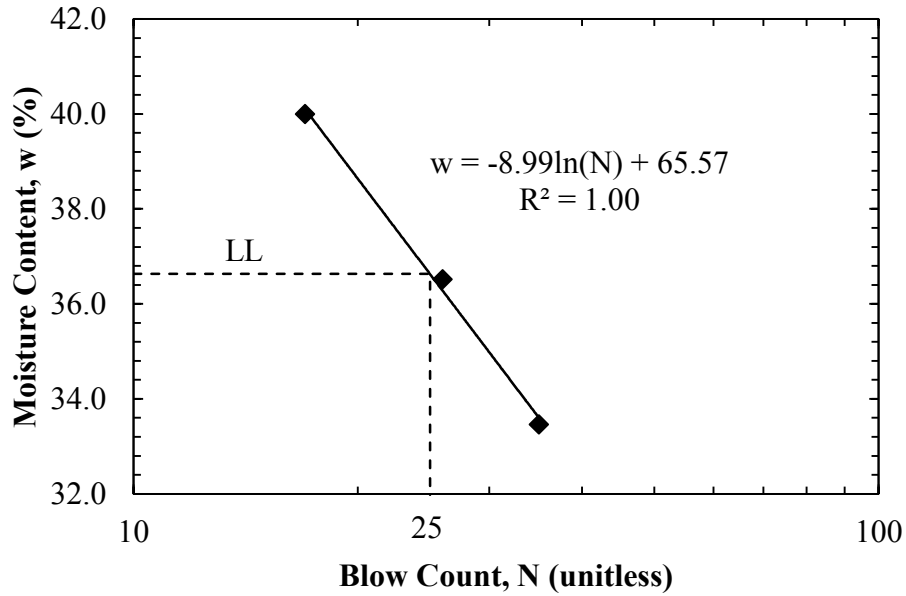


Figure D.17. Liquid limit results from Test Pad 1 Southwest Shelby Tube Lift 1 sample (SW ST-TP1).

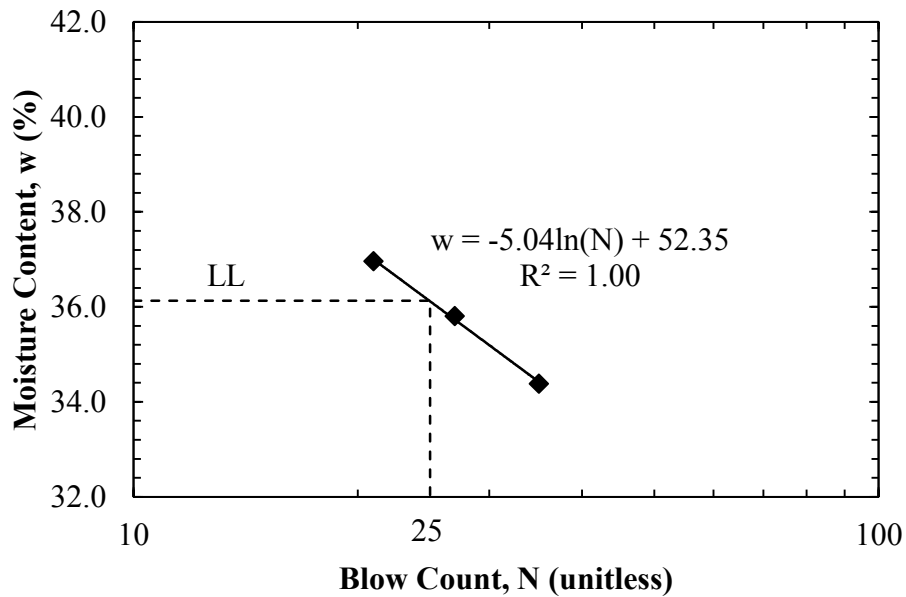


Figure D.18. Liquid limit results from Test Pad 1 Southwest Shelby Tube Lift 2 sample (SW ST-TP1).

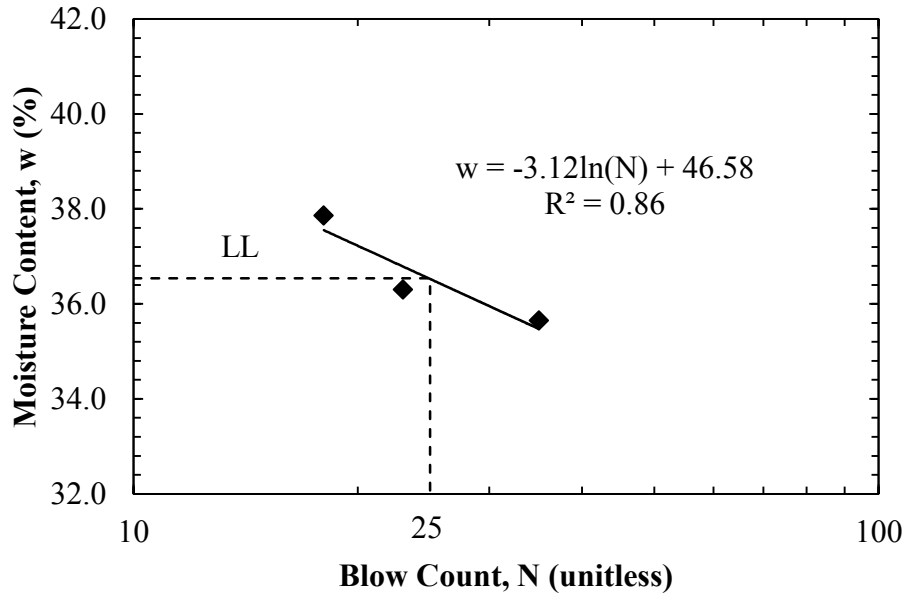


Figure D.19. Liquid limit results from Test Pad 1 Southwest Shelby Tube Lift 3 sample (SW ST-TP2).

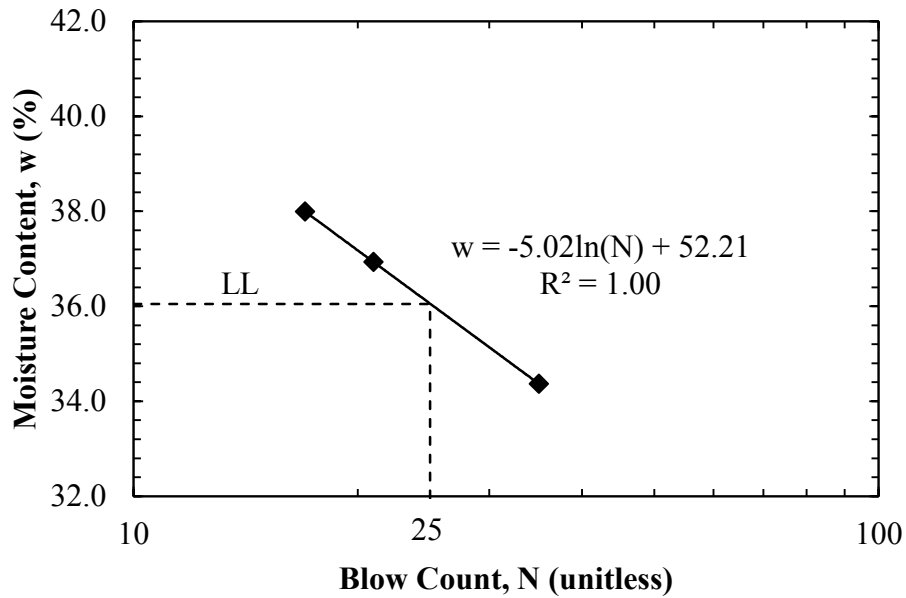


Figure D.20. Liquid limit results from Test Pad 1 Southwest Shelby Tube Lift 4 sample (SW ST-TP1).

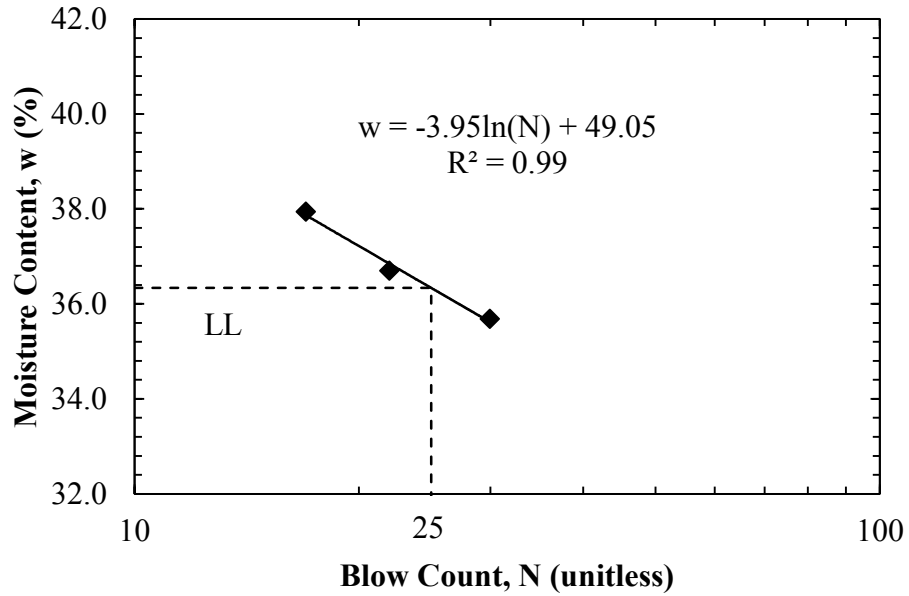


Figure D.21. Liquid limit results from Test Pad 2 Southwest Shelby Tube Lift 1 sample (SW ST-TP2).

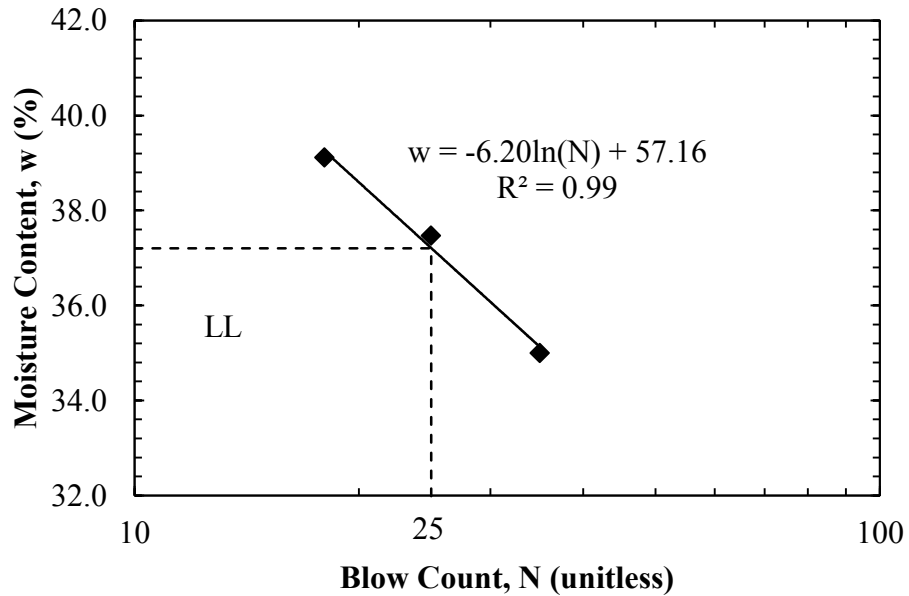


Figure D.22. Liquid limit results from Test Pad 2 Southwest Shelby Tube Lift 2 sample (SW ST-TP2).

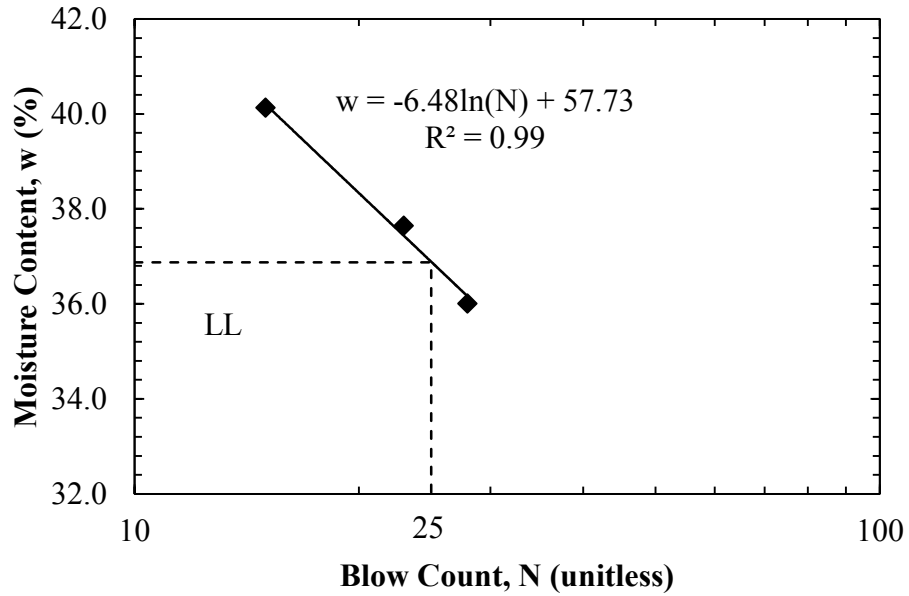


Figure D.23. Liquid limit results from Test Pad 2 Southwest Shelby Tube Lift 3 sample (SW ST-TP2).

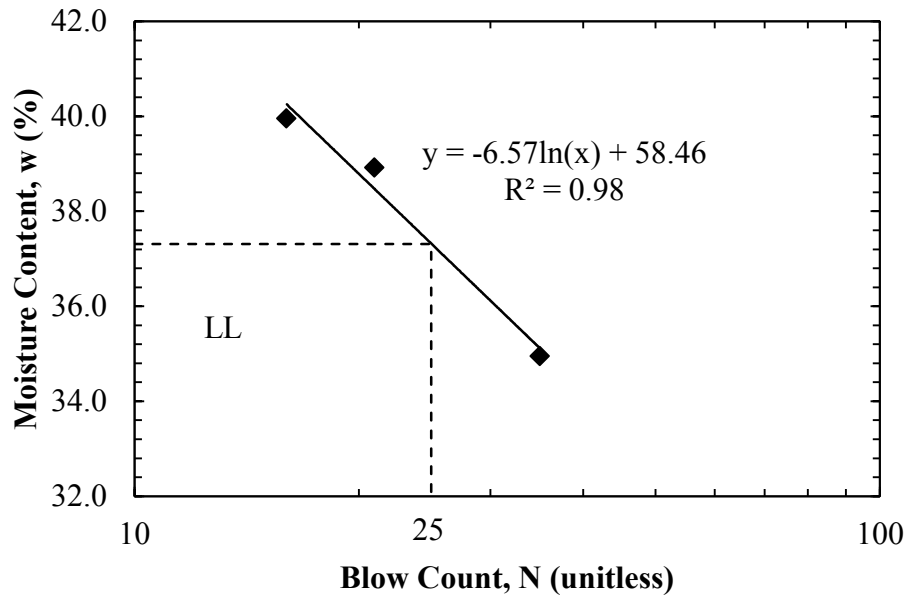


Figure D.24. Liquid limit results from Test Pad 2 Southwest Shelby Tube Lift 4 sample (SW ST-TP2).

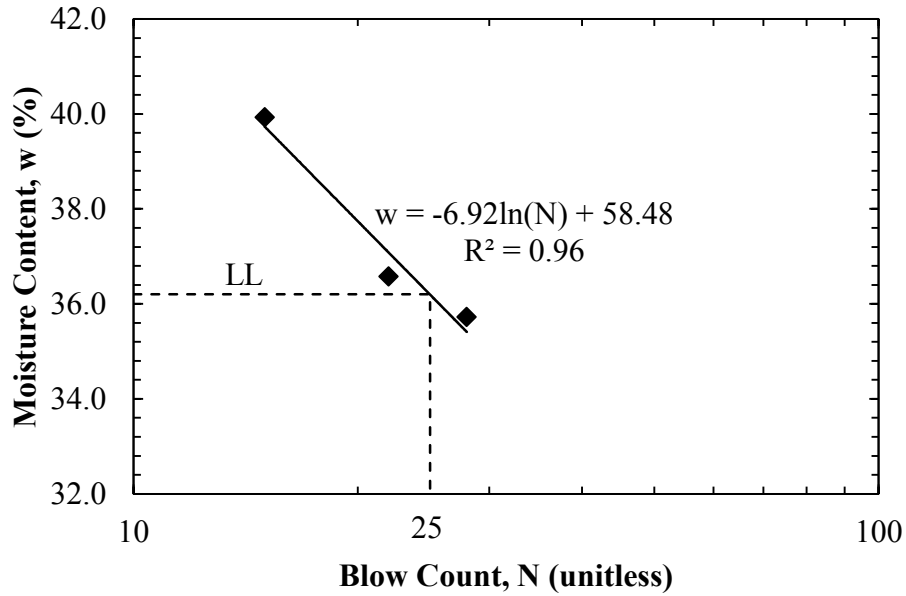


Figure D.25. Liquid limit results for sample from Test Pad 2 TSB borehole (0-2in.) obtained prior to TSB testing.

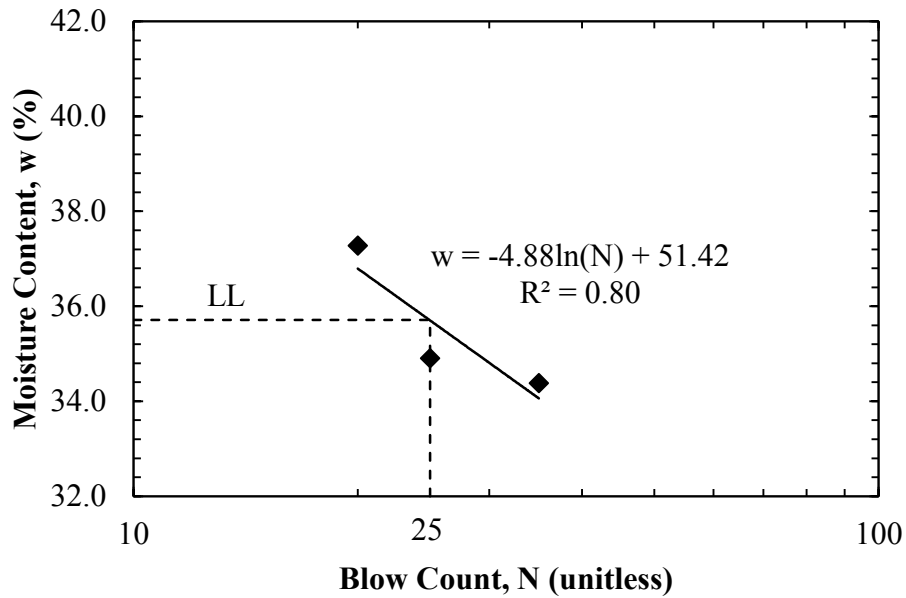


Figure D.26. Liquid limit results for sample from Test Pad 2 TSB borehole (2-4in.) obtained prior to TSB testing.

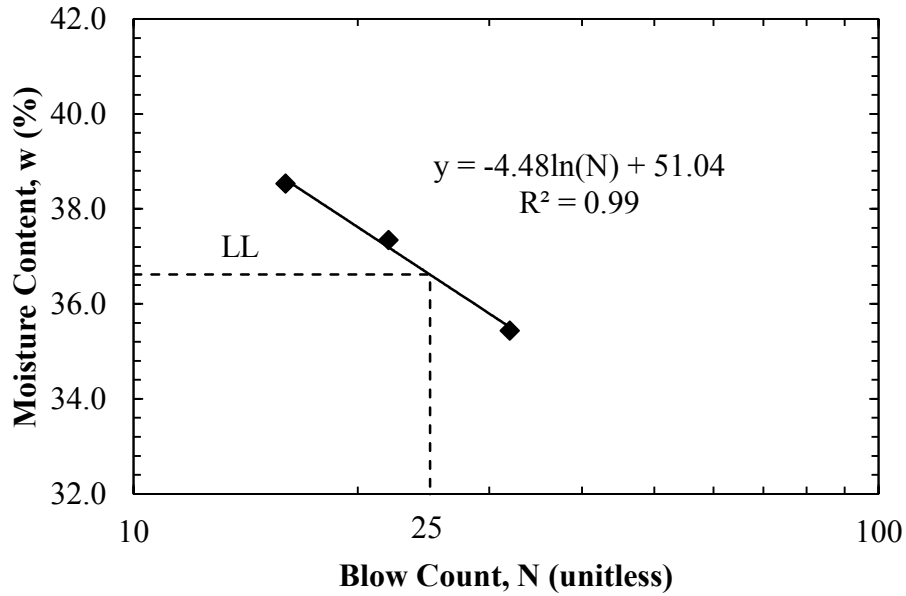


Figure D.27. Liquid limit results for sample from Test Pad 2 TSB borehole (4-6in.) obtained prior to TSB testing.

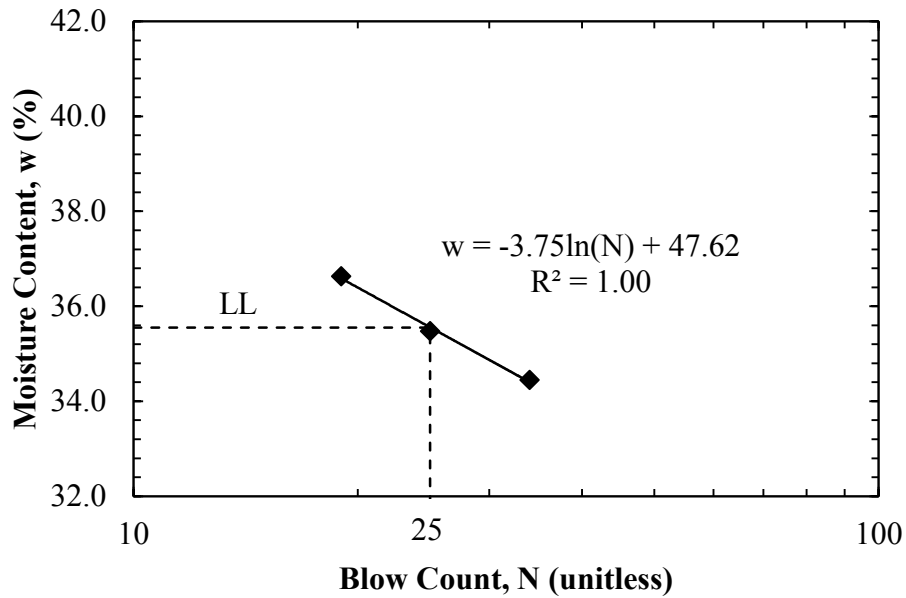


Figure D.28. Liquid limit results for sample from Test Pad 2 TSB borehole (6-8in.) obtained prior to TSB testing.

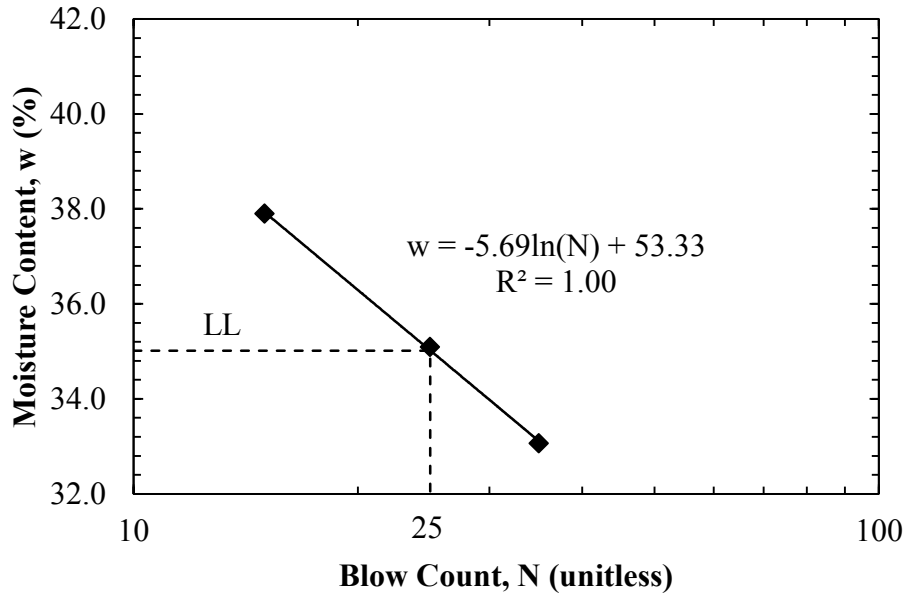


Figure D.29. Liquid limit results for sample from Test Pad 2 TSB borehole (8-10in.) obtained prior to TSB testing.

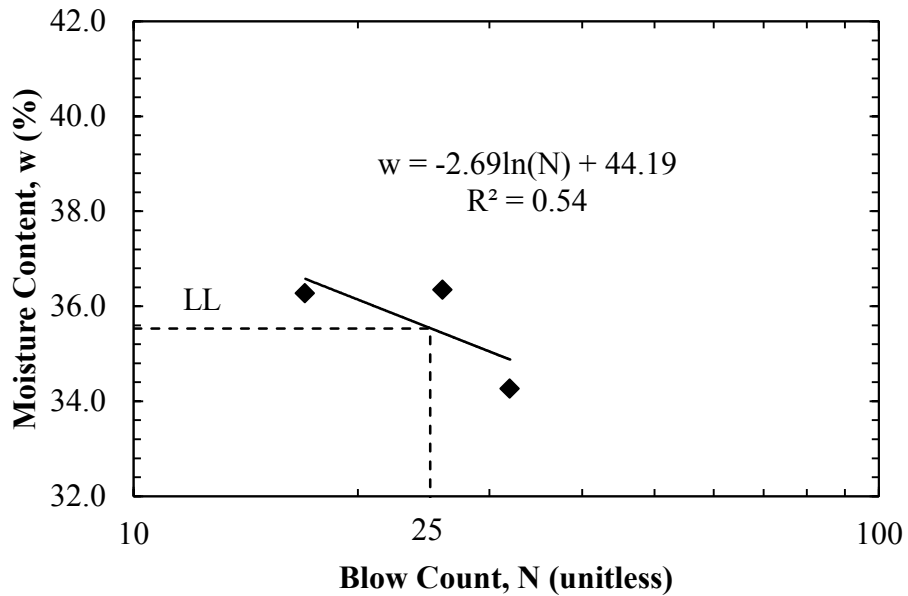


Figure D.30. Liquid limit results for sample from Test Pad 2 TSB borehole (10-12in.) obtained after Stage 1 of TSB testing.

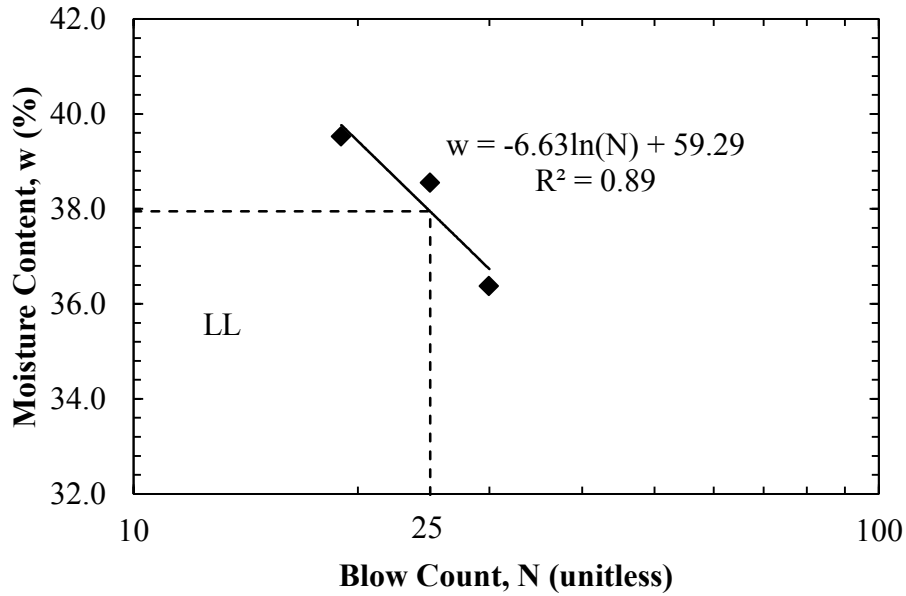


Figure D.31. Liquid limit results for sample from Test Pad 2 TSB borehole (12-14in.) obtained after Stage 1 of TSB testing.

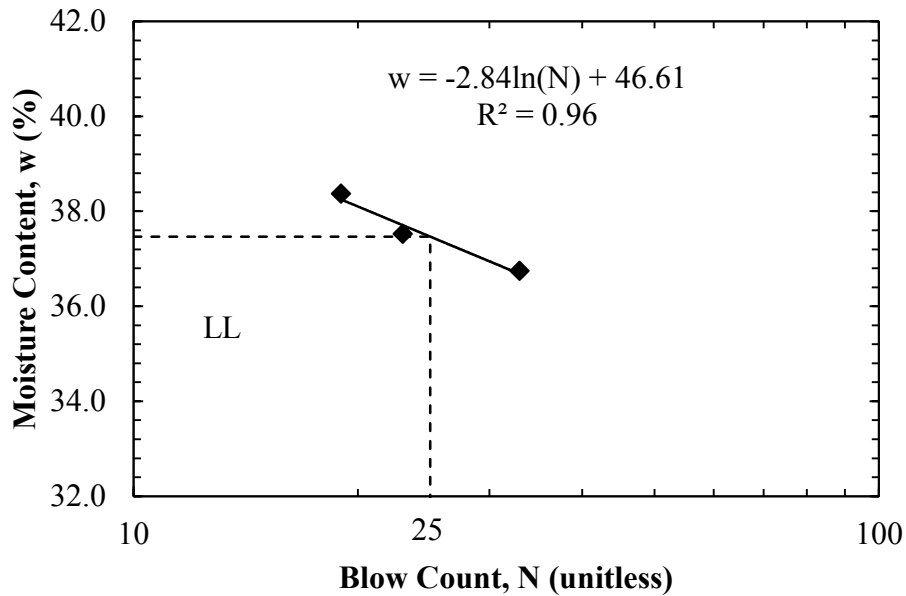


Figure D.32. Liquid limit results for sample from Test Pad 2 TSB borehole (14-16in.) obtained after Stage 1 of TSB testing.